



TECHNICAL UNIVERSITY – SOFIA
Department Theoretical Electrical Engineering

9TH SUMMER SCHOOL

ADVANCED ASPECTS
OF THEORETICAL ELECTRICAL ENGINEERING

Sozopol'12

PROCEEDINGS

Edited by: Valeri Mladenov
Snejana Terzieva

in the framework of

DAYS OF SCIENCE
OF THE TECHNICAL UNIVERSITY OF SOFIA

Sozopol'12, BULGARIA, 7-9.IX.2012



ORGANIZATION

The Summer School is organized by the Department of Theoretical Electrical Engineering at the Technical University of Sofia in the framework of the “Days of Science of the Technical University of Sofia”, Sozopol, Bulgaria, September 2012



TECHNICAL UNIVERSITY OF SOFIA, BULGARIA

under the patronage of the INTERNATIONAL SYMPOSIUM ON THEORETICAL ELECTRICAL ENGINEERING (ISTET) and it is a regular ISTET event



INTERNATIONAL SYMPOSIUM ON THEORETICAL ELECTRICAL ENGINEERING (ISTET)

SUPPORT

The main sponsor of the Summer School is:



RESEARCH & DEVELOPMENT SECTOR, TECHNICAL UNIVERSITY – SOFIA

Other sponsors:



IEEE BULGARIA CAS CHAPTER



THE WORLD SCIENTIFIC AND ENGINEERING ACADEMY AND SOCIETY (WSEAS)





TECHNICAL UNIVERSITY OF SOFIA



FACULTY AUTOMATION



DEPARTMENT THEORETICAL ELECTRICAL ENGINEERING

9th SUMMER SCHOOL

ADVANCED ASPECTS OF THEORETICAL
ELECTRICAL ENGINEERING -
SOZOPOL'12

Sozopol'12

in the framework of

THE DAYS OF SCIENCE OF THE TECHNICAL UNIVERSITY
OF SOFIA, SOZOPOL, BULGARIA, SEPT. 2012

Edited by: Valeri Mladenov
Snejana Terzieva

Organizing Committee

Honorary Chairmen:

V. Georgiev – Bulgaria
S. Farchy – Bulgaria
L. Kolev – Bulgaria
S. Papasow – Bulgaria
V. Savov – Bulgaria

Co Chairs:

V. Mladenov, TU-Sofia, Bulgaria
S. Terzieva, TU-Sofia, Bulgaria

Members:

Zh. Georgiev, TU-Sofia, Bulgaria
K. Brandisky, TU-Sofia, Bulgaria
I. Yacheva, TU-Sofia, Bulgaria
A. Chervenkov, TU-Sofia, Bulgaria
S. Petrakieva, TU-Sofia, Bulgaria
I. Tabahnev, TU-Sofia, Bulgaria
N. Petkova, TU-Sofia, Bulgaria
I. Trushev, TU-Sofia, Bulgaria
G. Tsenov, TU-Sofia, Bulgaria
S. Vladov, TU-Sofia, Bulgaria
S. Guninski, TU-Sofia, Bulgaria
K. Todorova, TU-Sofia, Bulgaria

International Programme Committee

Honorary Chairmen:

N. Mastorakis, Greece
R. Sikora, Poland
L. Chua, Berkeley-USA

Members:

D. Baldomir, Spain
A. Bossavit, France
A. Brykalski, Poland
H. Butterweck, Netherlands
T. Chady, Poland
K. Demirtchyan, Russia
S. Gratkowski, Poland
K. Hameyer, Germany
W. John, Germany
L. Klinkenbusch, Germany
L. Kolev, Bulgaria
A. Kost, Germany
Z. Leonowicz, Poland
W. Mathis, Germany
V. Mladenov, Bulgaria
M. Ogorzałek, Poland
S. Osowski, Poland
L. Pichon, France
B. Reljin, Serbia
L. Sumichrast, Slovakia
J. Sykulski, UK
M. Tadeusiewicz, Poland
R. Tetzlaff, Germany
H. Toepfer, Germany
H. Uhlmann, Germany
R. Weigel, Germany

PREFACE

This Proceedings contains the plenary lectures and the regular papers presented at the 9th Summer School *Sozopol'12*, which took place in Sozopol, Bulgaria, between 07 and 09 Sept. 2012 in the framework of the "Days of the Science of the Technical University of Sofia". The Summer School covers the advanced aspects of Theoretical Electrical Engineering and it is a platform for postgraduate training of Ph.D. students and young scientists. During the Summer School well-known experts presented some advanced aspects of circuits and systems theory, electromagnetic field theory and their applications. Apart from the educational part of the Summer School a presentation of original authors' papers took place.

The main topics of the Summer School *Sozopol'12* include Circuits and Systems Theory and Applications, Signal Processing and Identification Aspects, Electromagnetic Fields, Theoretical Concepts, Applications and New Approaches in Educating Theoretical Electrical Engineering. The Summer School *Sozopol'12* has been organized by the Department of Theoretical Electrical Engineering of the Technical University of Sofia with the main sponsorship of the Research and Development Sector of the Technical University of Sofia. At the time of this year's Summer School, a 7th FP project "South-East European TSO Challenges - SEETSOC" workshop took place. The papers presented during the workshop are also included in the proceedings.

This has been the ninth edition of the event, after the Summer Schools in 1986, 1988, 2001, 2002, 2005, 2007, 2009 and 2010. The Summer School is under the patronage of the International Symposium on Theoretical Electrical Engineering (ISTET) and it is a regular ISTET event. There were 63 participants from 8 different countries at the Summer School this year. There were 7 plenary lectures and 39 regular papers that are published in this Proceedings. Providing the recent advances in Theoretical Electrical Engineering the Proceedings will be of interest to all researchers, educators and Ph.D students in the area of Electrical Engineering.

Special thanks are due to the Research and Development Sector, Faculty of Automation and the Section of Social Services of the Technical University of Sofia about the overall support of the event. We would like to thank to the company h.o.-COMPUTER Software GmbH, a reseller of Intel Software Tools. Because of the good collaboration with ISTET, this year the company had a booth, presented their new products and partially sponsored the Summer School. We also would like to thank to the IEEE Bulgaria CAS Chapter and the World Scientific and Engineering Academy and Society (WSEAS), which also partially sponsored the event. We hope to meet again in the following edition of the Summer School to continue the good tradition and collaboration in the field of Theoretical Electrical Engineering.

Organizing Committee
Sofia, October 2012

CONTENTS

PLENARY LECTURES

1. *Elissaveta Dimitrova Gadjeva*, Computer-aided approaches to diagnosis of analog circuits 1
2. *Tuan D. Pham*, Image and signal analysis for personalized modeling in medicine and mental health 14
3. *Simona Kirilova Filipova-Petrakieva*, Stationary states analysis in linear electric circuits by graphs theory 20
4. *I. G. Koprinkov, K. A. Stankov*, A watt-level femtosecond fiber laser working in dissipative soliton regime 32
5. *Georgi A. Nenov*, A method for transformation of nullor RC-networks into equivalent OA-OTA-C- circuits 40
6. *R. P. Tasheva, V. Taneva-Toncheva, S. Tasheva*, Physical parameters and possible excitation mechanisms for a sample of seyfert galaxies 50
7. *Stefcho Georgiev Guninski*, Determination of the parameters of measurement scheme by shock excitation using FEM..... 56

SECTION 1 - CIRCUITS AND SYSTEMS THEORY, APPLICATIONS

1. *Galina Cherneva, Elena Dimkina*, A simulink model of synchronization of Lorenz-based chaotic system..... 64
2. *Rumen Yordanov, Georgi Tsenov, Valeri Mladenov*, Application of neural networks with different parameters for daily electric load forecast prediction..... 68
3. *Zvezditzia Nenova, Toshko Nenov, Stephan Kozhukharov, Nedyu Nedev*, Humidity sensing elements based on ce-doped SiO₂ films prepared via a sol-gel method..... 74
4. *Vasilina Georgieva Zlatanova, Nikola Petrov Georgiev*, Researching of tactile sensors resonant type 80

5.	<i>Irena Nikolova, Milka Vicheva, Kalinka Todorova</i> , European requirements for electromagnetic compatibility	86
6.	<i>Kalinka Mitkova Todorova, Stefcho Georgiev Guninski</i> , Study in modern software impact of electrical conductivity the signal output with pulse eddy current NDT	91
7.	<i>Kalinka Mitkova Todorova, Jivko Asenov Daskalov</i> , Study of a promiscuous T – shaped bridge circuit with eddy current transducer	95
8.	<i>Vasil Bachvarov</i> , Performance comparison of GPU and CPU implementations of the conjugate gradient method.....	99
9.	<i>Stoyan Kirilov, Simona Petrakieva, Valeri Mladenov</i> , Analysis of RM, LM and CM circuits with one memristor and sources of a sine voltage and current	105
10.	<i>Stoyan Kirilov, Svetoslav Dichev, Ivan Trushev, Valeri Mladenov</i> , Analysis of a LCM equivalent circuit of memristor and impulse voltage sources.....	111
11.	<i>Georgi Komsalov, Georgi Tsenov, Valeri Mladenov</i> , Optimisation procedure for determination of the optimal parallel lines for 110 KV electric power distribution systems.....	117
12.	<i>Антонио Андонов, Силвия Андонова, Марияна Михова</i> , Инварианти на чувствителността на честотно селективни комуникационни вериги	123
13.	<i>Валентина Танева-Тончева, Иван Танев Иванов, Радостина Пенева Ташева</i> , Универсален ултравиолетов оптичен микроскоп и rife beam ray (RBR) – две открития без авторство	129

SECTION 2 - THEORETICAL CONCEPTS, SIGNAL PROCESSING AND IDENTIFICATION ASPECTS

1.	<i>Lubomir Kolev</i> , Real eigenvalue range determination for the interval generalized eigenvalue problem	142
2.	<i>Lubomir Kolev</i> , Relations between margin of stability, stability radius and regularity radius	149

3.	<i>Valentin S. Mollov, Yancho Z. Kolev</i> , Hardware authentication module using feige-fiat-shamir zero-knowledge algorithm	155
4.	<i>Jordan Shopov, Galia Georgieva-Taskova, Simona Filipova-Petrakieva</i> , Electrical losses in semi-conductive devices	162
5.	<i>Stoyan Hristov Bozhkov</i> , Matlab oriented model of photovoltaic module considering the enviironmental factors.....	168
6.	<i>Stoyan Hristov Bozhkov</i> , Factors infliencing electrical performance of photovoltaic systems	174
7.	<i>Atanas Chervenkov</i> , Automating determination of the optimum power and number of transformation station in the residential part of settlements	180
8.	<i>Nikolina Petkova</i> , A new method for a real state of power transformers based on the area of partial discharge.....	185
9.	<i>Ivan Mitkov Trushev</i> , A simulink model of a DC/DC buck converter controller based on the general sliding mode control	190
10.	<i>Таня Методиева Стоянова, Адриана Найденова Бороджиева</i> , Синтез и анализ на нискочестотни и високочестотни активни биквадратни филтрови звена с използването на Matlab и Microcap.....	196
11.	<i>Таня Методиева Стоянова, Адриана Найденова Бороджиева</i> , Синтез и анализ на реактивни (LC) филтри с използването на Matlab и Microcap	203
12.	<i>Таня Методиева Стоянова, Адриана Найденова Бороджиева</i> , Синтез и анализ на трептящи кръгове с използването на Matlab и Microcap.....	209
13.	<i>Георги Рашков Георгиев, Таня Методиева Стоянова, Надежда Лиозовна Евстатиева, Димчо Василев Киряков</i> , Оценяване на ролята на мястото и големината на капацитета на кондензатора в параметричните индуктивно-капацитивни стабилизатори на ток и напрежение	215

SECTION 3 - ELECTROMAGNETIC FIELDS, NEW APPROACHES IN EDUCATING THEORETICAL EE

1. *Kostadin Brandisky*, Optimization of 4-pole small DC machine using fem and evolution strategy 221
2. *Snejana Terzieva, Ivan Tabahnev, Simeon Vladov*, An application of Matlab and Orcad PSpice for the education on the subject "Circuits and signals", Part I 227
3. *Snejana Terzieva, Ivan Tabahnev, Simeon Vladov*, An application of Matlab and Orcad PSpice for the education on the subject "Circuits and signals", Part II..... 234
4. *Kiril Stoyanov Stoykov*, Transformer windings with big section, high current and low voltage 241
5. *Ivan Stefanov Bozev*, Equations for electromagnetic induction in electromagnetism 247
6. *Elissaveta Dimitrova Gadjeva, Dimitar Yordanov Shikalanov*, Behavioral spice modeling of photovoltaic cells 258
7. *Nikolay Gourov, George Milushev*, Implementation of "Power quality teaching toy" (PSL) in the educational process in Bulgaria 263
8. *Tsvetomir Dobrev, Rosen Pasarelski, Teodora Pasarelska*, The e-learning of theoretical electrical engineering..... 268
9. *Таня Методиева Стоянова, Георги Рашков Георгиев*, Оптимизиране на организацията при провеждането и на резултатите от олимпиадите по теоретична електротехника със студентите от електротехническите специалности на техническите ВУЗ..... 273

SECTION 4 - SEETSOC WORKSHOP

1. *Petar Krstevski, Rubin Taleski, Jordancho Angelov, Aleksandra Krkoleva, Kliment Naumoski, Aleksandar Paunoski*, Creation of regional electric transmission network models by using database related software solution..... 278

2.	<i>Costin Cepisca, Alexandru Lazar, George Seritan, Sorin dan Grigorescu, Mircea Covrig</i> , Seetsoc RBM programm - structure and implementation.....	285
3.	<i>Nikolay Baldzhiev, Ivan Evgeniev, Velizar Bodurski, Valeri Mladenov</i> , Calculation of network transfer capacities using UCTE file format.....	291
4.	<i>Nikolay Baldzhiev, Velizar Bodurski, Georgi Tzenov, Ivan Evgeniev, Valeri Mladenov</i> , Using geographical information system in power networks	297

COMPUTER-AIDED APPROACHES TO DIAGNOSIS OF ANALOG CIRCUITS

Elissaveta Dimitrova Gadjeva

Department of Electronics, Technical University of Sofia,
8 Kliment Ohridski Blvd., 1000 Sofia, Bulgaria,
phone +395 2 3725, e-mail: egadjeva@tu-sofia.bg

Abstract. *In the present paper, computer-aided approaches to diagnosis of analog circuits using general-purpose circuit analysis programs are considered. Nullor approaches at subcircuit and at component levels are developed. The test voltages of the accessible nodes and the current through the voltage supply are selected as test quantities. A nullor diagnosis model of the circuit under test is constructed. The automated fault localization and identification of single and multiple faults is reduced to simulation of a nullor diagnosis model. A fault observability investigation is performed based on sensitivity analysis. The concepts fault masking, fault dominance, fault equivalence and fault isolation are defined. The fault coverage is obtained using oscillation-based approach in combination with statistical analysis.*

Keywords: *Analog circuit diagnosis; Fault models; Fault identification; Nullor models; Spice simulation*

1. INTRODUCTION

The fault diagnosis is a very important problem of analog circuit testing. Localization of faulty elements and determination of the changed parameter values using measurement data for the test voltages of the faulty circuit represent a typical inverse problem. The increasing complexity of the analog and mixed-signal VLSI circuits, the limited number of accessible nodes and the lack of efficient fault models complicate the fault localization and fault identification.

Many approaches have been developed to automate diagnosis of analog and analog-discrete circuits before and after test: model-based approaches [1, 2], branch decomposition diagnosis at subcircuit and component levels [3], nullator-norator approach [4], fault dictionary techniques, sensitivity-based, symbolic, spectral, neural network, optimization approaches [5, 6, 7], etc. The fault identification in circuits of analog-discrete type such as switched-capacitor circuits is considered in [8]. The monitoring of the I_{dd} current offers the opportunity to perform reliable diagnosis of faulty circuits with insufficient number of accessible (test) nodes [9, 10].

The contemporary general-purpose analog circuit analysis programs such as *PSpice* [11] are characterized by powerful analysis tools which allow to perform accurate and fast simulation. The development of analog circuit diagnosis approaches in the environment of the contemporary CAD systems are motivated by the extended possibilities of the circuit simulators:

- The abilities of the input languages allow to built user-defined computer models. In this way the construction and solving the test equations is reduced to analysis of corresponding diagnosis model;

- The circuit simulators such as *PSpice* are based on sparse matrix approach and modified nodal analysis, which permit to achieve a high speed of simulation for circuits having a large number of nodes. The sparse matrix approach used in contemporary analysis programs leads to computational efficiency of the simulation. The possibility for accuracy and convergence control allows to diagnose circuits consisting of subcircuits with a large number of inner (inaccessible) nodes;
- The automated fault localization and identification of single and multiple faults can be reduced to simulation of the nullator-norator diagnosis model of the circuit under test;
- One of the most important advantage of the realization of diagnosis approach in the environment of standard circuit simulators consists in the use of accurate computer models of electrical and electronic elements. This allows to obtain adequate diagnosis results;
- The sensitivity analysis can be applied to optimal test frequency selection in order to increase the fault observability and to avoid fault equivalence and fault masking;
- The tolerance (Monte Carlo and worst-case) analysis tools can be used in order to take into account the design and process tolerances and to determine automatically the non-faulty limits for the test quantities;
- The determination of magnitude and phase spectral components can be used for fault detection of catastrophic and parametric faults. It allows to improve the fault coverage by the use of the power supply current against the output voltage signal.

2. NULLOR APPROACH TO ANALOG CIRCUIT DIAGNOSIS

2.1. Diagnosis model

A nullor approach to analog circuit diagnosis at subcircuit and at component levels is developed in [4]. The diagnosis technique proposed solves the inverse problem for the fault localization and for obtaining the faulty parameter values of the circuit components and is based on measurements of test voltages at the accessible nodes. A nullor diagnosis model of the circuit under test is constructed and analyzed. The automated fault localization and identification of single and multiple faults is reduced to simulation of the nullor diagnosis model.

The concept for the pair fixator (nullator plus source) and norator is used in the diagnosis model approach proposed in [4,12]. A nullator-norator (nullor) based DC-test generation approach is developed in [12]. The topological conditions for diagnosability investigation using graphs containing nullators and norators, are considered in [13].

The circuit under test N shown in Fig. 1a consists of subcircuits S_1, S_2, \dots, S_l and branches in the main circuit (links). The nodes $n_{T1}, n_{T2}, \dots, n_{Tm}$ in N are accessible for

measurement of the voltages $V_{T1}, V_{T2}, \dots, V_{Tm}$ (test voltages), where m is the number of accessible (test) nodes. The voltage supply current I_{DD} is also accessible for testing. The localization of the faulty links and subcircuits is performed using testing of the accessible nodes which is based on analysis of nullor diagnosis model N_d of the tested circuit [4]. The N_d model is obtained from the model N_{nom} of the nominal circuit applying the measured test voltages V_{Ti} of the faulty circuit to the test nodes $n_{Ti} = 1, 2, \dots, m$ using independent voltage source $E_{Ti} = V_{Ti}$ connected in series with a nullator (voltage fixator) (Fig. 1b). The role of the fixators is to apply the measured test voltages to corresponding accessible nodes. The role of the norators is to ensure path for the difference currents due to the fault.

According to its definition, the nullator element is characterized by $i = u = 0$ [14]. As a result, the test voltage V_{Ti} , corresponding to a faulty circuit, is applied to the corresponding test node n_{Ti} . The correctness of the node n_{Ti} is tested by connecting a norator between the node n_{Ti} and the reference node (Fig. 1b) [4]. The norator ensures a path for the difference current $I_{nor,i}$ flowing as a result of faults in subcircuits or links connected to the test node n_{Ti} . If $I_{nor,i} = 0$, the node n_{Ti} is non-faulty. The subcircuit S_k is non-faulty, if all its poles are non-faulty nodes. A link is correct if it is incident to at least one non-faulty node [4]. The rest of the elements are potentially faulty.

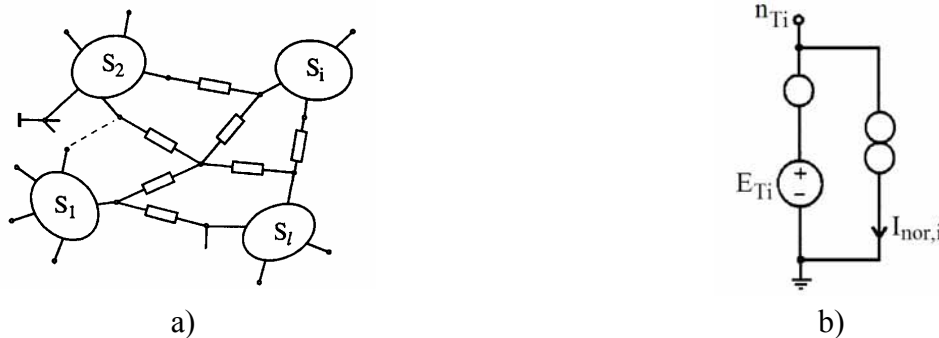


Fig. 1. Circuit under test N with accessible nodes (a) and nullor model for testing the accessible node n_{Ti} (b)

The topological conditions for existence of a unique solution of the nullator-norator diagnosis model are discussed in [4,13]. The circuit containing nullators and norators has a unique solution if the structural graph of the circuit G contains two trees T_1 and T_2 , where the tree T_1 includes all nullators but does not include norators while the tree T_2 includes all norators but does not include nullators.

The testing of the eventually faulty elements is performed using the nullor model shown in Fig. 2. In order to test a k -fold fault, the test voltages V_{Ti} are applied to the test nodes $n_{Ti}, i=1, 2, \dots, k$ and the norator element is connected in parallel with the tested element $Y_i, i=1, 2, \dots, k$. The correctness of the remaining $n_T = m - k$ test nodes is checked using the nullor equivalent circuits shown in Fig. 1b. The number of the test nodes defines the maximal multiplicity of tested faults.

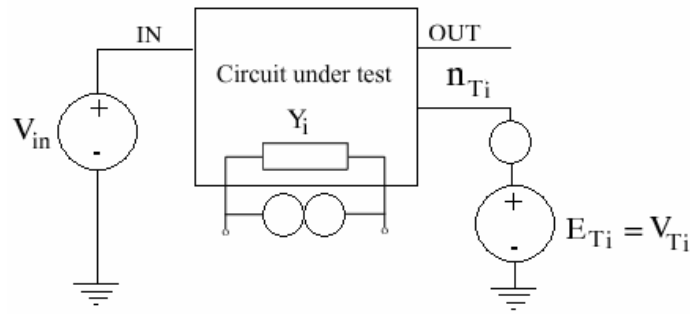


Fig. 2. Nullator-norator model for diagnosis of the faulty element Y_i

The fault diagnosis at subcircuit level is reduced to testing the corresponding sub-circuit poles using the nullor model shown in Fig. 1b.

The diagnosis algorithm consists of the following steps:

1. Decomposition of the circuit to a number of subcircuits which poles coincide with the accessible (test) nodes;
2. Carrying out diagnosis of the accessible nodes and subcircuits. If at least two poles of a subcircuit S_i are faulty nodes, the subcircuit is faulty. Otherwise the subcircuit is correct;
3. Carrying out diagnosis of the elements in the faulty subcircuits using the pairs fixator – norator as shown in Fig. 2.

2.2. Computer implementation of the diagnosis approach

The nullor element can be approximately represented in the input language of the general-purpose circuit simulators by a dependent source having a large value of the gain. The nullor element in Fig. 3a can be efficiently modelled by the *PSpice* circuit simulator [11] using a dependent current or voltage source, controlled by voltage (VCCS or VCVS), with a large controlling coefficient, for example 1×10^{12} . The nullor as a part of the pair fixator – norator, can be also easily modelled in the *PSpice* program by an ideal operational amplifier (OPAMP element), which is included in the symbol and model libraries.

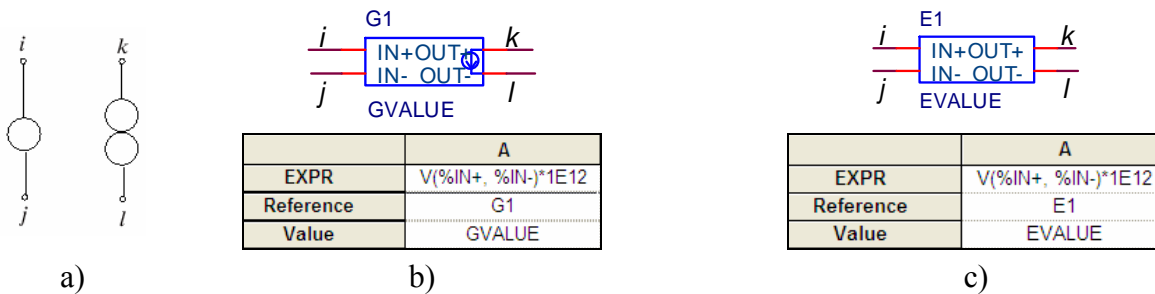


Fig. 3. Computer model of the nullor:
 (a) nullator-norator pair (nullor); (b) PSpice model of the nullor using VCCS;
 (c) PSpice model of the nullor using VCVS

2.3. Assessment of the design tolerances

Based on *Monte Carlo* simulation, the design and process tolerances of the circuit elements are taken into account in order to obtain the nonfaulty limits of the norator currents.

The fault prediction approach can be applied to reduce the influence of the design tolerances and to improve the diagnosis results. In the proposed in [15] fault prediction algorithm, the component values are evaluated according to the consecutive voltage measurements that are continuously monitored at the accessible test points at each periodic maintenance. Based on this approach, a difference diagnosis nullor model is constructed. Instead the measured test voltages V_{Ti} , the differences between two successive measured test voltages ΔV_{Ti} are applied to the test nodes n_{Ti} by fixators. In this way, the influence of the design tolerances is significantly reduced.

2.4. Computer diagnosis of example circuits

In order to test the lowpass filter shown in Fig. 4, consisting of 6 subcircuits S_1, S_2, S_3, S_4, S_5 and S_6 , the diagnosis model N_d is composed and analyzed. The calculated norator currents I_i at the accessible nodes are given in Table 1.

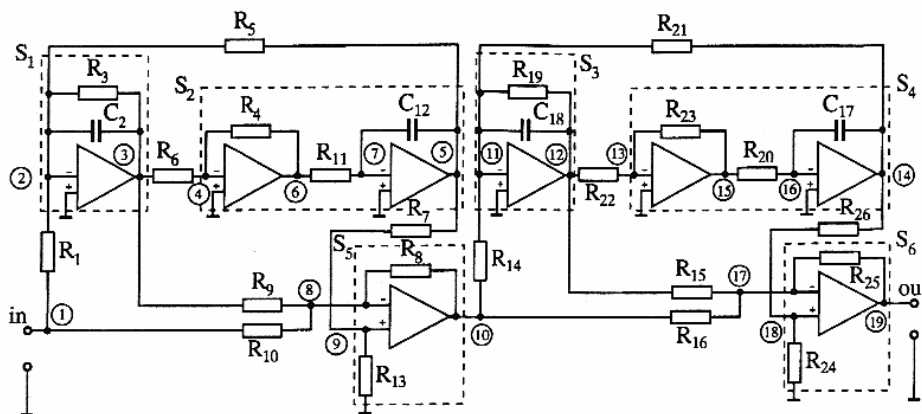


Fig. 4. Lowpass filter

Table 1. Diagnosis of faulty nodes of the lowpass filter

Node i	V_i (V)	I_i (A)
1	$9.56 \times 10^{-1} + j 3.155 \times 10^{-3}$	$4.307 \times 10^{-3} + j 1.359 \times 10^{-5}$
2	$1.17 \times 10^{-5} + j 1.38 \times 10^{-4}$	$-4.334 \times 10^{-3} - j 1.126 \times 10^{-5}$
3	$-1.17 \times 10^{-1} - j 1.328$	$2.655 \times 10^{-5} - j 2.34 \times 10^{-6}$
4	$-1.2 \times 10^{-5} - j 1.36 \times 10^{-4}$	$0 + j 0$
5	$-25.18 + j 2.167$	$0 + j 0$
8	$-3.9281 + j 0.338$	$0 + j 0$
9	$-3.9285 + j 0.338$	$0 + j 0$
10	$-4.406 + j 0.385$	$0 + j 0$
11	$-8.86 \times 10^{-6} - j 7.03 \times 10^{-5}$	$0 + j 0$
12	$8.8 \times 10^{-2} + j 0.692$	$0 + j 0$
13	$5.44 \times 10^{-6} + j 4.28 \times 10^{-5}$	$3.5 \times 10^{-6} + j 2.75 \times 10^{-5}$
14	$8.957 - j 1.12$	$4.79 \times 10^{-2} + j 0.2728$
17	$1.0868 - j 0.1358$	$0 + j 0$
18	$1.087 - j 0.1358$	$0 + j 0$
19	$1.6012 - j 0.1992$	$0 + j 0$
0	$0 + j 0$	$-4.79 \times 10^{-2} - j 0.273$

Nodes 4, 5, 8, 9, 10, 11, 12, 17, 18 and 19 are non-faulty since their norator currents $I_i = 0$ and nodes 0, 1, 2, 3, 13 and 14 are faulty ($I_i \neq 0$). The subcircuits S_2 , S_3 , S_5 and S_6 are non-faulty as they are connected to only one faulty node (node 0). The subcircuits S_1 and S_4 and the connection R_1 are faulty since they are incident to faulty nodes. The rest of the connections are non-faulty as they are incident to at least one non-faulty node.

In order to test the bandpass SC-filter shown in Fig. 5, consisting of 4 subcircuits S_1 , S_2 , S_3 and S_4 , the diagnosis model N_d is composed and analyzed. The calculated norator charges ΔQ_i are given in Table 2.

Nodes 3, 9, 11 and 13 are test nodes. The norator test quantities ΔQ_i are presented in Table 2. Nodes 3, 9 and 11 are non-faulty since $\Delta Q_i = 0$ and nodes 13 and 0 are faulty ($\Delta Q_i \neq 0$). The subcircuits S_1 , S_2 and S_3 are non-faulty as they are connected to non-faulty nodes. The subcircuit S_4 is faulty as it is incident to faulty nodes 13 and 0.

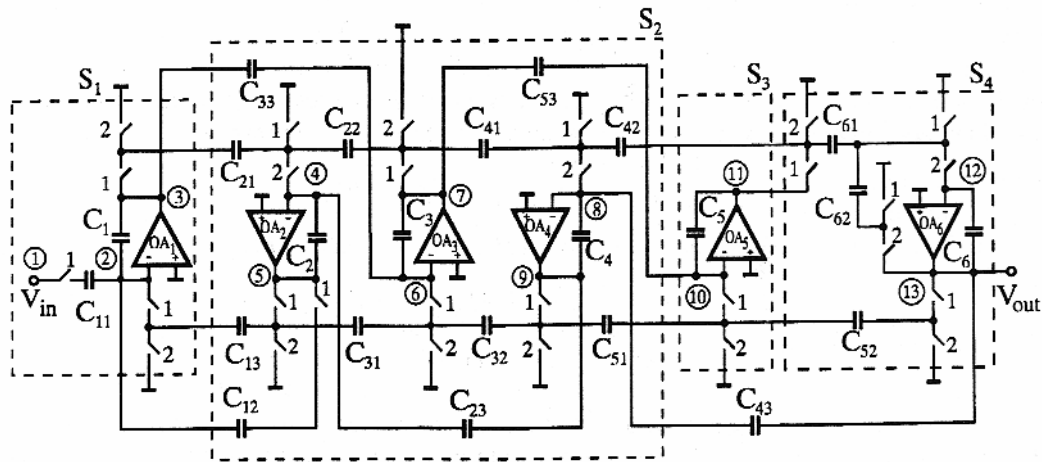


Fig. 5. Bandpass SC-filter

Table 2. Diagnosis of faulty nodes of the bandpass SC-filter

Node i	Phase j	V_i^j (V)	$\Delta Q_i^j(z) \times 10^{12}$ (C)
3	1	$-4.902 \times 10^{-1} - j2.218 \times 10^{-1}$	$0 + j0$
	2	$-5.089 \times 10^{-1} - j1.747 \times 10^{-1}$	$0 + j0$
9	1	$-4.193 \times 10^{-2} - j5.905 \times 10^{-1}$	$0 + j0$
	2	$1.382 \times 10^{-2} - j5.918 \times 10^{-1}$	$0 + j0$
11	1	$6.581 \times 10^{-1} + j6.595 \times 10^{-1}$	$0 + j0$
	2	$7.172 \times 10^{-1} + j5.947 \times 10^{-1}$	$0 + j0$
13	1	$1.004 - j3.767 \times 10^{-1}$	$0 + j0$
	2	$1.035 - j2.806 \times 10^{-1}$	$-0.1816 + j4.925 \times 10^{-2}$
0	1	$0 + j0$	$0 + j0$
	2	$0 + j0$	$0.1816 - j4.925 \times 10^{-2}$

The nullator-norator approach can be applied to fault diagnosis of RF circuits. It is based on the measured phasors of the S -parameters, introduced using fixators in the diagnosis model. High frequency models of passive and active components are submitted by the vendors [16] in the form of model and symbol libraries for *Cadence Capture* and *Cadence PSpice*.

3. FAULT OBSERVABILITY INVESTIGATION OF LINEAR ANALOG CIRCUITS

In [7] a method is developed for improving fault detection in the frequency domain of linear analog circuits based on sensitivity analysis. The test frequencies are selected maximizing the sensitivity of the magnitude and phase of the output characteristics. The concepts fault masking, fault dominance, fault equivalence and fault isolation are defined. A masking exists if $S_{x_i}^{y_j} = -S_{x_k}^{y_j}$ for each frequency. Fault dominance exists if $S_{x_i}^{y_j} \square S_{x_k}^{y_j}$ for each frequency, and the faults are equivalent if $S_{x_i}^{y_j} = S_{x_k}^{y_j}$ for each frequency. Based on sensitivity analysis, test nodes and test frequencies selection is performed for every category of faults (single, double, multiple). The method developed in [17] is based on sensitivity investigation of the test characteristics. The sensitivity model approach is realized using the *PSpice* simulator and parameterized sensitivity *PSpice* macromodels are built in order to calculate the sensitivity characteristics in the frequency domain. The determination of the needed sensitivities is reduced to a parametric analysis of the constructed sensitivity model. Applying post-processing of the simulation results using macro-definitions in the graphical analyzer *Probe*, a fault observability investigation of the circuit is performed. The frequency ranges, corresponding to maximal sensitivity measures, are automatically obtained for the multiple fault isolation.

3.1. Sensitivity model

The sensitivity model approach is used to calculate the sensitivity coefficients of the output characteristics in the frequency domain. According to this method, in order to obtain the derivative of the output voltage V_{out} in respect to the admittance Y_i in the circuit, an analysis of the original circuit N is performed and the resulting voltage V_{Y_i} is used as a control voltage for the sensitivity model N_d . A voltage controlled current source is connected in parallel with the element Y_{id} with controlling coefficient of $Y_c = 1S$. The output voltage $V_{out,d}$ of the circuit N_d is equal to the derivative $\partial V_{out} / \partial Y_i$: $V_{out,d} = \partial V_{out} / \partial Y_i$. In order to automatically obtain the sensitivity

$$S_{Y_i}^{V_{out}} = \frac{\partial V_{out}}{\partial Y_i} \cdot \frac{Y_i}{V_{out}} \quad (1)$$

in the computer *PSpice* model, the controlling coefficient of Y_c is multiplied by Y_i in the model and the result $V_{out,d}$ is divided by V_{out} in the graphical analyzer *Probe*.

3.2. Computer realization of the fault observability approach

The sensitivity model of the resistor is represented in Fig. 6. It is built using a block definition. In order to analyze simultaneously the circuits N and N_d , the equivalent circuit contains the element R_1 from the original circuit N and the element R_{1sen} from the sensitivity model N_d . The VCCS G_{gen} is added in parallel with R_{1sen} in the sensitivity model. The attributes of the block are shown in Fig. 6b. The ID number is assigned to the element. In order to obtain the sensitivities for a group of elements simultaneously in the graphical analyzer *Probe*, a parametric sweep is used. A parameter par is defined with a linear variation from 1 to n with increment 1. When the current value of par is equal to the ID number of a given element, the controlling coefficient G_{gen} of its VCCS is equal to the nominal element value val and the sensitivity with respect to this element is calculated, otherwise $G_{gen}=0$. This is accomplished by the **IF-THEN-ELSE** statement, included in the expression for G_{gen} (Fig. 6c). The sensitivity models of the capacitor and inductor elements are built similarly. They are represented in Fig. 7 and Fig. 8 correspondingly.

A number of fault observability measures can be defined based on sensitivity calculation [18]: M_1^n , M_2^n and M_3^n . The measure M_1^n is defined as a sum of modules of the sensitivities with respect to the element parameters Y_1, Y_2, \dots, Y_n .

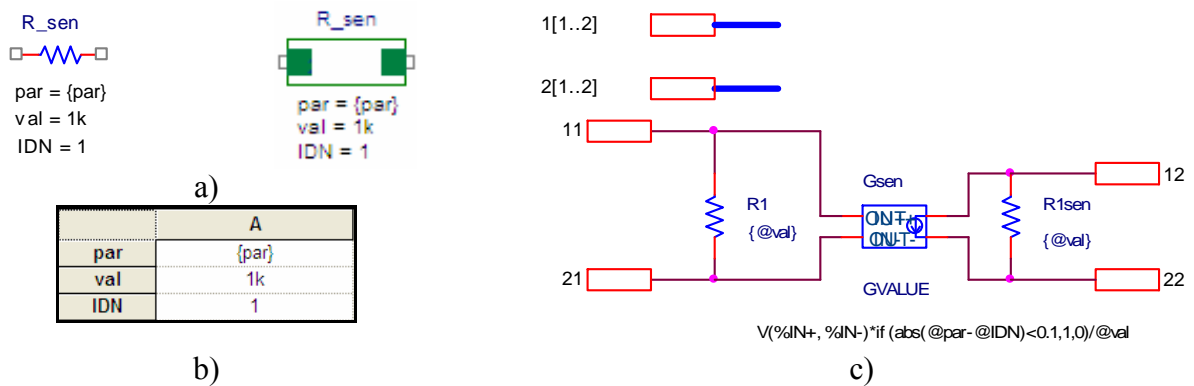


Fig. 6. Sensitivity model of the resistor

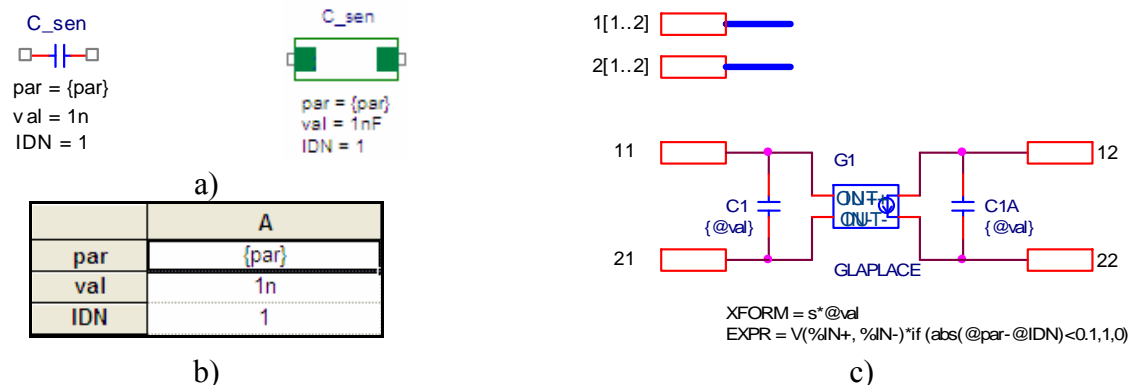


Fig. 7. Sensitivity model of the capacitor

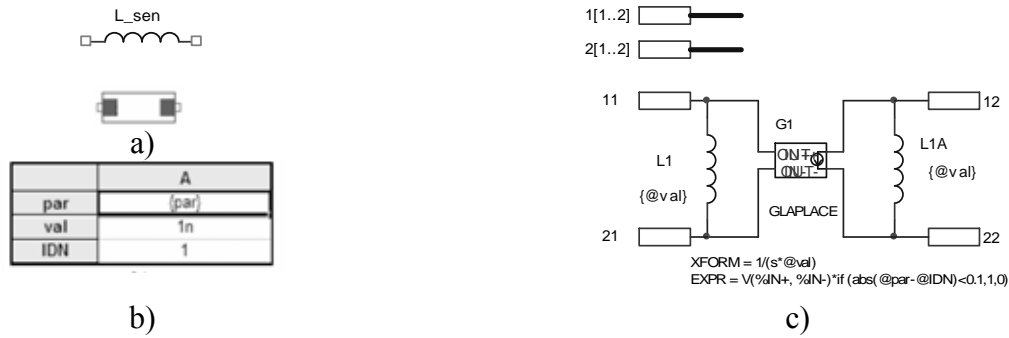


Fig. 8. Computer realization of the sensitivity model of inductor element using hierarchical block

$$M_1^n = \sum_{i=1}^n \left| S_{Y_i}^{V_{out}} \right|. \quad (2)$$

N -fold fault of the defined group of elements can be detected in the frequency ranges, where the measure M_1^n has a maximum value.

In order to avoid fault dominance, the measure M_2^n can be used in the form:

$$M_2^n = M_1^n \prod_{i=1}^n \left| S_{Y_i}^{V_{out}} \right|. \quad (3)$$

Multiplying the measure M_1^n by the product of sensitivities, the frequency ranges corresponding to low sensitivity values for some of the elements, are skipped and the fault dominance is avoided. N -fold fault of the defined group of elements can be detected in the frequency ranges, where the measure M_2^n has a maximum value.

A variant of the measure M_1^n is the measure M_3^n . It is defined in the following way:

$$M_3^n = M_1^n E, \quad (4)$$

where E is enable function:

$$E = \prod_{i=1}^n E_i \quad ; \quad E_i = \begin{cases} 1 & \text{if } \left| S_{Y_i}^{V_{out}} \right| \geq \varepsilon M_1^n \\ 0 & \text{if } \left| S_{Y_i}^{V_{out}} \right| < \varepsilon M_1^n \end{cases}, \quad (5)$$

where ε is a threshold parameter, defining the minimal allowed ratio between the individual sensitivity and the measure M_1^n . It is needed to avoid the fault dominance. If $E = 0$, a fault dominance exists and the value of the measure M_3^n in these frequency ranges is set to zero.

The sensitivities $S_{Y_i}^{V_{out}}$ and the measures: M_1^n , M_2^n and M_3^n are calculated in the graphical analyzer *Probe*.

For example, the measure M_1^1 for testing the circuit parameter with *ID* number p has the form:

$$\text{SEN}(p)=M(V(\text{OUT2})@p/V(\text{OUT1})@p)$$

where $V(\text{OUT1})$ is the output voltage of the circuit N and $V(\text{OUT2})$ is the output voltage of the circuit N_d .

The measures M_1^2 , M_2^2 and M_3^2 for testing a double fault in circuit elements with *ID* numbers p_1 and p_2 , have the form:

$$\begin{aligned} \text{MS1_2}(p_1,p_2)&=\text{SEN}(p_1)+\text{SEN}(p_2) \\ \text{MS2_2}(p_1,p_2) &= (\text{SEN}(p_1)+\text{SEN}(p_2))*\text{SEN}(p_1)*\text{SEN}(p_2) \\ \text{E_2}(p_1,p_2) &= 0.5*(\text{sgn}(\text{SEN}(p_1)/\text{MS2_2}(p_1,p_2))-\text{eps})+1)* \\ &+ 0.5*(\text{sgn}(\text{SEN}(p_2)/\text{MS2_2}(p_1,p_2))-\text{eps})+1) \\ \text{MS3_2}(p_1,p_2) &= \text{MS2_2}(p_1,p_2) * \text{E_2}(p_1,p_2) \end{aligned}$$

The approach developed in [21] is used for the S -parameter determination in the *PSpice* environment using parametric analysis (Fig. 9). Macrodefinitions in *Probe* are used for the S -parameter determination defined by the following expressions:

$$\begin{aligned} S_{11} &= \frac{2\dot{V}_1}{\dot{V}_{g1}} - 1; \quad S_{21} = \frac{\dot{V}_2}{\dot{V}_{g1}} \quad \text{for } V_{g2} = 0, \\ S_{12} &= \frac{\dot{V}_1}{\dot{V}_{g2}} \quad ; \quad S_{22} = \frac{2\dot{V}_2}{\dot{V}_{g2}} - 1 \quad \text{for } V_{g1} = 0. \end{aligned} \tag{6}$$

The corresponding macrodefinitions have the form:

$$\begin{aligned} S11 &= 2*V(1)@1-1 \\ S12 &= V(1)@2 \\ S21 &= V(2)@1 \\ S22 &= 2*V(2)@2-1 \end{aligned} \tag{7}$$

where @1 is used for the data of the first simulation ($par = 0$) and @2 is used for the data of the second simulation ($par = 1$).

The low-noise amplifier [17] is used to illustrate the fault observability of electronic circuits at RF based on sensitivity analysis of the two-port S -parameters. AC sweep is performed in the frequency range (3GHz – 7GHz). The macrodefinitions (7) are used for the S -parameter calculation in the graphical analyzer *Probe*.

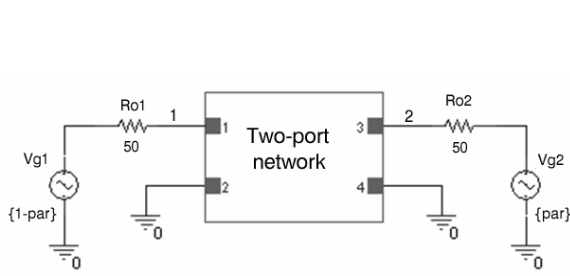


Fig. 9. S-parameter determination using PSpice

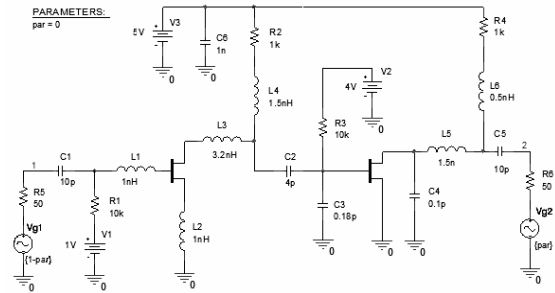


Fig. 10. Schematic of the low-noise amplifier

The result for the module of S_{21} in dB is shown in Fig. 11. The measures $M_1^2(L_2, L_5)$ and $M_2^2(L_2, L_5)$ are presented in Fig. 12. The frequencies, which ensure maximal observability of double faults, correspond to the maximum values of the defined measures. For the considered case, similar frequency values are obtained for the maximal fault observation (4.82GHz applying the measure $M_1^2(L_2, L_5)$ and 4.87GHz applying the measure $M_2^2(L_2, L_5)$).

4. STATISTICAL OBT APPROACH TO FAULT COVERAGE INVESTIGATION

The fault coverage FC is defined as a ratio of the number of recognized faults to the total number of modeled faults:

$$FC = \frac{F_2}{F_1 + F_2}, \tag{8}$$

where F_1 is the number of nonrecognized faults and F_2 is the number of recognized faults.

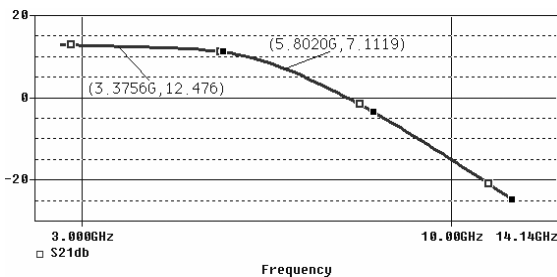


Fig. 11. Module of S_{21}

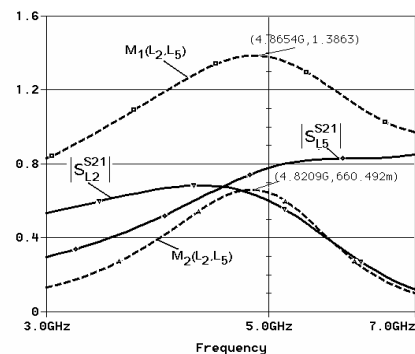


Fig. 12. Measures $M_1^2(L_2, L_5)$ and $M_2^2(L_2, L_5)$

The oscillation based testing (OBT) strategy is often used to achieve satisfactory fault coverage. The principle of OBT consists in reconfiguring the circuit under test (CUT) in test mode to an oscillator [18, 19, 20] (Fig. 13). The existence of catastro-

phic and parametric faults in the CUT results in deviation of the oscillation frequency from its normal value or in loss of oscillation. The fault coverage can be increased by monitoring the oscillation frequency, the amplitude of the oscillation voltage signal, as well as the supply current. The average and the peak-to-peak value of the current through the voltage supply I_{dd} are monitored for the I_{dd} testing. The fault coverage is obtained using *Monte Carlo* simulation of the diagnosis model taking into account the design tolerances. The modeled parametric faults of -50% and +100% and design tolerances of 5% are defined as shown in Fig. 14. As a result, the optimal test node set and test quantities, maximizing the fault coverage, can be selected.

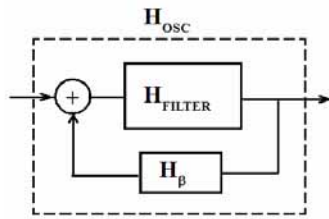


Fig. 13. The circuit in test mode

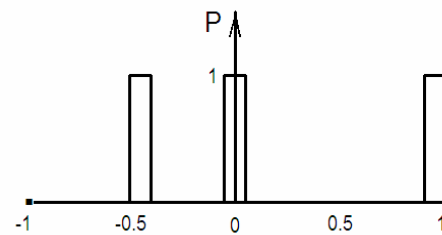


Fig. 14. Statistical distribution for defining the parameter value

4. CONCLUSION

The possibilities of general-purpose circuit analysis programs have been considered for realization of computer-aided approaches to analog circuit diagnosis. A nullator-norator approach to fault localization and identification is proposed based on monitoring the test voltages of the accessible nodes and the current through the voltage supply. Sensitivity analysis is used for the fault observability investigation. The concepts fault masking, fault dominance, fault equivalence and fault isolation are considered. The fault coverage is obtained in the PSpice environment applying oscillation-based approach in combination with statistical analysis.

5. ACKNOWLEDGEMENT

The investigations are supported by the project № DTK 02/50/17.12.2009.

References

- [1] I. Mozetic, C. Holzbaur, F. Novak and M. Santo-Zarnik, "Model-based analogue circuit diagnosis with CLP(R)", Proc. 4-th Intern. GI Congress, Munich, W. Brauer (editor), Springer Verlag, pp. 343-353, 1990.
- [2] E. Dimitrova, E. Gadjeva, A. Van den Bossche and V. Valchev, "A model-based approach to automatic diagnosis using general purpose circuit simulators", IEEE International Symposium on Industrial Electronics - ISIE 2006, July 9-12, 2006, Montreal, Quebec, Canada, 4, pp. 2972-2977.

- [3] A.E. Salama, J.A. Starzyk, and J.W. Bandler, "A unified decomposition approach for fault location in large analog circuits", *IEEE Trans. on Circuits and Systems*, 31, pp. 609-622, 1984.
- [4] S. Farchy, E. Gadzheva, L. Raykovska and T. Kouyoumdjiev, "Nullator-norator approach to analogue circuit diagnosis using general-purpose analysis programmes", *International Journal of Circuit Theory and Applications*, John Wiley & Sons, Ltd., 23, Issue 6, pp. 571-585, 2006.
- [5] T. C. Lin, M.J. Kuo and Y.C. Chen, "Frequency domain analog circuit fault diagnosis based on radial basis function neural network", *VLSI Design/Cad Symposium*, 2007.
- [6] J. Rutkowski and T. Golonek, "Application of genetic algorithms to analog fault diagnosis", *European Conference on Circuit Theory and Design - ECCTD'01*, August 28-31, 2001, Espoo, Finland, v.1, pp. 253-256, 2001.
- [7] M. Slamani and B. Kaminska, "Fault observability analysis of analog integrated circuits in frequency domain", *IEEE Transactions on Circuits and Systems*, pp. 134-139, 1996.
- [8] S. Farchy, E. Gadjeva and T. Kouyoumdjiev, "Fault identification in analog-discrete circuits using general-purpose analysis programs", *IEEE International Conference on Electronics, Circuits and Systems*, Lisboa, v.1, pp. 495-498, 1998.
- [9] C.D. Chalk and M. Zwolinski, "A Design for test technique to increase the resolution of supply current monitoring in analogue circuits", *Electronics Letters*, v. 33, Issue: 21, pp. 1746-1748, 1997.
- [10] D. Papakostas and A. Hatzopoulos, "Analogue fault detectability comparison between power supply current and output voltage magnitude and phase spectrum components", *Electronics Letters*, v. 40 Issue: 8, pp. 457-458, 2004.
- [11] *PSpice Reference Guide*, Cadence PCB Systems Division, USA, 2000.
- [12] B. Straube and W. Vermeiren, "A nullator-norator-based analogue circuit DC-test generation approach", *8th Intern. Mixed-signal testing workshop*, June 18-21, 2002, Montreux, Switzerland, pp. 133-136. 2002.
- [13] L. Hernandez-Martinez and A. Sarmiento-Reyes, "Topological considerations for the diagnosability conditions of analogue circuits using a pair of conjugate trees", *Journal of Electronic Testing: Theory and Applications*, Kluwer Academic Publishers, 19, pp. 29-36, 2003.
- [14] H. Carlin, "Singular network elements", *IEEE Trans. Circuit Theory*, v. 11, no. 3, March, pp. 67-72, 1964.
- [15] B.L. Jiang, C. L. Wey and L.J. Fan, "Fault prediction for analog circuits", *Journal Circuits, Systems, and Signal Processing*, v.7, No.1, pp. 95-109, 1988.
- [16] <http://www.cadence.com/products/orcad/pages/downloads.aspx#models>
- [17] E. Gadjeva, D. Shikalanov and A. Atanasov, "Automated observability investigation of analog electronic circuits using SPICE", *Annual Journal of Electronics*, ISSN 1313-1842, 2011.
- [18] A. Raghunathan, J. Chun, J. Abraham and A. Chatterjee, "Quasi-oscillation based test for improved prediction of analog performance parameters", *Proceedings of the International Test Conference, ITC 2004*, 26-28 Oct. 2004, pp. 252 - 261.
- [19] E. Gadjeva, D. Shikalanov and A. Atanasov, "Statistical approach to fault observability investigation in analog circuits", *Advanced Aspects of Theoretical Electrical Engineering*, 20.09- 23.09 2009, Sozopol, Bulgaria.
- [20] K. Arabi and B. Kaminska, "Oscillation-test methodology for low-cost testing of active analog filters", *IEEE Transactions on Instrumentation and Measurement*, Vol. 48, No. 4, pp. 798 - 806. 1999.
- [21] E. Gadjeva, T. Kouyoumdjiev, S. Farchy, M. Hristov, A. Popov, "Computer modeling and simulation of electronic and electrical circuits using Cadence PSpice", *Meridian* 22, 2009.

IMAGE AND SIGNAL ANALYSIS FOR PERSONALIZED MODELING IN MEDICINE AND MENTAL HEALTH

Tuan D. Pham

Aizu Research Cluster for Medical Engineering and Informatics
Center for Advanced Information Science and Technology
The University of Aizu
Aizuwakamatsu, Fukushima 965-8580, Japan

Abstract. *The concept of personalized medicine and patient-specific treatment is a trendy topic in computational systems medicine and systems biology. This paper presents a specific overview how computational models have been applied to the construction of typical personalized medicine and health systems. Discussions are focused on techniques developed in electrical engineering and information science which have been utilized for addressing problems with reference to studies in computational neuroscience and cardiovascular disease.*

Keywords: *Personalized medicine; image analysis; signal processing; computational models; neuroscience; cardiovascular disease.*

1. INTRODUCTION

Personalized medicine and targeted treatment [1] have recently emerged as revolutionary breakthrough in medicine and biology going hand in hand with engineering computation, computer science, information and communication technology (<http://www.itfom.eu/>). Major diseases such as cancer and heart disease have a genetic component; therefore the elucidation of the human genetic code and ensuing understanding of cellular processes at the molecular level will enable scientists and physicians to predict the relative risk and potential therapy for such conditions on a person-to-person basis.

It is expected that soon personalized medicine provides medical doctors with more precise information not only a cancerous tumor shown on a magnetic resonance imaging scan or cells under a microscope, but the biological makeup of each patient at molecular level. Such a provision of individual profile is very useful to physicians and medical researchers to identify treatments customized at specific patients. Just like an engineer working on some mathematical functions to determine optimal materials for building an electronic device; based on the genetic mapping, medical researchers are able to design a course of optimal treatment and targeted therapy to suppress the disease the way it works in individual patients (<http://www.personalizedmedicine.com/>). In addition, tissue-derived molecular information can utilized together with the personal medical record of an individual to develop more effective treatments for a wider variety of conditions. Obviously, this ambition is hardly achieved without the power of computational methods.

2. COMPUTATIONAL MODELING IN PERSONALIZED NEUROSCIENCE

The problem is explained as follows. High blood pressure, atherosclerosis, inflammation and other basic disease processes may travel the brain by means of the white matter (WM), causing some of the most mysterious and troubling disorders of neurology. If the nervous system were a computer network, gray matter would be the computers and white matter the cables. The white matter (WM) of the brain contains myelinated nerve fibers. WM transmits signals between areas of the brain that process information, known as the gray matter (GM), which contains nerve cell bodies. WM and GM, the two distinct parts of the brain, work simultaneously to perform basic brain functions [2]. When WM is damaged, vital communication between the two collaborating areas becomes slow or blocked, and as a consequence, causes brain dysfunctions. Multiple scattered damages of the white matter appear as 'bright signals' typically on T2-weighted FLAIR magnetic resonance imaging (MRI) scans. These areas are referred to as white matter hyperintensities (WMH).

It is still unclear what causes WMH, which are consistently associated with aging and cerebral hypertension. Moreover, several chronic disorders such as Alzheimer's disease and depression have been found to be associated with WMH. Therefore, understanding complex patterns of white matter changes may contribute to answering questions on the etiology and consequences of WMH. However, the rating of white matter hyperintensities, which are defined as areas of high signal intensities on MRI, requires skill and knowledge of experts, who read the MRI scans independently, discuss any differences and agree a final standard rating for each case.

At present neither human-based nor computer-based rating scheme can provide rigorous outcomes for the analysis of white matter hyperintensities. On the other side, the WMH rating scheme either established by human experts or computer models can provide different useful sources of information. This suggests possible improvements by 1) taking both sources of information into account for every new rating of WMH, or 2) keeping established consensus knowledge of WMH patterns based on which new patterns can be inferred to reduce variability among various rating methods. The latter view is our pursuit of technical innovation towards the reliability of WMH quantification.

We have proposed is to build a hidden Markov model (HMM) for constructing the pattern of WMH on the MRI of each participant [3]. This model can be studied using the notion of phylogeny, which is used to discover the pattern of relationships of organisms. By defining a relationship, we can then identify groups that have different scales of similarity. This information of grouping will have potential usage in several aspects: 1) inference of the rating of the WMH of the new data can be made as being the best current approximation to its grouping, 2) reducing uncertainty when there are different expert opinions about the new rating of WMH, 3) being capable of processing different aspects of image information where these are very difficult for human intervention, 4) reproducibility of the result can be ensured with the same inference model, and 5) the knowledge of the relationships of WMH. For this work, we

improve the model by incorporating the vectors of fractal dimensions [59] in the vector quantization (VQ) process, where each region of interest on the MRI is subdivided to extract the fractal dimension. By doing so, we can better capture the detailed information of the morphology and intensity of the brain. The sequential steps of the computational procedure for constructing the proposed phylogenetic tree of hidden-Markov brain models for WMH pattern/rating inference is summarized as follows.

We used the MRI data of individuals, who took part in an interdisciplinary population-based cohort study of healthy ageing described in [3], to illustrate the effectiveness of the proposed procedure for automated inference of WMH patterns.

We performed the similarity comparisons of WMH on MRI of the five participants. The results of the inference of the similarity/dissimilarity among various patterns of WMH of the participants can be illustrated using the phylogenetic trees based on the HMMs of the MRI scans. Figure 1 shows a typical MRI scan showing WMH of the brain.

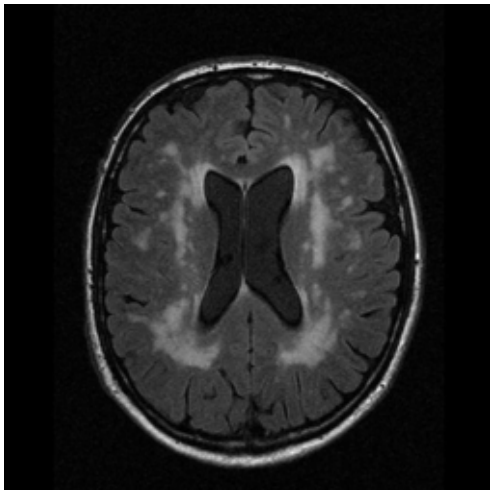


Fig. 1

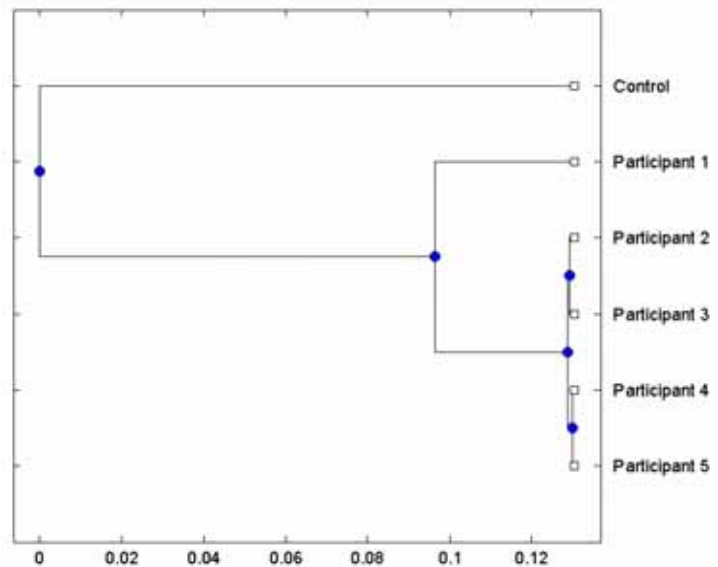


Fig. 2

All MRI scans of the five participants which contain information about WMH were used to extract the fractal dimensions and build the HMMs for constructing the phylogeny-based tree of the brains. To ensure the correction of the phylogenetic tree construction, we built HMMs for control subjects by modifying the HMMs of the participants. The HMMs of the control were imposed a virtual reality of WMH in order to allow the similarity comparison of the HMMs using the KLD. The virtual WMH was modeled by replacing the values of the transition and observation matrices of the WMH with appropriate values that simulate the existence of a very tiny fraction of WMH. Figure 2 shows a phylogenetic tree of WMH patterns of 5 participants and a control subject. The phylogenetic trees of the brain models can give us many insights; however, to ensure they are properly constructed, we need a collection of patterns of all the population in the tree. For each of these patterns, we can determine the characters as we are able to recognize the same characters in different subjects.

This is not a problem in this study which only consists of a so-called homogeneous population of participants; whereas it can be a problem if we are working with a collection of broad species as being encountered in biology. We used the similarity matrix of the HMM-based brain models to construct the tree using the following three distance methods: nearest distance (single linkage method), furthest distance (complete linkage method), and unweighted average distance (UPGMA). The experimental results interestingly show the agreement of the three methods, which imply the validity of the proposed phylogenetic tree.

3. COMPUTATIONAL MODELING IN PERSONALIZED CARDIOLOGY

The Human Genome Project has provided a significant landmark in mapping the human genome and identifying key genes that regulate cell and tissue function. More recently, however, the research focus has shifted to the study of proteomics to gain insight into cell function through determining how proteins are expressed, processed, recycled, and localization in cells. Proteomics opens new doors in the search for clinically useful biomarkers of disease, treatment response and aging. In particular, mass-spectrometry (MS) based proteomics is a rapidly emerging approach to the identification of biomarkers of specific human disorders.

The motivation for this research stemmed from the work by Brennan et al [4] on the identification of a new cardiac biomarker using mass spectral data, and the application of molecular imaging in the development of personalized medicine. Given the advanced development in proteomic technology and molecular imaging, it has become apparent that the potential success of each of these two new paradigms and their combination for enhanced outcomes rely heavily on advanced computational techniques for information processing. However, image and pattern recognition methods have not been well-explored in the field of proteomics-based biomarker discovery, especially when compared with other fields of computational life sciences.

Recent methods developed for cancer classification using MS data include the work by Petricoin et al [5] who applied cluster analysis and genetic algorithms to detect early stage ovarian cancer, Lilien et al [6] applying principal component analysis and a linear discriminant function to classify ovarian and prostate cancers, Sorace and Zhan [7] detecting early ovarian cancer, and Tibshirani et al [8] proposing a probabilistic approach for sample classification. Despite these examples, research into proteomics-based biomarker discovery is still in its infancy and offers several challenges in order to become a mature platform for clinical diagnostics and biomarker discovery. Because of the complexity of such data, some of major challenges in the analysis of mass spectrometry data for biomarker discovery include data preprocessing, feature extraction and reduction, and effective computational models for robust classification and validation.

Our proposed approach is to utilize the data already generated by a clinical proteomic approach to identify biomarkers or biomarker patterns that can be used to predict the risk of major adverse cardiac events (MACE) with greater accuracy than us-

ing MPO testing alone. We have used high throughput, low-resolution SELDI MS (see more information about SELDI technique at www.ciphergen.com) to acquire the protein profiles from patients and controls. More details about the mass spectrometry data are described as follows.

Control group: This group includes 60 patients who presented in emergency with chest pain but where a subsequent troponin T (biomarker for heart attack) test was negative. In addition, for these patients there was no subsequent heart attack or need for intervention within 6 months of this presentation date, and patients were still surviving 5 years later.

MACE group: This group includes 60 patients who presented in emergency with chest pain but again with a troponin T test. However, the patients in this group had either a heart attack, died or needed revascularization in the subsequent 6 months. The serum samples used in this study were the same as those used in the study reported in the paper of Hazen's group (Brennan et al [4]). MPO data measured with FDA approved CardioMPO kit for these two groups are available: for 56 (out of 60) patients in control group and 55 (out of 60) patients in the MACE group. Statistical analysis showed that MPO alone could distinguish MACE from control with accuracy of greater than 60%.

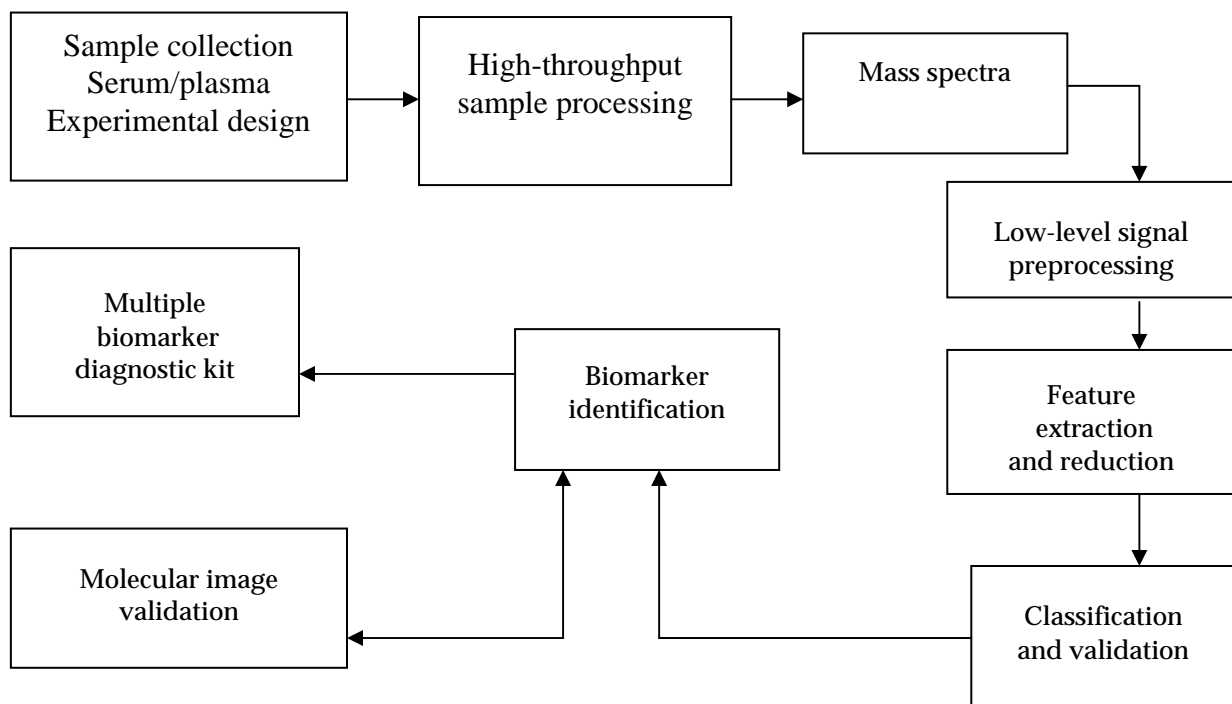


Fig. 3. Computational framework of proteomics-based biomarker discovery

The general computational framework for the biomarker discovery is shown in Figure 3. We applied the theory of linear predictive coding (LPC) and geostatistics for extracting the effective features of mass spectrometry data that could be useful for the classification of MS spectra [9]. The results in comparing with other methods are

shown in Table 1. The distortion measure derived from geostatistics gave the best prediction rate (97.10%), which is significantly higher than the MPO value. These experimental results using the cardiovascular SELDI-MS datasets showed the potential application of the proposed techniques for predicting patient's major adverse cardiac risk.

Table 1. Average MACE prediction rates (%) provided by different methods

MPO value	T-test	Genetic Algorithms	Statistical Distortion	Geostatistical Distortion
55.25	62.23	69.05	83.34	97.10

4. CONCLUSION

Review on typical computational models developed in electrical engineering and geostatistics have been presented in the foregoing sections. Technical extensions on the presented models for improvement of results and applying to similar challenging problems in medicine and biology are possible as the MRI-based age prediction has been studied [10] based on other signal processing methods and models applied in [3].

References

- [1] G. S. Ginsburg and J. J. McCarthy, Personalized medicine: revolutionizing drug discovery and patient care, *Trends Biotechnol.*, vol. 19, pp. 491-496, 2001.
- [2] A. J. Thomas et al, Pathologies and pathological mechanisms for white matter hyperintensities in depression, *Ann. N.Y. Acad. Sci.*, vol. 977, pp. 333-339, 2002.
- [3] T. D. Pham et al, The hidden-Markov brain: comparison and inference of white matter hyperintensities on magnetic resonance imaging (MRI), *J Neural Eng.*, vol. 8, 016004, 2011.
- [4] M.-L. Brennan et al, Prognostic value of myeloperoxidase in patients with chest pain, *The New England J Medicine*, vol. 13, pp. 1595-1604, 2003.
- [5] E. F. Petricoin et al., Use of proteomic patterns in serum to identify ovarian cancer, *Lancet*, vol. 359, pp. 572-577, 2002.
- [6] R. H. Lilien, H. Farid, B.R. Donald, Probabilistic disease classification of expression-dependent proteomic data from mass spectrometry of human serum, *J. Computational Biology*, vol. 10, pp. 925-946, 2003.
- [7] J. M. Sorace, M. Zhan M, A data review and re-assessment of ovarian cancer serum proteomic profiling, *BMC Bioinformatics*, vol. 4: 24, 2003.
- [8] R. Tibshirani et al, Sample classification from protein mass spectrometry, by `peak probability contrasts, *Bioinformatics*, vol. 20, pp. 3034-3044, 2004.
- [9] T. D. Pham et al, Computational prediction models for early detection of risk of cardiovascular events using mass spectrometry data, *IEEE Trans Information Technology in Biomedicine*, 12 (2008) 636-643.
- [10] B. Wang, T. D. Pham, MRI-based age prediction using hidden Markov models, *J. Neuroscience Methods*, vol. 199, pp. 140– 145, 2011.

STATIONARY STATES ANALYSIS IN LINEAR ELECTRIC CIRCUITS BY GRAPHS THEORY

Simona Kirilova Filipova-Petrakieva

Theory of Electrical Engineering, Technical University of Sofia,
8, Kl. Ohridsku, blvd., 1000 Sofia, Bulgaria,
Country, phone: +359 895 590 433, e-mail: petrakievas-te@tu-sofia.bg

Abstract: *Stationary states analysis in direct current (DC) or alternating current (AC) linear electric circuits brings to solving linear equations system with constant coefficients, got by either Kirchoffs' laws either mesh or nodal analysis. With regard to this a method for DC or AC circuit's analysis, based on graphs theory is suggested. It consists of the following steps. Firstly, the linear equations system considered presents as a directed graph's model with initial vertexes, respecting to the energy sources (voltages and currents) and immediate vertexes, associated to the unknown variables (currents, voltages and etc.). Second, it determines all possible paths reached to the unknown variables from the initial vertexes of the graph studied. Third, these paths aggregates, taking in mind the respective coefficient of the graph arcs and it gets the expressions about the studied currents and voltages with respect to the power sources in the circuit considered. The method proposed is simpler than traditional methods solving the linear equation systems and it requires smaller number of calculations than using the Mason's gain formula. The applicability of the method proposed is illustrated to AC analysis of the stationary states in real electric circuit which behavior explains with 3-rd order the linear equations system got by mesh analysis.*

Keywords: *stationary states in linear DC and AC electric circuits, Kirchoff's laws, mesh analysis, nodal analysis, graphs theory, Mason's gain formula*

1. INTRODUCTION

It is well known that the behavior of arbitrary linear electric circuit can be obtained by the following linear system:

$$\left\{ \begin{array}{l} a_{11}x_1 + a_{12}x_2 + \dots + a_{1n}x_n = f_1 \\ a_{21}x_1 + a_{22}x_2 + \dots + a_{2n}x_n = f_2 \\ \dots\dots\dots \\ a_{n1}x_1 + a_{n2}x_2 + \dots + a_{nn}x_n = f_n \end{array} \right. , \quad (1)$$

where:

$x = [x_1, x_2, \dots, x_n]^T$ – vector of unknown variables (currents, voltages, potentials) which can include either instantaneous values or complexes;

$f = [f_1, f_2, \dots, f_n]^T$ – vector consists of input power sources (voltage and current sources) which can include either instantaneous values or complexes and electric circuit's parameters (resistors R , coils L , capacitors C and mutual inductances M);

a_{ij} , $i, j = \overline{1, n}$ – coefficients, taking in mind the electric circuit parameters (resistors R , coils L capacitors C and mutual inductance M) variation over its behavior.

The standard linear system (1) has constant coefficients and it can be solved using the some traditional numerical methods, based on Gause’s method, Gause-Jordan’s method, Kramer’s formulas [1, 2] which are built in software products as MathLab, Matematica and etc.

To simplify the graph presentation of linear system (1) it can be rewritten as follows:

$$\begin{aligned} x_1 &= && + b_{12}x_2 + \dots + b_{1(n-1)}x_{(n-1)} + b_{1n}x_n + b_1f_1 \\ x_2 &= b_{21}x_1 + && + \dots + b_{2(n-1)}x_{(n-1)} + b_{2n}x_n + b_2f_2 \\ &..... \\ x_n &= b_{n1}x_1 + b_{n2}x_2 + \dots + b_{n(n-1)}x_{(n-1)} && + b_nf_n \end{aligned} \tag{2}$$

where:

$$\left. \begin{aligned} b_{ss} &= 0, b_s = \frac{1}{a_{ss}} \\ b_{ks} &= -\frac{a_{ks}}{a_{kk}}, k = \overline{1, n} \end{aligned} \right\} s = \overline{1, n}.$$

Then the system (2) can be modeled by the following directed graph $G = \langle V, L \rangle$:

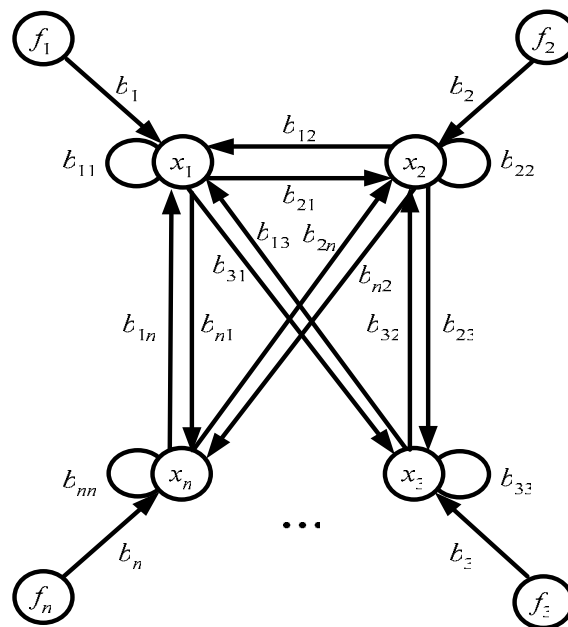


Fig. 1. Directed graph model associated to the linear equation system

where:

$V = \{x_1, x_2, \dots, x_n\}$ – set of vertexes, associated to the unknown variables in the linear electric circuit studied;

$L = \{L_{ij}, L_i\}$ – set of arcs, taking in mind the direction of the interaction between the elements x_i and x_j of the set V , i.e. $L_{ij} = (x_i \rightarrow x_j)$.

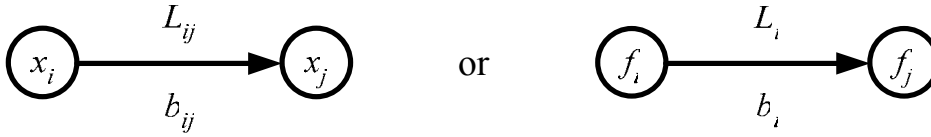


Fig. 1a. Directed graph presentation of the multiplications in linear equations

2. PROBLEM STATEMENT

The main aim of the linear electric circuit analysis problem is obtaining the analytical expressions of the unknown variables x_i , $i = \overline{1, n}$ as functions of the input power sources f_i , $i = \overline{1, n}$ using the parameters of the electric circuit studied.

The basic linear equation system can be written in form (1) as a result of applying the basic methods for circuit analysis – Kirchhoff's laws, mesh or nodal analysis ((4a) and (5a), respectively). We get the transformed system (2) using the same above methods, in forms ((4b) and (5b), respectively).

2.1. Stationary states analysis based on Kirchhoff's laws

If the electric circuit considered has n nodes, m branches, N_e independent voltage sources, N_{je} independent current sources and $k = m - (n - 1) - N_{je}$ independent closes loops, then it composes $(n - 1) - N_e$ and k equations by Kirchhoff's current law (KCL) and Kirchhoff's voltage law (KVL), respectively (see (3a and 3b)).

$$\left\{ \begin{array}{l} \pm \sum_{s_1 \in a} i_{s_1}(t) \pm \sum_{r_1 \in a} j e_{r_1}(t) = 0 \\ \pm \sum_{s_2 \in a} i_{s_2}(t) \pm \sum_{r_2 \in a} j e_{r_2}(t) = 0 \\ \dots \\ \pm \sum_{s_{n-1} \in a} i_{s_{n-1}}(t) \pm \sum_{r_{n-1} \in a} j e_{r_{n-1}}(t) = 0 \end{array} \right. , \quad (3a)$$

where: + – when the branch current (resp. current source) point to the node;
- otherwise.

$$\left\{ \begin{array}{l} \pm \sum_{h_1 \in k_1} u_{h_1}(t) = \pm \sum_{h_1 \in k_1} e_{h_1}(t) \\ \pm \sum_{h_2 \in k_2} u_{h_2}(t) = \pm \sum_{h_2 \in k_2} e_{h_2}(t) \\ \dots \\ \pm \sum_{h_k \in k_k} u_{h_k}(t) = \pm \sum_{h_k \in k_k} e_{h_k}(t) \end{array} \right. , \quad (3b)$$

where: + – when the directions of the voltage (resp. voltage source) and the closed loop are the same;
- otherwise.

Note: Without lost of the generality of the analysis only mesh and nodal analysis will be presented, because of the fact that these analyses are corollaries of the base linear system for electric circuit analysis, composed by Kirchhoff's laws.

2.2. Stationary states analysis based on mesh analysis

The final linear equations system describing mesh analysis approach is following:

$$\begin{cases} Z_{11}\dot{I}'_1 + Z_{12}\dot{I}'_2 + \dots + Z_{1k}\dot{I}'_k = \pm \dot{E}'_1 \\ Z_{21}\dot{I}'_1 + Z_{22}\dot{I}'_2 + \dots + Z_{2k}\dot{I}'_k = \pm \dot{E}'_2 \\ \dots \\ Z_{k1}\dot{I}'_1 + Z_{k2}\dot{I}'_2 + \dots + Z_{kk}\dot{I}'_k = \pm \dot{E}'_k \end{cases}, \quad (4a)$$

where:

$\dot{I}' = [\dot{I}'_1, \dot{I}'_2, \dots, \dot{I}'_k]^T$ – vector of loop's currents;

$Z_{ss}, s = \overline{1, k}$ – own's impedances in loop s , i.e. the sum of impedances in loop s ;

Z_{ps} – joint's impedances between the loops p and s , i.e. the sum of the impedances, both included in p and s loops;

$\dot{E}'_s, s = \overline{1, k}$ – an algebraic sum of voltage sources, included in loop s .

This system is a result from equations composed on KVL (formulae 3b) after introducing the fictive currents, passed through each independent closed loop $p = \overline{1, k} = m - (n - 1) - N_{je}$ in the linear electric circuit considered.

After writing (4a) in form (2) the final linear system for mesh analysis is:

$$\begin{cases} \dot{I}'_1 = -\frac{Z_{12}}{Z_{11}}\dot{I}'_2 - \dots - \frac{Z_{1k}}{Z_{11}}\dot{I}'_k \pm \frac{1}{Z_{11}}\dot{E}'_1 \\ \dot{I}'_2 = -\frac{Z_{21}}{Z_{22}}\dot{I}'_1 - \dots - \frac{Z_{2k}}{Z_{22}}\dot{I}'_k \pm \frac{1}{Z_{22}}\dot{E}'_2 \\ \dots \\ \dot{I}'_k = -\frac{Z_{k1}}{Z_{kk}}\dot{I}'_1 - \frac{Z_{k2}}{Z_{kk}}\dot{I}'_2 - \dots - \frac{Z_{k(k-1)}}{Z_{kk}}\dot{I}'_{(k-1)} \pm \frac{1}{Z_{kk}}\dot{E}'_k \end{cases}. \quad (4b)$$

The respective directed graph model associated to (4b) is following:

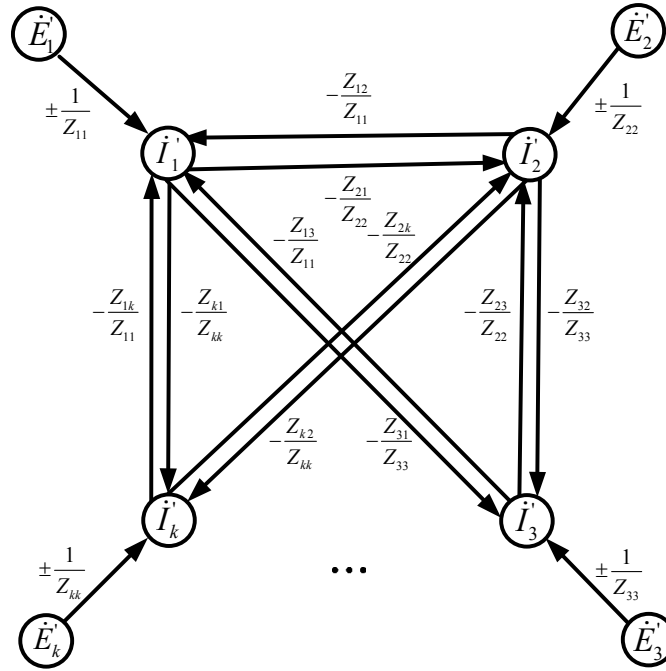


Fig. 2. Directed graph model associated to the linear equation system based on mesh analysis

2.3. Stationary states analysis based on nodal analysis

The final linear equations system describing nodal analysis approach is following:

$$\begin{cases}
 Y_{11}\dot{V}_1 - Y_{12}\dot{V}_2 - \dots - Y_{1n}\dot{V}_n = \pm \sum_{j=1, j \neq 1}^n Y_{1j} \cdot \dot{E}_1 \pm \sum_{j=1, j \neq 1}^n \dot{J}e'_j = \pm \dot{J}e''_1 \\
 -Y_{21}\dot{V}_1 + Y_{22}\dot{V}_2 - \dots - Y_{2n}\dot{V}_n = \pm \sum_{j=1, j \neq 2}^n Y_{2j} \cdot \dot{E}_2 \pm \sum_{j=1, j \neq 2}^n \dot{J}e'_j = \pm \dot{J}e''_2 \\
 \dots \\
 -Y_{(n-1)1}\dot{V}_1 - Y_{(n-1)2}\dot{V}_2 - \dots - Y_{(n-2)(n-1)}\dot{V}_{(n-2)} + Y_{(n-1)n}\dot{V}_{(n-1)} = \pm \sum_{j=1, j \neq (n-1)}^n Y_{(n-1)j} \cdot \dot{E}_{(n-1)} \pm \sum_{j=1, j \neq (n-1)}^n \dot{J}e'_j = \pm \dot{J}e''_{n-1}
 \end{cases} \tag{5a}$$

where:

$\dot{V} = [\dot{V}_1, \dot{V}_2, \dots, \dot{V}_{n-1}, \dot{V}_n = 0]^T$ – vector of potentials in the circuit's nodes;

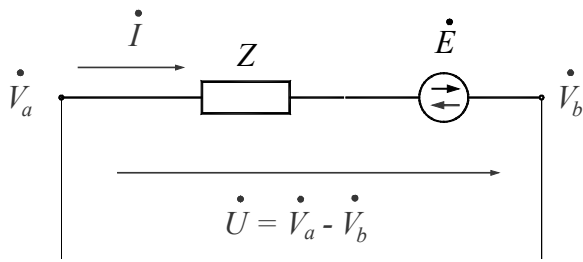
$Y_{ss}, s = \overline{1, (n-1)}$ – owns admittances of the node s -th, i.e. the sum of admittances of the branches, connected to the node s ;

Y_{ps} – an admittance of the branches lied between the nodes p and s ;

$\dot{J}e'_s, s = \overline{1, (n-1)}$ – an algebraic sum of current sources in the branches, connected to node s ;

\dot{E}'_j – an algebraic sum of voltage sources, lied between the nodes j and s .

This system is a result from equations composed on KCL (formulae 3a) after substituting in (5a) each branch current with its equivalent by Ohm's law:



$$i = \frac{\dot{U} \pm \dot{E}}{Z} = \frac{\dot{V}_a - \dot{V}_b \pm \dot{E}}{Z}$$

where: (+) – current \dot{I} and voltage source \dot{E} has the same direction;
 (-) – otherwise.

Fig. 3. Ohm's law for active branch

She is written for $(n - 1) - N_e$ nodes of the linear electric circuit considered. After notation system (5a) in form (2) the final linear system for nodal analysis is:

$$\begin{cases} \dot{V}_1 = +\frac{Y_{12}}{Y_{11}} \dot{V}_2 + \dots + \frac{Y_{1(n-1)}}{Y_{11}} \dot{V}_{n-1} \pm \frac{1}{Y_{11}} \dot{J}e_1'' \\ \dot{V}_2 = +\frac{Y_{21}}{Y_{22}} \dot{V}_1 + \dots + \frac{Y_{2(n-1)}}{Y_{22}} \dot{V}_{n-1} \pm \frac{1}{Y_{22}} \dot{J}e_2'' \\ \dots \\ \dot{V}_{n-1} = +\frac{Y_{(n-1)1}}{Y_{(n-1)(n-1)}} \dot{V}_1 + \frac{Y_{(n-1)2}}{Y_{(n-1)(n-1)}} \dot{V}_2 + \dots + \frac{Y_{(n-1)(n-2)}}{Y_{(n-1)(n-1)}} \dot{V}_{n-2} \pm \frac{1}{Y_{(n-1)(n-1)}} \dot{J}e_{n-1}'' \\ \dot{V}_n = 0 \end{cases} \quad (5b)$$

The respective directed graph model associated to (5b) is following:

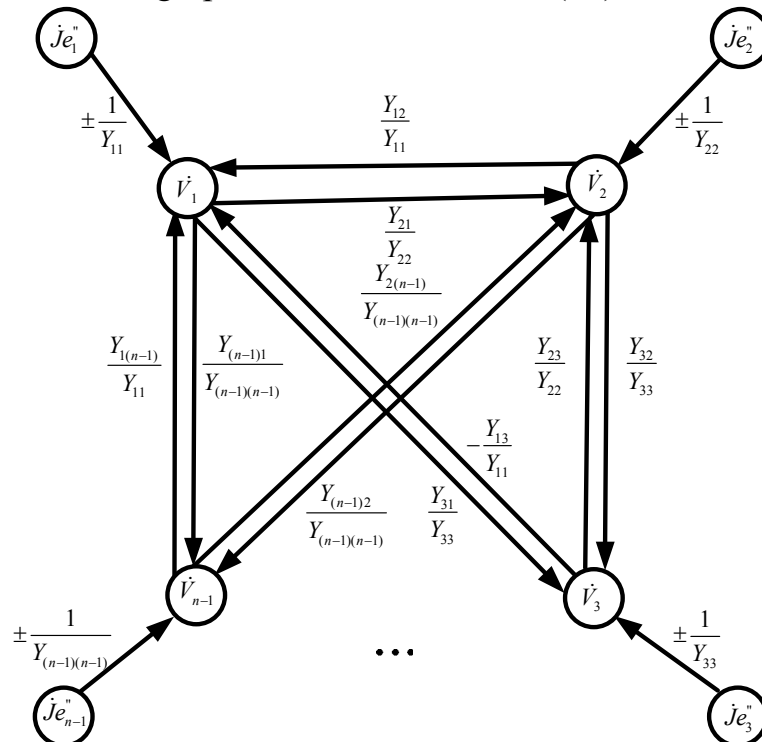


Fig. 4. Directed graph model associated to the linear equation system based on nodal analysis

3. ALGORITHM FOR SOLVING LINEAR EQUATION SYSTEM WITH CONSTANT COEFFICIENTS BASED ON GRAPHS THEORY

The present algorithm, solving the system (2), requires the following input data:

n – the numbers of graph vertexes, where n' - the number of initial graph vertexes, n'' – the number of intermediate graph vertexes and $n = n' + n''$;

Note: In particular (Fig. 2 and 3), n' and n'' are the numbers of the power voltages' and loop's currents' and current's sources and node's potentials in the linear electric circuit considered, respectively.

$V^{start} = \{V_i, i = \overline{1, r_{start}}, r_{start} < n\}$ – set of all initial graph vertexes;

$V^{end} = \{V_i, i = \overline{1, r_{end}}, r_{end} < n\}$ – set of all end graph vertexes.

It can be described with the following procedure.

Step 1

It determines two squared ($n \times n$) matrices associated to each vertex $V_k, k = \overline{1, n}$

$$H_{in}(k) = \left[h_{ij}^{in} \right]_{i,j=\overline{1,n}}$$

$$h_{ij}^{in} = \begin{cases} 1, & \exists \text{arc from } V_i \text{ to } V_j; \\ 0, & \text{otherwise.} \end{cases} \quad k = \overline{1, n} \quad (6a)$$

and

$$H_{out}(k) = \left[h_{ij}^{out} \right]_{i,j=\overline{1,n}}$$

$$h_{ij}^{out} = \begin{cases} 1, & \exists \text{arc from } V_j \text{ to } V_i; \\ 0, & \text{otherwise.} \end{cases} \quad k = \overline{1, n}. \quad (6b)$$

The matrices $H_{in}(k)$ and $H_{out}(k)$ take in mind the arcs inputting in and outputting from the vertex considered V_k , respectively.

Step 2

For each intermediate graph's vertex $V_k, k = \overline{1, n''}$ it determines:

2.1. 1-st iteration – 1-step reachability

2.1.1. The reachability matrix:

$$H_{in}^{k(1)} = H_{in}(k), \quad k = \overline{1, n''}. \quad (7)$$

2.1.2. All possible paths from the initial graph vertexes $V_k, k = \overline{1, n'}$ to each intermediate graph vertex $V_k, k = \overline{1, n''}$ obtain taking in mind the 1-elements in matrix $H_{in}(k)$.

2.1.3. The expressions about the considered variables $x_k, k = \overline{1, n''}$ as functions of the input power sources $f_k, k = \overline{1, n'}$ determine using the information from 2.1.2.

2.2. 2-nd iteration – 2-step reachability

2.2.1. The reachability matrix:

$$H_{in}^{k(2)} = H_{out}(1).H_{in}^{k(1)} + H_{out}(2).H_{in}^{k(1)} + \dots + H_{out}(n).H_{in}^{k(1)}. \quad (8)$$

2.2.2. All possible paths from the initial graph vertexes $V_k, k = \overline{1, n'}$ to each intermediate graph vertex $V_k, k = \overline{1, n''}$ obtain taking in mind the 1-elements from the multiplications in resulting matrix, calculating by (8).

2.2.3. The expressions about the considered variables $x_k, k = \overline{1, n''}$ as functions of the input power sources $f_k, k = \overline{1, n'}$ determine using the information from 2.2.2.

2.s. s-th iteration – s-step reachability

2.s.1. The reachability matrix:

$$H_{in}^{k(s)} = H_{out}(1).H_{in}^{k(s-1)} + H_{out}(2).H_{in}^{k(s-1)} + \dots + H_{out}(s).H_{in}^{k(s-1)}. \quad (9)$$

2.s.2. All possible paths from the initial graph vertexes $V_k, k = \overline{1, n'}$ to each intermediate graph vertex $V_k, k = \overline{1, n''}$ obtain taking in mind the 1-elements from the multiplications in resulting matrix, calculating by (9).

2.s.3. The expressions about the considered variables $x_k, k = \overline{1, n''}$ as functions of the input power sources $f_k, k = \overline{1, n'}$ determine using the information from 2.s.2.

The stop criteria for calculating process on step s is arising the multiplications $b_{ij}.b_{ji}$ above the line of some of the fractions of the resulting expressions from 2.s.3.

The final expressions obtain after dividing the expressions from 2.s.3 to the determinate of the matrix of coefficients from the right side of the system (2).

4. ILLUSTRATIVE EXAMPLE

The applicability of the method proposed is illustrated to AC analysis of stationary states in the following linear electric circuit (in complex form) – see Fig. 5:

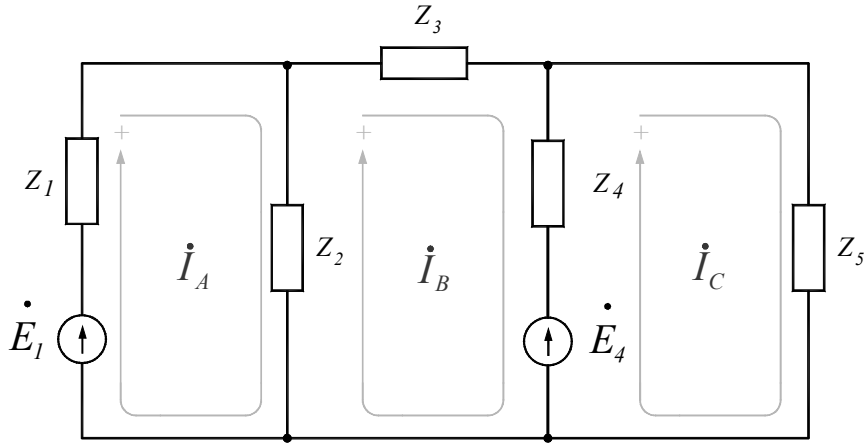


Fig. 5. Complex equivalent of the real linear electric circuit

The circuit behavior can be described by mesh analysis. The respective linear equation system is on 3-rd order:

$$\begin{cases} (Z_1 + Z_2)\dot{I}_A - Z_2\dot{I}_B + 0\dot{I}_C = \dot{E}_1 \\ -Z_2\dot{I}_A + (Z_2 + Z_3 + Z_4)\dot{I}_B - Z_4\dot{I}_C = -\dot{E}_4 \\ 0\dot{I}_A - Z_4\dot{I}_B + (Z_4 + Z_5)\dot{I}_C = \dot{E}_4 \end{cases} \begin{array}{l} | : (Z_1 + Z_2) \\ | : (Z_2 + Z_3 + Z_4) \\ | : (Z_4 + Z_5) \end{array} \quad (10)$$

After transformation and introducing some notation system (10) can be written as follows:

$$\begin{cases} x_1 - b_{12} \cdot x_2 - b_{13} \cdot x_3 = b_1 \cdot f_1 \\ -b_{21} \cdot x_1 + x_2 - b_{23} x_3 = b_2 \cdot f_2 \\ -b_{31} \cdot x_1 - b_{32} \cdot x_2 + x_3 = b_3 \cdot f_3 \end{cases} \quad (11)$$

$$\Downarrow$$

$$A \cdot x = b \cdot f$$

$$\text{where: } A = \begin{bmatrix} 1 & -b_{12} & -b_{13} \\ -b_{21} & 1 & -b_{23} \\ -b_{31} & -b_{32} & 1 \end{bmatrix}, \quad x = \begin{bmatrix} \dot{I}_A \\ \dot{I}_B \\ \dot{I}_C \end{bmatrix}, \quad b = \begin{bmatrix} b_1 \\ b_2 \\ b_3 \end{bmatrix}^T, \quad f = \begin{bmatrix} f_1 \\ f_2 \\ f_3 \end{bmatrix}$$

The notation of (11) in form (2) is:

$$\begin{cases} x_1 = & + b_{12}x_2 + b_{13}x_3 + b_1f_1 \\ x_2 = b_{21}x_1 + & + b_{23}x_3 + b_2f_2 \\ x_3 = b_{31}x_1 + b_{32}x_2 + & + b_3f_3 \end{cases} \quad (11a)$$

The equivalent directed graph model associated to the linear system (11a) is:

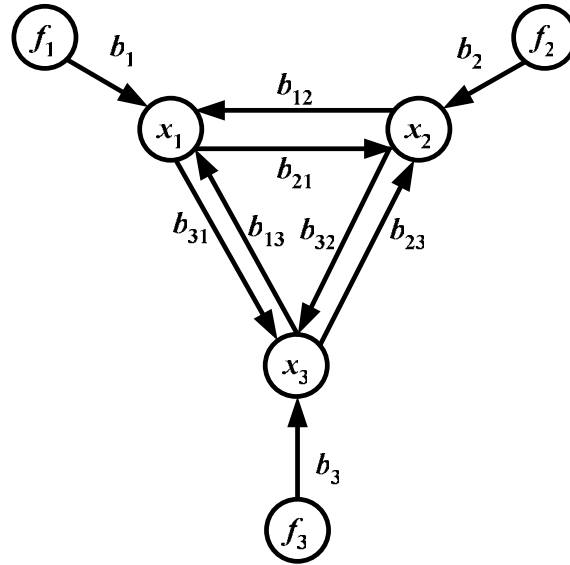


Fig. 6. Directed graph model associated to the linear electric circuit studied

Using traditional methods, the solution of linear equation system (11) (resp. (11a)) is following:

$$x = \begin{bmatrix} x_1 \\ x_2 \\ x_3 \end{bmatrix} = \begin{bmatrix} \frac{(-1+b_{23}*b_{32})*b_1*f_1-(b_{12}+b_{13}*b_{32})*b_2*f_2-(b_{12}*b_{23}+b_{13})*b_3*f_3}{\det(A)} \\ \frac{-(b_{21}+b_{31}*b_{23})*b_1*f_1+(-1+b_{13}*b_{31})*b_2*f_2-(b_{23}+b_{13}*b_{21})*b_3*f_3}{\det(A)} \\ \frac{-(b_{21}*b_{32}+b_{31})*b_1*f_1-(b_{32}+b_{12}*b_{31})*b_2*f_2+(-1+b_{12}*b_{21})*b_3*f_3}{\det(A)} \end{bmatrix} \quad (12)$$

$$\det(A) = -1+b_{23}*b_{32}+b_{12}*b_{21}+b_{13}*b_{31}+b_{21}*b_{13}*b_{32}+b_{31}*b_{12}*b_{23}$$

Applying the new method, based on graphs' theory, the final solution gets as follows:

1-st iteration

$$x^{(1)} = \begin{bmatrix} x_1^{(1)} \\ x_2^{(1)} \\ x_3^{(1)} \end{bmatrix} = \begin{bmatrix} \frac{-b_1*f_1}{\det(A)} \\ \frac{-b_2*f_2}{\det(A)} \\ \frac{-b_3*f_3}{\det(A)} \end{bmatrix} \quad (13)$$

2-nd iteration

$$x^{(2)} = \begin{bmatrix} x_1^{(2)} \\ x_2^{(2)} \\ x_3^{(2)} \end{bmatrix} = \begin{bmatrix} x_1^{(1)} + \frac{b_{23} * b_{32} * b_1 * f_1 - b_{12} * b_2 * f_2 - b_{13} * b_3 * f_3}{\det(A)} \\ x_2^{(1)} + \frac{-b_{21} * b_1 * f_1 + b_{13} * b_{31} * b_2 * f_2 - b_{23} * b_3 * f_3}{\det(A)} \\ x_3^{(1)} + \frac{-b_{31} * b_1 * f_1 - b_{32} * b_2 * f_2 + b_{12} * b_{21} * b_3 * f_3}{\det(A)} \end{bmatrix} \quad (14)$$

3-rd iteration

$$x^{(3)} = \begin{bmatrix} x_1^{(3)} \\ x_2^{(3)} \\ x_3^{(3)} \end{bmatrix} = \begin{bmatrix} x_1^{(2)} + \frac{b_{23} * b_{32} * b_1 * f_1 - b_{12} * b_2 * f_2 - b_{13} * b_3 * f_3}{\det(A)} \\ x_2^{(2)} + \frac{-b_{21} * b_1 * f_1 + b_{13} * b_{31} * b_2 * f_2 - b_{23} * b_3 * f_3}{\det(A)} \\ x_3^{(2)} + \frac{-b_{31} * b_1 * f_1 - b_{32} * b_2 * f_2 + b_{12} * b_{21} * b_3 * f_3}{\det(A)} \end{bmatrix} \quad (15)$$

4-th iteration

$$x^{(4)} = \begin{bmatrix} x_1^{(4)} \\ x_2^{(4)} \\ x_3^{(4)} \end{bmatrix} = \begin{bmatrix} x_1^{(3)} + \frac{(b_{21} * b_{13} * b_{32} + b_{31} * b_{12} * b_{23}) * (b_1 * f_1 + b_2 * f_2 + b_3 * f_3)}{\det(A)} \\ x_2^{(3)} + \frac{(b_{21} * b_{13} * b_{32} + b_{31} * b_{12} * b_{23}) * (b_1 * f_1 + b_2 * f_2 + b_3 * f_3)}{\det(A)} \\ x_3^{(3)} + \frac{(b_{21} * b_{13} * b_{32} + b_{31} * b_{12} * b_{23}) * (b_1 * f_1 + b_2 * f_2 + b_3 * f_3)}{\det(A)} \end{bmatrix} \quad (16)$$

$$\det(A) = -1 + b_{23} * b_{32} + b_{12} * b_{21} + b_{21} * b_{13} * b_{32} + b_{31} * b_{12} * b_{23} + b_{13} * b_{31}$$

It is obvious, that the final solution (16) of the linear system (11) (resp. (11a)) obtains on the 3-rd iteration of the proposed procedure because of the fact that the multiplications on type $(b_{21} * b_{13} * b_{32} + b_{31} * b_{12} * b_{23})$ arise on the 4-th iteration of the algorithm proposed. It shows that we “go” between vertexes $x_1 - x_2 - x_3$, forming the closed loop in graph’s model considered (Fig. 6).

5. CONCLUSION

The graph method suggested is better than traditional math’s methods, solving the linear equations system for DC and AC circuits analysis, because it consists of n multiplications of squared ($n \times n$) matrices on the i -th iteration and the most of elements of these matrices are 0, compared with the Gauss method which has a $(i+1)$ multiplications on the i -th iteration. The number of necessary iterations in both methods is n .

The current graph method proposed is simpler than well known method based on Mason's gain formulae because of the fact that it is necessary to determine only all possible paths in graph considered from initial to intermediate graph's vertexes and to take in mind the respective weight coefficients of these arcs, while Mason's gain formula requires obtaining of all possible paths between the arbitrary graph vertexes; all pairs loops, which have no joint arcs; all three loops, which have no joint arcs; all four loops, which have no joint arcs and etc. and to take in mind the associated coefficients on these paths.

References

- [1] W. Press, B. Flannery, S. Teukolsky, W. Vetterling, Numerical Recipes, Cambridge University Press.
- [2] Дж. Форсайт, М. Малкълм, К. Мольр, "Компютърни методи за математични пресмятания", Наука и изкуство, София 1986.
- [3] В. П. Сигорский, "Матрицы и графы в электротехнике", Энергия, Москва 1968, 176 стр.
- [4] С. Фархи, С. Папазов. Теоретична электротехника, ч. I, Издателство Техника, София, 1992, 664 стр.

A WATT-LEVEL FEMTOSECOND FIBER LASER WORKING IN DISSIPATIVE SOLITON REGIME

I. G. Koprinkov

Department of Applied Physics, Technical University of Sofia, 8 Kl. Ochriski Blvd,
1000 Sofia, Bulgaria, phone: +359 2 965 3072, e-mail: igk@tu-sofia.bg

K. A. Stankov

APHALAS GmbH, Bertha-von Suttner-Str.5, D-37085 Göttingen, Germany,
phone: 0049 551 7706147, e-mail: stankov@alphalas.com

Abstract: *A reliable watt-level femtosecond fiber laser working in dissipative soliton regime is created. The laser is built on conventional double-clad ytterbium doped optical fibers and pumped by a multimode laser diode using pump-signal combiner. The mode-locking is based on the nonlinear polarization rotation mechanism. The laser typically generates around 5 ps long chirped optical pulses of average power up to 1.8 W that can be dechirped down to 150 fs in an external pulse compressor.*

Keywords: *fiber laser, mode locking, femtosecond pulses, dissipative solitons.*

1. INTRODUCTION

The introduction of high-power femtosecond lasers has opened up new prospects in the modern science and technology. In that field, titan sapphire lasers remain the main laser system as they are still unsurpassed in the generation of extremely short and high power pulses. On the other hand, the titan sapphire lasers are relatively bulky, expensive and require highly qualified maintenance, which limits the wide spreading of the ultrafast technologies. That is why, other laser systems are subject to intensive research as an alternative to the titan sapphire lasers. Among these, the fiber lasers show great potential for development. Their complex features like stable, reliable and maintenance free operation, excellent beam profile, good thermal properties and simplified cooling, compactness and low cost make them the best candidate for to bring the ultrafast technologies to a broad range of users.

One may distinguish four main pulse propagation regimes in the mode-locked fiber oscillators: soliton regime [1, 2], dispersion managed soliton regime [3], self-similar regime [4, 5], and all-normal dispersion regime [6, 7]. The basic properties of these regimes have been systematically presented in [8], see also [9]. Among these, the all-normal dispersion regime, implemented typically in ytterbium fibers lasers of around 1 μ m generation wavelength, seems to be the most perspective for scaling up the oscillator's power [10]. The all-normal dispersion lasers may support dissipative temporal solitons [11].

The recent advances in the high-power femtosecond ytterbium doped fiber lasers prove their great capabilities. A watt-level average power and sub-100 fs pulses have

been obtained using ordinary ytterbium doped double-clad fibers [10]. A dramatic increase of the output power has been achieved using large mode area single mode photonic crystal fibers [12-14]. The average power from the oscillator has been increased from slightly above 10 W [12, 13] up to 27 W [14] and megawatt peak power of the individual pulses. These results are highly impressive, but the price paid to be achieved is the strong departure of the laser design from that of the usual fiber laser concept - the only fiber element in these oscillators is the doped optical fiber. On the other hand, the ordinary fiber lasers show still unexhausted capabilities. Recently, we have generated the shortest soliton pulses (around and below 50 fs) by compression through amplification in an all-fiber erbium laser-amplifier system [15]. The aim of the present work is to create a reliable watt-level femtosecond ytterbium fiber laser working in dissipative soliton regime using conventional optical fibers only. Attention has been paid to the further optimization of the laser design. In particular, mode matching in the ytterbium doped and the passive fibers is carefully done in order to reduce the cavity losses. At the maximal pump power of 6 W, the laser generates up to 1.8 W chirped pulses of around 5 ps duration that can be dechirped to sub-150 fs pulses in an external pulse compressor.

2. EXPERIMENTAL SETUP

The entire experimental setup is shown in Fig. 1. It includes a fiber oscillator, a grating pulse compressor and associated equipment for monitoring and characterization of the laser parameters. The spectrum of the laser emission is analyzed by an optical spectrum analyzer Agilent 86140B type having a spectral sensitivity range 600-1700 nm. The temporal structure of the generation down to about 15 ps range is analyzed by a 50GHz sampling oscilloscope Tektronix 11801C, a 50 GHz (7 ps risetime) sampling head Tektronix SD-32, and a 30 GHz optical-to-electrical convertor Tektronix SD-48. The pulse duration is measured by self-made scanning autocorrelator and GRENOUILLE-FROG. The laser power is measured by a Coherent Fieldmaster GS power meter with LM10 HTD measuring head.

The fiber oscillator is shown in Fig. 2. It consists of a fiber section and a free space section. The fiber section includes a double-clad ytterbium doped fiber and two parts of passive single mode fiber. The ytterbium doped fiber is about 1.5 m long and has 10 μm core with 130 cladding. The single mode fiber is carefully selected so as to match its core diameter and numerical aperture to those of the ytterbium doped fiber. This reduces the cavity losses and improves the laser operation. The pump laser diode is coupled by means of a multimode fiber of 105/125 μm core/cladding diameter. Its emission around 976 nm is delivered into the ytterbium doped fiber by means of a pump signal combiner PSC. The free space section is formed between collimators C_1 and C_2 having 50 cm working distance, which incorporates the optical elements of the mode locking device and the band pass filter.

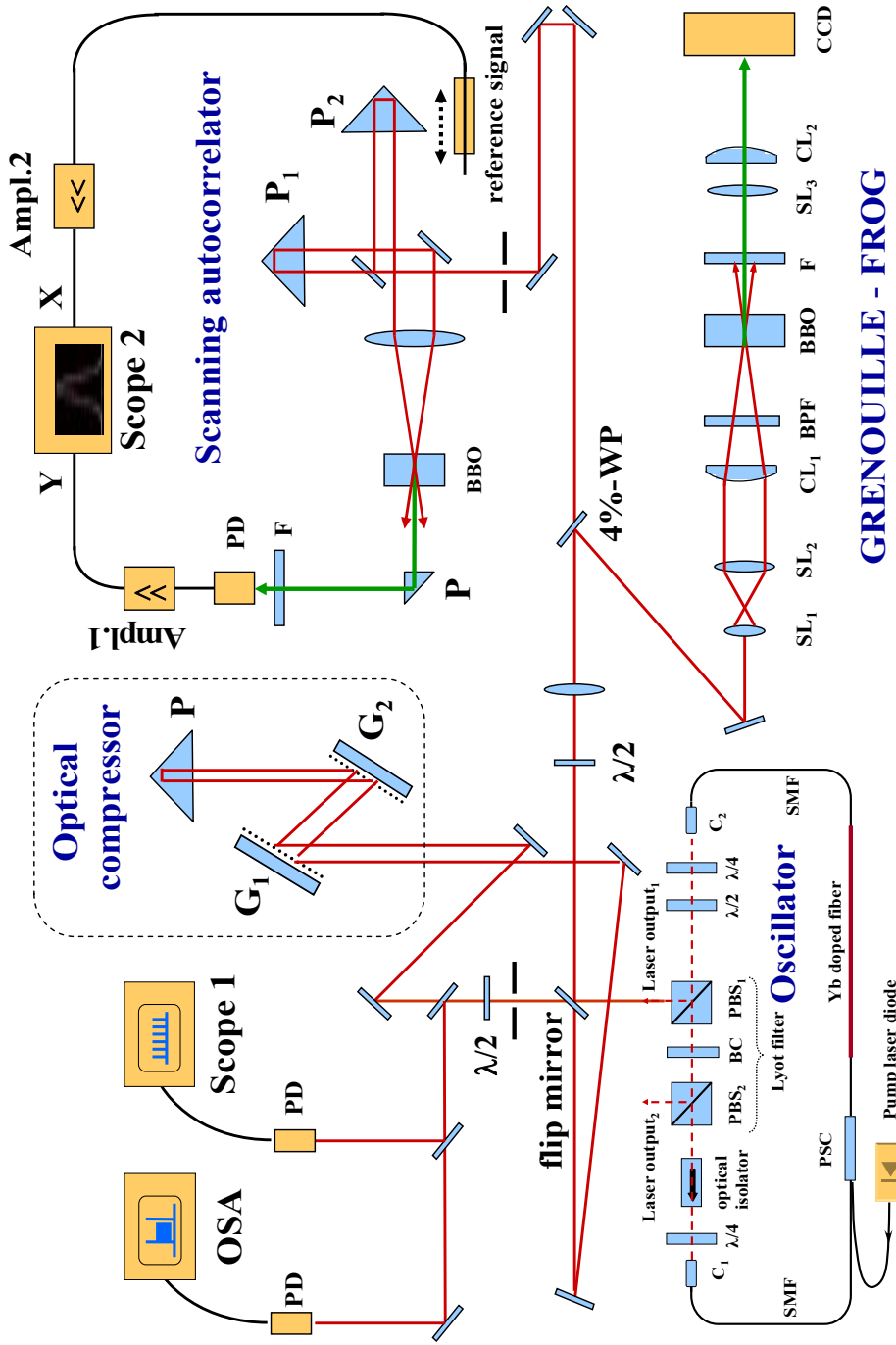


Fig.1. Experimental setup. PD-photodiode, P- prism, SL - spherical lens, CL-cylindrical lens, F- filter, BPF - band pass filter, WP – wedge plate, OSA – optical spectrum analyzer.

The mode-locking of the laser is based on the nonlinear polarization rotation mechanism whose main advantages are the instantaneous and nonabsorptive way of operation. The mode locking device of this oscillator consists of three wave plates (two quarter-wave plates $\lambda/4$ and a half-wave plate $\lambda/2$) and a polarizer, in our case, polarization beam splitter PBS_1 . The laser output is taken from the reflected part of the pulse from the PBS_1 . The PBS_1 together with a second PBS_2 and a birefringent crystal BC (a 3.2 mm thick quartz plate) placed between them form a Lyot filter. It plays role of a bandpass filter of sinusoidal transmission curve of, in our case, 20 nm bandwidth (FWHM) and variable central wavelength that can be tuned at the maximal laser power. At the emission wavelength of the ytterbium fiber laser, all optical

elements fall in the positive dispersion region and the pulse should broaden continuously in time while it propagates along the cavity. There are two non-dispersion mechanisms in the all normal dispersion oscillators that may lead to stable pulse formation: the mode locking and the bandpass filter. As it has been revealed [6-8, 10], the band pass filter plays a crucial role in the formation of the dissipative soliton in the all normal dispersion oscillators. According to the numerical simulations [10], the mode locking leads to shortening of the pulses in each cavity round trip, but it is the band pass filter that restores the initial pulse and keeps it from excessive time broadening and, eventually, splitting into a number of sub pulses. This ensures a stable mode locking operation of the laser in a continuous pulse train.

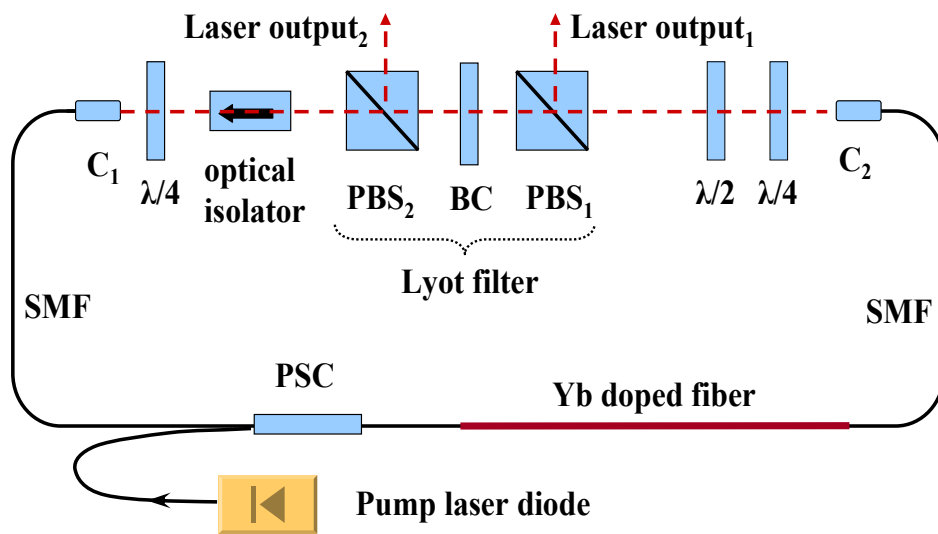


Fig. 2. Femtosecond fiber oscillator working in dissipative soliton regime: C – collimator, SMF – single mode fiber, PBS – polarization beam splitter, PSC – pump signal combiner, BC – birefringent crystal, $\lambda/2$, $\lambda/4$ – waveplates

The group delay dispersion GDD, $D_2 \equiv \partial^2 \phi / \partial \omega^2$, of the entire laser cavity is estimated to be about $D_2 = +0.05 \text{ ps}^2$. To compensate the positive chirp acquired in the oscillator and, thus, to compress the output pulse, the latter is sent through a double pass pulse compressor. The compressor consists of two gratings of 1200 l/mm placed at 45 degrees angle of incidence, Fig.1. The distance between the gratings can be varied continuously in order to achieve the best compression of the pulse.

3. RESULTS AND DISCUSSION

Mode locking operation of the laser can be achieved at different settings of the waveplates. The different mode locking regimes can be distinguished in the spectral shape, time duration of the generated pulses, average power, and the stability of the pulse train. The reduction of the overall cavity losses by proper design of the laser cavity and reduction of the splice losses between the fiber components strongly improves the operation characteristics of the laser and increases the number of the

waveplate settings at which mode locking can be obtained. The mode locking is self-starting at given pump power and suitable setting of the waveplates.

It has been confirmed experimentally in our case too that the laser operation is highly sensitive on the settings of the mode locking waveplates as well as on the tuning of the bandpass filter. The mechanism of operation of the bandpass filter in the mode locked laser at all normal dispersion regime can be explained by the following. The common action of self-phase modulation and the dispersion at positive dispersion regime results in continuous broadening of the pulse in time. In that case, the longer spectral components travel faster than the shorter spectral components. Thus, after some distance of propagation, the longest and the shortest spectral components appear at the leading and the trailing edges of the pulse, respectively. Generally speaking, the spectral components become arranged in a way that the wavelength gradually decreases along the local time of the pulse, *i.e.*, the pulse becomes chirped. The spectral filtering, *i.e.*, cutting the extreme spectral components outside the filter transmission bandwidth, leads, in fact, to cutting of the extreme time edges of the pulse. This keeps the pulse duration within certain time limits and results in generation of chirped pulses. It means that such pulses can be further shortened by means of dechirping in an external pulse compressor.

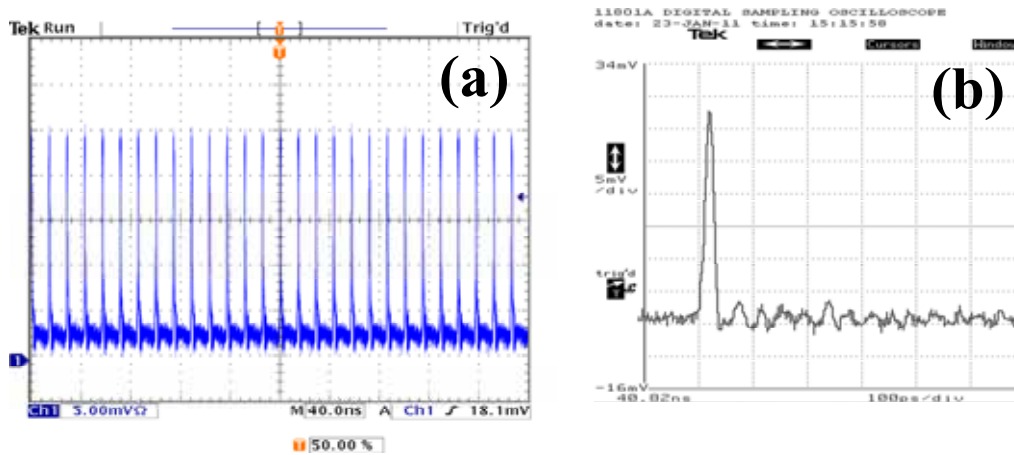


Fig. 3. The pulse train (a) and a single pulse (b) illustrate a stable mode locking operation of the laser without pulse splitting

At proper adjustment of the waveplates and the pump power, a highly stable mode locking operation can be achieved, Fig. 3(a). A flat top pulse train of identical pulses is observed at slow time sweep of the oscilloscope. The repetition rate of the pulses, depending on the actual cavity length, is 71 MHz in this particular case. Single pulse operation of the laser down to about 15 ps is monitored electronically by a fast oscilloscope and optical detectors Fig. 3(b), as specified in the preceding section, as well as by a scanning autocorrelator, in the shorter time domain. The autocorrelation trace of a single pulse measured directly after the laser output is shown in Fig. 4. The time duration of the autocorrelation function is 6.7 ps, which corresponds to about 4.7 ps pulse duration assuming Gaussian temporal shape of the pulse. The output power of

the laser at that working regime reaches 1.8W from output 1, Fig. 2, at about 6 W power of the pump laser diode. At 71 MHz repetition rate, it corresponds to about 25 nJ energy per pulse and 5.3 kW peak power. After some time of operation, the average power of the laser from output 1 drops to about 1.2 W. It is attributed to a gradual degradation of the collimator C_2 due to the lack (in the present design of the laser) of pump stripper to absorb the transmitted part of the pump radiation. In that case, the non-absorbed part of the pump power leaks from the inner cladding of the double clad ytterbium doped fiber to the cladding of the single mode fiber pigtail of the collimator. If no lasing takes place at given settings of the waveplates, the pump transition easily saturates and less absorption of the pump emission takes place. As a result, substantial part of the pump power hits the collimator, which may lead to its degradation. The power emitted from output 2, Fig. 2, is about 0.6 W.

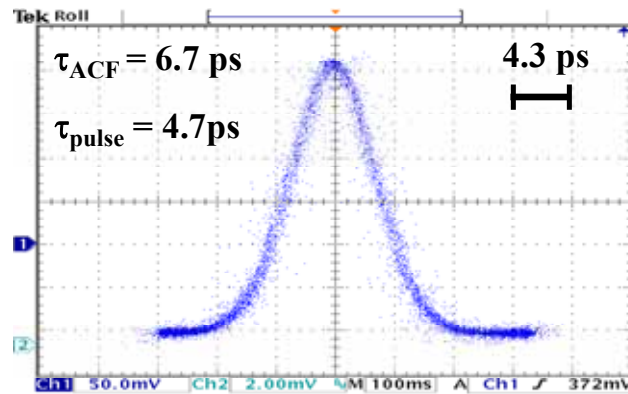


Fig. 4. Autocorrelation trace of the output pulse directly at the laser output

The chirped pulses from the oscillator have been compressed in an optical pulse compressor, Fig. 1. The group delay dispersion of the grating compressor in double pass configuration is given by the following expression

$$D_2 \equiv \frac{\partial^2 \varphi}{\partial \omega^2} = - \frac{\lambda^3 L}{\pi c^2 d^2} \left[1 - \left(\frac{\lambda}{d} - \sin \alpha \right)^2 \right]^{-3/2},$$

where L is distance between the gratings, d is grating constant, α is angle of incidence, λ is the wavelength, and c is the vacuum speed of light. The optimal group delay dispersion of the compressor has been determined experimentally by varying the distance between the gratings so as to obtain the shortest pulse duration. By this procedure we have obtained that the optimal dispersion of the compressor is about -0.1 ps^2 , *i.e.*, twice the magnitude of that of the laser cavity.

The spectrum of the compressed pulse is shown in Fig. 5(a). The laser emission is centered at about $1.045 \text{ } \mu\text{m}$ and has a 37 nm bandwidth. The shortest pulse duration, measured by the scanning autocorrelator, has been determined at 147 fs, Fig. 5(b). The average power of the compressed pulses from the laser output 1 is about 0.8 W. The energy of the compressed pulse is 14 nJ, which corresponds to 95 kW peak

power. The gratings used are not specially designed for pulse compressor, and the throughput of the entire compressor is about 65 percent. Nowadays, diffraction gratings especially designed for pulse compressor of efficiency exceeding 90 percent are available. It means that the present laser system, built on conventional optical fibers only, is capable to generate femtosecond pulse of average power well above one watt and the peak power substantially above 100 kW.

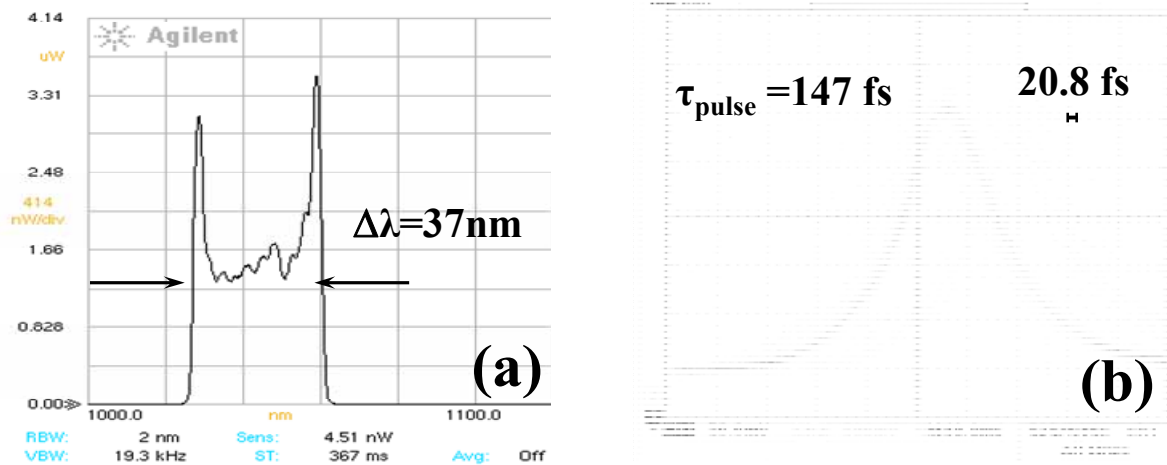


Fig. 5. Spectrum (a) and the autocorrelation trace (b) of the compressed pulse

3. CONCLUSIONS

In conclusion, a reliable high average and peak power fiber oscillator working in dissipative soliton regime is created using conventional optical fibers. The average and peak power are among the highest reported to date for that kind of femtosecond fiber oscillators working in dissipative soliton regime. The further development of the all-normal-dispersion oscillators' concept seems perspective.

4. ACKNOWLEDGEMENTS

This work was done in the frame of the Contract for joint research activities between the Department of Applied Physics, Technical University of Sofia, and ALPHALAS GmbH. I. G. Koprnikov acknowledges with thanks the hospitality and the research support from ALPHALAS GmbH, where this work has been done.

References

- [1] J. D. Kafka, T. Baer, Opt. Lett. **14**, 1269 (1989)
- [2] I. N. Duling III, Opt. Lett. **16**, 539 (1991)
- [3] K. Tamura, E. P. Ippen, H. A. Haus, L. E. Nelson, Opt. Lett. **18**, 1080 (1993)
- [4] M. E. Fermann, V. I. Kruglov, B. C. Thomsen, J. M. Dudley, J. D. Harvey, Phys. Rev. Lett., **84**, 6010 (2000)

- [5] F. Ö. Ilday, J. R. Buckley, W. G. Clark, F. W. Wise, *Phys. Rev. Lett.* **94**, 213902 (2004)
- [6] A. Chong, J. Buckley, W. Renninger, F. Wise, *Opt. Express* **14**, 10095 (2006)
- [7] A. Chong, W. H. Renninger, F. W. Wise, *Opt. Lett.* **32**, 2408 (2007).
- [8] F. W. Wise, A. Chong, and W. H. Renninger, High-energy femtosecond fiber lasers based on pulse propagation at normal dispersion, *Laser & Photon. Rev.*, **2**, 58 (2007).
- [9] I. G. Koprinkov, Femtosecond fiber lasers: basic characteristics and operation regimes, “Advanced Aspects of Theoretical Electrical Engineering”, Sozopol 2010 Summer School, Part I, pp.102-120, (2010).
- [10] K. Kieu, W. H. Renninger, A. Chong., and F. W. Wise, Sub-100fs pulses at watt-level powers from a dissipative-soliton fiber laser, *Opt. Lett.*, **34**, 593 (2009).
- [11] W. H. Renninger, A. Chong and F. W. Wise, Dissipative solitons in normal dispersion fiber lasers, *Phys. Rev. A* **77**, 023814 (2008).
- [12] S. Lefrançois, K. Kieu, Y. Dong, J. D. Kafka, and F. W. Wise, Scaling of dissipative soliton fiber laser to megawatt peak powers by use of large-area photonic crystal fiber, *Opt. Lett.*, **35**, 1569 (2010).
- [13] C. Lecaplain, B. Orta, G. Machinet, J. Bouillet, M. Baumgartl, T. Schreiber, E. Cormier, and A. Hideur, High-energy femtosecond photonic crystal fiber laser, *Opt. Lett.*, **35**, 3156 (2010).
- [14] M. Baumgartl, F. Jansen, F. Stutzki, C. Jauregui, B. Orta, J. Limpert, and A. Tünnermann, High average and peak power femtosecond large-pitch photonic-crystal-fiber laser, *Opt. Lett.*, **36**, 244 (2011).
- [15] I. G. Koprinkov, K. A. Stankov, Generation of sub-50-femtosecond pulses by compression through amplification from soliton based erbium fiber laser“, Advanced Aspects of Theoretical Electrical Engineering”, Sozopol 2010 Summer School, Part II, pp.103-108, (2010).

A METHOD FOR TRANSFORMATION OF NULLOR RC-NETWORKS INTO EQUIVALENT OA-OTA-C- CIRCUITS

Georgi A. Nenov

Higher School of Transport “Todor Kableshkov”, Sofia
1574 Sofia, 158 Geo Milev Str. BULGARIA
phones: 0359 2 9709232; 0359 896617007
gnenov1@gmail.com

Abstract: *An approach to the transformation of nullor RC-networks into resistorless circuits containing only operational amplifiers (OA), operational transconductance amplifiers (OTA) and capacitors on the base of admittance matrix equivalence is proposed. This is done by using pseudoinverse matrices which correspond to the rectangular matrices normally used for the transformation of the passive part of the examined nullor network into an reduced admittance matrix. In this way we reach to a new pseudopassive admittance matrix realisable by using OTA's, OA's and capacitors only and without resistors. A practical example sustains the theoretical results obtained.*

1. INTRODUCTION

Despite of the wide application of the digital devices for signal processing, the use of the analogue devices of different kinds not only do not lose their significance but mark an ascending evolution. One of the main advantages of the digital circuits in the competition with the analogue ones is that they allow to be realized on the base of the unified integrated technology. The analogue devices and technologies however successfully pursue a similar aim – to reduce the element basis used. The arising of active RC-, SC-, OTA-C-, switched-current (SI-) and translinear (TL-) -circuits are important steps of this way. But it seems the basic aspiration that impulses the improvement of the analogue techniques, started after the “active RC-epoch” is the desire to remove resistors in the corresponding decisions. Such a possibility possesses the use only of transistors and capacitors which realization as integrated circuits is well worked out. Some works are published [8, 9] that describe a variety of methods for synthesis of OTA-C-filters on the base of LC-ladders or signal-flow graphs, whereas others [13-15] propose procedures for transformation of active RC-structures into OTA-ones. The nullor model of an operational transconductance amplifier used in the literature and in the present paper is given in Fig. 1.

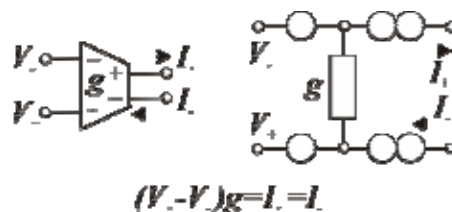


Fig. 1

In the paper an approach to the transformation of active RC-networks into ones containing operational amplifiers (OA), operational transconductance amplifiers (OTA) and capacitors is proposed. Consequently, this transformation responds to the trend discussed above and leads to “resistorless” results.

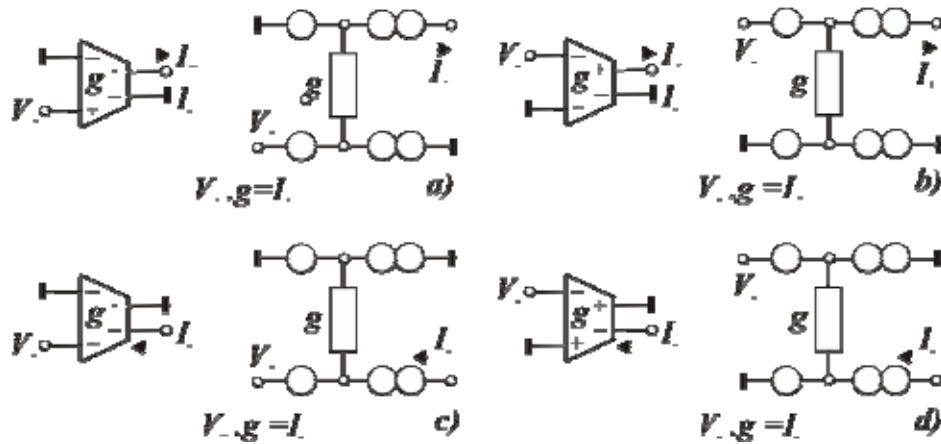


Fig. 2

2. THEORETICAL BASIS

Let us consider a nullor network N with $m+1$ nodes (the node with label $m+1$ is the grounded one) which contains n nullators and n norators (i.e. n nullors). According to classical works of Davies [1, 3] we can form the definite square admittance matrix \mathbf{Y}_p of size m for the passive part of N . In order to find the admittance matrix \mathbf{Y} of the network N taking into account the nullor influence it is necessary firstly to write the matrices \mathbf{K}_N and \mathbf{K}_n of size $(m-n) \times m$ and $m \times (m-n)$, respectively. A simplest way to find these two matrices is to start from two identity matrices $\mathbf{1}$ of size m . Then one obtains the matrix \mathbf{K}_N (\mathbf{K}_n) by adding all columns (rows) in $\mathbf{1}$ which correspond to the nodes in N interconnected by norators (nullators) and by replacing by 0 the entry 1 in the columns (rows) which correspond to nodes connected with the ground node by norators (nullators). Then the searched admittance matrix \mathbf{Y} is

$$\mathbf{Y} = \mathbf{K}_N \cdot \mathbf{Y}_p \cdot \mathbf{K}_n \quad (1)$$

Having in mind the equalities [2, 16, 17]

$$\begin{cases} \mathbf{K}_N \cdot \mathbf{K}_N^+ \cdot \mathbf{K}_N = \mathbf{K}_N; \\ \mathbf{K}_n \cdot \mathbf{K}_n^+ \cdot \mathbf{K}_n = \mathbf{K}_n \end{cases} \quad (2)$$

where \mathbf{K}_N^+ and \mathbf{K}_n^+ are the *Moor-Penrose* pseudoinverse matrices [2] of \mathbf{K}_N and \mathbf{K}_n , respectively. After substituting the expressions (2) in (1) we obtain an other expression for \mathbf{Y} :

$$\mathbf{Y} = \mathbf{K}_N \cdot \mathbf{K}_N^+ \cdot \mathbf{K}_N \mathbf{Y}_p \cdot \mathbf{K}_n \cdot \mathbf{K}_n^+ \cdot \mathbf{K}_n, \quad (3)$$

or

$$\mathbf{Y} = \mathbf{K}_N \cdot \mathbf{Y}_x \cdot \mathbf{K}_n \quad (4)$$

for

$$\mathbf{Y}_x = \mathbf{K}_N^+ \cdot \mathbf{K}_N \mathbf{Y}_p \cdot \mathbf{K}_n \cdot \mathbf{K}_n^+ = \mathbf{K}_N^+ \cdot \mathbf{Y} \cdot \mathbf{K}_n^+. \quad (5)$$

If we compare the last result with (1) we can see that the new matrix \mathbf{Y}_x in (4) plays the same role as the matrix \mathbf{Y}_p in (1) but obviously

$$\mathbf{Y}_p \neq \mathbf{Y}_x. \quad (6)$$

Because the matrix \mathbf{Y}_p corresponds to the passive structure of N, its entries (admittances) in every row or column satisfy the dominant condition (nonnegative sum of entries, nonnegative entry on the main diagonal and nonpositive entries outside of it). On the other hand the products $\mathbf{K}_N^+ \cdot \mathbf{K}_N$ and $\mathbf{K}_n \cdot \mathbf{K}_n^+$ in (5) are nonidentity matrices and the entries of \mathbf{Y}_x do not satisfy the dominant condition. Consequently, the matrix \mathbf{Y}_x does not correspond of a passive structure (it is pseudopassive matrix). This conclusion submits for discussion the problem of a suitable realization of \mathbf{Y}_x as it will present below.

3. POSSIBLE REALIZATIONS OF MATRIX \mathbf{Y}_x

Without loss of generality in what follows we suppose that the entries of \mathbf{Y}_x are of the kind $\pm g_{ij}$ (resistive admittance) or sC_{ij} (capacitive admittance) on i^{th} row and j^{th} column, $i, j=1, 2, \dots, m-n$. The matrix \mathbf{Y}_x can be synthesized according to the methods, proposed in [4-7, 10-12] but all they lead again to nullor structures. Here we propose two ways to the decision of this task, namely:

Direct realization. The circuit implementation of the frequency independent entries of \mathbf{Y}_x locate as below

$$\mathbf{Y}_x = \begin{bmatrix} \vdots & \vdots & \vdots & \vdots & \vdots \\ \vdots & \vdots & \vdots & \vdots & \vdots \\ \vdots & \vdots & \pm g_{ij} & \vdots & \vdots \\ \vdots & \vdots & \vdots & \vdots & \vdots \\ \vdots & \vdots & \vdots & \vdots & \vdots \end{bmatrix} \quad (7)$$

causes no problems and it is possible by using OTA's from Fig. 2. When however the entries depend on the frequency:

$$\left\{ \begin{array}{l}
 \mathbf{Y}_x = \begin{bmatrix} \vdots & \vdots & \vdots & \vdots & \vdots \\ \vdots & \vdots & \pm sC_{ij} & \vdots & \vdots \\ \vdots & \vdots & \vdots & \vdots & \vdots \\ \vdots & \vdots & \vdots & \vdots & \vdots \\ \vdots & \vdots & \vdots & \vdots & \vdots \end{bmatrix}; \\
 \mathbf{Y}_x = \begin{bmatrix} \vdots & \vdots & \vdots & \vdots & \vdots & \vdots \\ \vdots & \vdots & \pm sC_{ij} & \vdots & sC_{ii} & \vdots \\ \vdots & \vdots & \vdots & \vdots & \vdots & \vdots \\ \vdots & \vdots & \vdots & \vdots & \vdots & \vdots \\ \vdots & \vdots & \vdots & \vdots & \vdots & \vdots \\ \vdots & \vdots & \vdots & \vdots & \vdots & \vdots \end{bmatrix}; \\
 \mathbf{Y}_x = \begin{bmatrix} \vdots & \vdots & \vdots & \vdots & \vdots & \vdots \\ \vdots & \vdots & \vdots & \vdots & \vdots & \vdots \\ \vdots & \vdots & sC_{ii} & \vdots & \pm sC_{ij} & \vdots \\ \vdots & \vdots & \vdots & \vdots & \vdots & \vdots \\ \vdots & \vdots & \vdots & \vdots & \vdots & \vdots \\ \vdots & \vdots & \vdots & \vdots & \vdots & \vdots \end{bmatrix}; \\
 C_{ij} = C_{ii} > 0
 \end{array} \right. \quad (8)$$

the corresponding blocks consist of one or two operational amplifiers and one or two OTA's – Fig. 3.

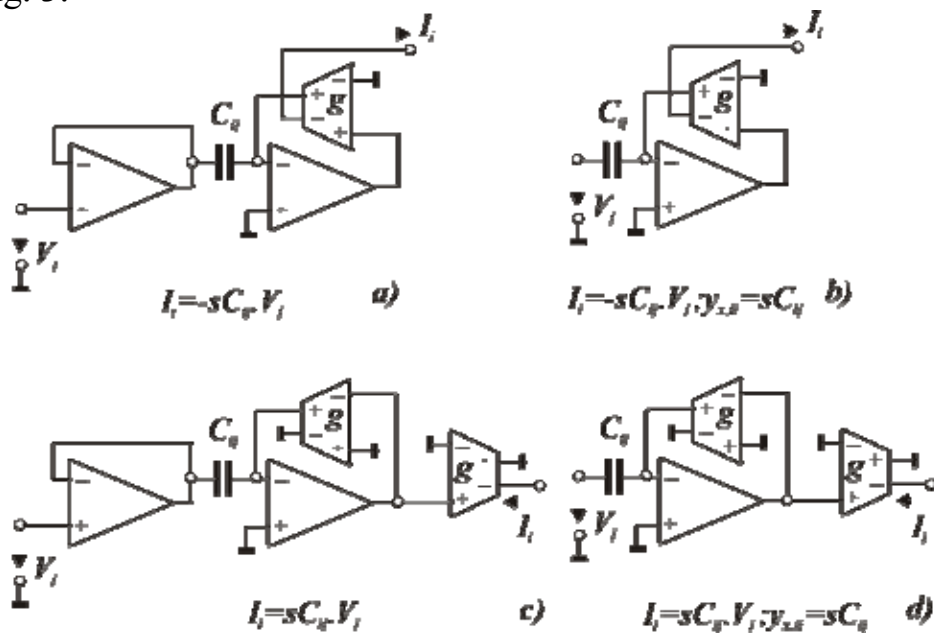


Fig. 3

Realization of transformed matrix \mathbf{Y}_x . Here we aspire to obtain the matrix $k \cdot \mathbf{Y}_x/s$ instead of \mathbf{Y}_x where k is a positive real constant. Then all frequency independent entries of \mathbf{Y}_x become frequency dependent and vice versa. Note that the multiplication given above does not change all voltage transfer functions connected with network examined. The circuit implementation of the frequency independent entries uses again OTA's, whereas the realization of frequency dependent entries needs OTA-integrators [13-15] – Fig. 4. To our mind this approach is preferable because as it is clear from Fig. 3 the direct realization of \mathbf{Y}_x uses differentiating blocks whereas the cells for the second approach are integrators and they reduce the noises.

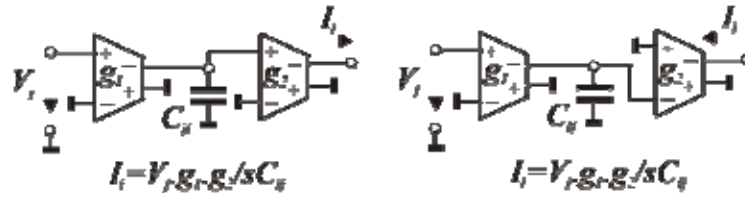


Fig. 4

4. EXAMPLE

The well known Tow’s lowpass filter structure is given (Fig. 5a). Now we shall try to transform it into an equivalent OA-OTA-C- structure according to the method proposed above. The corresponding nullor representation of the filter is drawn in Fig. 5b. Firstly, on the base of the last one we write the matrix Y_p :

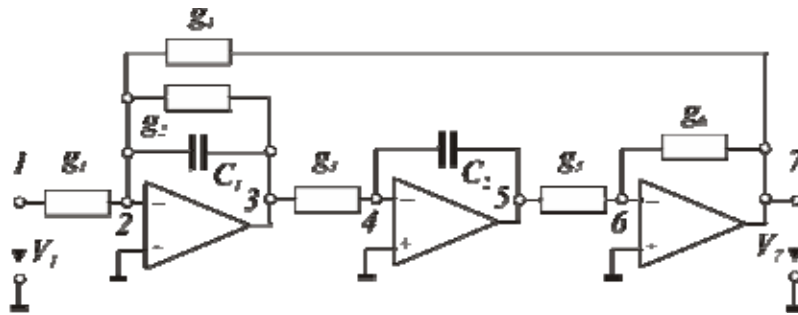


Fig. 5a

$$Y_p = \begin{bmatrix} g_1 & -g_1 & 0 & 0 & 0 & 0 & 0 & 0 \\ -g_1 & g_1 + g_2 + g_4 + sC_1 & -g_2 - sC_1 & 0 & 0 & 0 & 0 & -g_4 \\ 0 & -g_2 - sC_1 & g_2 + g_3 + sC_1 & -g_3 & 0 & 0 & 0 & 0 \\ 0 & 0 & -g_3 & g_3 + sC_2 & -sC_2 & 0 & 0 & 0 \\ 0 & 0 & 0 & -sC_2 & g_3 + sC_2 & -g_5 & 0 & 0 \\ 0 & 0 & 0 & 0 & -g_5 & g_5 + g_6 & -g_6 & 0 \\ 0 & -g_4 & 0 & 0 & 0 & -g_6 & g_4 + g_6 & 0 \end{bmatrix} \quad (9)$$

We assume a low-pass second-order Butterworth filter transfer function

$$T_U(s) = \frac{U_o(s)}{U_i(s)} = -\frac{\alpha_0}{b_0 + b_1 \cdot s + b_2 \cdot s^2}, \quad (10)$$

for

$$\{\alpha_0 = b_0 = 1; b_1 = 4,503 \cdot 10^{-4}; b_2 = 1,014 \cdot 10^{-7}\}. \quad (11)$$

The analysis of the circuit in Fig. 4a yields

$$T_U(s) = \frac{U_o(s)}{U_i(s)} = -\frac{1}{1 + \frac{g_2 g_5 C_2}{g_1 g_2 g_3} s + \frac{g_6 C_1 C_2}{g_1 g_3 g_5} s^2} \quad (12)$$

and for $g_1=g_2=g_3=g_4=g_5=g_6= 1mS$ from (10) and (11) one obtains $C_1= 0,225 \mu F$; $C_2= 0,4503 \mu F$.

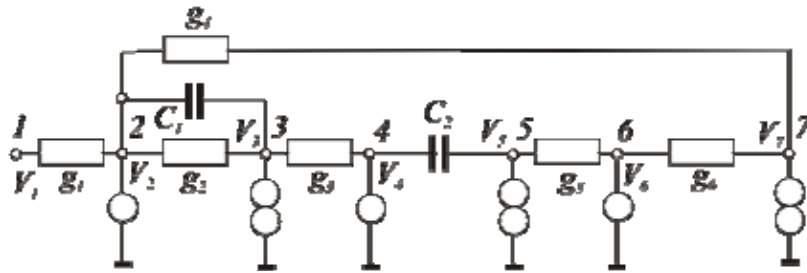


Fig. 5b

Taking into account the location of the nullators and norators in Fig. 5b the matrices \mathbf{K}_N and \mathbf{K}_n are [1]

$$\mathbf{K}_N = \begin{bmatrix} 1 & 0 & 0 & 0 & 0 & 0 & 0 \\ 0 & 1 & 0 & 0 & 0 & 0 & 0 \\ 0 & 0 & 0 & 1 & 0 & 0 & 0 \\ 0 & 0 & 0 & 0 & 0 & 1 & 0 \end{bmatrix}; \mathbf{K}_n = \begin{bmatrix} 1 & 0 & 0 & 0 \\ 0 & 0 & 0 & 0 \\ 0 & 1 & 0 & 0 \\ 0 & 0 & 0 & 0 \\ 0 & 0 & 1 & 0 \\ 0 & 0 & 0 & 0 \\ 0 & 0 & 0 & 1 \end{bmatrix}. \tag{13}$$

Because [2]

$$\mathbf{K}_N = \mathbf{B}_N \cdot \mathbf{C}_N; \mathbf{K}_n = \mathbf{B}_n \cdot \mathbf{C}_n \tag{14}$$

and $\text{rank } \mathbf{K}_N = 5$; $\text{rank } \mathbf{K}_n = 5$, it is suitable the choice

$$\mathbf{B}_N = \begin{bmatrix} 1 & 0 & 0 & 0 \\ 0 & 1 & 0 & 0 \\ 0 & 0 & 1 & 0 \\ 0 & 0 & 0 & 1 \end{bmatrix}; \mathbf{B}_n = \begin{bmatrix} 1 & 0 & 0 & 0 \\ 0 & 0 & 0 & 0 \\ 0 & 1 & 0 & 0 \\ 0 & 0 & 0 & 0 \\ 0 & 0 & 1 & 0 \\ 0 & 0 & 0 & 0 \\ 0 & 0 & 0 & 1 \end{bmatrix}. \tag{15}$$

Then from (14) one follows

$$\mathbf{C}_N = \begin{bmatrix} 1 & 0 & 0 & 0 & 0 & 0 & 0 \\ 0 & 1 & 0 & 0 & 0 & 0 & 0 \\ 0 & 0 & 0 & 1 & 0 & 0 & 0 \\ 0 & 0 & 0 & 0 & 0 & 1 & 0 \end{bmatrix}; \mathbf{C}_n = \begin{bmatrix} 1 & 0 & 0 & 0 \\ 0 & 1 & 0 & 0 \\ 0 & 0 & 1 & 0 \\ 0 & 0 & 0 & 1 \end{bmatrix}. \tag{16}$$

Now for the pseudoinverse matrices \mathbf{K}_N^+ and \mathbf{K}_n^+ we obtain

$$\mathbf{K}_N^+ = \mathbf{C}_{N,t} \cdot (\mathbf{C}_N \cdot \mathbf{C}_{N,t})^{-1} \cdot (\mathbf{B}_{N,t} \cdot \mathbf{B}_N)^{-1} \mathbf{B}_{N,t} = \begin{bmatrix} 1 & 0 & 0 & 0 \\ 0 & 1 & 0 & 0 \\ 0 & 0 & 0 & 0 \\ 0 & 0 & 1 & 0 \\ 0 & 0 & 0 & 0 \\ 0 & 0 & 0 & 1 \\ 0 & 0 & 0 & 0 \end{bmatrix}; \quad (17)$$

$$\mathbf{K}_n^+ = \mathbf{C}_{n,t} \cdot (\mathbf{C}_n \cdot \mathbf{C}_{n,t})^{-1} \cdot (\mathbf{B}_{n,t} \cdot \mathbf{B}_n)^{-1} \mathbf{B}_{n,t} = \begin{bmatrix} 1 & 0 & 0 & 0 & 0 & 0 & 0 \\ 0 & 0 & 1 & 0 & 0 & 0 & 0 \\ 0 & 0 & 0 & 0 & 1 & 0 & 0 \\ 0 & 0 & 0 & 0 & 0 & 0 & 1 \end{bmatrix}. \quad (18)$$

From (5), (17) and (18) we obtain the pseudopassive matrix

$$\mathbf{Y}_x = \begin{bmatrix} g_1 & 0 & 0 & 0 & 0 & 0 & 0 \\ -g_1 & 0 & -g_2 - sC_1 & 0 & 0 & 0 & -g_4 \\ 0 & 0 & 0 & 0 & 0 & 0 & 0 \\ 0 & 0 & -g_3 & 0 & -sC_2 & 0 & 0 \\ 0 & 0 & 0 & 0 & 0 & 0 & 0 \\ 0 & 0 & 0 & 0 & -g_5 & 0 & -g_6 \\ 0 & 0 & 0 & 0 & 0 & 0 & 0 \end{bmatrix}. \quad (19)$$

Of course this matrix can be realized directly by using the blocks given in Fig. 3. We prefer however to follow the second approach commented in item 3 – this realizing the matrix $k \cdot \mathbf{Y}_x / s$. Then from (19) one obtains

$$k \cdot \mathbf{Y}_x / s = \begin{bmatrix} k \cdot g_1 / s & 0 & 0 & 0 & 0 & 0 & 0 \\ -k \cdot g_1 / s & 0 & -k \cdot g_2 / s - k \cdot C_1 & 0 & 0 & 0 & -k \cdot g_4 / s \\ 0 & 0 & 0 & 0 & 0 & 0 & 0 \\ 0 & 0 & -k \cdot g_3 / s & 0 & -k \cdot C_2 & 0 & 0 \\ 0 & 0 & 0 & 0 & 0 & 0 & 0 \\ 0 & 0 & 0 & 0 & -k \cdot g_5 / s & 0 & -k \cdot g_6 / s \\ 0 & 0 & 0 & 0 & 0 & 0 & 0 \end{bmatrix} \quad (20)$$

or for $k=10^3$ and taking into account the values of $g_1, g_2, g_3, g_4, g_5, g_6, C_1$ and C_2 the matrix (20) takes the form

$$k \cdot \mathbf{Y}_x / s = \begin{bmatrix} 10^6 / s & 0 & 0 & 0 & 0 & 0 & 0 \\ -10^6 / s & 0 & -10^6 / s - 0,225 \cdot 10^{-3} & 0 & 0 & 0 & -10^6 / s \\ 0 & 0 & 0 & 0 & 0 & 0 & 0 \\ 0 & 0 & -10^6 / s & 0 & -0,4503 \cdot 10^{-3} & 0 & 0 \\ 0 & 0 & 0 & 0 & 0 & 0 & 0 \\ 0 & 0 & 0 & 0 & -10^6 / s & 0 & -10^6 / s \\ 0 & 0 & 0 & 0 & 0 & 0 & 0 \end{bmatrix} \quad (21)$$

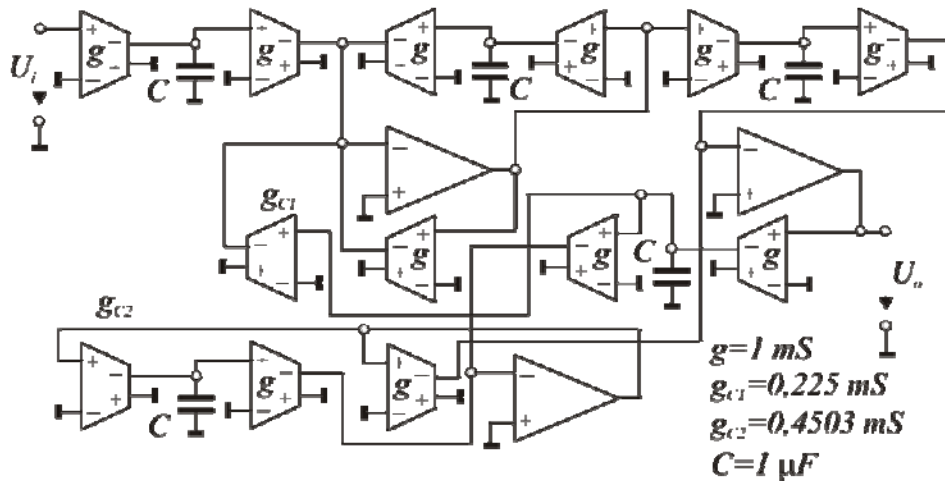


Fig. 6

The filter structure synthesized on the base of the last matrix is shown in Fig. 6. It contains 3 OA's, 13 OTA's and 5 grounded capacitors without resistors. It was simulated through the product *Multisim 10* (Fig. 7) and the characteristic of attenuation A , dB vs frequency f , Hz is given in Fig. 8.

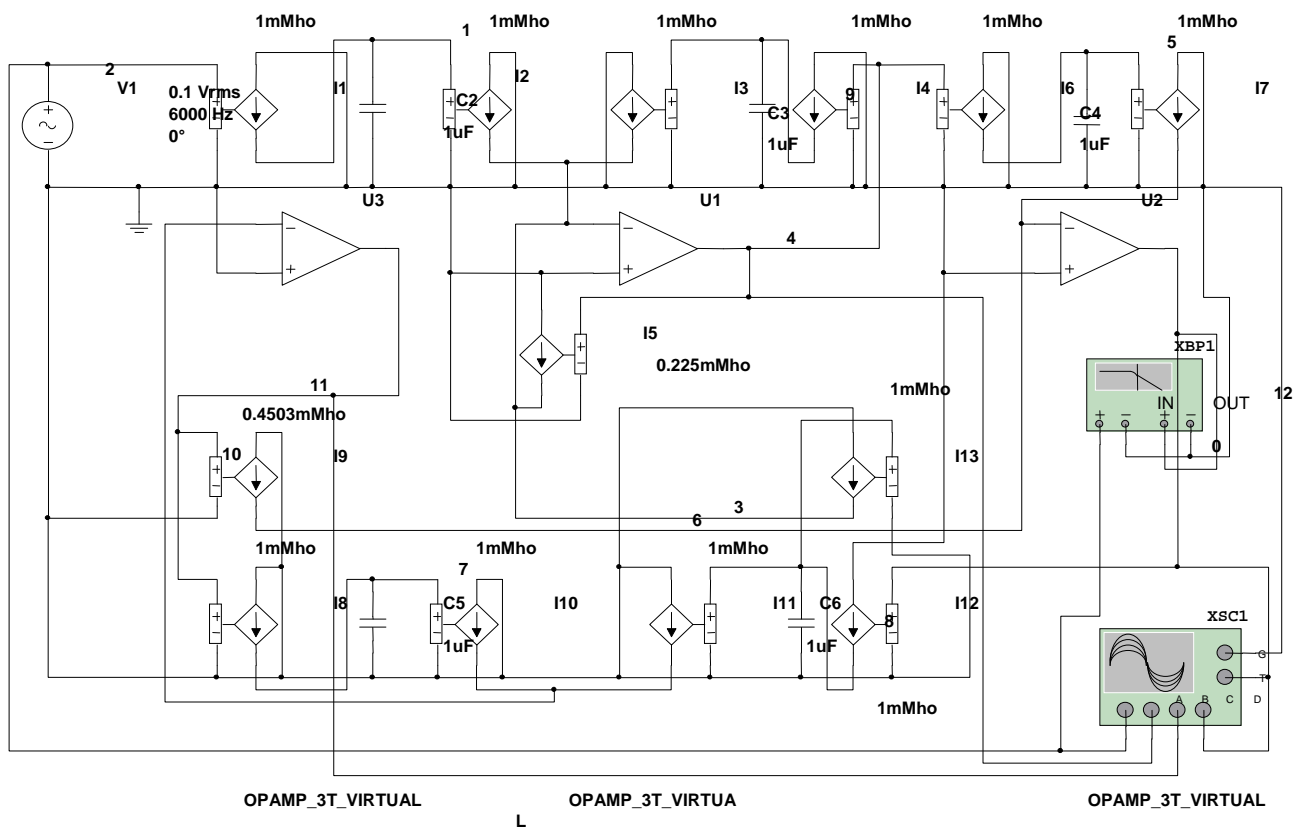


Fig. 7

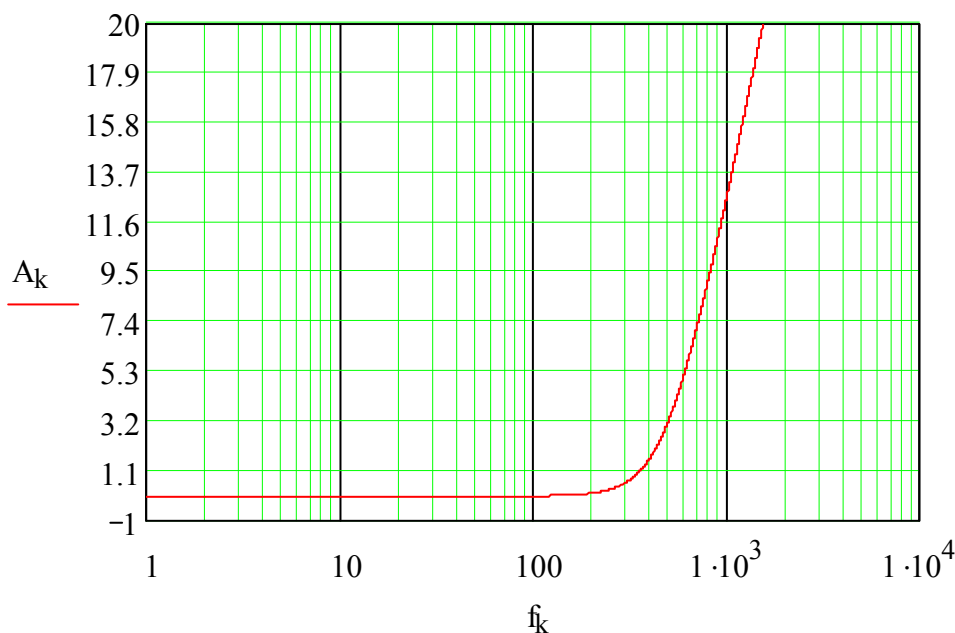


Fig. 8

5. CONCLUSIONS

The approach presented in the paper is based on the use of pseudopassive transforming matrices for equivalent conversion of RC-nullor networks (usually networks containing operational amplifiers, resistors and capacitors) into structures with operational amplifiers, operational transconductance amplifiers and grounded capacitors. This element basis does not contain resistors and simplifies the practical realization of the transformed objects as integrated circuits. The theoretical results are applied to the concrete active RC-network.

References

- [1] A. C. Davies, "Matrix Analysis of Network Containing Nullators and Norators", *Electronics Letters*, vol. 2, 2, 1966, 48-49
- [2] Ф. Р. Гантмахер, „Теория матриц”, Изд. „Наука”, Москва, 1966
- [3] A. C. Davies, "The Significance of Nullators, Norators and Nullors in Active- Network Theory", *Radio and Electronic Engineer*, vol. 54, 11, 1967, pp. 259-267
- [4] R. W. Daniels, "A Nullator-Norator Synthesis Procedure Applied to Gyration", *Proc. of IEEE MWCAS, Texas, 1969*, pp. IX.3.1 – IX.3.8
- [5] B. B. Stamenkovic, "Realization of Open-Circuit Voltage-Transfer Matrices by Grounded Nullors", *Electronics Letters*, vol. 11, 6, 1975, pp. 134-136
- [6] T. Yanagisawa, N. Kanbayashi, "Realization of Arbitrary Conductance Matrix Using Operational Amplifiers", *Proc. of IEEE ISCAS, Munich, 1976*, pp. 532-535
- [7] J. K. Stevenson, "Network Synthesis by Admittance Matrix Expansion", *Proc. of IEE Colloquium on Electronic Filters, London, 1978*, pp. 5-9
- [8] M. A. Tan, R. Schaumann, "Generation of Transconductance Grounded Capacitor Filters by Signal-Flow Graph Simulation of LC_Ladders", *Proc. IEEE ISCAS, 1988*, 2407-2410
- [9] C. M. Antonio de Queiros, L.P.Galoba, E.S.-Sinencio, "Signal-Flow Graph OTA-C Integrated Filters", *Proc. IEEE ISCAS, 1988*, 2165-2168

- [10] D. Haigh, P. Radmore, “Systematic Synthesis Method for Analogue Circuits, Part I: Notation and Synthesis Toolbox”, Proc. of IEEE ISCAS, 2004, pp. I-701 – I-704
- [11] D. Haigh, F. Q. Tan, C. Papavassiliou, “Systematic Synthesis Method for Analogue Circuits, Part II: Active RC-Circuit Synthesis”, Proc. of IEEE ISCAS, 2004, pp. I-705 – I-708
- [12] D. Haigh, F. Q. Tan, C. Papavassiliou, “Systematic Synthesis Method for Analogue Circuits, Part III: All-Transistor Circuit Synthesis”, Proc. of IEEE ISCAS, 2004, pp. I-709 – I-712
- [13] R. F. Ahmed, I. A. Awal, A. M. Soliman, “New OpAmp-RC to Gm-C Transformation Method”, Analog Integrated Circuits and Signal Processing, vol. 49, 1, 2006, pp. 79-86
- [14] Johana-M. Garcia-Ortega, E. Tlelo-Cuautle, C. Sanchez-Lopez, “Design of Current-Mode Gm-C Filters From the Transformation of OpAmp RC Filters”, Journal of Applied Sciences, 7(9), 2007, p. 1321-1326
- [15] E. Tlelo-Cuautle et al., “Behavioral Modeling of Mixed-Mode Integrated Circuits”, “Advances in Analog Circuits”, ed. E. Tlelo-Cuautle, Rijeka (Croatia), InTech, 2011, pp. 85-108.
- [16] http://en.wikipedia.org/wiki/Moore%E2%80%93Penrose_pseudoinverse
- [17] http://en.wikipedia.org/wiki/Generalized_inverse
- [18] <http://books.google.bg/books?id=E4O662eBlu8C&pg=PA639&lpg=PA639&dq=OTA+resistor+equivalent&source=bl&ots=Ue6ZZX02qn&sig=ev0I2kvPgRRcQgGoUY4mpBJjCd4&hl=bg#v=onepage&q=OTA%20resistor%20equivalent&f=false>

PHYSICAL PARAMETERS AND POSSIBLE EXCITATION MECHANISMS FOR A SAMPLE OF SEYFERT GALAXIES

R.P. Tasheva¹, V. Taneva-Toncheva¹, S.T. Tasheva²

¹Technical University of Sofia, Bulgaria, e-mail: rpt@tu-sofia.bg, uraa@dir.bg

²University of Sofia “St. Kliment Ohridski”, Bulgaria e-mail: Snezhana.Tasheva@cern.ch

Abstract. *Using spectroscopic data found in the literature for a sample of 55 nearby ($z < 0.4$) Seyfert galaxies and working under assumption that a black hole is the central AGN engine in them, corresponding black hole masses and accretion disk luminosities are derived. Possible composite character of some of the nuclei is discussed utilizing Veilleux @ Osterbrock (1987) [OIII] $\lambda 5007/H\beta$ vs [NII] $\lambda 6583/H\alpha$ diagnostic diagram.*

Keywords: *Seyfert galaxies – black holes – active galactic nuclei*

1. INTRODUCTION

Seyfert galaxies belong to the class of Active Galactic Nuclei (AGN). According to the standard model, in active galaxies an accretion disk around a massive black hole produces a hard X-ray continuum, which photoionizes the Broad Line Region (BLR, where broad emission lines originate) and the Narrow Line region (NLR, where narrow emission lines originate) located at $< 1\text{pc}$ and at $< 100\text{pc}$ from the nuclear engine respectively. Seyfert galaxies are classified as type 1 or type 2. Type 1 have both narrow forbidden lines ($\text{FWHM} \sim 10^3 \text{ km s}^{-1}$) and broad Balmer lines ($\text{FWHM} \sim 10^4 \text{ km s}^{-1}$) in their optical spectrum, while type 2 have only narrow lines. Actually they are the same object: type 2 Seyferts harbour a BLR, but this is obscured in some direction by a molecular torus (Antonucci [1]).

Black holes have been the leading candidate to power central engines in AGN for over three decades, but direct evidence for their presence has been elusive. In nearby galaxies, spatially resolved kinematics have provided strong evidence for the ubiquity of nuclear black holes with dynamical black hole detection reported for 37 galaxies by Woo and Urry [2].

Black hole mass, along with accretion ratio is a fundamental property of AGNs. Via the Eddington limit, a maximum luminosity for the idealized case of spherical accretion ($L_{\text{Edd}} = 1.25 \cdot 10^{38} M_{\text{BH}}/M_{\odot} \text{ ergs s}^{-1}$), the black hole sets an approximate upper limit to AGN energetics summarizing the accretion history of the AGN.

2. RESULTS AND DISCUSSION

Direct cinematic observations of the black holes are limited by finite spatial resolution, not to mention that scattered light from the bright central source dilutes any cinematic signal from orbiting material. For these reason various less direct methods for estimating black hole mass have been devised. One set of methods assumes that

the BLR is gravitationally bound by the central black hole potential, so that the black hole mass can be estimated from the orbital radius R_{BLR} and the Doppler velocity.

We attempt an approximate evaluation of the black hole mass for the 55 objects for which we have data of the broad H_α component [3]. Assuming that broad-line clouds are virialized, the black hole mass can be estimated as:

$$M_{\text{BH}} = v^2 R_{\text{BLR}}/G \quad (1)$$

making some suggestions [4]. The virial assumption may not be correct, however; radiation pressure and or magnetic field may contribute significantly to the dynamics, and outflows or winds could cause the observed lines to exceed those induced by the black hole potential itself. Additionally, the calculations require measurement of the broad H_β , which is not detected because it is swamped by the narrow line produced by starburst and/or by the AGN continuum which is not measured directly. We substitute the FWHM of H_β with the FWHM of the broad H_α that we attribute to AGN. H_α is usually broader than the H_β so this is another factor that leads to black hole mass overestimation.

Assumptions about the orbital shape and inclinations of the broad-line clouds introduce additional uncertainties. McLure @Dunlop [5] suggest $f = 1,5$ for the relationship between orbital velocity and **FWHM**:

$$v = 1,5 \text{ FWHM} \times H_\beta \quad (2)$$

and $R_{\text{BLR}} = 32,9 (\lambda L_{5100\text{\AA}}/10^{44} \text{ ergss}^{-1})^{0,7}$ in light days [4]. We adopt $\text{FWHM} \approx 1500$ km/s for the galaxies that are likely to be Sy 1 type and $\text{FWHM} \approx 500$ km/s for those that are probably Sy 2 type.

Assuming accretion scenario, the energy of the falling matter can be transferred into energy or fast-moving particles with coefficient η ,

$$0,572 \leq \eta \leq 0,423$$

This coefficient shows how much of the mass moving toward the black hole is transferred into energy and does not reach the black hole. The so obtained luminosity of the accretion disk is

$$L_{\text{disk}} = \eta (dM/dt) c^2 \quad (3)$$

From here we can derive the accretion ratio $dM/dt = L_{\text{disk}} / \eta c^2$, assuming $\eta = 0,1$. Every accretion disk emits only part of boundary Eddington luminosity, for Seyfert galaxies between 0,01 and 0,1. We adopt $L_{\text{disk}} = 0,1 L_{\text{Edd}}$.

If the the black hole is fast rotating and massive enough we will expect the accretion disk surrounding it to be a source of photons and accepting $R = 0,5 R_s$ for the radius of the inner edge of the accretion disk, where

$$R_s = 2GM/c^2 \quad (4)$$

e Schwarzschild's radius.

The presumed temperature of the disk can be derived accepting that the accretion disk emits like a black body:

$$(dM/dt) c^2 = 4\pi R_s^2 \sigma T^4 \quad (5)$$

From where

$$T_{\text{disk}} = (c^6(dM/dt)/8\pi G^2 M^2) \quad (6)$$

i.e. the temperature of the disk depends on the accretion ratio of the matter reach the black hole.

The results are presented in the Table 1. The Table 1 lists names, luminosity of the broad component of H_α in units of ergs s^{-1} , relative intensities $[\text{OIII}]/H_\beta$ and $[\text{NII}]/H_\alpha$, the calculated black hole masses and approximate luminosities of the nuclei, according to Eddington's formula $L/L_c \leq L_{\text{Edd}}/L_c = 1,25 \cdot 10^{38} M_{\text{BH}}/M_c \text{ ergs s}^{-1}$, accretion ratio and the temperature of the accretion disk.

Table 1

Name	$\lg L_{H\alpha}$	$[\text{OIII}]/H_\beta$	$[\text{NII}]/H_\alpha$	$\lg M_{\text{BH}}$	$\lg L_{\text{disk}}$	$dM/dt, \text{yr}^{-1}$	$\lg T_{\text{disk}}$
NGC 185	34,75	3,32	0,61	4,96	42,06	0,0002	5,53
NGC 676	38,44	10,13	0,94	7,54	44,63	0,07	4,88
NGC 777	38,73	3,68	1,79	7,74	44,84	0,12	4,84
NGC 1052	40,16	2,01	1,20	8,67	45,77	1,03	4,60
NGC 1058	37,40	3,81	1,23	6,81	43,91	0,01	5,06
NGC 1068	41,55	12,82	0,76	9,72	46,82	11,57	4,34
NGC 1167	40,21	5,66	2,01	8,78	45,88	1,33	4,57
NGC 1275	41,14	14,88	1,36	9,44	46,54	6,07	4,41
NGC 1358	40,36	11,33	2,01	8,89	45,99	1,71	4,54
NGC 1667	40,54	7,58	2,38	9,01	46,11	2,25	4,52
NGC 2273	40,46	5,77	0,86	8,92	46,02	1,83	4,54
NGC 2336	38,39	2,97	1,79	7,51	44,61	0,07	4,89
NGC 2639	39,68	3,46	4,25	8,41	45,51	0,57	4,66
NGC 2655	39,55	3,83	2,91	8,32	45,42	0,46	4,67
NGC 2683	37,21	2,93	1,49	6,68	43,78	0,01	5,1
NGC 2685	38,66	3,11	0,93	7,70	44,80	0,11	4,84
NGC 2841	38,53	1,86	1,83	8,56	45,66	0,80	4,63
NGC 3031	37,64	4,11	2,23	6,99	44,09	0,02	5,02
NGC 3079	38,76	4,15	1,59	7,77	44,87	0,13	4,82
NGC 3147	39,47	6,14	2,71	8,27	45,37	0,41	4,70
NGC 3185	39,60	3,42	0,87	8,36	45,46	0,50	4,68
NGC 3227	40,38	5,91	1,33	8,90	46,00	1,75	4,54
NGC 3254	38,43	9,57	1,14	7,54	44,64	0,08	4,88
NGC 3486	37,79	4,54	1,05	7,09	44,19	0,03	5,00

NGC 3516	40,21	9,28	1,31	8,78	45,88	1,33	4,57
NGC 3608	38,28	2,94	1,30	7,44	44,54	0,06	4,91
NGC 3627	38,50	2,90	1,44	7,56	44,66	0,08	4,88
NGC 3738	37,72	2,96	0,10	7,04	44,14	0,02	5,01
NGC 3941	38,67	3,52	1,56	7,71	44,81	0,11	4,84
NGC 3976	39,21	3,58	1,96	8,06	45,16	0,25	4,75
NGC 3982	39,21	21,35	0,87	8,10	45,20	0,28	4,74
NGC 3998	40,00	1,98	1,08	8,64	45,74	0,96	4,61
NGC 4051	40,04	4,50	0,64	8,67	45,77	1,03	4,60
NGC 4138	38,54	5,94	1,47	7,62	44,72	0,09	4,86
NGC 4151	41,22	11,56	0,68	9,50	46,60	6,97	4,39
NGC 4168	37,60	3,79	2,85	6,94	44,04	0,02	5,03
NGC 4235	39,25	12,86	2,57	9,05	46,15	2,47	4,50
NGC 4258	38,35	10,32	0,80	7,46	44,56	0,06	4,90
NGC 4378	38,80	4,09	2,78	7,77	44,87	0,13	4,82
NGC 4388	40,07	11,15	0,57	8,68	45,78	1,06	4,60
NGC 4395	37,88	6,22	0,44	7,16	44,26	0,03	4,98
NGC 4472	37,59	5,08	3,43	6,93	44,03	0,02	5,04
NGC 4477	38,84	3,70	1,87	7,82	44,92	0,14	4,81
NGC 4501	38,93	5,31	2,10	7,90	45,00	0,18	4,79
NGC 4565	37,97	8,73	2,50	7,20	44,30	0,03	4,97
NGC 4579	37,44	3,07	1,89	8,22	45,32	0,37	4,71
NGC 4639	38,34	3,77	1,12	7,46	44,56	0,06	4,90
NGC 4698	38,69	4,29	1,31	7,72	44,82	0,12	4,84
NGC 4725	38,19	6,64	1,14	7,35	44,45	0,05	4,93
NGC 5033	39,32	4,69	2,36	8,14	45,24	0,30	4,73
NGC 5194	38,88	8,96	2,90	7,84	44,94	0,15	4,81
NGC 5273	39,27	11,08	1,14	8,10	45,20	0,28	4,74
NGC 5395	38,87	3,03	1,23	7,83	44,93	0,15	4,81
NGC 5548	40,70	10,09	0,88	9,11	46,21	2,84	4,49
NGC 5631	38,87	3,45	2,61	7,83	44,93	0,15	4,81
NGC 6482	39,23		2,33	8,08	45,18	0,26	4,75
NGC 6503	37,56		0,65	6,91	44,01	0,02	5,21
NGC 6951	39,07	6,62	2,48	8,00	45,10	0,22	4,77
NGC 7479	39,53	3,87	1,16	8,31	45,41	0,45	4,69
NGC 7743	39,59	5,68	1,65	8,35	45,45	0,49	4,68

The masses of the black hole are between 10^5 and 10^9 solar masses but they could possibly undergo strong changes in their accretion ratios when they brighten. The obtained disk luminosities are consistent with those of the typical AGN ($L \approx 10^{42}$ - 10^{46} ergs s^{-1}).

If we suppose that the velocity of gas outflow from AGN nuclei is approximately the same as the accretion ratio, the so obtained value for dM/dt – less than 1 solar mass for 80% of the sample is way lesser from the typical outflow velocities for Seyfert galaxies ($10 \div 100$ solar masses), as well typical outflow velocities for quasars

($1 \div 10 M_{\odot}$). This suggests that only a tiny fraction of the available gas gets accreted (which means that the rest is driven out by winds).

3. OPTICAL CLASSIFICATION

All objects In Table 1 with few exceptions are reported as Seyfert 2 or transition objects. In order to check NED Seyfert 2 classification accurately we have employed an optical diagnostic diagram by Veilleux @ Osterbrock [6] which use line-intensity ratios that are relatively insensitive to reddening and are considered good excitation indicators. Line ratios $[\text{OIII}] \lambda 5007/\text{H}\beta$ and $[\text{NII}] 6583/\text{H}\alpha$ delineate the different excitation which operate in HII regions, high – excitation AGNs (Seyferts) and low-excitation AGNs (LINERS) – Fig. 1.

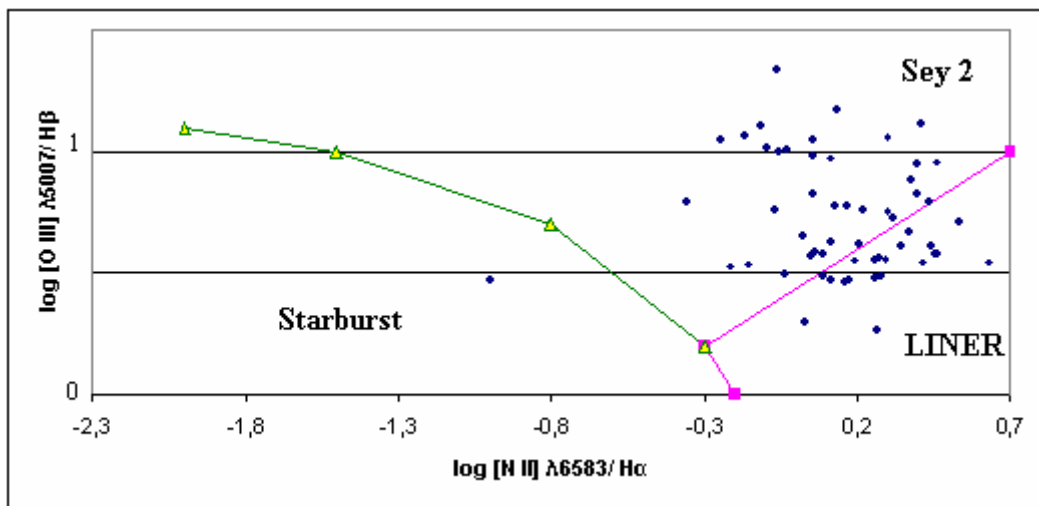


Fig. 1. Diagnostic diagram $[\text{OIII}] \lambda 5007/\text{H}\beta$ versus $[\text{NII}] 6583/\text{H}\alpha$

Although the boundaries between these three classes are not rigorously defined this diagram represents a valid system to distinguish between various types of narrow emission objects. Five of the objects that are in the LINERS area - NGC№№ 2639, 2655, 3941, 4168 and 4378 are reported to be Sy2 by Ho L.C. at all, 1997 [2] and 7 of the objects in the same area - NGC№№ 2336, 2683, 3608, 3627, 4579, 5395 and 5395 are most likely to be LINER 2, but may actually to be Sy2 according to the same authors. NGC 2639 is composite object, LINER + Sy 2, according to [7] and NGC 3998 is a LINER confirmed by [8].

4. CONCLUSION

The main conclusions of this study can be summarized as follows:

- the obtained black hole masses, disk luminosities and temperatures are consistent with the typical data for Seyfert galaxies;
- accretion ratios are smaller than expected;

- Veilleux @ Osterbrock diagnostic diagram produces a well distinguished groups of Seyfert 2 galaxies, starbursts and LINERs except form the cases when the objects are composite (for example LINER+Sy2)

References

- [1] Antonucci, R.R.J. 1993, *ARA@A*, 31, 473
- [2] Woo, J. H@ Urry C. M. 2002, *ApJ*, 579, 530
- [3] Ho L.C., Filippenko A.V. @ Sargent W.L. 1997, *ApJ Suppl. Ser.*, 112, 315
- [4] Panessa F., Wolter A., Pellegrini S., Fruscione, Bassani L., Ceca R., Palumbo G., Trichieri G., *Ap J*, 2005, V.631, P.707-719.
- [5] McLure R.J.@ Dunlope J.S. 2001 *MNRAS*, 327, 199
- [6] Veilleux S.@ Osterbrock D.E.1987, *ApJ Supll Ser*, 63, 295
- [7] Kinney R.G., Bohlin D., Galzetti N.D., Rosemary F.G. 1993, *APj Suppl. Ser*, 86,5
- [8] Jonnele L.W., van den Bosh R.C.E., Aaron J.B., Marc S., 2012, *Ap J*, 753,79

DETERMINATION OF THE PARAMETERS OF MEASUREMENT SCHEME BY SHOCK EXCITATION USING FEM

Stefcho Georgiev Guninski

Dep. „Electrical Engineering”, Technical university of Sofia,
8, „Kl.Ohridski”blvd., 1000 Sofia, tel. (+359 2) 965 2318,
e-mail: sgg@tu-sofia.bg

Analytical expressions are given for the basic parameters of the multiple impulse signal of Eddy current transducer (ECT), included in a scheme with shock excitation. The expressions are presented in a different form and are analyzed in view of their use for preliminary calculations in the development of various methods and instruments for the eddy current nondestructive testing. Through these expressions are determined the initial values of the elements in the measuring scheme. The necessary values of the parameters of the output signal of the pulse ECT (PECT) are determined by Finite element method (FEM).

Keywords: pulse ECT, shock excitation, FEM

1. INTRODUCTION

Since their introduction the pulse methods (PM) for eddy current nondestructive testing (NDT) have shown several advantages [1, 2]. It is not coincidence that recent publications in this field [3, 4, 5] has increased. However their theoretical study is very difficult because, in general, it leads to a simultaneous decision of the transient process in non-linear electrical circuit (measuring scheme) in which participates an eddy current transducer (ECT), whose parameters (inductance/mutual inductance and active resistance) has to be dynamically determined by parallel solving of the electrodynamic field task. Many attempts have been made [2] for the analytical solution to the problem, but end (in terms of the output signal) and practically applicable (even at the modern computing equipment) results are not known to the author. Until recently there were not any available software products, based on the numerical methods, which to solve the combined task (electrical circuit - electromagnetic field). Currently already there are available software products, which very successfully are solving the problem, for example the latest versions of the product MagNet [6].

In the present work, this product is used not for the full modeling of eddy current device, but for solving a simpler, but also practically difficult for analytical solving task for determination of the parameters of the elements, participating in one of the most widespread measurement impulse schemes - the one with shock excitation [2].

In the work it is demonstrated that it is very useful the complex simulation with the use of modern software to be preceded, wherever possible, by a partial analytical analysis of some aspects of the problem.

2. ANALYTICAL DETERMINATION OF THE OUTPUT SIGNAL OF THE MEASURING SCHEME WITH SHOCK EXCITATION

The replacement scheme of the impulse eddy current method with shock excitation is shown in Fig. 1.

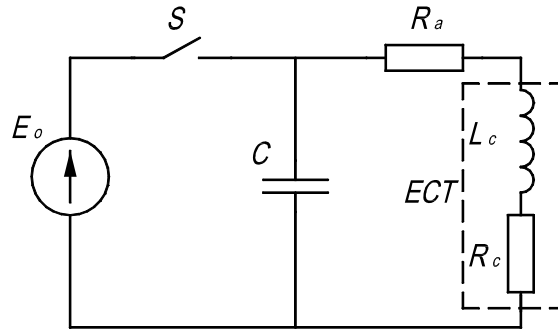


Fig. 1

Before the commutation at $t = 0$ the switch S has been closed for enough time t_1 , that the scheme practically to reach the steady-state conditions:

$$u_c(0-) = U_0, \quad i_{L_c}(0-) = U_0 / R \quad (1)$$

$$U_0 = E_0, \quad R = R_c + R_a \quad (2)$$

Apparently for an error below 0,1% the following inequality should be fulfilled In order to fulfill (4) with an error below 0,1% should:

$$t_1 \geq 7\tau_L = 7L_c / R. \quad (3)$$

Currently $t = 0$ the switch S is opened for time t_2 , enough to reach the new steady-state conditions:

$$u_c(t_2) \approx u_c(\infty) = 0, \quad i_{L_c}(t_2) \approx i_L(\infty) = 0. \quad (4)$$

In order to fulfill (4) with an error below 0,1% should:

$$t_2 \geq 7\tau, \quad (5)$$

where τ is the time constant of the closed loop $C - R_a - ECT$.

Almost always it is working in mode of damped oscillations of the currents and voltages, in which in most cases an output signal is the voltage at the ends of the capacitor u_c or the current i in the loop:

$$u_c = \frac{U_0}{\Omega CR} e^{-\beta t} \sin(\Omega t + \psi), \quad (6)$$

$$i = -\frac{\omega U_0}{\Omega R} e^{-bt} \sin(\Omega t + \varphi), \quad (7)$$

where

$$\text{a) } \omega = \frac{1}{\sqrt{L_c C}}, \quad \text{b) } b = \frac{R}{2L_c}, \quad (8)$$

$$\Omega = \sqrt{\omega^2 - b^2}, \quad (9)$$

$$\psi = \arctg\left(\frac{\Omega CR}{bCR-1}\right) + \pi \cdot \eta(1 - bCR), \quad (10)$$

$$\varphi = \arctg\left(\frac{\Omega}{b}\right). \quad (11)$$

$\eta(x - a)$ is Heaviside step function.

Although it is not obvious, it can be demonstrated that:

$$\psi = 2\varphi \quad (12a)$$

and

$$\pi > \psi > 0, \quad \pi/2 > \varphi > 0. \quad (12b)$$

From (6) and (7) taking into account (8b) and (3) it is seen that the time constant of the circuit after commutation from (5) is:

$$\tau = \frac{1}{b} = \frac{2L_c}{R} = 2\tau_L. \quad (13)$$

From (3), (5) and (13) is easily found that at the same accuracy of the requirement for attenuation of both transient processes

$$t_2 = 2 t_1. \quad (14)$$

The graphics of u_c and the current i in the circuit are shown in Fig. 2:

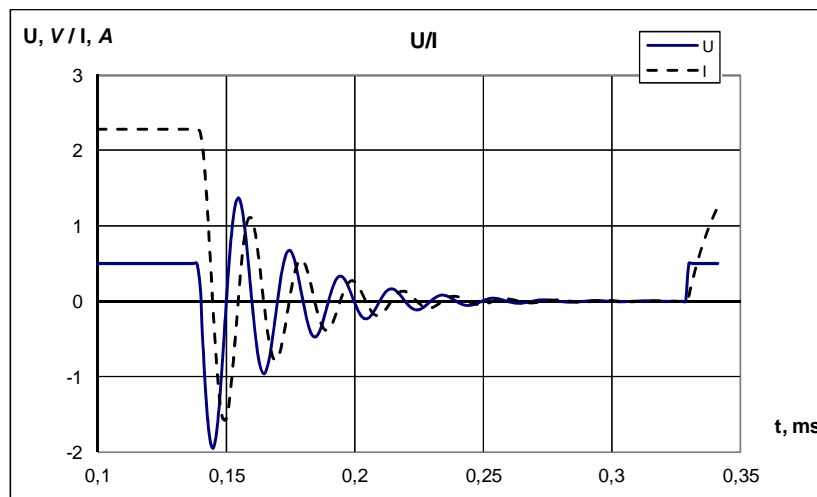


Fig. 2

If the characteristic resistivity ρ and the quality factor q are introduced:

$$\text{a) } \rho = \sqrt{\frac{L_C}{C}}, \quad \text{b) } q = \frac{\rho}{R}, \quad (15)$$

the requirement for damping oscillation mode can be written in the following ways

$$\text{a) } \omega > b, \quad \text{b) } R < 2\rho, \quad \text{c) } q > 1/2. \quad (16)$$

The expression for u_C can be expressed as a function of q :

$$u_C = \frac{2q^2 U_0}{\sqrt{4q^2 - 1}} e^{-bt} \sin(\Omega t + \psi) \quad (17)$$

$$\Omega = \frac{\omega}{2q} \sqrt{4q^2 - 1} \quad (18)$$

$$\psi = \arctg\left(\frac{\sqrt{4q^2 - 1}}{1 - 2q^2}\right) + \pi \cdot \eta \left(q - \frac{\sqrt{2}}{2}\right) \quad (19)$$

It turns out that all the parameters of the output signal can be expressed by the quality factor q and the own frequency ω of the circuit in Fig. 1, which reflects the influence of the electro-physical parameters and geometry of the controlled object:

$$q = \frac{\rho}{R} = \frac{\sqrt{L_C}}{\sqrt{C}(R_C + R_0)}, \quad (20)$$

$$\omega = \frac{1}{\sqrt{L_C C}}. \quad (21)$$

Moreover

$$\text{a) } L_C = L_0 - L_{EC}, \quad \text{b) } R_C = R_0 + R_{EC}. \quad (22)$$

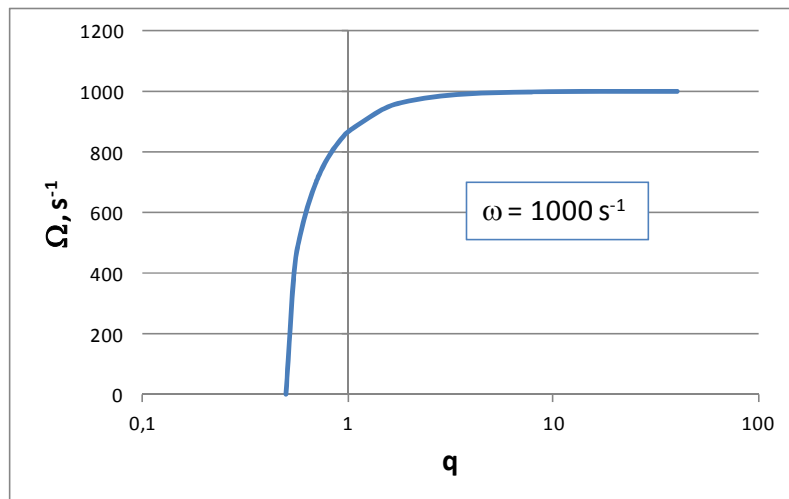


Fig. 3

With L_0 and R_0 are indicated the inductivity and the resistance of PECT in the absence of the controlled object (sample), and with L_{EC} and R_{EC} – the appropriate components caused by the magnetic field of the eddy currents (the inserted components).

On Fig. 3 it is shown the dependence of the angular frequency of the damping fluctuations Ω as a function of the quality factor for $\omega = 1000 \text{ s}^{-1}$, and on Fig. 4 – the dependence on the initial phases ψ and ϕ from q in logarithmic scale.

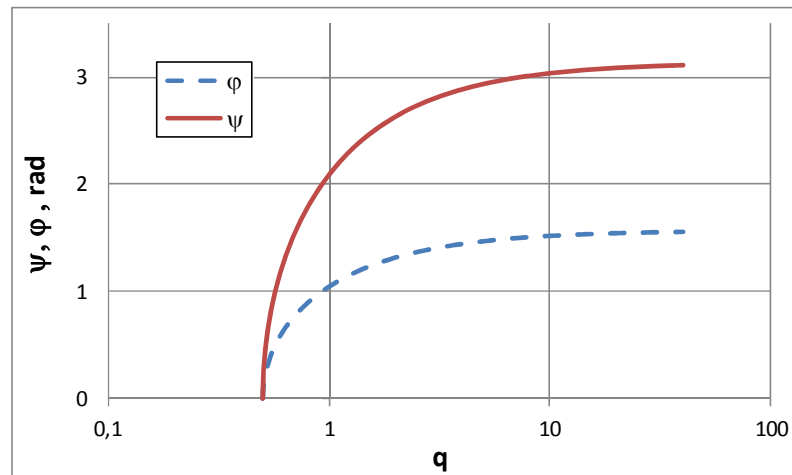


Fig. 4

There is clearly the very strong dependence of Ω from q in the range $(1/2 \div \sqrt{2}/2)$ and respectively very weak dependence at $q > 10$ (Fig. 3). Similarly the initial phases ϕ and ψ strongly depend on q in the range $(1/2 \div \sqrt{2}/2)$ and are slightly influenced by the quality factor at $q > 10$ (Fig. 4).

3. DETERMINING THE PARAMETERS OF THE MEASURING SCHEME

Development of a device for nondestructive eddy current testing or measurement based on the method with shock excitation is a complex engineering task. In the present work an attempt is made to determine only the values of the elements of the measuring scheme from Fig. 1 - the capacity of the capacitor C and the resistance R_a of the auxiliary resistor. And the times should be determined t_1 of a closed switch S and respectively t_2 , when it is opened (Fig. 1).

It is considered that developed impulse ECT is available, or there is a vision for its shape, size and number of turns. If it has a magnetic core, it is necessary to be modeled precisely enough as linear.

According to the selected informative parameter (first negative/positive amplitude, average of the detection voltage, etc.) the number n is set of the periods of the damping oscillations, whose amplitudes are attenuated not more than k times. In most cases, it is appropriate that $k = e^2$.

Also it is suggested that the shape and dimensions are known, as well as electro-physical parameters (μ и γ) of the potential controlled (measured) object, which can

be ferromagnetic, but its characteristics to allow its examination as linear. Also it is considered, that with taking into account the purpose of the device, the area of control in the sample is known, expressed as the depth d from its surface, where significant eddy currents will be inducted. This allows determining the depth of penetration

$$\delta = \sqrt{\frac{2}{\mu\gamma\Omega}} = d, \quad (23)$$

and from there the angular frequency Ω of the induced eddy currents:

$$\Omega = 2\pi F = \frac{2}{\mu\gamma d^2}. \quad (24)$$

The next stage involves modeling using some of the latest software products for numerical analysis of electromagnetic fields of the system ECT – controlled object (Fig. 5). Very suitable for this purpose are the latest versions of the software product **MagNet** [6], which is used by the author to verify the effectiveness of the proposed algorithm. The model contains a component type "coil", presenting ECT from Fig. 5, powered by a sinusoidal current source with a frequency defined in (24). Due to the linearity of the model the effective value of the current may be random, but it is more convenient for the calculations, if it is taken to be 1A. The second component is the controlled object (*Sample*) from Fig. 5, from material which is user-defined and characterized by the given $\gamma = \text{const}$ and $\mu = \mu_0 \mu_r = \text{const}$. Of course, the thickness of this component must be greater than the given depth d of the control area (measurement). If the unit will be universal, i.e. various controlled (measured) objects will be controlled (measured), quick and sufficiently accurate results are obtained, if the second component is right circular conductive cylinder. Recommended for tasks from the field of NDT options and settings [7, 8] are set, and the model is solved using the solver "TIME HARMONIC" - 3D or 2D, depending on is there a proper symmetry.

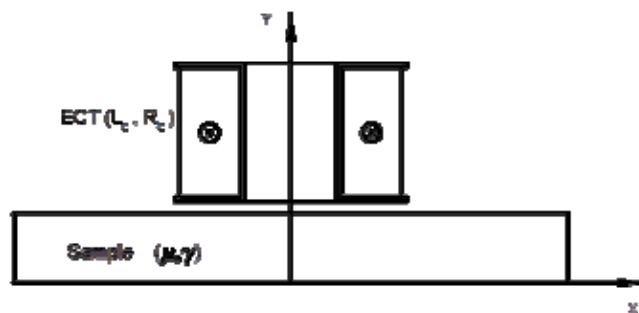


Fig. 5

The global variables full magnetic flux – Ψ , joule's losses – ΔP_C and the current through *ECT* (the component “coil”) are reported, and the parameters of the converter are defined:

$$\text{a) } L_C = \frac{\Psi}{i}; \quad \text{b) } R_C = \frac{\Delta P_C}{i^2}. \quad (25)$$

From (2), (6), (13), (24) and (25a) the equivalent resistance of the circuit after the commutation is determined:

$$R = R_c + R_a = \frac{\Omega L_c \ln k}{n\pi}, \quad (26)$$

and from (26) and (25b) – and the value of the additional resistor:

$$R_a = R - R_c. \quad (27)$$

From (9) a convenient expression is defined for calculating the capacity of the capacitor from Fig. 1:

$$C = \frac{4L_c}{4\Omega^2 L_c^2 + R^2}. \quad (28)$$

Participating in the above expression values are replaced by (25a), (24) and (26).

The time t_1 , during which the switch S is closed, is determined by (3) where the values are replaced by (25a) and (26). The time t_2 of closed switch S is easily determined from (14) and (3).

4. EXAMPLE

4.1. Input data

ECT					
Outer diameter	Inner diameter	Height	Number of turns	Core	Lift-off
10 mm	4 mm	6 mm	30	No	0,2 mm
SAMPLE					
Diameter	Height	γ	μ_r	d	
18 mm	4 mm	2 MS/m	1	1,5 mm	
CIRCUIT					
Current	n		k		
1 A	4		e^2		

4.2. Calculations

Ω	ΔP_C	S	L_C	R_C	R
353678 s^{-1}	0,019 W	$3,03 \cdot 10^{-6} \text{ Wb}$	3,03 μH	0,019 Ω	0,17 Ω

4.3. Output data

R_a	C	t_1	t_2
0,151 Ω	2,62 μF	0,124 ms	0,248 ms

4.4. Other useful quantities

ρ	q	ψ	φ
1,07 Ω	6,3	2,98 rad	1,49 rad

References

- [1] Weidelich D. L., An Analysis and Discussion of the Response of a Metal Plate to Pulsed Eddy Currents, International Conference on NDT, Hannover, 1970.
- [2] Grozdanova D. B., Study of electromagnetic processes in linear conductive environments quasi stimulant pulse field, Sofia, 1983 (in bulgarian).
- [3] Krause T.W., Prof., D. Harley, V.K. Babbar, Dr. and K. Wannamaker, Evaluation of Selective Phase Corrosion Thickness on Nickel Aluminum Bronze Valves using Transient Eddy Current, NDT in Canada National Conference, 25-27, 2009, London, Ontario, Canada.
- [4] Babbar V. K., D. Harley and T. W. Krause, Study of the Variations of Probe Parameters by Finite Element Modeling of Transient Eddy Currents in Multilayer Aluminum Structures, 6th International Workshop – NDT-Signal Processing, August, 25-27, 2009, London, Ontario, Canada.
- [5] Scottini R., H.J. Quakkelsteijn, Monitoring Average Wall Thickness of insulated or difficult to access objects with Pulsed Eddy Current, IV Conferencia Panamericana de END, Buenos Aires, Octubre, 2007.
- [6] www.ifolytica.com.
- [7] 2D Tutorial, Preparing, Solving and Interpreting NDT Problems, Infolytica Corporation, 2005.
- [8] 3D Tutorial, Preparing, Solving and Interpreting NDT Problems in 3D, Infolytica Corporation, 2006.

A SIMULINK MODEL OF SYNCHRONIZATION OF LORENZ-BASED CHAOTIC SYSTEM

Galina Cherneva, Elena Dimkina

Department of Electrical Engineering, Todor Kableshkov University of Transport,
Geo Milev Str. No158, 1574 Sofia, Bulgaria, phone: +359 888 498478,
e-mail: cherneva@vtu.bg, elena.dimkina@abv.bg

Abstract: *The Lorenz system is one of paradigms of chaos since it captures many features of chaotic systems. The chaotic Lorenz system appears frequently in theoretical studies of chaos communications. Chaotic signal transmission is based on chaos synchronization. This paper presents the computer modeling and simulation of the Lorenz-based chaotic circuit in the transmitter and in the receiver of a communication scheme by Simulink. The synchronization between the transmitter and receiver has been proved by analyzing the stability of the error signal.*

Keywords: *Lorenz system, synchronization, chaos, Simulink model, simulation*

1. INTRODUCTION

Chaotic signal transmission is based on chaos synchronization [1, 2, 3, 4]. Synchronization of chaotic oscillators is one of the fundamental phenomena of nonlinear dynamics. A typical and most widely-used scenario of the chaotic synchronization is identical synchronization, where the state of response system converges asymptotically to the state of the drive system. The drive chaotic system is located in the transmitter and the response chaotic system in the receiver in a communication scheme (Fig1). This driving response synchronization is described in [1], in which the Lorenz system is used in the transmitter and the receiver.

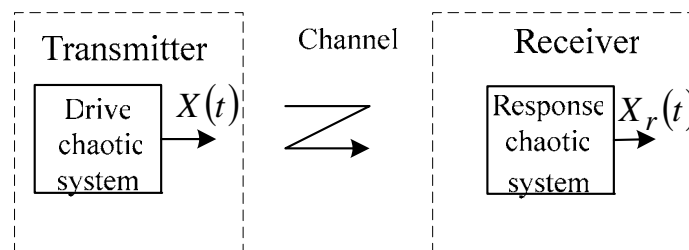


Fig. 1

This paper presents the Simulink model of synchronization between two Lorenz-based chaotic systems. According to numerical simulations, by a choice of parameters the synchronization error states converge to zero and hence the synchronization between Lorenz systems is achieved.

2. MODEL DESCRIPTION

The Lorenz system of differential equations exhibiting chaos is the simplest nonlinear three dimensional system of first order. The non-dimensional form of Lorenz system is:

$$\begin{aligned}\dot{x} &= \sigma(y - x) \\ \dot{y} &= \rho x - y - xz, \\ \dot{z} &= xy - \beta z\end{aligned}\quad (1)$$

where σ, ρ, β are parameters, and $[x \ y \ z]$ is the state vector.

Interpret equation (1) as a dynamic drive system. The response system is structurally similar to the drive system and can be written as

$$\begin{aligned}\dot{x}_r &= \sigma(y_r - x_r) \\ \dot{y}_r &= \rho x(t) - y_r - x(t)z_r. \\ \dot{z}_r &= x(t)y_r - \beta z_r\end{aligned}\quad (2)$$

The signal used for synchronization is $x(t)$.

The system is implemented with the following standard parameters [2]:

$$\sigma = 10; \rho = 28; \beta = \frac{8}{3}.$$

The parameter σ is modulated by a digital informational signal, so that it is $\sigma \pm \Delta\sigma$ if the bit is “0” or “1”. For the different values of σ is observed different chaotic attractor [5].

The coefficients of the receiver are chosen identical to that of the transmitter.

The synchronization between the transmitter (1) and receiver (2) has been proved [2] by analyzing the stability of the error signal:

$$\mathbf{e} = (x - x_r, y - y_r, z - z_r). \quad (3)$$

According to the Lyapunov theorem [1], $\mathbf{e}(t) \rightarrow 0$ asymptotically as $t \rightarrow \infty$, which implies that the synchronization between the transmitter and receiver occurs.

3. SIMULATION MODEL AND RESULTS

The Simulink model of the communication scheme with the Lorenz system in the transmitter and the receiver is shown in Fig. 2.

The communication channel is anticipated only with additive white Gaussian noise.

Figure 3 shows the error signal $\mathbf{e}(t)$ of scope:

- curve 1 – without noise added to the transmission channel;
- curve 2 – with Gaussian noise of zero mean and with a variance of 1;
- curve 3 – with Gaussian noise of zero mean and with a variance of 25.

After the synchronizing the error state of the transmitter and receiver systems is zero.

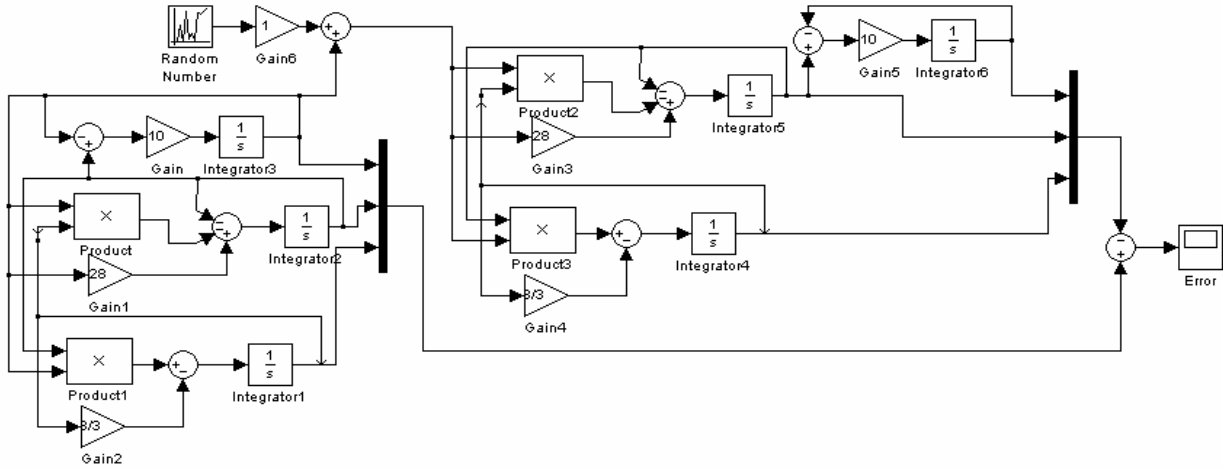


Fig. 2

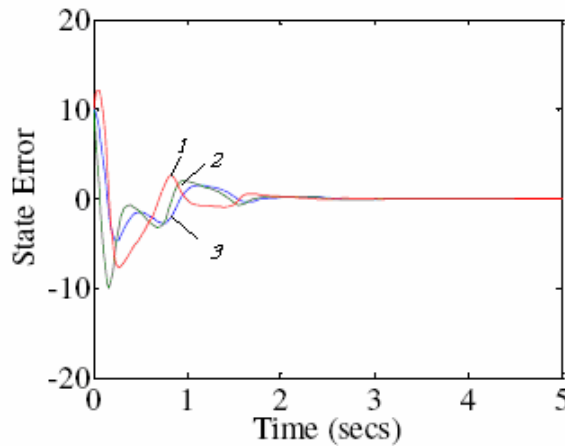


Fig. 3

4. CONCLUSION

The curve 1 (without noise) shows that the response systems states synchronize within a short period. The synchronization time is of the same order as periodic type oscillations of the chaotic system, which implies that synchronization occurs within a small number of orbits of the trajectory around the chaotic attractor.

The state errors in the second case are reasonably acceptable and it is clear that the system has indeed synchronized. That synchronization has been achieved, can be judged qualitatively by the fact that the response system states do follow the drive system's states over the simulation period.

However, in the third case the state errors are similar, throughout the simulation, to the initial errors and it is quite unclear that synchronization has been achieved.

Again from a qualitative point of view the response system's states do not follow the drive system's states. However this approximate synchronization may be acceptable dependent on the application.

References

- [1] Pecora, L. M., and Carroll, T. L. Synchronization in chaotic systems. *Phys. Rev. Lett.* 64, 8 1990
- [2] J.F. Heagy, T.L. Carroll, L.M. Pecora, Synchronization chaos in coupled oscillator systems. *Phys. Rev. E*50. 1994.
- [3] Kocarev, L., and Parlitz, U. General approach for chaotic synchronization with applications to communication. *Physical Review Letters* 74 .1995.
- [4] Celikovsk'y, S., and Chen, G. Secure synchronization of a class of chaotic systems from a nonlinear observer approach. *IEEE Transactions on Automatic Control* 50, 1 .2005.
- [5] Cherneva G., E. Dimkina. A Pspice-aided Simulation and Examination of Lorenz-Based Chaotic Circuit. XXXIV International Conference on Fundamentals of Electrotechnics and Circuit Theory IC-SPETO-2011 , 18-21.05.2011, Gliwice, Poland, p.73-74

APPLICATION OF NEURAL NETWORKS WITH DIFFERENT PARAMETERS FOR DAILY ELECTRIC LOAD FORECAST PREDICTION

Rumen Yordanov¹, Georgi Tsenov², Valeri Mladenov²

¹Department of Microelectronics, ²Department of Theoretical Electrical Engineering,
Technical University of Sofia, 8 St. Kliment Ohridski Str., 1000 Sofia, Bulgaria;
e-mail:gogotzenov@tu-sofia.bg

Abstract. *The successful electric grid load forecast prediction is an important task for the companies involved in the energy distribution industry when the economy is deregulated. The electric consumption forecasting finds many applications as is in the cases of planned inclusion or removal of power plants from the electric grid, when planning the future energy distribution infrastructure or in the markets of electrical energy trading between states and etc. In this paper are given results for energy load daily forecasting, when presenting the consumer power load as time series dataset, using Feedforward Error Backpropagation Neural Networks from the MATLAB Neural Networks Toolbox, when changing the resulting Neural Networks structure. An comparison with forecasts based on mean average value of the power load data from the previous week is also presented.*

Keywords: *time series forecasting, grid electric load, neural networks*

1. INTRODUCTION

In the electric power distribution systems the prediction of the consumed electric power is very important. An essential element of electric utility resource planning is the successful short or long term forecast of the electrical consumption. It is so, because in order the delivery of electric energy to be efficient the operators from the distribution companies will need to know for instance, which are the nodes with higher expected instantaneous load, in which hours of the day are the peak network distribution loads, what is the quality of the supplied electrical energy, what are the effects from power savings and etc.

A definite prerequisite for development of an accurate forecast model is the understanding of the characteristics of the consumers that are going to be analysed. The knowledge about the load behavior can be learned from experience with usage of consumer data and statistical analysis of electrical consumption from the past. Usually electricity consumers are operating in a similar economic and climate environment, and usually we have similar consumer behavior and consumption forecast models developed for a consumer can usually be easily adapted for use with another consumer. Load that is supplied by a power distribution system has a dynamic development and reflects directly the activities and conditions in the environment.

In this paper is presented an approach for adequate forecast of electricity consumption. The forecast is done by usage of artificial neural networks (ANN) based on historical data for several transmission nodes in Bulgaria. It involves the development

of several ANN designs and selection of the best network that can produce the best results in terms of its accuracy. Also, a comparison is presented between prediction using mean average of several preceding days and ANN method.

2. SHORT INTRODUCTION IN THE NEURAL NETWORK THEORY

The neural networks are parallel processing systems with the capability of storing experimental knowledge. Basically every neural network consists of simple information processing elements named neurons. Every neuron is interconnected with the others and the weights of these connections determine their strength. Every neuron input data is the weighted sum of the signals of the other neurons connected to it, while the neuron output is determined by a transfer function based on the weighted input sum value. The information in one neural network is accumulated in a training process, where the strength of the connections between the various nodes is modeled with weights on the according connections, which are used for information storage.

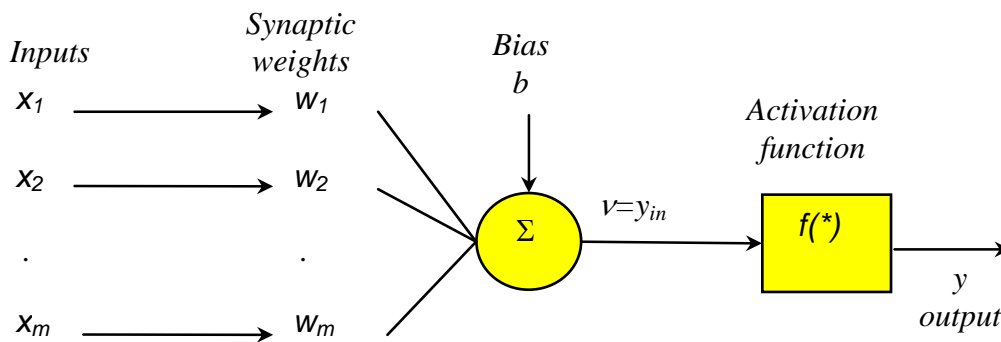


Fig. 1. Single neuron abstract mathematical model

Every neuron have many inputs and one output. Inputs x_1, x_2, \dots, x_m are the signals coming to the neuron and can be external signals or other neuron outputs. Every input is connected with weight $w_j, j=1,2, \dots, m$, that models the strength of the transduced signal. The aggregated input signals are modeled with sumator unit:

$$v = y_{in} = \sum_{j=1}^m w_j x_j + b \tag{1}$$

For convenience, constant signals are modeled with bias b . In most of the cases the activation function is nonlinear and the single neuron output is:

$$y = f(y_{in}) = f\left(\sum_{j=1}^m w_j x_j + b\right) \tag{2}$$

Neural networks can be realized in different structures, but the classical structure is with two layers of neurons Feedforward error backpropagation as shown on Fig. 2.

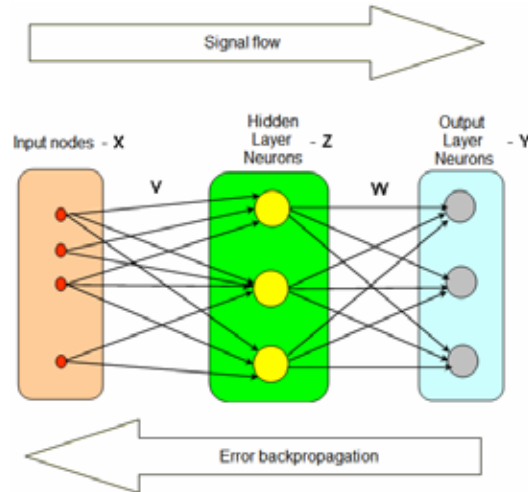


Fig. 2. Two layer Feedforward neural network architecture

Neuron number in the input layer is determined by the input data dimensions, and the same is valid for the output layer. For this structure by a rule of thumb defined by Oja the optimal neuron number in the hidden layer can be determined. If with Z is denoted the hidden layer neuron number, with P number of samples in the training dataset, m is input numbers and n is the output layer dimension, then:

$$Z = \frac{P}{5(m + n)} \tag{3}$$

3. SIMULATION MODELING AND RESULTS

The forecasting results are based on data from preceding time intervals. For training the neural network we have the daily data of consumption in 24 high voltage nodes for year 2006 and the data from year 2007 is used for testing and validation. This data we have was in the for as shown on Table 1.

Table 1. Data from 24 high voltage nodes

Year	Month	Day	Node 1	Node 2	Node 3	Node 4	***	Node 22	Node 23	Node 24	P daily summed
2006	1	1	4293	4186	4026	3877	***	4301	4346	4335	29364
2006	1	2	4030	3823	3678	3571	***	4806	4809	4684	29401
2006	1	3	4307	4045	3897	3811	***	5017	5044	4868	30989
2006	1	4	4568	4319	4119	4024	***	5136	5229	4990	32385
2006	1	5	4625	4289	4128	4088	***	5248	5281	5045	32704
2006	1	6	4741	4412	4268	4183	***	5379	5389	5310	33682
2006	1	7	4872	4612	4445	4362	***	5107	5213	5147	33758
2006	1	8	4915	4614	4421	4282	***	5514	5631	5343	34720
2006	1	9	4936	4538	4494	4379	***	5609	5800	5512	35268
2006	1	10	5116	4775	4646	4589	***	5688	5806	5574	36194
2006	1	11	5139	4749	4652	4514	***	5801	5879	5593	36327

From this data that we have the training dataset is formed by packing every n number of days consecutive sequence as input sample and the next following sample as desired output. One example for the timeseries training dataset formation for forecast based on 7 preceding days and 8-th day used for desired output is shown on Fig. 3.

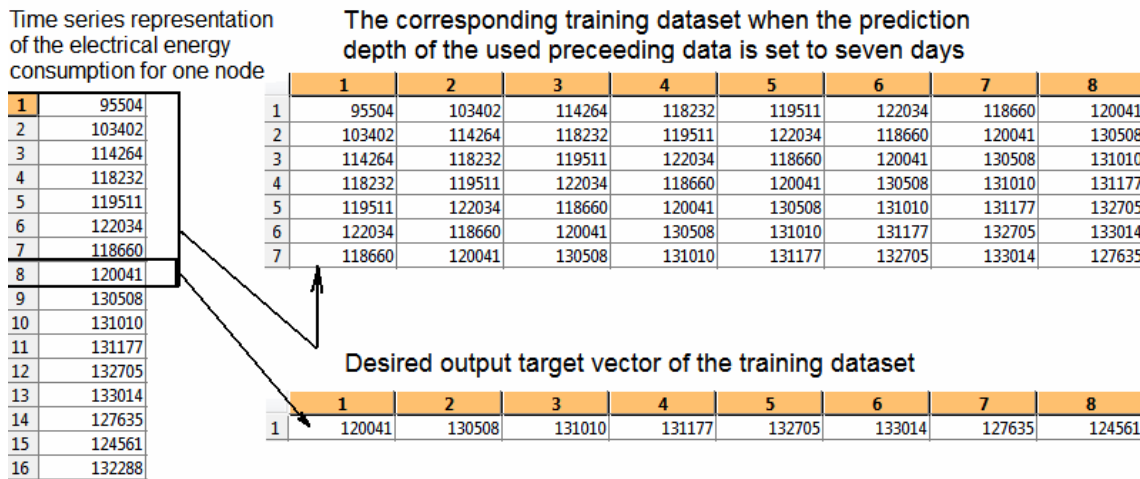


Fig. 3. Training dataset formation

We used generation of ANN in MATLAB with the Neural Network Toolbox function newff for creation of multilayer feedforward networks. After forming the training dataset a training is performed on the created structures. For the example when using prediction depth $n=7$ days for only next day forecast window, this results in 7 ANN inputs representing the preceding day 1, day 2, ..., day 7 and one output neuron for day 8. The number of neurons in the hidden layer can be determined with (3), which in this particular case gives 9 neurons forming the hidden layer.

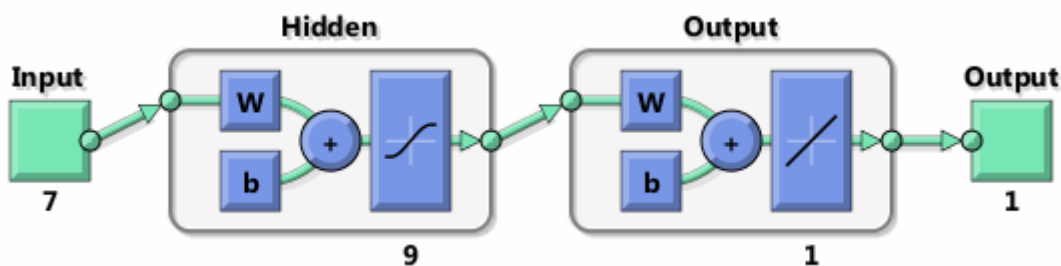


Fig. 4. ANN for daily forecast based on data from the preceding week

After training the ANN with data from year 2006 for testing the adequateness we used the data from 2007. On Fig. 5 is shown an result comparison between actual and predicted value for the energy consumption. From the graph easily is seen that the ANN approximates very well the data and that there are no big differences between predicted and actual data.

In the industry practice one simple method for electricity load consumption prediction is used with having the forecast being mean average of n preceding days:

$$P_{\text{prognosed}} = \frac{\sum_{\text{day}=1}^n P_{\text{day}}}{n} \quad (4)$$

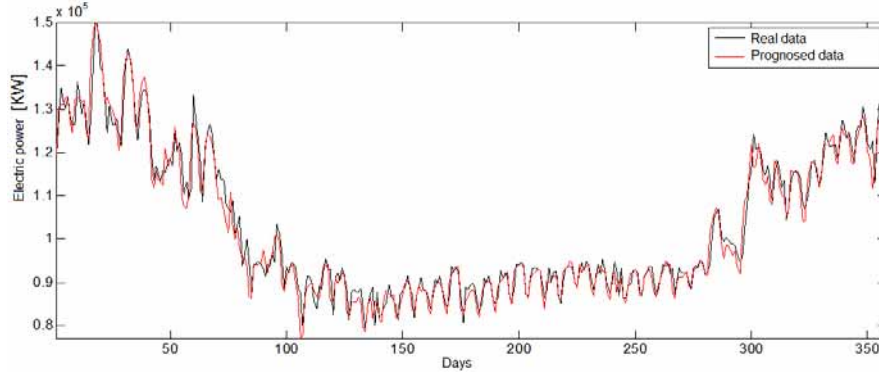


Fig. 5. Comparison of daily consumption between real and prognosed data in one node for one year

We made a comparison with this technique showing the results on Fig. 6 and Fig. 7. As it can be seen the ANN method is better as it yields more adequate and correct data forecast prediction. We also created a variation of the number of neurons in the hidden layer ranging them from -2 to +2 from the Oja rule (3) and variation on the prediction depth from 4 to 9 days. The results from the tested data and the corresponding percentage error are presented in Table 2 and they don't vary much.

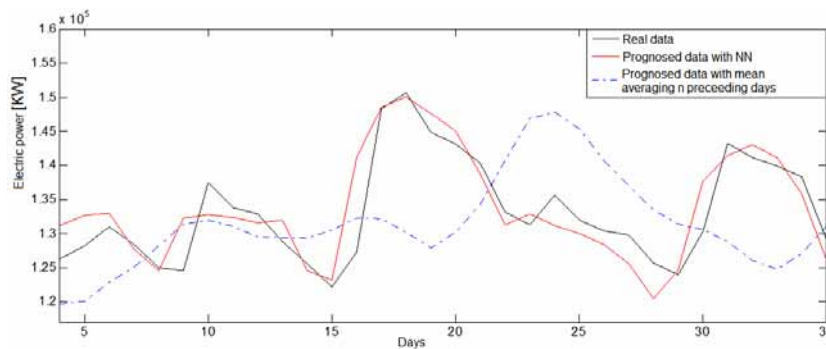


Fig. 6. Prediction methods comparison for n=4 days

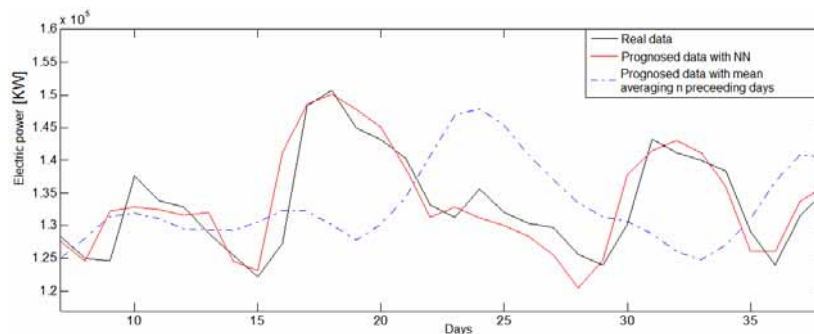
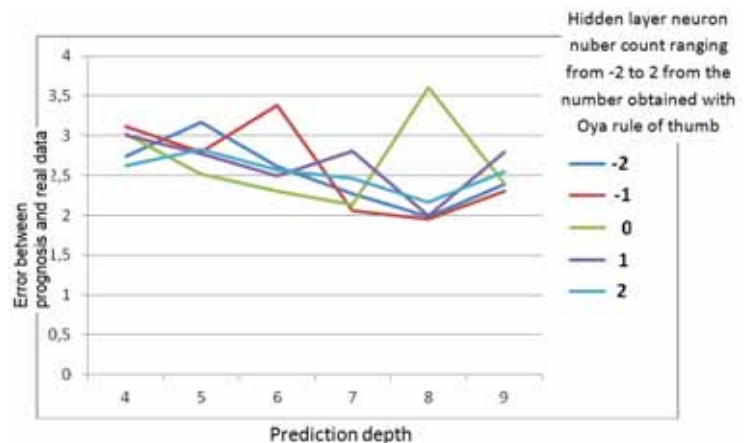


Fig. 7. Prediction methods comparison for n=7 days

Table 2. Percent error between forecast and actual data for ANN hidden layer neuron and prediction depth variation

	Prediction depth						
	4	5	6	7	8	9	
Hidden layer neuron nuber count ranging from -2 to 2 from the number obtained with Oja rule of thumb	-2	2,74%	3,17%	2,61%	2,27%	1,98%	2,39%
	-1	3,12%	2,8%	3,38%	2,06%	1,95%	2,3%
	0	3,02%	2,52%	2,3%	2,13%	3,61%	2,4%
	1	3,01%	2,77%	2,5%	2,81%	1,99%	2,79%
	2	2,62%	2,83%	2,57%	2,46%	2,16%	2,55%



4. CONCLUSION

After making comparison with forecasting on the electricity consumption based on mean average of preceding days samples or with neural networks shows that the prognosis with neural networks are more accurate than the classical approach. The developed neural network model yield very satisfactory results and this leads to the conclusion that, the range of electricity consumption can be successfully obtained when needed.

References

- [1] S. Haykin, "Neural Networks", Macmillan College Publishing Co. Inc. 1994.
- [2] F. F. Wu and P. Varaiya, "Coordinated multilateral trades for electric power networks: theory and implementation 1", *Electrical Power and Energy Systems* 21, pp.75-102, 1999
- [3] Othman, M.S.M. , Artificial neural network-based forecast for electricity consumption in Malaysia, *Power and Energy (PECon) 2010 IEEE International Conference*, pp. 24 - 28
- [4] Danilo Bassi, Oscar Olivares, Medium Term Electric Load Forecasting Using TLFN Neural Networks, *International Journal of Computers, Communications & Control* Vol. I (2006), No. 2, pp. 23-32.
- [5] The MathWorks, Inc., MATLAB 2010b, 24 Prime Park Way, Natick MA, 2010.

HUMIDITY SENSING ELEMENTS BASED ON CE-DOPED SiO₂ FILMS PREPARED VIA A SOL-GEL METHOD

Zvezditzia Nenova¹, Toshko Nenov¹, Stephan Kozhukharov², Nedyu Nedev¹

¹Technical University of Gabrovo, 4 H.Dimitar Str., 5300 Gabrovo, Bulgaria
phone: (+359) 66 827 376, e-mail: nenova@tugab.bg

²University of Chemical Technology and Metallurgy, 8 Kliment Ohridski Blvd.,
1756 Sofia, Bulgaria

Abstract. Humidity sensing elements are developed using a sol-gel method to deposit SiO₂ films with additions of Ce-compounds on alumina substrates. The samples are sintered at temperatures 400°C and 800°C in order to investigate its influence on the properties and characteristics of the sensing elements. The surface morphology, chemical composition of the films, and their electrical characteristics have been investigated. An equivalent electric circuit of the sensing element has been obtained. The results obtained show that using Ce(NO₃)₃ as a dopant and a sintering temperature of 400°C lead to SiO₂-based sensing elements with good humidity sensitivity.

Keywords: humidity, sensing elements, sol-gel method, silica, cerium-dopant

1. INTRODUCTION

Humidity measurement in gas mixtures, and in air, in particular, is a relevant problem in many scientific and technical fields. This measurement is necessary for industrial processes (textile, chemical, metallurgy, microelectronics, etc.), in meteorology, agriculture, storage of products, art works, etc. This necessitates the improvement of existing and development of new humidity sensors. One such direction is the preparation of thin film humidity sensing elements based on oxide materials by a sol-gel method [1, 2]. This method enables the synthesis of nanostructured ceramic films. The specific features of the nanostructured materials should lead to humidity sensing elements with improved parameters and characteristics and leads to decrease in the size of these elements.

Various metallic oxides are available for preparation of this kind of sensor elements, as for instance: TiO₂, ZnO, Fe₂O₃, Al₂O₃, SnO₂, etc. [3]. Humidity sensing elements based on SiO₂ are less studied. Its application for the preparation of humidity sensing elements with nanostructure is promising, since it enables their integration with other elements in the semi-conductor technology. Previous studies [4 - 6] have investigated SiO₂-based sensor elements obtained by the sol-gel route, using tetraethyl orthosilicate (TEOS) as a precursor. The influence of humidity on sol-gel derived SiO₂-based films, doped with Fe₂O₃ has also been studied [7, 8].

The present paper proposes thin film humidity sensing elements based on SiO₂, doped with Ce and prepared via a sol-gel method. The characteristics and parameters of the sensing elements obtained at different sintering temperatures have been investigated. Their impedance characteristics and equivalent electric circuit have also been determined.

2. EXPERIMENTAL

2.1. Sample preparation

Initially, 60 ml TEOS, produced by Alfa Aesar (Germany), were added to 40 ml n-Butanol (n-BuOH), preliminary heated up to 70°C in a covered beaker, by dripping for 30 minutes, while stirring by magnetic stirrer. Afterwards, 1.0056g cerous nitrate $Ce(NO_3)_3$ – Alfa Aesar (Germany) and 2ml concentrated HNO_3 was added to the obtained solution. It was left at 70°C for 1 hour, while being stirred, and then, cooled at room temperature for 20 min. The sol-gel system obtained in this way was left for one day at 5°C, in a covered vessel, in order to avoid whatever evaporation of its ingredients, during the polymerization process.

The film was deposited via a dip-coating procedure [1] by triple dipping of alumina substrates with preliminary deposited interdigitated silver-palladium electrodes. The procedure was performed by subsequent dipping of the substrates in the solution for 30 minutes at 70°C, and drying at the same temperature. Finally, the samples were sintered for 30 min either at 400 °C, or at 800°C. The samples are market as: S_400 or S_800, respectively.

2.2. Measurements

Surface morphology and chemical characterization: Observations by Scanning Electronic Microscopy (SEM), together with Energy Dispersive X-ray Spectroscopy (EDX) were performed in order to determine the features of the respective surface films. They were done by Scanning Electronic Microscope TESCAN, SEM/FIB LYRA I XMU and Energy Dispersion Spectrometer (Quantax 200 of BRUKER detector), respectively.

Electrical characteristics and parameters: The measurement of the impedance of the obtained samples was performed by Precision Impedance Analyzer 6505P product of Wayne Kerr Electronics Ltd, at 1 kHz frequency and 500 mV amplitude of the excitation signal. The influence of frequency was investigated in the range of 100Hz to 1 MHz. The samples were put inside a humidity conditioning chamber VAPORTRON H-100BL, produced by BUCK RESEARCH INSTRUMENTS L.L.C., which provides conditioning of accurate controlled humidity in a range of 15 to 95% with maximal deviation of up to 1.5% of relative humidity.

3. RESULTS AND DISCUSSIONS

3.1. Scanning Electronic Microscopy

Figure 1 presents low magnification SEM-images of the surface of prepared samples S_400 and S_800. These images show that the sintering temperature affects the size of the crystals and intercrystalline areas. It can be concluded that after sintering

at 800°C, the respective crystals and intercrystalline areas have larger sizes than after sintering at 400°C.

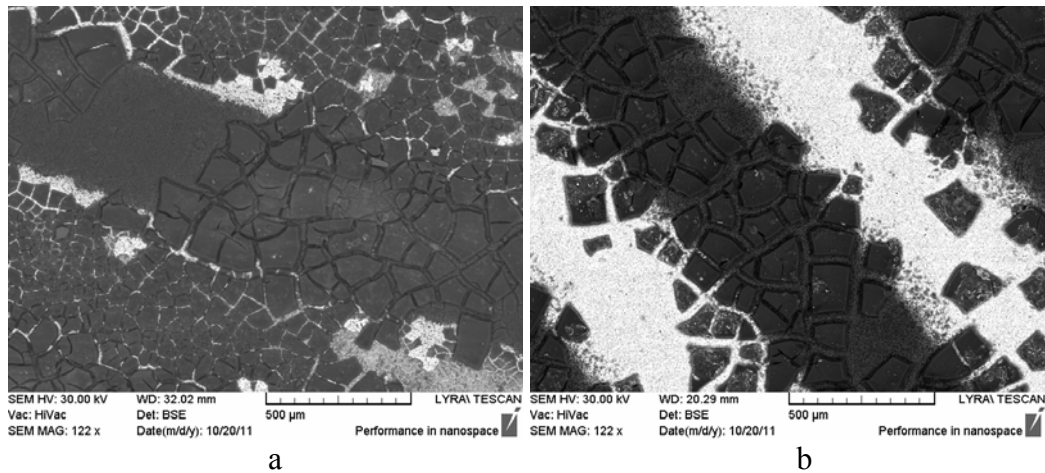


Fig. 1. SEM – images of samples: (a) S_400; (b) S_800

3.2. Energy Dispersive X-ray Analysis

A point-quantitative analysis has been performed on the surfaces of selected crystals obtained from the sol-gel derived films. Figure 2 shows the compositions by elements of sample S_400, determined by EDX analysis. The results obtained show that the crystals are built from Ce, Si, and oxygen. The simultaneous presence of both metallic elements in the oxide crystals indicates that they are likely composed of partially Ce- substituted SiO_2 . This fact suggests that the crystals are composed of $\text{Ce}_x\text{Si}_{(1-x)}\text{O}_{3-\delta}$ solid solution, or Ce- doped SiO_2 in Ce/ SiO_2 sol-gel products.

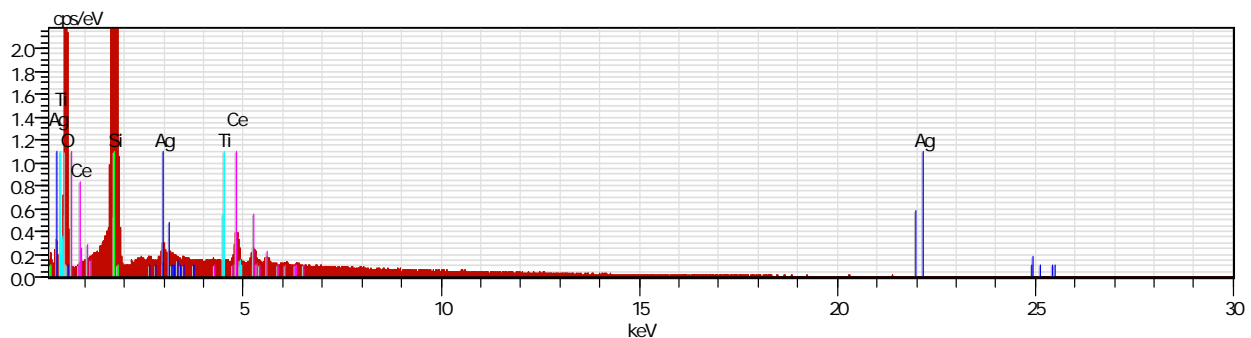


Fig. 2. Point-quantitative analysis for sample S_400

3.3. Electrical measurements

The humidity sensing elements of metaloxide materials are characterized by ionic conductivity given water adsorption [9]. As a result, there are polarization effects in measurements with direct current. This necessitates their investigation with alternating current. The elements are normally represented by an equivalent circuit of resistors and capacitors connected in parallel [10].

Figure 3 presents the characteristics $R=f(RH)$ of the samples S_400 and S_800 at a temperature of 25°C, where R is their electric resistance and RH is relative humidity.

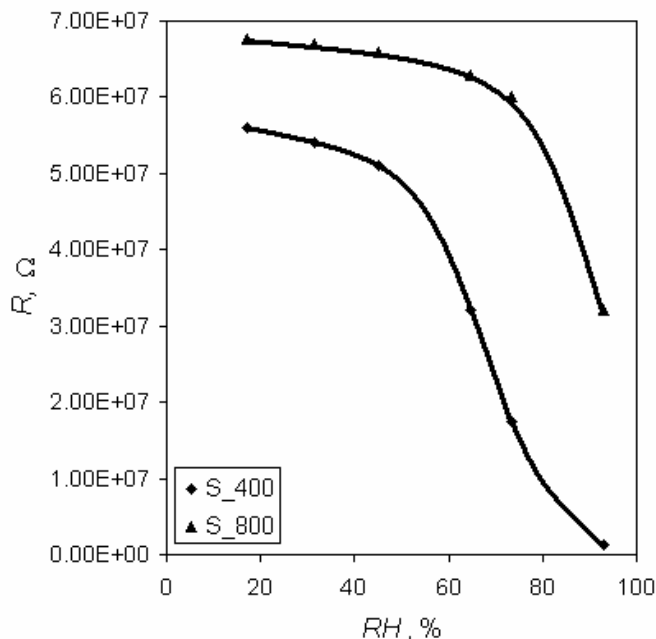


Fig. 3. Characteristics $R=f(RH)$ of samples S_400 and S_800 at a temperature of 25°C

The sample S_400, sintered at temperature 400°C, reveal higher sensitivity of resistance, S_R , to changes in relative humidity, RH , compared to the sample S_800, sintered at 800°C temperature. Sample S_400 has the highest sensitivity of about 1.7 MΩ/%RH in the range 40...82 %RH, and in the range 15...40%RH and over 82%RH this sensitivity is lower, being around 220kΩ/%RH. Sample S_800 has relatively lower sensitivity than sample S_400. It is around 150kΩ/%RH in the 15 to 80%RH range and there is also a sharp increase of its sensitivity for relative humidity above 80%RH, where it reaches 1.8 MΩ/%RH.

As mentioned above, the ionic conductivity of the type of humidity sensing elements investigated here changes as a result of adsorption and desorption of water. The resistance of the sensor element decreases with an increase in the relative humidity due to the physical adsorption and condensation of water molecules in the inter-crystalline areas. The operating principle of such sensors is described in [11, 12]. In the initial stage of adsorption there is chemical adsorption of water molecules on the surface of crystals. The active role in this process is played by metallic atoms, M . They interact with the water molecules to form hydroxyl groups $M-OH$. In this way the surface of crystals is covered by a monolayer of water molecules.

After the formation of the first chemically adsorbed layer there is physical adsorption of water molecules on it. The physically adsorbed layer is more weakly connected to the surface of crystals. The process of condensation of water vapors depends on the size and distribution of the intercrystalline areas in the thin film. The filling of areas with smaller size starts at lower humidity, while the filling of areas with larger size happens at higher humidity.

Based on the structure of the samples from the SEM images in Figure 1 and investigations of the electrical properties (Figure 3), it can be concluded that an increase in the sintering temperature increases the size of the intercrystalline areas, lowers the sensitivity of the elements at lower humidity, and increases the sensitivity at higher humidity. This correlation between intercrystalline area size and sensitivities corresponds to the water vapor adsorption mechanism described above.

Therefore, the samples sintered at 400°C, has better properties, compared to those

sintered at 800°C. On the basis of the characteristics obtained it can be concluded that the samples S_400 can be used as sensing elements in the range 15...93%RH, and samples S_800 can be used as key-elements for humidity sensing.

The frequency characteristics of the samples were also investigated. The characteristics $z(f)$ and $\theta(f)$ for the samples S_400 at $RH = 93\%$ and a temperature of 25°C are shown in Figure 4. An increase in frequency leads to a decrease in the impedance z , and an increase in the phase angle of the sensor elements S_400.



Fig. 4. Frequency characteristics of sample S_400 at $RH = 97\%$ and a temperature of 25°C

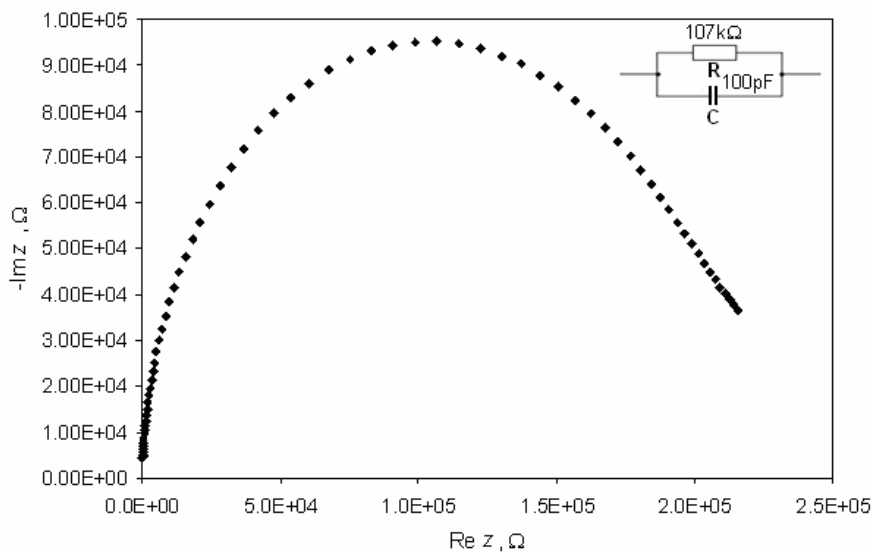


Fig. 5. Dependence of reactive resistance on active resistance for sample S_400 at relative humidity of 97% and a temperature of 25°C

Based on the dependences $z(f)$ and $\theta(f)$ the dependence of reactive resistance on active resistance for sample S_400 at relative humidity of 97% and a temperature of 25°C has been obtained. This is shown in Figure 5. An equivalent electric circuit for the sensor element has also been determined. It is a resistor and capacitor connected in parallel.

4. CONCLUSIONS

Humidity sensing elements were obtained based on SiO₂ films with additions of Ce-compounds using a sol-gel method. Among the samples investigated in the present work, increasing the sintering temperature from 400°C to 800°C increases the size of the crystals and intercrystalline areas, which in turn leads to a change in the samples' electrical characteristics and parameters. Regarding the application of the obtained samples as humidity sensing elements the best humidity sensing properties have the samples treated for 30 minutes in solution with Ce(NO₃)₃ and sintered at 400°C. The samples, sintered at 800°C, can be used as key-elements.

References

- [1] Brinker C.J., G.W. Scherer, "Sol-Gel Science: The Physical and Chemistry of Sol-Gel Processing," Academic Press. San Diego-New York-Boston, 1990.
- [2] E. Traversa, "Ceramic sensors for humidity detection: the state-of-the-art and future developments," Sensors and Actuators B 23, 1995, pp. 135–156.
- [3] Nenov, T., S.Yordanov, "Ceramic Sensors: Technology and Applications," TECHNOMIC Publ. Co., Inc. Lancaster-Basel, 1996.
- [4] P. Innocenzi, A. Martucci, M. Guglielmi, A. Bearzotti, E. Traversa, "Electrical and structural characterization of mesoporous silica thin films as humidity sensors," Sensors and Actuators B 76, 2001, pp. 299–303.
- [5] C.-T. Wang, C.-L. Wu, I.-C. Chen, Yi-H. Huang, "Humidity sensors based on silica nanoparticle aerogel thin films," Sensors and Actuators B 107, 2005, pp. 402–410.
- [6] J. Tua, N. Li, W. Geng, R. Wang, X. Lai, Y. Cao, T. Zhang, X. Li, S. Qiu, "Study on a type of mesoporous silica humidity sensing material," Sensors and Actuators B 166-167, 2012, pp. 758–764.
- [7] R. Tongpool, S. Jindasuwan, "Sol-gel processed iron oxide-silica nanocomposite films as room-temperature humidity sensors," Sensors and Actuators B 106, 2005, pp. 523–528.
- [8] Q. Qia, T. Zhanga, X. Zheng, L. Wan, "Preparation and humidity sensing properties of Fe-doped mesoporous silica SBA-15," Sensors and Actuators B 135, 2008, pp. 255–261.
- [9] T. Seiyama, N. Yamazoe, H. Arai, "Ceramic humidity sensors," Sensors and Actuators, Vol.4, 1983, pp. 85-96.
- [10] M.K. Jain, M.C. Bhatnagar, G.L. Sharma, "Electric circuit model for MgO-doped ZrO₂-TiO₂ ceramic humidity sensor," Applied Physics Letters, Vol.73, 1998, No 26, pp.3854-3856.
- [11] J.H. Anderson, G.A. Parks, "The electrical conductivity of silica gel in the presence of adsorbed water," J. Phys.Chem., Vol.72, 10, 1968, pp.3662-3668.
- [12] E. McCafferty, A.C. Zettlemoyer, "Adsorption of water vapour on α -Fe₂O₃," Discuss. Faraday Soc., Vol.52, 1971, pp.239-254.

RESEARCHING OF TACTILE SENSORS RESONANT TYPE

Vasilina Georgieva Zlatanova, Nikola Petrov Georgiev

Department "Electrical Engineering", Technical University of Sofia, Branch Plovdiv,
25 Tsanko Dyustabanov Str., 4000 Plovdiv, *phone:*
0359 895 587257, e-mail: v_zlatanowa@abv.bg;
032 659 592, e-mail: geotek@abv.bg

Abstract. *This paper presents an opportunity to investigate tactile sensors operating in resonant mode, based on theoretical and experimental results. The substitutional electrical circuit consists of a series-connected coil and a capacitor controlled by introduced resistance. Modeling and simulation of the performance of the sensor used is carried out by means of the software OrCAD PSpice 9.2. An analysis of the change of the output voltage, the resonant frequency and the sensitivity is done at change in the parameters of the electrical circuit.*

Keywords: *sensors, tactile, resonance, sensitivity*

1. INTRODUCTION

For the purpose of recognizing images, determining the size of objects, searching for objects, perceiving the mechanical movement of a sensitive element under the influence of a force, the so called tactile sensors are used.

Sensor devices absorb information at different distances from the source. According to this indicator the sensors can be categorized into such with: long-range action in the work area and overly long-range action (outside the work area); action near the work area and contact ones (with overly short range action) [1].

The tactile sensors are used in the production of touch screens, keypads and other devices where physical contact is needed to be sensed.

Based on the fact that the sense of touch is always associated with a direct contact with the object, the tactile sensors studied in this work are defined as part of the contact group converters.

For the contact sensing devices the mechanical interaction between the sensor and the object is directly converted into electrical signal. These devices are characterized by simple technical realization and low cost both in terms of the sensors used and in the schemes for control and processing the signals coming from them [1].

The aim of this study is to investigate tactile sensors whose operation is based on an effect associated with the conductivity of a living tissue, i.e. when touched with a finger.

2. THEORETICAL JUSTIFICATION AND SIMULATION WITH ORCAD PSpICE

The wiring diagram of the investigated tactile sensor is presented in Fig. 1, as a simplified version of an *RLC* circuit, operating in resonant mode [2]. Reactive ele-

ments C and L with different values are used, as given in Table 1, and the goal is to determine both the resonant frequency and the output voltage recorded on the capacitor C , while the key is in position 1 (Fig. 2).

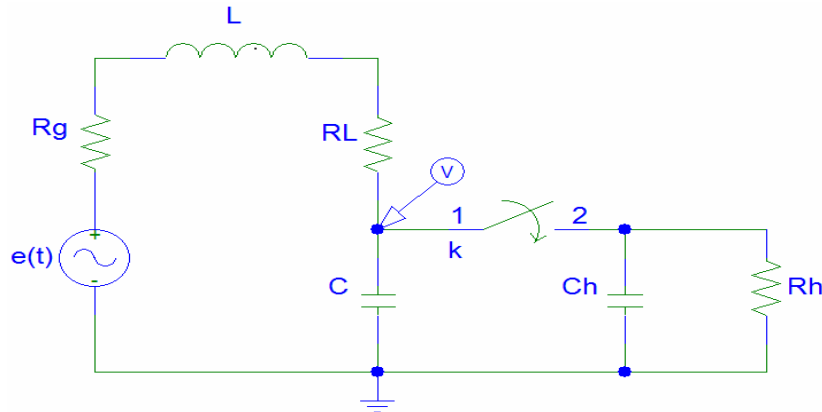


Fig. 1. Principal scheme

Together with closing the switch, activation of the sensor is simulated by a human touch. The complex impedance introduced by the human is modeled in the form of a simplified circuit consisting of a resistor and a capacitor in parallel (R_h and C_h). The resistance of the human body is a variable depending nonlinearly both on various physiological factors and on the parameters of the circuit [3]. The inner resistance of the generator used in the experiment is marked with $R_g = 50\Omega$ and the active resistance of the real coil is noted as R_L .

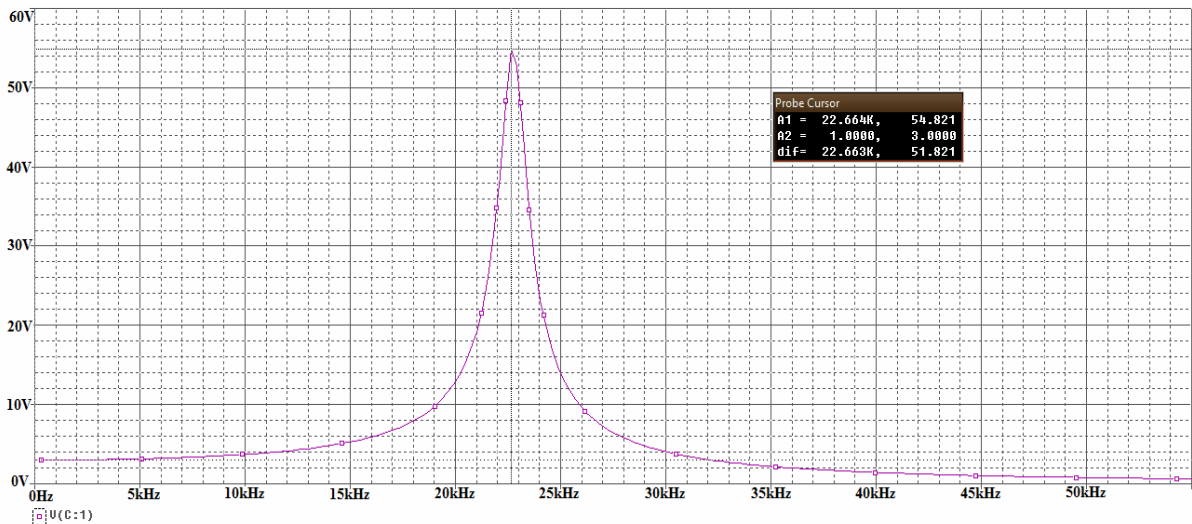


Fig. 2. Output voltage before switching

The graph in Fig. 2 shows the operation of the circuit before the commutation (when in idle mode), by which the resonant frequency and the value of the voltage on the capacitor C are determined.

From the simulations it is clear that the resulting graphs have quite steep character around the point of resonance and the small change in the resonant frequency range

leads to large changes in the output voltage. This is of great significance for the further practical measurements.

After closing the switch, the circuit goes out of resonance and the output voltage U_C reduces.

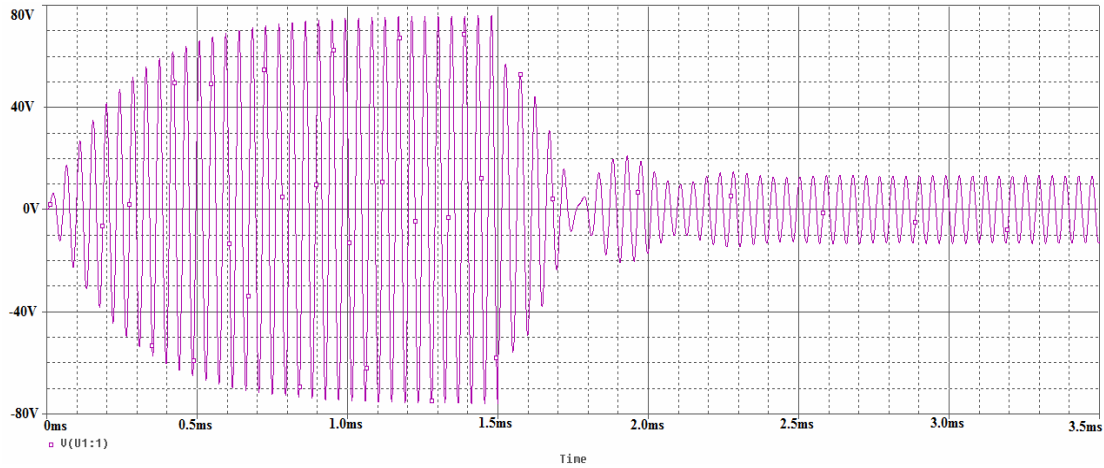


Fig. 3. Changes in the output voltage before and after contact

Fig. 3 clearly shows the voltage before and after the commutation (analogous to the touch by hand), as well as the ongoing transition process, whose duration is about 1ms.

The results of all simulations are shown graphically in comparison with those of the experimental studies (fig. 4, fig. 5 and fig. 6).

For the used electric circuit the following equations are worked out for the resonant frequency and the effective value of the output voltage:

– unloaded

$$U_C = \frac{E}{\sqrt{(1-\omega^2 LC)^2 + \omega^2 (R_g + R_L)^2 C^2}}; \quad \omega_p = \frac{1}{\sqrt{LC}} \quad (1)$$

– with imported resistance

$$U_{U3X} = \frac{E}{\sqrt{\left[1 + \frac{R_g + R_L}{R_h} - \omega^2 L(C + C_h)\right]^2 + \omega^2 \left[(R_g + R_h)(C + C_h) + \frac{L}{R_h}\right]^2}} \quad (2)$$

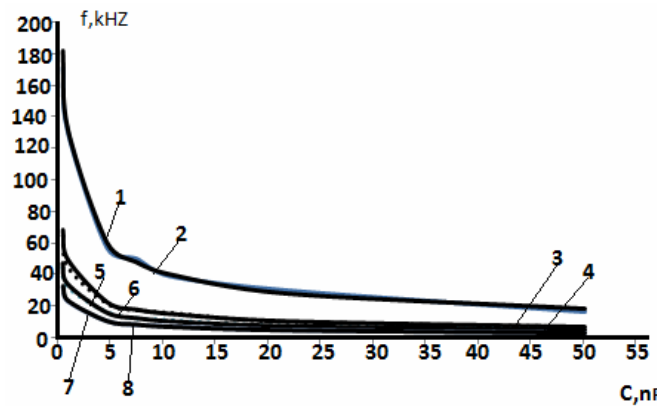
3. EXPERIMENTAL RESEARCH

Experimental data were collected for the circuit shown in Fig. 1, for different values of the reactive elements, given in Table. 1. Combinations of six capacitors and four coils are implemented.

Table 1. Parameters of the reactive elements

L, mH	1.484	10.4	22.2	45.7		
R_L, Ω	14.3	30.7	61.4	131.4		
C, nF	0.52	1	4.72	7.51	10.68	50.2

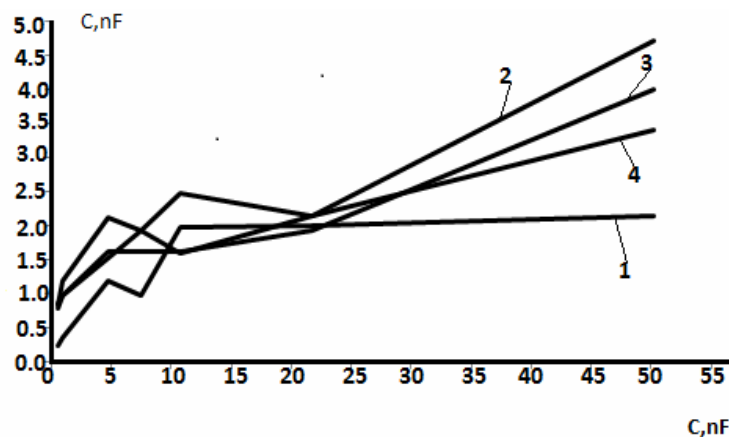
The graphs in fig. 4 show the change in the resonant frequency, which, at the lower values of the capacitor and of the coil can reach up to several hundred kilohertz. The experimental values are very close to the simulation ones.



1,2 – experimental and simulation graphics for $L=1.484 mH$;
 3,4 – respective for $L=10.4 mH$; 5,6 – for $L=22.2 mH$; 7,8 – for $L=45.7 mH$

Fig. 4. Resonance frequency

During the experiment, the activation of the sensor is done by hand touch. The conductivity of the living tissue differs from that of a conventional conductor not only in physical properties, but also in the higher complexity of biochemical and biophysical processes. In the substitutional circuit for the resistance of the human body the active resistance $R_h = 100k\Omega$ is taken for constant and the change in the human capacity is measured. In Fig. 5 it can be seen that C_h increases with the growth of the capacitor, used in the circuit.



1–for $L=1.484 mH$
 2– for $L=10.4 mH$
 3– for $L=22.2 mH$
 4– for $L=45.7 mH$

Fig. 5. Changes in the capacity of the human body

The measured values of the output voltage at idle run are shown in Fig. 6 compared with those in the simulations. Differences are observed mainly in the capacitors, which are lower in value, i.e., at the higher resonant frequencies. Best results are reported in the coils $L = 1.484mH$ and $L = 10.4mH$.

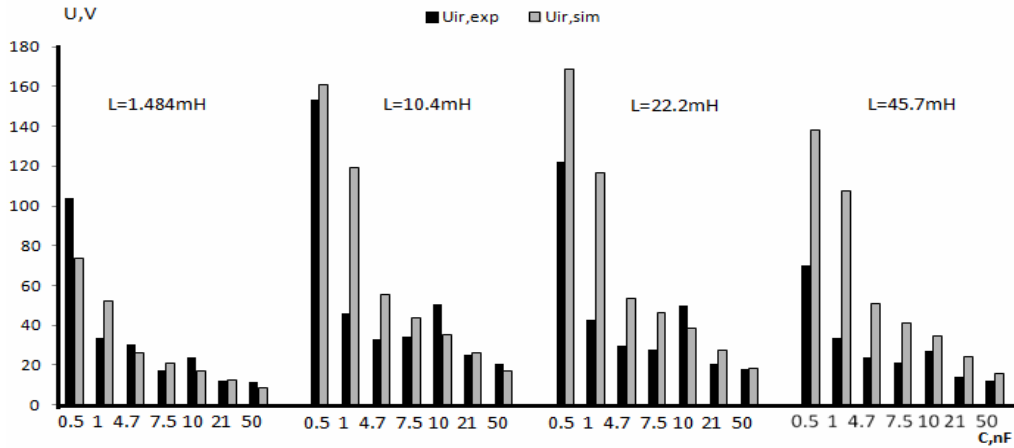


Fig. 6. Change in the voltage at idle run

Essential to the operation of the sensor is the magnitude of the change in the output voltage after its activation (touch by a man). The greater the difference, the better the sensitivity of the sensor. The graphs in Fig. 7 show that this is achieved for the capacitor C , having a lower value.

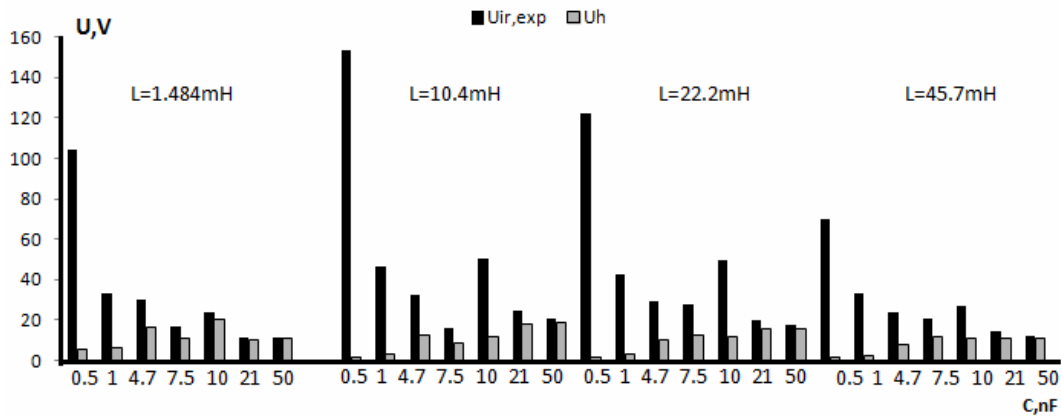


Fig. 7. Changes in the output voltage after activation of the sensor

Table 2. Percentage change in the output voltage

	C, nF	0,520	1	4,72	7,51	10,68	21,7
$L=1,484mH$	$\delta_U, \%$	94,81	81,54	45,16	37,86	13,88	13,90
$L=10,4mH$	$\delta_U, \%$	98,79	92,19	61,75	58,67	76,10	25,81
$L=22,2mH$	$\delta_U, \%$	98,53	92,47	66,30	54,36	76,91	24,56
$L=45,7mH$	$\delta_U, \%$	95,99	76,58	50,72	47,07	58,44	19,49

The data in Table 2, show that with the capacitor $C = 0.520, 1 nF$, the voltage drop after the activation of the sensor exceeds 90%.

4. CONCLUSIONS AND RECOMMENDATIONS

There are software simulations and experimental studies of tactile sensors operating in resonant mode, activated when touched by a person. In the process of determining the resonant frequency very good match is found between the experimental results and those from the computer simulation.

In terms of the output voltage when idling, there are some differences between the experimental and simulation results, especially in the range of the higher frequencies. At the same time, in the same range the sensor sensitivity is the highest. Taking into account the complex and nonlinear character of the human resistance, the selection of the sensor elements becomes more complicated.

A disadvantage of the investigated sensors is the error caused by the parasitic capacity of the connecting conductors. Therefore in further investigations special attention should be paid to shielding the connecting conductors and right choice of the grounding point.

References

- [1] M. Valtchev, 'Labour Safety "Technique, Sofia, 1990, pp.82-85.
- [2] Y. Marinov and V. Dimitrov, "Sensor devices for robots" Technique, Sofia, 1982, pp.9-15.
- [3] L. Genov, "Theoretical Foundations of Electrical Engineering", Technique, Sofia, 1991, pp. 146-150.
- [4] K. Brandisky, V. Mladenov and K. Stanchev, "Guidance for solving problems in electrical engineering with PSpice", Sofia, 2010.
- [5] P. Georgiev, "Sensory Engineering", University Press, Technical University of Gabrovo, 1999.

EUROPEAN REQUIREMENTS FOR ELECTROMAGNETIC COMPATIBILITY

Irena Nikolova, Milka Vicheva, Kalinka Todorova

Fundamentals and Technical Means of Design, Technical University of Sofia,
blvd. Kliment Ohridski 8, 1000, Sofia, Bulgaria, 00359 2 965 2786,
e-mail: inikolova@tu-sofia.bg,
mvicheva@tu-sofia.bg, ktodorova@tu-sofia.bg

Abstract. *To have free movement in the European Market products produced in Bulgaria should respond to the requirements determined in the European technical legislation. The Directive 2004/108/EC relating to electromagnetic compatibility is one of the basic directives of the New Approach whose requirements should be met by a significant number of products. The application of those essential requirements for safety is fulfilled through using harmonized with the corresponding directive standards. The essential requirements for electromagnetic compatibility of products determined in the directive are considered in the report. Harmonized standards related to electromagnetic compatibility are analyzed.*

Keywords: *electromagnetic compatibility, Directive 2004/108/EC, harmonized standards, essential requirements, European technical legislation*

1. INTRODUCTION

Through the European Union (EU) a common economic space between countries with different levels of law and economics is created. Taking into account these differences, the single market mechanism is built in the member states. To achieve this purpose the European Technical Legislation (ETL) plays a unique role.

ETL is built on the basic principle: "Any good that moves on the market of a country should be free to move on the markets of other member states." To satisfy this principle a system formed by the ETL and European standards is needed. Thus all matters for harmonizing standards and requirements to products are resolved and products can free move on the market of each country member of EU. ETL governs the legal aspects of the public interest of the citizens of the member states, because it obliges governments to harmonize their regulatory requirements in its regulations and standards. For achieving that the conditions for doing business in different countries should be equalized. As a result of these two areas of impact of ETL the prerequisites for real opening of frontiers between countries and functioning of the Single European Market (SEM) are created.

2. LEGISLATIVE REQUIREMENTS ABOUT ELECTROMAGNETIC COMPATIBILITY

Creating of SEM could not be achieved without New approach to technical harmonization and standards [1], which is a typical example of regulation, not market

management. This approach removes the hardest non-tariff barriers. The harmonization of the technical legislation limits to essential requirements that must be met by the products placed on the EU market. The New approach requires the essential requirements to be harmonized and made mandatory by directives.

One of the major New approach directives is Directive 2004/108/EC of the European Parliament and of the Council on the harmonization of the laws of Member States relating to electromagnetic compatibility [2]. Its purpose is to ensure the functioning of the SEM by requiring equipment to comply with an appropriate level of electromagnetic compatibility.

For the purposes of the considered directive "electromagnetic compatibility" means the ability of equipment to function satisfactorily in its electromagnetic environment without introducing excessively electromagnetic disturbances to other equipment in that environment. The "Equipment" means any apparatus or fixed installation, such as:

- "Equipment" means any finished device or combination of such devices commercially available as a single functional unit intended for the end user and liable to generate electromagnetic disturbance, or the performance of which is liable to be affected by such disturbance;

- "Fixed installation" means a particular combination of several types of apparatus and other devices, which are assembled, installed and intended to be used permanently at a predefined location.

"Electromagnetic disturbance" means any electromagnetic phenomenon which may degrade the performance of equipment. An electromagnetic disturbance may be electromagnetic noise, an unwanted signal or a change in the propagation medium.

Directive 2004/108/EC defines the essential requirements of the electromagnetic compatibility (EMC) facilities, which are divided into the following groups:

Group I. Requirements regarding the protection

The equipment should be designed and manufactured to adhere to current achievements in this field and provide the following:

- Generated electromagnetic disturbances should not exceed the level above which radio and telecommunications equipment or other equipment does not work as intended;

- Distinguished by a level of immunity to electromagnetic interference, as expected to be encountered during the operation, which allows the level to operate without unacceptable degradation in operating as intended.

Group II. Specific requirements for fixed installations

When installing a fixed installation apply best practice excellence in technique and take into account information on the performance of its components to meet the requirements for protection. These best practice advances in technology are documented and documents are kept by the person and available to the relevant domestic authorities to check for the entire life of the fixed installation.

3. PROVISION OF LEGISLATIVE REQUIREMENTS ON ELECTROMAGNETIC COMPATIBILITY

The technical specifications of products that meet essential requirements of the New Approach Directives are formulated in harmonized standards. The application of these standards is voluntary, and the manufacturer can always use other technical specifications to satisfy the requirements. But harmonized standards offer a guaranteed level of protection with respect to the essential requirements set out in the directives. The presumption of conformity with the essential requirements only applies to products manufactured in accordance with harmonized standards.

The following harmonized standards for EMC Directive are discussed:

- EN 60947-1:2007 Low-voltage switchgear and controlgear. Part 1: General rules [3];
- EN 60947-2:2006 Low-voltage switchgear and controlgear. Part 2: Circuit-breakers [4].

Switchgear apparatus is designed to switch on or off electricity in one or more electric circuits. A switchgear apparatus may perform either or both functions.

Through the EN 60947-1:2007 the rules and of general scope requirements for switchgear for low voltage are harmonized in order to achieve uniformity of requirements and tests for all relevant equipment and to avoid testing under different standards. This standard includes all the common parts of the standards for different apparatus. Therefore, to determine all requirements and tests for all types of switchgear only two standards are needed:

- a) EN 60947-1:2007 in the role of basic standard relating to different types of switchgear for low voltage;
- b) Standard for the particular apparatus called product standard. (EN 60947-2:2006 is product standard)

EN 60947-1:2007 applies when required by the product standard for distribution switchgear and control switchgear designed for connecting to circuits with rated voltage not exceeding 1000V AC or 1500V DC. This standard includes terms and definitions; characteristics; product information; legal conditions for operating, installation and transportation; requirements for construction, performance and electromagnetic compatibility; testing for compliance with the requirements for construction, operating, testing of electromagnetic compatibility.

Two types of electromagnetic environment of products under the scope of the standard are discussed:

- Electromagnetic environment A;
- Electromagnetic environment B.

Electromagnetic Environment A applies to non-public or industrial low voltage networks / locations / installations, including sources with strong disturbance.

Electromagnetic Environment B refers to public low-voltage networks, such as housing, commercial locations / installations. Sources with strong disturbing effects such as arc welding apparatus are not covered by the electromagnetic environment.

Requirements regarding electromagnetic compatibility are related to sustainability and emission. They are different for:

- Apparatus, not containing electronic circuits;
- Apparatus containing electronic circuits.

Testing the stability and the emission are performed to determine type and must be performed under representative operating conditions and environment, using the manufacturer's instructions for installation.

EN 60947-2:2006 applies to circuit breakers, the main contacts of which are intended for connection to circuits whose rated voltage does not exceed 1000V AC or 1500V DC. It also contains additional requirements for circuit-breakers with integral fuses. This standard includes: terms and definitions; classification; characteristics; product information; legal conditions for operating, installation and transportation; requirements for construction, functionality, electromagnetic compatibility; tests.

Circuit breaker is a mechanical switchgear apparatus capable to switch on, to conduct and to switch off currents in the circuit under normal conditions, but also to switch on, to conduct for some time and to switch off currents in prescribed abnormal conditions in the circuit, such as for short circuit.

Requirements and tests for electromagnetic compatibility prescribed in EN 60947-2:2006 are for sustainability and for radiation.

For the stability test, the following performance criteria are determined:

– Performance criterion A: during test check the stability of unwanted activations and functional characteristics. Each function for monitoring and control should show the correct status.

– Performance criterion B: during test check the stability of unwanted activations. Functions for monitoring and control may show incorrect status. After the test check functional characteristics.

For sustainability in the standard are considered: Testing of electrostatic discharge; Exposure to radio frequency electromagnetic fields emitted; Electrical fast transient processes / pulse packages; Jumps; Conducted Disturbances induced from radio frequency fields (asymmetric mode).

For radiation are considered: Conductive radio frequency disturbances (150 kHz-30MHz); Irradiation radio frequency disturbances (30 MHz-1000 MHz).

4. CONCLUSIONS

To apply the European requirements for electromagnetic compatibility exposed in the New Approach Directive of the ETL it is advisable to use harmonized European standards. This will facilitate the industry as using safety norms set out in these

standards, a guaranteed level of protection with respect to the essential requirements would be achieved.

References

- [1] Guide to the implementation of directives based on the New Approach and the Global Approach, European Commission Office for Official publications of the European communities, Luxembourg, 2000.
- [2] Directive 2004/108/EC of the European Parliament and of the Council on the approximation of the laws of the Member States relating to electromagnetic compatibility.
- [3] EN 60947-1:2007 Low-voltage switchgear and controlgear. Part 1: General rules.
- [4] EN 60947-2:2006 Low-voltage switchgear and controlgear. Part 2: Circuit-breakers.

STUDY IN MODERN SOFTWARE IMPACT OF ELECTRICAL CONDUCTIVITY THE SIGNAL OUTPUT WITH PULSE EDDY CURRENT NDT

Kalinka Mitkova Todorova, Stefcho Georgiev Guninski

Dep. „Electrical Engineering”, Technical University of Sofia,
8, „Kl.Ohridski” blvd., 1000, Sofia, tel. tel. (+359 2) 965 3665, (+359 2) 965 2318,
e-mails: ktodorova@tu-sofia.bg, sgg@tu-sofia.bg

Abstract. *The influence of electrical conductivity on the main parameters of the eddy current transducer (ECT), included in the shock excitation measurement scheme is investigated. MagNet model is created, which solves the transition process in an electrical circuit with setting ECT parameters in FEM. The simulation accurately reflects the geometric shapes and sizes and different electrical parameters of ECT and samples. As a result of the computational experiments the relationships of the main parameters of the pulse output of the electrical conductivity are obtained and analyzed.*

Keywords: *eddy current testing, shock excitation, FEM*

1. INTRODUCTION

Pulse techniques are increasingly applied in eddy current nondestructive testing (NDT). They are used mostly for measuring the thickness of coatings and defects detection [3, 4, 5]. Pulse signals given many opportunities [1] to obtain necessary information for the control parameters. They have consistency between multi-parametric input and output of multidimensionality. This advantage is very strong in the inclusion of pulse eddy current transducer (PECT) in measuring circuit with shock excitation. Data output parameters are numerous and can easily be handled electronically. This gives reason to believe that success can be used when one of the control parameters is the electrical conductivity γ .

2. FORMULATION OF THE PROBLEM

2.1. Measuring circuit

Consider the circuit (Fig. 1) consisting of a capacitor C , resistor R_a , switch S and eddy current transducer (ECT) with parameters L_c and R_c , powered by a voltage source E_0 . For $t < 0$ the switch S is closed for a time t_{on} , long enough so that the voltage of the capacitor C and the current through ECT practically reach their steady state values $U_C(0.) = E_0$ and $I_{ECT}(0.) = E_0 / (R_a + R_c)$. At the moment $t = 0$ the switch S is opened and remains open for a time t_{off} until the new steady state mode is established $U_C \cong 0$ and $I_{ECT} \cong 0$.

Most often output is the voltage at the terminals of the capacitor $C - U_C(t)$. The current in the loop (voltage drop at the ends of the auxiliary resistor R_a) is rarely used. In this case the voltage $U_C(t)$ (Fig. 3) is used as output signal. It shows the main parameters of the information signal: U_{I+} - first positive amplitude; t_{I+} - time for reaching U_{I+} ; U_{I-} - first negative amplitude; t_{I-} - time for reaching U_{I-} ; U_{0+} -mean value of positive the envelope; U_{0-} -mean value of negative the envelope.

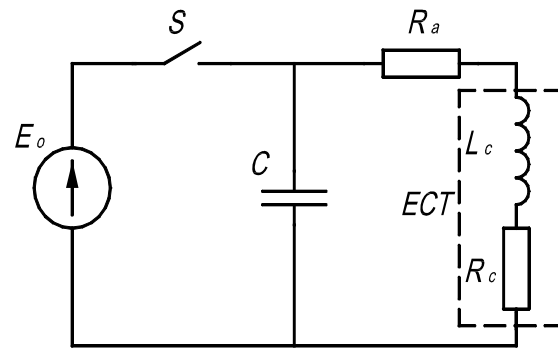


Fig. 1

2.2. Physical model

With product MagNet [6] a model is created. It consists of a sample (Component 1) and ECT (Component 2) with parameters L_c and R_c , located close enough above the sample. Table 1 shows components data. ECT is included in the measuring circuit on Fig. 1. By MagNet the transition process in the circuit is solved with the determination of the parameters of the ECT for a series of values of electrical conductivity from 0.02 MS/m to 50000 MS/m.

Table 1

Component 1 - SAMPLE		Component 2 - ECT		Circuit	
Diameter, mm	14	Outer diameter, mm	10	Capacitor C , μF	3
Height, mm	4	Inner diameter, mm	4	Resistor R_a , Ω	0.2
Permeability	1	Height, mm	6	t_{on} , ms	0.14
Conductivity, MS/m	0.02÷50000	Material	Cu	t_{off} , ms	0.33
		LIFT OFF, mm	0.2	E_0 , V	0.5

One advantage of this pulse method is that information parameters are more than three, as in the classic single-frequency eddy current NDT.

The influence of the electrical conductivity on the basic parameters of pulse output signal - first positive amplitude; time for reaching first positive amplitude; first negative amplitude; time for reaching first negative amplitude – is investigated in the work. These parameters have been chosen based on theoretical analysis [2] and the experience of the Department of Electrical Engineering in the development of devices for eddy current nondestructive testing.

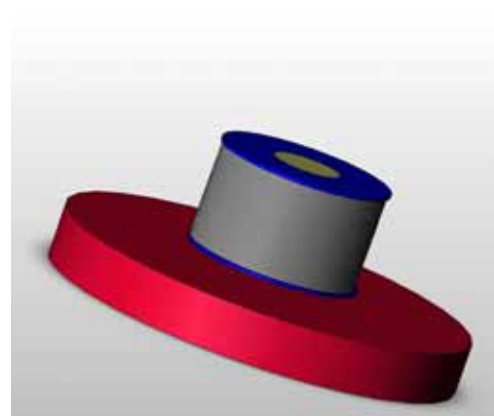


Fig. 2

3. ANALYSIS OF OBTAINED RESULTS

Fig. 3 shows the output pulse signal - voltage $U_C(t)$. Main parameters of the information signal: U_{1+} - first positive amplitude; t_{1+} - time for reaching U_{1+} ; U_{1-} - first negative amplitude; t_{1-} - time for reaching U_{1-} ; U_{0+} - mean value of positive the envelope; U_{0-} - mean value of negative the envelope are shown.

Fig. 4 shows the dependence of $t_{1+/-}$ as function of the electrical conductivity γ of the sample. It is seen that the sensitivity of this parameter in terms of electrical conductivity is not large and therefore not suitable for use. There are of course ranges of change, which could be used, but only in case of sophisticated and expensive electronic circuitries.

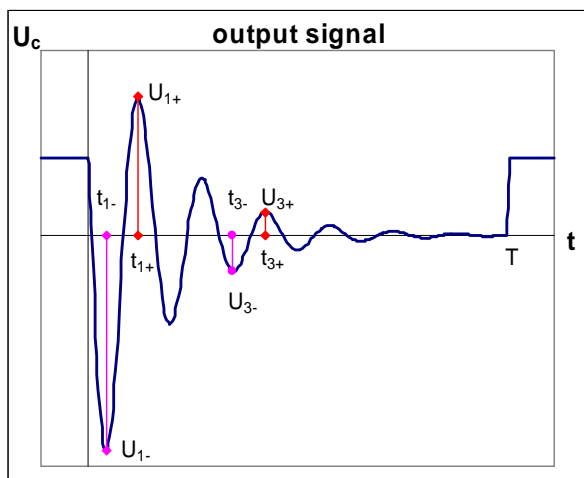


Fig. 3

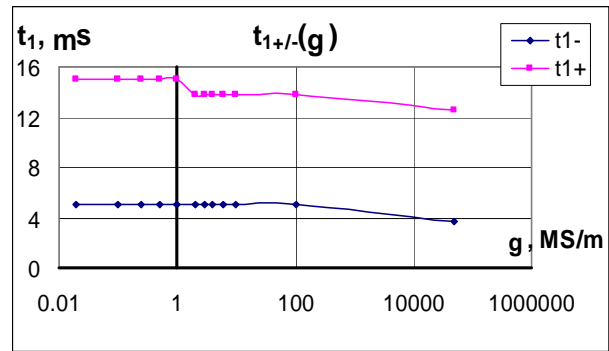


Fig. 4

Dependences $U_{1+}(\gamma)$ and $U_{1-}(\gamma)$ in a very wide range of variation of the electrical conductivity are given in Fig. 5. It is seen that in both dependencies sensitivity is highest in the interval for γ of 0.1 MS / m to 2 MS / m, as shown in Fig. 6.

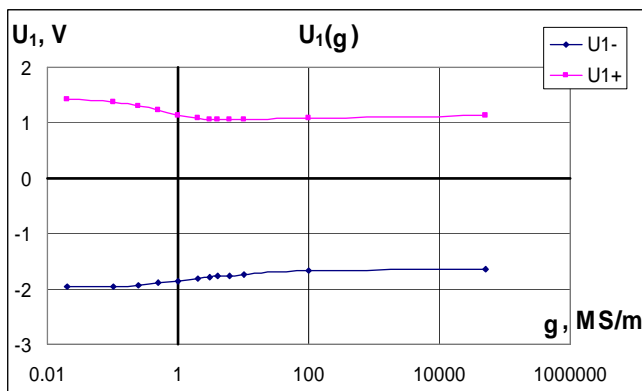


Fig. 5

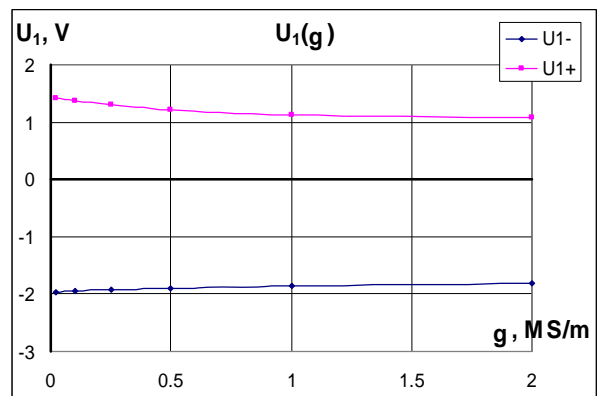


Fig. 6

Dependences $U_{0+}(\gamma)$ and $U_{0-}(\gamma)$ in logarithmic scale are given in Fig. 7. This is the most commonly used parameter of data pulse output for measuring shock excitation scheme [1, 2].

Again, it is seen that a range of greater sensitivity to γ (of 0.1 MS/m to 2 MS/m). Dependencies $U_{0+}(\gamma)$ and $U_{0-}(\gamma)$ in this range are shown in Fig. 8.

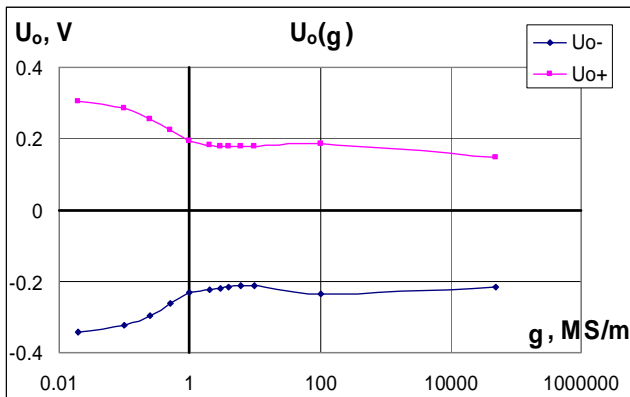


Fig. 7

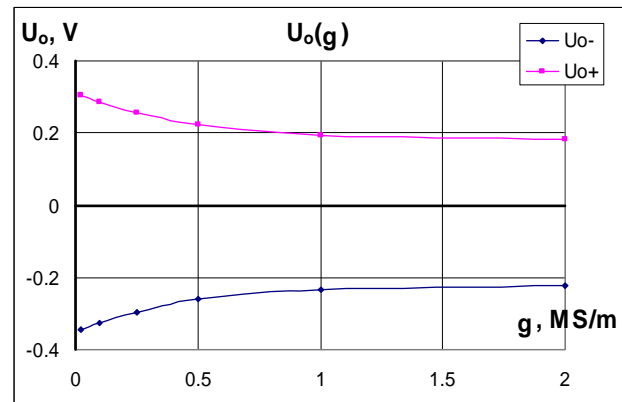


Fig. 8

4. CONCLUSION

A. The analysis shows that measuring shock excitation scheme has advantages in measuring and control and electrical conductivity.

B. Parameters related to the voltage values: U_{1+} , U_{1-} , U_{0+} , U_{0-} are more sensitive to changes in electrical conductivity than parameters related to the time t_{1+} , t_{1-} .

C. With product MagNet very accurately can be modeled and jointly solved the two tasks: the analysis of the transition process in the electrical measuring circuitry coupled with the solution of FEM field problem to determine the electromagnetic parameters involved in this scheme ECT.

D. Another advantage of the developed model is the possibility to carry out a series of numerical experiments to optimize the values of the elements in the measuring circuit and the shape and size of ECT.

References

- [1] Grozdanova D. B., Study of electromagnetic processes in linear conductive environments quasi stimulant pulse field, Sofia, 1983;
- [2] Guninski S. G., Determination Of The Parameters Of Measurement Scheme By Shock Excitation Using FEM, Advanced Aspects of Theoretical Electrical Engineering, Sozopol '2012;
- [3] Scottini R., H.J. Quakkelsteijn, Monitoring Average Wall Thickness of insulated or difficult to access objects with Pulsed Eddy Current, IV Conferencia Panamericana de END, Buenos Aires, Octubre, 2007;
- [4] Babbar V. K., D. Harley and T. W. Krause, Study of the Variations of Probe Parameters by Finite Element Modeling of Transient Eddy Currents in Multilayer Aluminum Structures, 6th International Workshop – NDT-Signal Processing, August, 25-27, 2009, London, Ontario, Canada;
- [5] Krause T.W., Prof., D. Harley, V.K. Babbar, Dr. and K. Wannamaker, Evaluation of Selective Phase Corrosion Thickness on Nickel Aluminum Bronze Valves using Transient Eddy Current, NDT in Canada National Conference, 25-27, 2009, London, Ontario, Canada;
- [6] www.ifolytika.com

STUDY OF A PROMISCUOUS T – SHAPED BRIDGE CIRCUIT WITH EDDY CURRENT TRANSDUCER

Kalinka Mitkova Todorova, Jivko Asenov Daskalov

Dep. „Electrical Engineering”, Technical University of Sofia,
8, „Kl.Ohridski” blvd., 1000 Sofia, tel. tel. (+359 2) 965 3665, (+359 2) 965 2136,
e-mails: ktodorova@tu-sofia.bg, jdaskalov@tu-sofia.bg

Abstract. In the presented paper a theoretical analysis of an unbalanced T – shaped bridge circuit, which included parametric eddy current transducer (ECT) with parameters inductance L and active resistance r is completed. Output is summarized expression of the complex transmission coefficient of the scheme. Based on this coefficient can be determined module and phase of the output signal and sensitivity of the voltage and phase of the output signal in relation to variations in ECT.

1. INTRODUCTION

One of the important issues that arise in the practical application of eddy current method to measure and control the choice of appropriate measurement schemes, which include parametric eddy current transducers (PECT). At reflection transducers output signal is voltage that can be directly used as a carrier of information about the measured parameter. Parametric eddy current transducers must be included in the scheme, transforming climate full resistance variation of the amplitude and phase (or frequency) of the output voltage.

The literature described different variants of measurement schemes involving parametric eddy current transducers. They can be attributed to two main groups: resonance and bridge.

In [1] and [2] has been proposed and experimentally tested a single T-shaped bridge circuit operating in unbalanced mode. In one side of the scheme is parametric eddy current transducer for nondestructive measurement of the thickness of conductive coatings applied on ferromagnetic base. A careful analysis of the experimental set time on the features and benefits of this scheme demonstrates the appropriateness of its use in other areas of eddy current nondestructive control.

2. PURPOSE OF THE STUDY

In the presented paper to make a theoretical analysis of this single T-bridge circuit. The scheme operates in unbalanced mode. In one shoulder included parametric eddy current transducer (PECT). The goal is to determine the complex transmission coefficient the scheme. Then derive analytical expressions for the output voltage sensitivity to changes in parameters (inductance L and active resistance r).

3. THEORETICAL ANALYSIS

Study surface eddy current transducer, which is included in measuring single unbalanced T-bridge circuit. Active resistance and inductance PECT are indicated by r and L . Parameters of the measuring circuit are R , R_1 , C_0 , C_1 and C_2 (Fig. 1) (scheme in Fig. 2 is a simplified version of the first scheme in which $C_1 = C_2 = C_0$ and $R_1 = 0$).

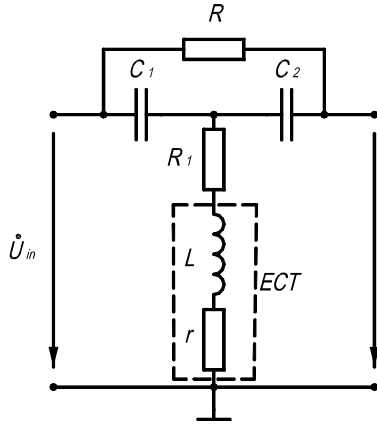


Fig. 1

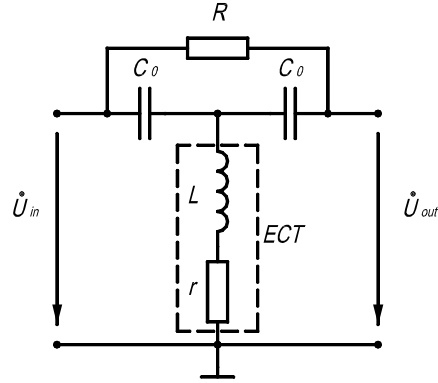


Fig. 2

The theoretical analysis is carried out based on scheme in Fig. 1. Application for $C_1 = C_2 = C_0$ and $R_1 = 0$ analogous expressions are obtained for the scheme in Fig. 2. It should be noted that the first scheme provides a rich opportunity to obtain different gear ratios, and hence a wide range of plane diagram of change of output voltage U_{out} . All theoretical conclusions are made on condition that the scheme is powered by a sinusoidal voltage $u(t) = U_m \sin \omega t$ source and works in idle mode.

After appropriate conversion of a scheme 1 for complex transmission coefficient K_1 expression is obtained:

$$\dot{K}_1 = \frac{\dot{U}_{out}}{\dot{U}_{in}} = \frac{1 - \omega^2 B + j\omega A}{1 - \omega^2 B + j\omega (C_2 R + A)} \quad (1)$$

where

$$A = (C_1 + C_2)(r + R_1) - \omega^2 L C_1 C_2 R \quad \text{and} \quad B = L(C_1 + C_2) + C_1 C_2 R (r + R_1)$$

The expression for the complex transmission coefficient K_2 for Scheme 2 is obtained after taking $C_1 = C_2 = C_0$ and $R_1 = 0$:

$$\dot{K}_2 = \frac{\dot{U}_{out}}{\dot{U}_{in}} = \frac{1 - \omega^2 C_0 B_1 + j\omega C_0 A_1}{1 - \omega^2 B_1 + j\omega (C_2 R + A_1)} \quad (2)$$

where

$$A_1 = 2r - \omega^2 L C_0 R \quad \text{and} \quad B_1 = 2L + C_0 R r \quad (3)$$

Obviously, A and A_1 - on the one hand and on the other - B and B_1 are connected to each other in the following way:

$$A = C_0 A_1 \quad \text{and} \quad B = C_0 B_1 \quad (4)$$

From formulas (1) and (2) determine the following expressions for the modules and arguments of complex coefficients of transmission of both of the schemes:

$$|\dot{K}_1| = \frac{\sqrt{(1 - \omega^2 B)^2 + \omega^2 A^2}}{\sqrt{(1 - \omega^2 B)^2 + \omega^2 (C_2 R + A)^2}} \quad (5)$$

$$\arg \dot{K}_1 = \varphi_1 = \arctg \frac{\omega A}{1 - \omega^2 B} - \arctg \frac{\omega (C_2 R + A)}{1 - \omega^2 B} \quad (6)$$

and accordingly:

$$|\dot{K}_2| = \frac{\sqrt{(1 - \omega^2 C_0 B_1)^2 + \omega^2 C_0^2 A_1^2}}{\sqrt{(1 - \omega^2 C_0 B_1)^2 + \omega^2 C_0^2 (R + A_1)^2}} \quad (7)$$

$$\arg \dot{K}_2 = \varphi_2 = \arctg \frac{\omega C_0 A_1}{1 - \omega^2 C_0 B_1} - \arctg \frac{\omega C_0 (R + A_1)}{1 - \omega^2 C_0 B_1} \quad (8)$$

In determining the sensitivity of the measurement schemes in amplitude and phase of their output voltages equivalent to changing parameters L and r number of their parametric eddy current transducers, it is convenient to work with relative sensitivity to voltage parameters (L and r).

$$(S_U^L)_{omh} = \frac{\partial |\dot{K}|}{\partial L} = \frac{1}{|\dot{U}_{in}|} \frac{\partial |\dot{U}_{out}|}{\partial L} \quad (9)$$

$$(S_U^r)_{omh} = \frac{\partial |\dot{K}|}{\partial r} = \frac{1}{|\dot{U}_{in}|} \frac{\partial |\dot{U}_{out}|}{\partial r} \quad (10)$$

and ultimate sensitivity to phase:

$$S_\varphi^L = \frac{\partial \varphi}{\partial L} \quad (11)$$

$$S_\varphi^r = \frac{\partial \varphi}{\partial r} \quad (12)$$

After differentiating the relevant expressions for the module and argument (phase) of the complex transmission coefficient of the second scheme we have the following results:

1. Relative sensitivity voltage to amend the inductance L of PECT

$$(S_U^L)_{omh} = \omega^4 C_0^3 R \frac{R(\omega^4 C_0^2 B^2 - 1) - A[\omega^2 C_0^2 R(R + A) + 4(1 - \omega^2 C_0 B)]}{\left[(1 - \omega^2 C_0 B)^2 + \omega^2 C_0^2 A^2 \right]^{\frac{1}{2}} \left[(1 - \omega^2 C_0 B)^2 + \omega^2 C_0^2 (R + A)^2 \right]^{\frac{3}{2}}}$$

2. Relative sensitivity voltage to amend the active resistance r of PECT

$$(S_U^r)_{omh} = \omega^2 C_0^2 R \frac{2\omega^2 C_0^2 (R + A)A - (1 - \omega^2 C_0 B)[\omega^2 C_0^2 R(R + 2A) + 2(1 - \omega^2 C_0 B)]}{\left[(1 - \omega^2 C_0 B)^2 + \omega^2 C_0^2 A^2 \right]^{\frac{1}{2}} \left[(1 - \omega^2 C_0 B)^2 + \omega^2 C_0^2 (R + A)^2 \right]^{\frac{3}{2}}}$$

3. Relative sensitivity to climate phase inductance L of PECT

$$S_\varphi^L = \omega^2 C_0^2 R \frac{\omega^2 C_0^2 [(\omega^2 C_0^2 R^2 + 4)(R + 2A)r - (R^2 + 2RA + 2A^2)] - 2(1 - \omega^2 C_0 B)^2}{(1 - \omega^2 C_0 B)^2 [(1 - \omega^2 C_0 B)^2 + \omega^2 C_0^2 (R^2 + 2RA + 2A^2)] + \omega^4 C_0^4 A^2 (R + A)^2}$$

4. Relative sensitivity to the phase variation of the active resistance r of PECT

$$S_\varphi^r = \omega^3 C_0^3 R \frac{(R + 2A)[2 - \omega^2 LC_0(\omega^2 C_0^2 R^2 + 4)] - R[(1 - \omega^2 C_0 B)^2 + \omega^2 C_0^2 A^2]}{(1 - \omega^2 C_0 B)^2 [(1 - \omega^2 C_0 B)^2 + \omega^2 C_0^2 (R^2 + 2RA + 2A^2)] + \omega^4 C_0^4 A^2 (R + A)^2}$$

4. CONCLUSIONS

A. Performed a theoretical analysis of two variants of a single T-shaped bridge circuit including at one shoulder parametric eddy current transducer.

B. Obtained in analytical form expressions: complex transmission coefficient of the considered schemes module and argument of this coefficient, equilibrium conditions, and sensitivity to voltage and phase of the output voltage to changes in parameters included parametric eddy current transducer.

C. The obtained expressions can be used for measuring dimensioning of schemes that examined type for their work with embedded parametric eddy current transducers.

D. Given a domain of variation of the values of the elements of the scheme can be found such value at which an eddy current transducer for the scheme will have maximum sensitivity to a given parameter transducer.

References

- [1] Daskalov J. A., Study of the interaction of electromagnetic field with ferromagnetic multi-layer environment, PhD – dissertation, TUS, 1984 (in Bulgarian).
- [2] Daskalov J. A., S. S. Staykov, D. N. Cvetkov, Experimental study of the possibilities of a T-shaped bridge circuit for measuring the thickness of conductive coatings on ferromagnetic base, scientific Session of TUS, 1978 (in Bulgarian).

PERFORMANCE COMPARISON OF GPU AND CPU IMPLEMENTATIONS OF THE CONJUGATE GRADIENT METHOD

Vasil Bachvarov

Department of Theoretical Electrical Engineering, TU – Sofia, 8 Kliment Ohridski Blvd., Sofia, Bulgaria, phone: (+359)-2-965-38-09

Abstract. *The purpose of this article is to study the performance of the numeric conjugate gradients algorithm by comparing it on computer CPUs opposed to GPUs, found in graphic adapters. By utilizing the high parallelization of GPUs it is expected to see substantial performance gain compared to the CPU implementation. The numerical experiments are based on a CUDA implementation of the conjugate gradients method and executed on an Intel Core i7 CPU with 4 CPU cores and NVIDIA NVS 3100M graphic card with 16 GPU cores. Sparse matrix formats have been used to increase computational efficiency by omitting substantial number of zero matrix elements in the calculations.*

Keywords: *GPU, conjugate gradients, sparse matrix*

1. INTRODUCTION

1.1. General computing with GPUs and CUDA

Parallel computation is often used to accelerate the search for numerical solutions to electrical engineering problems. Commonly available central processor units (CPUs) with multiple cores enable even personal computers to perform quick analysis of electromagnetic field in models with several thousands to hundreds of thousands of discrete elements.

With the introduction of the graphical processor unit (GPU) initially used for graphical calculations but later on for general computation as well, NVIDIA has opened new possibilities for further accelerating the execution of numerical algorithms. At the time of writing many GPU solutions with tens and even hundreds of cores are readily available on the market. The reason for the better performance of GPUs compared to CPUs when it comes to floating point calculations is explained in [3]:

“The GPU is specialized for compute-intensive, highly parallel computation [...] and therefore designed such that more transistors are devoted to data processing rather than data caching and flow control.”

CUDA is a general-purpose parallel computing architecture provided by NVIDIA, which enables the development of programs that run on the GPU. The programs are implemented in the C programming language. CUDA has its own compiler that provides extensions to C. A CUDA program consists of *host code* and *device code*. The host code is executed on the CPU like ordinary C programs. The device code (in CUDA called *kernel*) is executed on the GPU.

As described in [3], “a GPU is built around an array of Streaming Multiprocessors (SMs). [...] A multithreaded program is partitioned into blocks of threads that execute independently from each other, so that a GPU with more multiprocessors will automatically execute the program in less time than a GPU with fewer multiprocessors”. Figure 1 illustrates this.

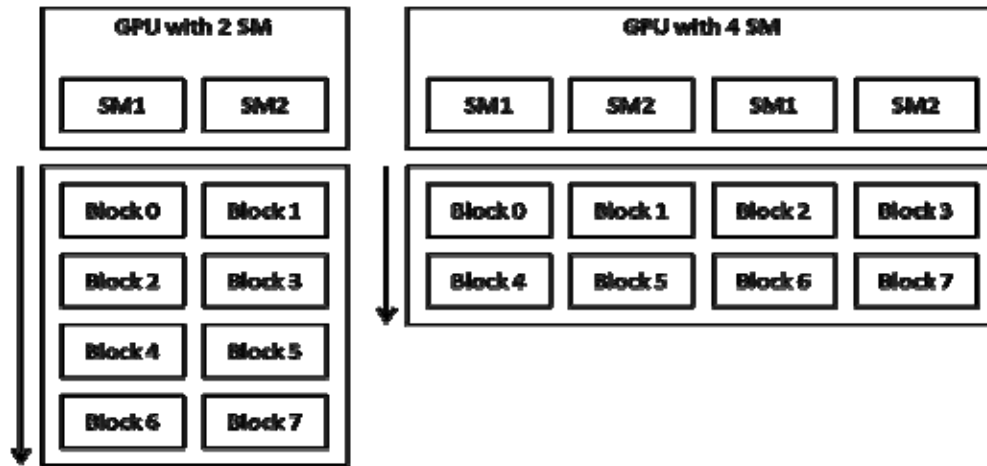


Fig. 1. Automatic scalability of a CUDA program (source: [3]).

Blocks and threads can be structured in one or more dimensions to facilitate 1D, 2D or 3D calculations.

In the device code (the kernel) it is necessary to determine uniquely the currently executed thread in order to perform the computation on the correct data entry. This is done through special data structures, called *blockIdx* (block index), *blockDim* (block dimension) and *threadIdx* (thread index within the current block). They can have x-, y- and z-component. For the purposes in this paper only the x-component is used. Each thread is assigned a unique thread number through the following formula:

$$k_{\text{thread}} = \text{blockIdx}_x \cdot \text{blockDim}_x + \text{threadIdx}_x \quad (1)$$

1.2. The conjugate gradients (CG) method

The method of conjugate gradients (as described in [2]) is an iterative algorithm for finding an approximate solution to the equation

$$Ax = b \quad (2)$$

where A is a positive definite symmetric matrix ($N \times N$), x is the unknown vector ($N \times 1$), b is the source or forcing function vector ($N \times 1$), and N is the order of the matrix.

The solution is found through generation of N vectors W_i orthogonal with respect to A or *conjugate*, such that:

$$W_i^T A W_j = 0, \text{ for } i \neq j \quad (3)$$

and

$$W_i^T A W_j \neq 0, \text{ for } i = j \quad (4)$$

The solution to the equation is representable as a linear combination of these vectors thus it can be found in not more than N steps. On each step a value is minimized, called *residual vector* r , which represents the deviation of the current step solution vector from the exact solution.

$$r = b - Ax \quad (5)$$

At the last step the residual r is sufficiently close to zero, thus the approximate solution is sufficiently close to the exact solution vector x .

The following formulas represent the CG calculation cycle [2]:

$$\begin{aligned} \text{(direction)} \quad & W_{i+1} = r_{i+1} + \beta_i W_i \\ \text{(new solution)} \quad & x_{i+1} = x_i + \alpha_i W_i \\ \text{(new residual)} \quad & r_{i+1} = b - A x_{i+1} \end{aligned} \quad (6)$$

$$\alpha_i = (W_i^T r_i) / (W_i^T A W_i) \quad (7)$$

$$\beta_i = - (r_{i+1}^T A W_i) / (W_i^T A W_i) \quad (8)$$

1.3. Sparse matrix storage formats

Matrices used when solving electrical engineering problems with methods like the Finite Elements Method (FEM) are typically sparse, i.e. with a large number of zero matrix elements. Considering this, the usage of sparse matrix format for computation is favorable because of omitting large number of operations on zero matrix elements.

Bell and Garland's [1] implementation for sparse matrix-vector multiplication has been used for matrix-vector operations in the numerical experiments. The latter paper offers GPU implementations based on several sparse matrix storage formats. In this article the author has used the DIA (diagonal) format and CSR (compressed row storage).

DIA stores the non-zero elements of a matrix A ($N \times N$) in a smaller matrix, containing only the elements of the diagonals, containing non-zero elements. An additional vector *indices* is used to store the indices of the diagonals.

With CSR the non-zero elements are stored in a vector *data* in the order in which they occur in the original matrix starting with the topmost row. Additional vector *ptr* of size $N+1$ stores the accumulated number of non-zero elements for each row. Another vector *indices* is used to store the column numbers of the non-zero elements for each vector entry in *data*.

1.4. Goals

With this article the author aims to compare the performance of the conjugate gradients algorithm on CPUs and GPUs in a common personal computer configuration and verify if usage of the GPU can increase the speed of the computation. The latter analysis is performed on synthetic matrices similar to the ones produced by the Finite Elements Method.

2. IMPLEMENTATION DESCRIPTION

All experiment procedures have the following structure:

- Definition of a matrix size N for the current experiment.
- Generation of a synthetic matrix ($N \times N$) with 5 non-zero diagonals, similar to the matrices produced by the FEM (Figure 2).
- Generation of an exact solution vector $x = [1 \dots 1]^T$ ($N \times 1$), consisting of values 1.
- Calculation of the vector $b = Ax$.
- Conversion of the matrix to a sparse matrix format (CSR or DIA).
- Execution of the conjugate gradients algorithm with the sparse matrix data using the corresponding matrix-vector multiplication code (CSR/DIA and CPU/GPU). The resulting approximate solution vector should be very close to the exact solution x .
- Execution time is measured only for the last step.

$$\begin{array}{cccccc} 4 & -1 & -1 & 0 & 0 & 0 \\ -1 & 4 & -1 & -1 & 0 & 0 \\ -1 & -1 & 4 & -1 & -1 & 0 \\ 0 & -1 & -1 & 4 & -1 & -1 \\ 0 & 0 & -1 & -1 & 4 & -1 \\ 0 & 0 & 0 & -1 & -1 & 4 \end{array}$$

Fig. 2. A sample 6×6 matrix.

The CG algorithm in the implementation is equivalent to the one described in Salton and Chari's book [2]. A sufficiently small number ε has been defined to determine when the CG algorithm converges, i.e. the approximate solution is found. The value of ε in the numerical experiments has been set to $\varepsilon = 10^{-4}$. The termination criterion for the CG cycle is:

$$|r_{\{k\}}| < \varepsilon, \text{ for } 0 \leq k < N \quad (9)$$

(each component of the residuum vector r must be sufficiently close to 0, i.e. the approximate solution is sufficiently close to the exact solution x).

2.1. CPU implementation of sparse matrix-vector multiplication

The matrix-vector multiplications in the CPU implementation are executed with multiple threads in order to use the advantage of multiple CPU cores. Each matrix row is assigned a single thread. All CPU multiplication algorithms are equivalent to their GPU counterparts.

2.2. GPU implementation of sparse matrix-vector multiplication

The GPU implementation is equivalent to the one described in [1]. The DIA and the scalar CSR kernels have been used.

3. SETUP OF THE NUMERICAL EXPERIMENTS

Algorithm performance is evaluated by applying the CG method to square equation matrices of sizes 10, 100, 1000 and 10000 equations. Two identical implementations are used – one multithreaded C++ application, run on Intel Core i7 CPU with 4 processor cores and one multithreaded CUDA C++ application run on NVIDIA NVS 3100M GPU with 16 cores (2 streaming multiprocessors with 8 cores each). The latter configuration has been chosen because it represents a common personal computer setup at the time of writing.

What is measured is the time it takes to execute the CG algorithm and find the approximate solution in each case. When comparing the CPU and GPU execution times an acceleration factor is calculated as follows:

$$k_{\text{acceleration}} = t_{\text{CPU}} / t_{\text{GPU}} \quad (10)$$

It illustrates how many times quicker the GPU execution is.

Early experiments showed some additional delay in the first run of the algorithm for each testing session, probably caused by initializations of the multithreading environment. In order to eliminate this side effect an empty execution call was introduced before doing the real experiments.

4. EXPERIMENT RESULTS

Table 1 and 2 present the measured execution times from the numerical experiments.

As expected, the measured times from the execution of the programs show performance improvement with the application of GPU compared to CPU.

Considering the GPU case, the performance of the CSR kernel is almost equal to the performance of the DIA kernel.

Table 1. Performance of the CG method with sparse matrices in CSR format

Number of equations	Solution time with CPU, ms	Solution time with GPU, ms	$k_{\text{acceleration}}$
10	15	4	3.75
100	867	21	41.29
1000	68168	739	92.24
10000	6671247	59997	111.19

Table 2. Performance of the CG method with sparse matrices in DIA format

Number of equations	Solution time with CPU, ms	Solution time with GPU, ms	$k_{\text{acceleration}}$
10	10	3	3.33
100	751	24	31.29
1000	67531	713	94.71
10000	6660968	58642	113.59

5. CONCLUSIONS

Application of GPU in all considered cases leads to acceleration of the computation. It is an interesting observation that the acceleration gain by using GPU opposed to CPU increases with the number of equations, thus using GPUs for CG computation with the provided input data is more beneficial with higher number of matrix elements.

The GPU results for CSR and DIA kernels show very similar performance. This is a consequence of the chosen input data format. The matrix under test consists of 5 diagonals without zero elements. This results in equal number of floating point multiplications in the CSR and DIA cases. If the matrix diagonals contained zero matrix elements, mixed with the non-zero ones, it is expected that the CSR kernel computes faster. The more zero elements in the diagonals, the better the CSR kernel should perform in relation to the DIA kernel.

If the structure of the matrix under test is changed so that each row contains a variable number of non-zero elements, the performance of the scalar CSR kernel used in this article should decline as described in [1]. Using the vector CSR kernel proposed by Bell and Garland in the latter paper can improve the performance, provided that “matrix rows contain a number of nonzeros greater than the warp size (32)”, where *warp* is defined as a group of 32 threads.

References

- [1] N. Bell and M. Garland, “Efficient Sparse Matrix-Vector Multiplication on CUDA”, NVIDIA Corporation, NVIDIA Technical Report NVR-2008-004, December 2008.
- [2] S. Salon and V. K. Chari, “Numerical Methods in Electromagnetism”, Academic Press, 1999, pp. 627-637.
- [3] NVIDIA Corp., “NVIDIA CUDA C Programming Guide” v. 4.2, April 2012.

ANALYSIS OF RM, LM AND CM CIRCUITS WITH ONE MEMRISTOR AND SOURCES OF A SINE VOLTAGE AND CURRENT

Stoyan Kirilov, Simona Petrakieva, Valeri Mladenov

Department of Theoretical Electrical Engineering, Faculty of Automatics, Technical University of Sofia, 1000, 8, Kliment Ohridski, Blvd., Sofia, Bulgaria, tel. 965-34-45,
e-mails: s_kirilov@tu-sofia.bg, petrakievas-te@tu-sofia.bg, valerim@tu-sofia.bg

Abstract. *In this material, an introduction of the Williams's memristor and its parameters is performed. The behavior of a circuit with one memristor and ideal sine current source is modeled with MATLAB. Three circuits including Resistor-Memristor (RM), Coil-Memristor (LM) and Capacitor-Memristor (CM) and with an ideal sine voltage source in series are discussed and analyzed using SIMULINK models. Based on this simulation, the basic characteristics of the memristor circuits are presented in graphical form. The harmonious structure of the current in the circuits studied is also performed. The extent of nonlinearity of Williams's memristor is discussed too. Finally, some final conclusions about properties and applications of the Williams's memristor and memristor circuits are made.*

Key words: *Williams's memristor, current source, computer simulation, harmonious structure.*

1. INTRODUCTION

The object of investigation in this publication is the Williams's memristor, invented in 2008 in scientific-research laboratory of "Hewlett-Packard". It is a new semiconductor element with unique property – ability for memorizing the quantity of electrical charge. Based on this property professor Leon Chua proposed in 1971 the basic model of memristor [1]. Its basic parameters are: $w=1\text{ nm}$, $D=10\text{ nm}$, $\mu_v=1.10^{-14}\text{ m}^2/(V.s)$, $R_{ON}=100\ \Omega$, $R_{OFF}=16\text{ k}\Omega$. Schematic image of Williams's memristor presented here is shown in Fig. 1.

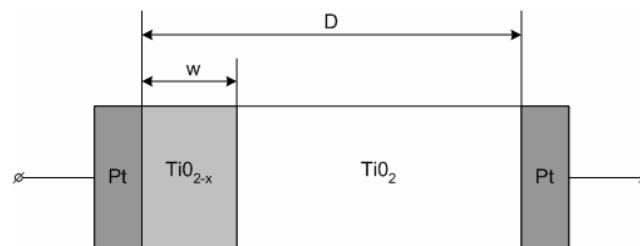


Fig. 1. Structure scheme of titanium dioxide memristor

The main application of Williams's memristor is in computer memories. In the present publication some nonlinear circuits, consist of one memristor in series with the basic passive elements – resistor, inductor and capacitor [3, 4], are discussed. The analysis is made with toolbox SIMULINK of MATLAB, because of the difficulties arising during the analytical solution.

2. PROBLEM STATEMENT

To analyze the circuit including an ideal current source it is necessary to find the relation as $u(t) = f(i(t))$. It is very difficult to find the exactly analytical solution of the relation $i(t) = f(u(t))$ for *RM*, *LM* and *CM* memristor circuits, so that approximate numerical methods, based on OPTIMIZATION and SIMULINK toolboxes in MATLAB environment will be used.

2.1. Analysis of a circuit with one memristor and an ideal sine current source

Let us consider a sine current source with the following instantaneous value:

$$i(t) = j_e(t) = i_m \sin(\omega t + \psi_i), \quad (1)$$

where: $i_m = 140 \mu A$, and $\omega = 3 \text{ rad/s}$.

The charge can be determined after integration of (1) [2, 3] as follows:

$$q(t) = \int_0^t i_m \sin(\omega t + \psi_i) dt = \frac{i_m}{\omega} [\cos \psi_i - \cos(\omega t + \psi_i)] = Q_D \left(1 - \sqrt{1 - \frac{2}{Q_D R_{OFF}} \psi(t)} \right) \quad (2)$$

The equation (2) is solved with respect to the magnetic flux $\psi(t)$ and the resulting connection between the charge and the magnetic flux is:

$$\psi(t) = -\frac{Q_D R_{OFF}}{2} \left\{ 1 - \frac{i_m}{\omega Q_D} [\cos \psi_i - \cos(\omega t + \psi_i)] \right\}^2 + \frac{Q_D R_{OFF}}{2} \quad (3)$$

Then the voltage on the memristor is obtained by the Faraday's law:

$$u(t) = \frac{d\psi(t)}{dt} = i_m \sin(\omega t + \psi_i) R_{OFF} \left\{ 1 - \frac{i_m}{Q_D \omega} [\cos \psi_i - \cos(\omega t + \psi_i)] \right\} \quad (4)$$

2.2. SIMULINK models of RM, LM and CM circuits

SIMULINK model of the memristor is based on the following formula:

$$q(t) = Q_D \left(1 - \sqrt{1 - \frac{2}{Q_D R_{OFF}} \psi(t)} \right). \quad (5)$$

The analytical base of the simulations is the Kirchhoff's voltage law and the respective expressions for voltages on the passive elements. The solutions are made at zero independent initial conditions, i.e. at the initial moment there is no energy stored in the conservative elements [2, 3].

The main goal of the present researches is obtaining the graphical characteristics of simple memristor circuits with one Williams’s memristor. For that reason Volt-Ampere Characteristics (VAC) and the spectral structure of the current in the circuits studied are analyzed (Section 3). Based on this, conclusions for the nonlinearity of circuits and appearance of higher harmonics are made (Section 4).

3. SIMULATION RESULTS FROM THE MEMRISTOR CIRCUITS STUDIED

In the present material simulations of behavior of simple memristor circuit with ideal sine current source and of series RM, LM and CM circuits with an ideal sine voltage source are made.

3.1. Analysis of a circuit with one memristor and ideal sine current source

The basic scheme of the studied circuit is presented in Fig. 2. The simulation is made based on formulae 1 – 4, combined in respective .m-file, started from the command window of MATLAB. The results are given in the Fig. 3, 4 and 5.

The magnetic flux as a nonlinear function of the charge accumulated in the element is presented in Fig. 3. Figure 4 shows the respective VAC, which has dual character and it looks like a “pinched hysteresis loop”. The distorting in form of the curve of the voltage on the memristor with respect to the sine curve of the current observed clearly with Fig. 5.

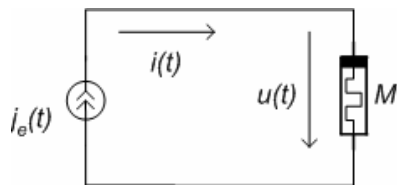


Fig. 2. Circuit with ideal sine current source and one memristor

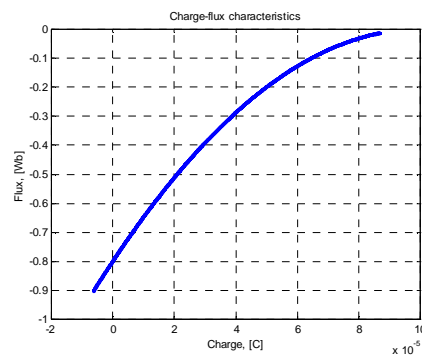


Fig. 3. Magnetic flux as function of the charge at $\omega = 3 \text{ rad/s}$ and magnitude of the current $i_m = 140 \mu\text{A}$

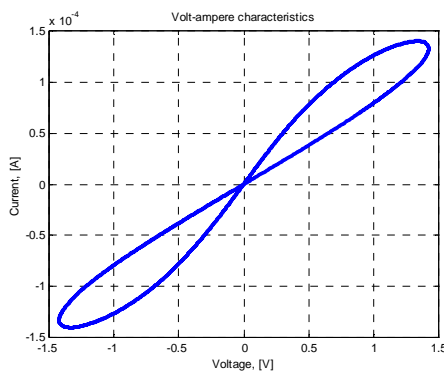


Fig. 4. Volt-ampere characteristic in frequency $\omega = 3 \text{ rad/s}$ and $i_m = 140 \mu\text{A}$

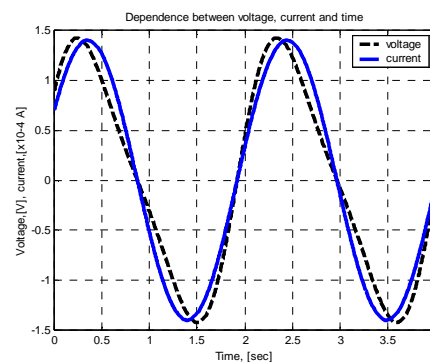


Fig. 5. The voltage and the current of the memristor as functions of time at frequency $\omega = 3 \text{ rad/s}$ and magnitude of the current $i_m = 140 \mu\text{A}$

3.2. Analysis of a series RM circuit supplied with a sine voltage source

The electrical scheme of a serial RM circuit with an ideal sine voltage source and parameters $R = 4,7 \text{ k}\Omega$, and $e_m = 1,8 \text{ V}$ is presented in Fig. 6. The resulting VAC of the studied memristor - $u_M(t) = f(i(t))$ - is shown in Fig. 7. Both the characteristics of the voltage of the analyzed memristor and the respective current, passed through the circuit studied, are non-sinusoidal (see Fig. 8). The spectral structure of the current in the circuit is presented in Fig. 9. As it was said in [3] the current simulations confirm contains of 1st, 2nd, 3rd and 4th harmonics of the current variation.

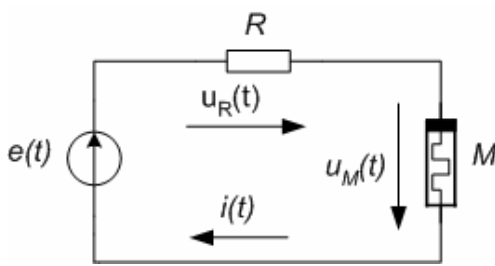


Fig. 6. Serial RM circuit with ideal sine voltage source

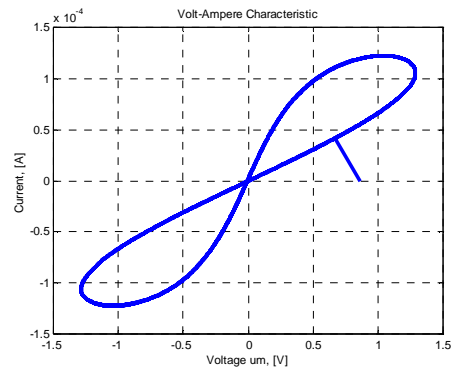


Fig. 7. Volt-ampere characteristics at frequency $\omega = 3 \text{ rad/s}$ and electromotive force $e_m = 1,8 \text{ V}$

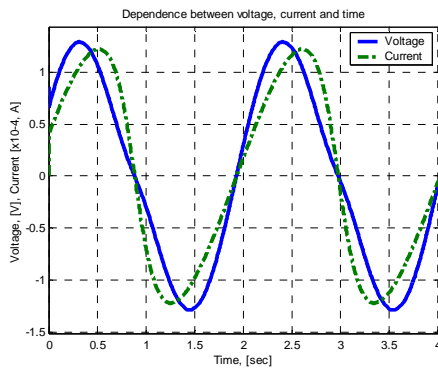


Fig. 8. The voltage and the current of the memristor at $\omega = 3 \text{ rad/s}$ and EMF $e_m = 1,8 \text{ V}$

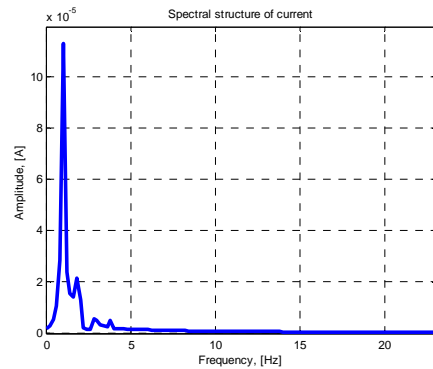


Fig. 9. Spectral analysis of the current in the circuit at $\omega = 3 \text{ rad/s}$ and EMF $e_m = 1,8 \text{ V}$

3.3. Analysis of a series LM circuit supplied with a sine voltage source

The electrical scheme of a series LM circuit with an ideal sine voltage source and parameters $L = 500 \text{ mH}$, and $e_m = 1,2 \text{ V}$ is presented in Fig. 10. The resulting VAC of the studied memristor - $u_M(t) = f(i(t))$ - is shown in Fig. 11.

The curves of the voltage on the memristor and current passed through the circuit studied are given in Fig. 12. There are non visible distortions on the voltage curve, so it has almost sine form. It can be explained with a very small voltage on the inductor at low frequencies of the current. Unfortunately, the current has significant distortions, according to the harmonics included – from 1st to 8th (see Fig. 13).

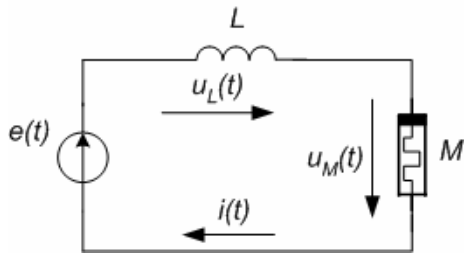


Fig. 10. Serial LM circuit with an ideal sine voltage source

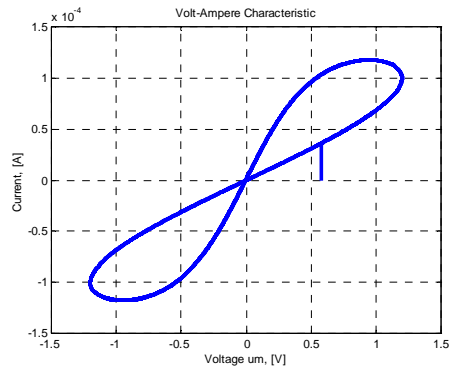


Fig. 11. Volt-ampere characteristics at frequency $\omega = 3 \text{ rad/s}$ and EMF $e_m = 1,2 \text{ V}$

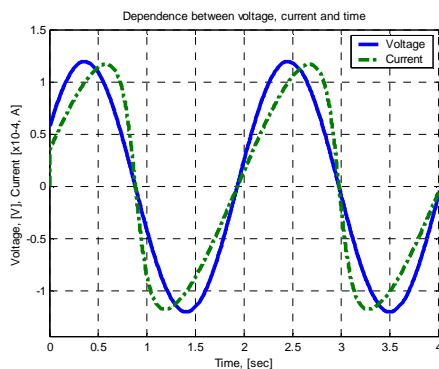


Fig. 12. The voltage and the current of the memristor at $\omega = 3 \text{ rad/s}$ and EMF $e_m = 1,2 \text{ V}$

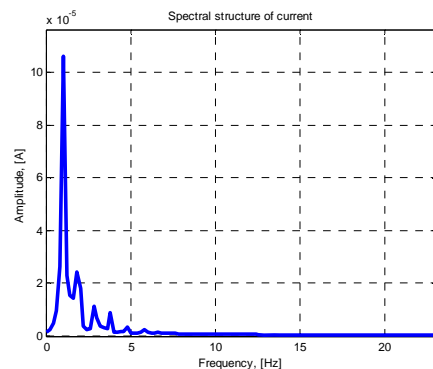


Fig. 13. Spectral structure of the current in the circuit at $\omega = 3 \text{ rad/s}$ and EMF $e_m = 1,2 \text{ V}$

3.4. Analysis of a series CM circuit supplied with a sine voltage source

The electrical scheme of a series CM circuit with an ideal sine voltage source and parameters $C = 1 \mu F$ and $e_m = 1,5 \text{ V}$ is presented in Fig. 14. The resulting VAC of the studied two-terminal CM circuit - $e(t) = f(i(t))$ – is shown in Fig. 15.

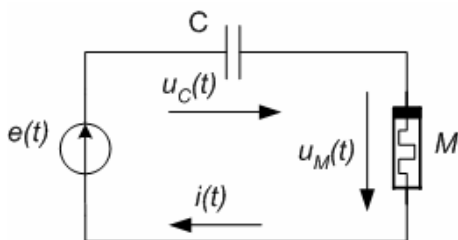


Fig. 14. Serial CM circuit with ideal sine voltage source

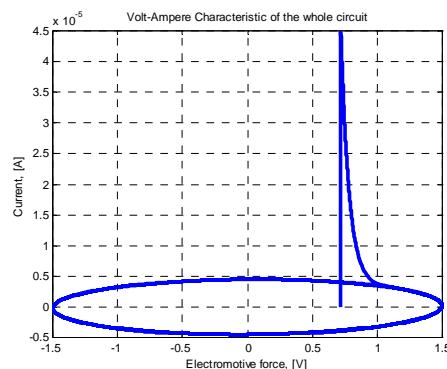


Fig. 15. Volt-ampere characteristics of the serial MC two-terminal circuit at $\omega = 3 \text{ rad/s}$ and EMF $e_m = 1,5 \text{ V}$

Analyzing the simulation results shown in Fig. 16, it can be seen that in the beginning of the experiment the current has a sharp local maximum due to the initial

charging of the capacitor. The spectral structure of the current is presented in Fig. 16. It includes only first harmonic and a very small value of DC component so that the curve of the current has a sine form.

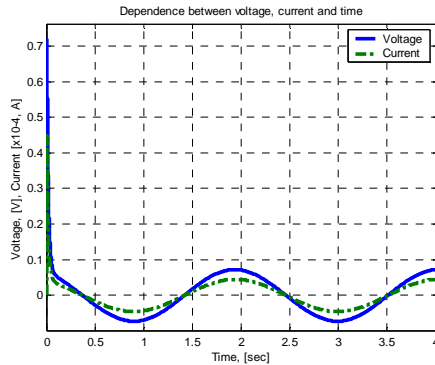


Fig. 16. The voltage and the current of the memristor at $\omega = 3 \text{ rad/s}$ and EMF $e_m = 1,5 \text{ V}$

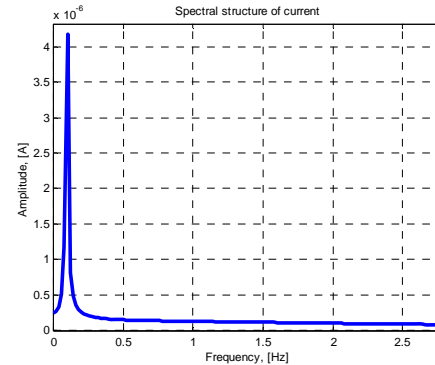


Fig. 17. Harmonic structure of the current in the circuit at $\omega = 3 \text{ rad/s}$ and EMF $e_m = 1,5 \text{ V}$

4. CONCLUSIONS

Currently, in the literature there are some publications, associated with the RM, LM and CM circuits analysis supplied by sinusoidal current and voltage sources [3]. Unfortunately, this is not sufficient for detailed analysis of these circuits. For this reason the present analysis is urgently needed. The simulation results show that there is a small nonlinear dependence between the current and the voltage of the memristor circuits. This fact explains the “poor” frequency spectrum of the current in the circuits studied – from 1st to 4th harmonics and from 1st to 8th, respectively. In both cases the DC-component has a small value.

Unfortunately, these passive two-terminal circuits cannot be fully linearized and couldn't be used well for filtering of electrical signals. Thus, they can be used only for analyzing of hybrid memristor-transistor circuits.

Acknowledgements: The results of the scientific researches, presented in this paper, are financed from the inner competition for scientific projects for help of PhD Students of Scientific-research sector of Technical University – Sofia for 2012 year, in the frames of project № 121ΠД0072-08 with topic: “Development of the algorithms for analysis of nonlinear electrical circuits with one, two or more memristor elements activated by sine and pulse supply”.

References

- [1] Chua, L. O. Memristor – The Missing Circuit Element. IEEE Trans. on Circuit Theory, Vol. CT-18, pp. 507-519, September 1971.
- [2] Strukov, D. B., G. S. Snider, D. R. Stewart, R. S. Williams. The missing memristor found. Nature, doi: 10.1038/nature06932, Vol 453, pp. 80–83, 2008.
- [3] Volos, C. K. et al. Memristors: A New Approach in Nonlinear Circuits Design, Department of mathematics and Engineering Sciences, Hellenic Army Academy, Athens, GR16673, Greece.
- [4] Yogesh, N., Joglekar and Stephen J. Wolf, The elusive memristor: properties of basic electrical circuits, Department of Physics, Indiana University Purdue, University Indianapolis, Indianapolis, Indiana 46202, pp. 1 – 24, January 13, 2009.

ANALYSIS OF A LCM EQUIVALENT CIRCUIT OF MEMRISTOR AND IMPULSE VOLTAGE SOURCES

Stoyan Kirilov, Svetoslav Dichev, Ivan Trushev, Valeri Mladenov

Department of Theoretical Electrical Engineering, Faculty of Automatics,
Technical University of Sofia, 1000, 8, Kliment Ohridski, Blvd., Sofia, Bulgaria,
tel. +3592/965-34-45,
e-mails: s_kirilov@tu-sofia.bg, s_dichev@tu-sofia.bg,
ivant@tu-sofia.bg, valerim@tu-sofia.bg

Abstract. *An equivalent inductance (L), capacitance (C) and memristance (M) (LCM) scheme of Williams's memristor with impulse voltage source is given in the presented paper. Computer simulation of the circuit is realized in MATLAB & SIMULINK environment. The parasitic inductance and capacitance of the memristor are obtained by approximate method and they are associated with a square memristor matrix with length of 3 cm and width of 3 cm. The transient response of investigated memristor circuit is obtained in graphical form. Sources of rectangular and triangular voltage pulses are also used in implementing the simulations. The basic diagrams in graphical form are obtained. Several basic conclusions and deductions in time domain and frequency domain properties of Williams's memristor are made. Conclusions for behavior of Williams's memristor at very high frequencies with rendering an account of its parasitic inductance and capacitance are also presented.*

Key words: *Williams's memristor, computer simulation, impulse mode, parasitic parameters.*

1. INTRODUCTION

Because of the importance of development of new effective computer memories with high storage a very crucial memristor investigation as a future memory element is being made. Its advantages are small dimensions (about 10 nm) and low power consumption [1, 2, 4]. The influence of parasitic inductances and capacitances and also of mutual inductances between rims of the memristor matrix must be rendered an account at high working frequencies. In the present paper the equivalent scheme of Williams's memristor is object of analysis. The parasitic parameters are shown in Fig. 1. The basic parameters of the circuit are: $w=1$ nm, $D=10$ nm, $\mu_v=1.10^{-14}$ m² / (V.s), $R_{ON} = 100$ Ω , $R_{OFF} = 16$ k Ω . The parasitic parameters of Williams's memristor have the values: $L_{par} = 1.10^{-15}$ H, $C_{par} = 3.10^{-17}$ F. The last two values are approximate. They are calculated at exemplary topologic structure of memristor matrix with length of 3 cm and width of 3 cm. Parasitic capacitance of Williams's memristor is calculated as capacitance of plane capacitor, and parasitic inductance of the element is obtained as inductance of semi-winding between platinum rims of the memristor. Because of the difficulty of obtained analytical relationships of Williams's memristor (Eq. 1), a numerical method in MATLAB environment with usage of SIMULINK toolbox is applied in investigation of the equivalent scheme of the memristor [6, 7].

2. PROBLEM STATEMENT

The main goal of present analysis is obtaining a visual concept for influence of parasitic inductance and capacitance of Williams's memristor in impulse mode. Transient voltage response is analyzed with an ideal input step voltage. The main tasks presented here are mainly associated with investigation of distortion of rectangular and saw-tooth voltage impulses in memristor circuit at very high frequencies up to 1000 GHz. The signals described here have very abundant frequency spectrum, especially the rectangular pulses with small coefficient of filling. The form and magnitude of current through signal source are analyzed too. On the base of presented simulations some conclusions of extent of influence of parasitic parameters and the memristor nonlinearity to exemplary impulse sequence are shown [3, 5].

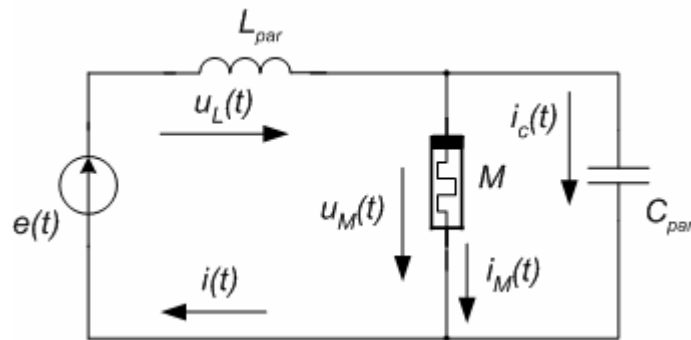


Fig. 1. Equivalent LCM scheme of Williams's memristor

3. SIMULATION RESULTS FROM THE MEMRISTOR CIRCUIT STUDIED

3.1. SIMULINK model of investigated circuit

A SIMULINK model of the memristor circuit is constituted – Fig. 1. For this task the Kirchhoff's laws and defining expressions of voltage drops of passive elements and currents through them are used. The main physical dependence for Williams's memristor is used too – see Eq.1:

$$i(t) = \frac{u(t)}{R_{OFF} \sqrt{1 - \frac{2\mu_D}{rD^2} \int u(t) dt}}. \quad (1)$$

The memristor circuits are examined under zero independent initial conditions, i.e. in the initial moment no energy is stored in conservative elements. The model obtained here is shown in Fig. 2. In the scheme a minimal number of differentiating parts are used. Therefore a formula about charge has not been used but Eq. (1) about current instead [6, 7].

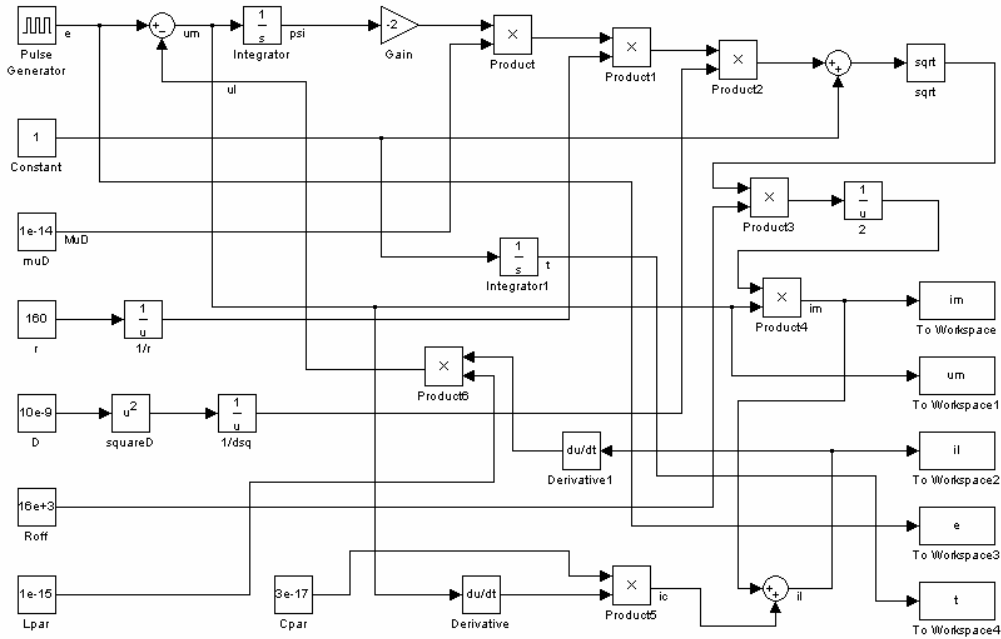


Fig. 2. SIMULINK model of investigated LCM memristor circuit

3.2. Obtaining transient response of examined circuit

For obtaining a transient response of analyzed circuit a step input voltage source with initial value of voltage 0 V and final value of 1 V has been used – see Fig.3. Output signal of analyzed circuit is voltage drop across the memristor. It represents the response of analyzed scheme – Fig. 4.

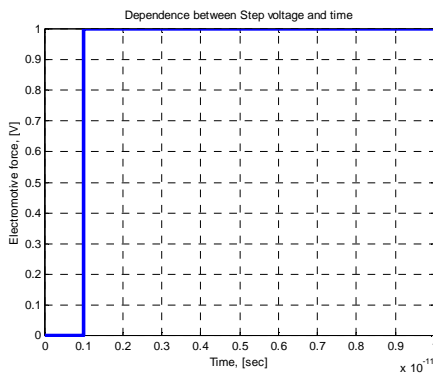


Fig. 3. Dependence between input stepped voltage and time

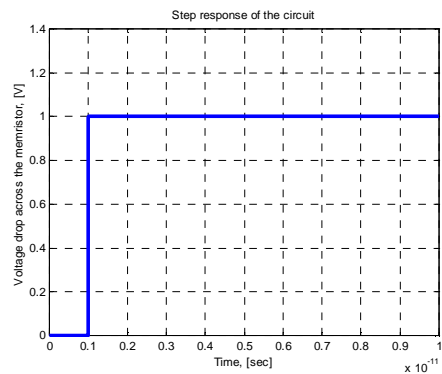


Fig. 4. Dependence between memristor voltage and time at stepped input impact

From simulation made here and from results obtained it is obvious that the signal hasn't obvious distortions. The circuit has behavior of a scheme built of only resistive elements. Because of very small values of memristor parasitic parameters in this case, they do not visibly affect transients [3].

3.3. Analysis of equivalent LCM scheme of memristor activated by rectangular pulse voltage source

The time diagram of EMF source is presented in Fig. 5. In the next Fig. 6 current through signal source has been shown. The current through the memristor and the voltage drop across it are presented in Fig. 7 and Fig. 8, respectively.

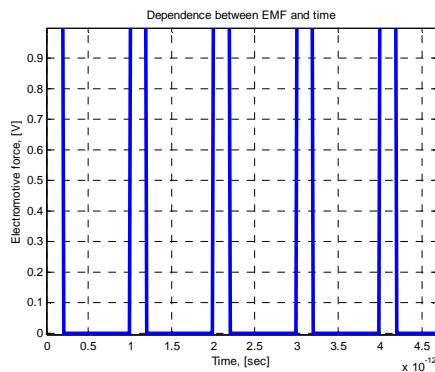


Fig. 5. Time diagram of rectangular pulse source EMF with frequency 1000 GHz and coefficient of filling 20 %

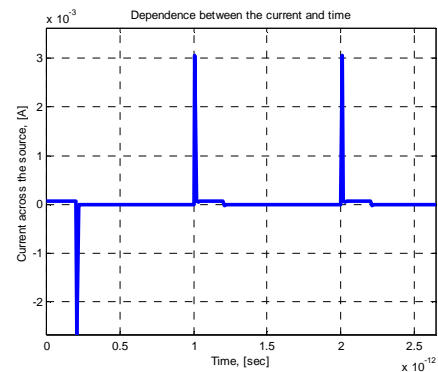


Fig. 6. Relationship between signal source current and time at rectangular pulse EMF

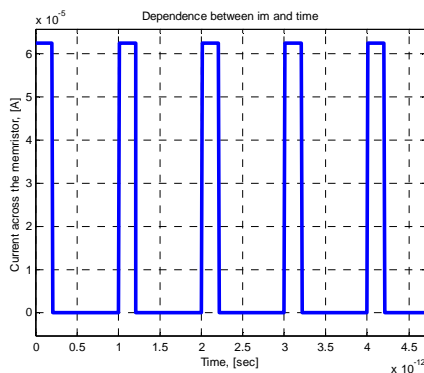


Fig. 7. Dependence between memristor current and time at rectangular pulse EMF

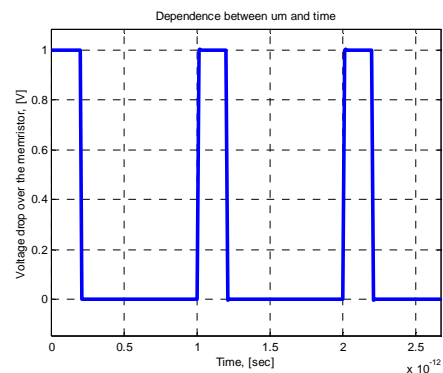


Fig. 8. Time diagram of memristor voltage drop u_m

Comparing the EMF impulses of the source and the voltage drop across the memristor u_M we can see that there are no visible distortions of voltage, i.e. the parasitic parameters do not affect quality of signals passing from input to the output of the circuit.

3.4. Analysis of equivalent LCM scheme of Williams's memristor activated by the saw-tooth voltage pulses

The dependence between saw-tooth voltage source and time at frequency 1000 GHz is presented in Fig. 9. In the next Fig. 10 a current through EMF source has been shown. This current represents a sequence of short duration pulses with steep fronts

and smooth back regions. This form of current pulses is due to transients in charging and recharging the parasitic capacitance. Current through the memristor and voltage drop across it are presented in Fig. 11 and Fig. 12, respectively.

Comparing Fig. 9 and Fig. 12 it is obvious that input saw-tooth impulses are not distorted at passing through examined circuit. This conclusion is the same as this in section (3.3), where rectangular pulses have been used.

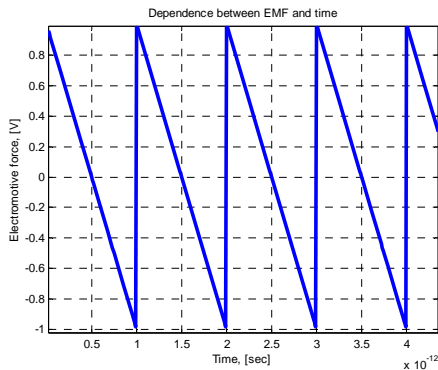


Fig. 9. Time diagram of saw-tooth pulse source EMF with frequency 1000 GHz

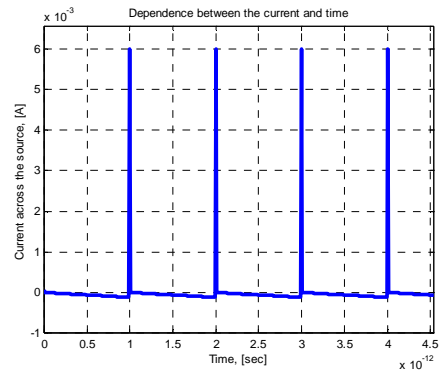


Fig. 10. Dependence between signal source current and time at saw-tooth pulse EMF

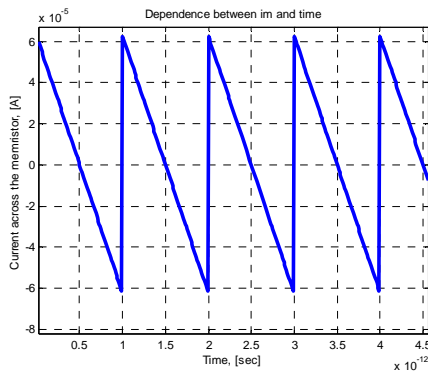


Fig. 11. Dependence between memristor current and time at saw-tooth pulse EMF

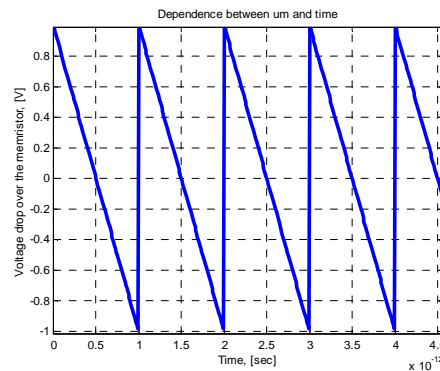


Fig. 12. Time diagram of voltage drop across the memristor

In spite of ultra high frequency pulse voltage sequences used in simulations in MATLAB & SIMULINK environment, parasitic parameters do not affect the form and magnitude of the input signal.

4. CONCLUSIONS

From the literature reference and simulations realized the following basic conclusions could be obtained. A few papers associated with investigations of memristor at impulse mode [3, 6] have been found. This fact has been a precondition for implementing the present analysis. The results obtained here confirm the assumption that at very high frequencies Williams’s memristor has a behavior of linear resistor, and parasitic inductances and capacitances do not distort the pulses. This fact is confirmed by investigation of transient response of the equivalent scheme. Because of that Wil-

Williams's memristor might work at ultra high frequencies – mainly in computer system memories, in neural networks in automatics, and in many other applied areas of technique.

The influence of mutual inductance between rims of memristor matrix and of capacitances between rims will be investigated in future papers.

Acknowledgements: The results of the scientific researches, presented in this paper, are financed from the inner competition for scientific projects for help of PhD Students of Scientific-research sector of Technical University – Sofia for 2012 year, in the frames of project № 121ПД0072-08 with topic: “Development of the algorithms for analysis of nonlinear electrical circuits with one, two or more memristor elements activated by sine and pulse supply”.

References

- [1] Chua, L. O. Memristor – The Missing Circuit Element. IEEE Trans. on Circuit Theory, Vol. CT-18, pp. 507-519, September 1971.
- [2] Strukov, D. B., G. S. Snider, D. R. Stewart, R. S. Williams. The missing memristor found. Nature, doi:10.1038/nature06932, Vol 453, pp. 80 – 83, 1 May 2008.
- [3] Torrezan, A. C., J. P. Strachan, G. Meederios-Ribeiro, R. S. Williams. Sub-nanosecond switching of a tantalum oxide memristor. Nanotechnology, Hewlett_packard Labs, pp.1 – 7, November 9, 2011.
- [4] Tour, J. M., T. He. The fourth element. Nature, Vol. 453, pp. 42 – 43, May 1, 2008.
- [5] Yogesh N. Joglekar and Stephen J. Wolf. The elusive memristor: properties of basic electrical circuits. Department of Physics, Indiana University Purdue, University Indianapolis, Indianapolis, Indiana 46202, pp. 1 – 24, January 13, 2009.
- [6] Zaplatilek, K. Memristor modeling in MATLAB & SIMULINK. Proceedings of the European Computing Conference, pp. 62 – 67.
- [7] The MathWorks, Inc. SIMULINK – dynamic system simulation for MATLAB. Users Guide, January 1999.

OPTIMISATION PROCEDURE FOR DETERMINATION OF THE OPTIMAL PARALLEL LINES FOR 110 KV ELECTRIC POWER DISTRIBUTION SYSTEMS

Georgi Komsalov, Georgi Tsenov, Valeri Mladenov

Theoretical Electrical Department, TU-Sofia, Kliment Ohridski N:8 blvd.,
3500, Sofia, Bulgaria, gogotzenov@tu-sofia.bg

Abstract. *Up to date in several power distribution systems there are main power lines without parallel connection between them. In such cases if there is a fault on some of the lines the consumers attached to the faulty line will be left without electricity. In order to avoid line faults if there are parallel lines interconnecting the main lines this problem can be avoided with electric energy redistribution from the healthy lines. When building such parallel lines in power distribution systems several aspects are to be taken into consideration when the exact connection places are to be determined. These aspects include the length of the parallel line, the type of cable required according to the peak energy consumption. This paper presents an optimisation procedure for determination of the optimal parallel line for connection of the main lines in one exemplar electric grid energy distribution system with three main lines.*

Keywords: *optimization, grid electric load, system modeling*

1. INTRODUCTION AND PROBLEM FORMULATION

Today the existing electrical power distribution systems in the big cities in Bulgaria are facing several problems in the present and especially in the future. With decentralization of the electric grid and making it managed by private companies without knowledge for the rest of the grid it's becoming harder to manage certain parts of the grid. There are many uncertainties that come into play that can harm the delivery of electric power to the consumers like fast addition of many new consumers in certain branches, increased probability for faults due to terrorist acts sabotage or by faults in the grid itself, as it is quite old. With the deregulation for the private electrical distribution companies several main 110KV transmission lines appear as connected in serial with no option to transfer energy from one to another in case of faults in certain parts of the grid. This can lead to lack of electrical energy supply, which is not acceptable in the 21st century. The solution – an multicriterial optimization procedure for determination of the optimal parallel line for connection of the main lines in one exemplar electric grid energy distribution system.

In this paper we present a method for determination of the best spots for creation of parallel lines in the existing grid, that will connect the main distribution line in a way that despite some of the sources is being cut from the grid, the distribution grid can be powered from the other sources. The best parallel reserve line connection spots are determined with optimization procedure by obtaining the minimal line length and minimal current going through the parallel line, while checking if the parts

of the existing grid will be able to hold on increased power flow. This is having an impact on the money invested in the parallel lines, as minimal distance means less cable length used, and minimal currents means that the cable requirements will be lessened meaning that cheaper cable type can be used.

One example is done in a power grid in Sofia and the data we have been provided to work with involves three serial 110kV distribution lines without parallel connection between them. Each line has many transformer stations for voltage reduction from 110 to 22kV. Unfortunately the data provided from the electric distribution company is confidential, resulting that the gps coordinates, energy consumption, peak currents, cable types, transformer station parameters and the other parameters used in the optimization procedure are not to be published, and that only partial general results can be given.

2. MODELING AND SIMULATION OF THE ELECTRIC GRID

For modeling the electric grid we used MATLAB. In this development environment in contrast to tools like PSpice there is a lot of freedom for circuit generation and parameter tune. We used a voltage potential method with functions to easily create the conductivity matrix of the grid by applying the conductance between two nodes. From the problem formulation we have several power distribution systems in which there are main power lines without parallel connection between them. In such cases if there is a fault on some of the lines the end result is that consumers attached to the faulty line will be left without electricity and in order to avoid line faults and increase reliability if there are parallel lines interconnecting the main lines this problem can be avoided with electric energy redistribution from the healthy lines. The grid taken into account is shown on Figure 1.

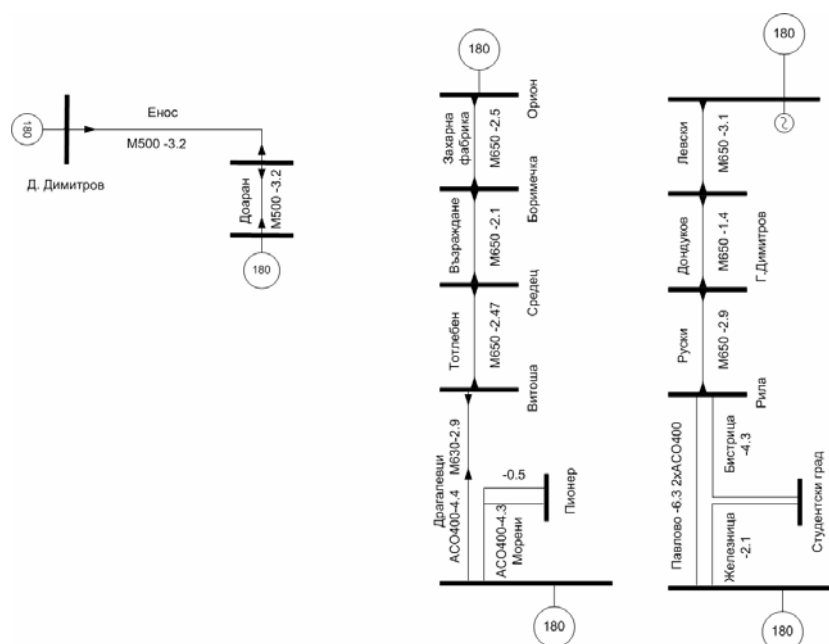


Fig. 1. The three main 110kV lines with transformer stations

When building the parallel lines in power distribution systems several aspects are to be taken into consideration when the exact connection places are to be determined.

These aspects include:

- The power supply system – nominal Voltage, nominal Frequency, Short circuit power, X/R ratio;
- cable line parameters – specific resistance and inductance per km;
- linear conventional loads – nominal active and reactive power;
- the length of the parallel line (if it's bigger it will be expensive);
- the type of cable required according to the peak energy consumption;
- capability of the existing infrastructure to handle the loads.

As already mentioned there are three serial 110 KV independent lines and each of the serial line consists of Voltage Transformers from 110 KV to 22 KV for distribution of electric energy for domestic needs. For simplicity the transformer stations with the exception of the endpoint stations are considered as an consumer. The line endpoint voltage transformer stations are connected to high power transmission lines and can deliver enough power to all of the consumers of entire line if needed (if the infrastructure can handle the load). Distances of the existing cable connections and cable types between the stations are known, and also the GPS coordinates on every single transformer station are known. By knowing the distance between the transformer stations and the cable type used the cable length can be modeled with cable resistance and cable inductivity per kilometer. From catalogue data per kilometer cable Resistance is 0.06 Ohm and the inductance is 0.4H. The distances considered are very small so modeling line capacitive behavior from line to ground is very small and will not be considered.

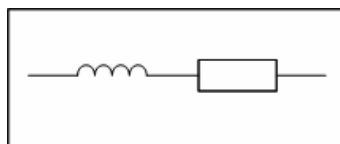


Fig. 2. Cable line modeling with 0.06 Ohm and 0.4H per km line length

The consumers are modeled with R and L according to the data for the consumed power. For domestic energy distribution $\cos\phi=0.9$

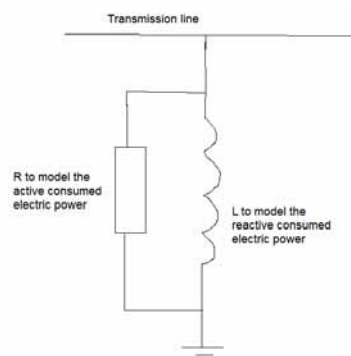


Fig. 3. Modeling the transformers as consumers

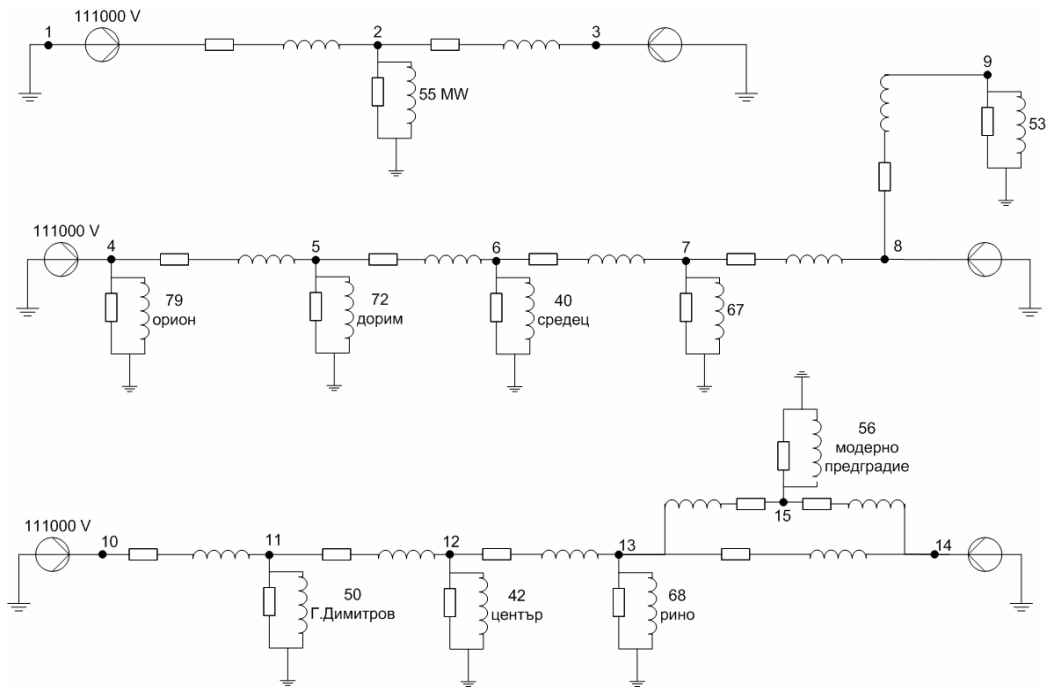


Fig. 4. Electrical model of the grid

A program code in MATLAB is generated that makes a electric grid bias point calculation. Then this code is inserted in a loop cycle where the sources are independently removed one by one for every possible combination of the parallel lines. Monitored are the peak currents passing through the transformer stations and the cable distance is calculated with the usage of GPS coordinates. With this calculated cable distance the parallel cable line R and L are also inserted into the model. This results in a various grid combinations as shown on Figure 5.

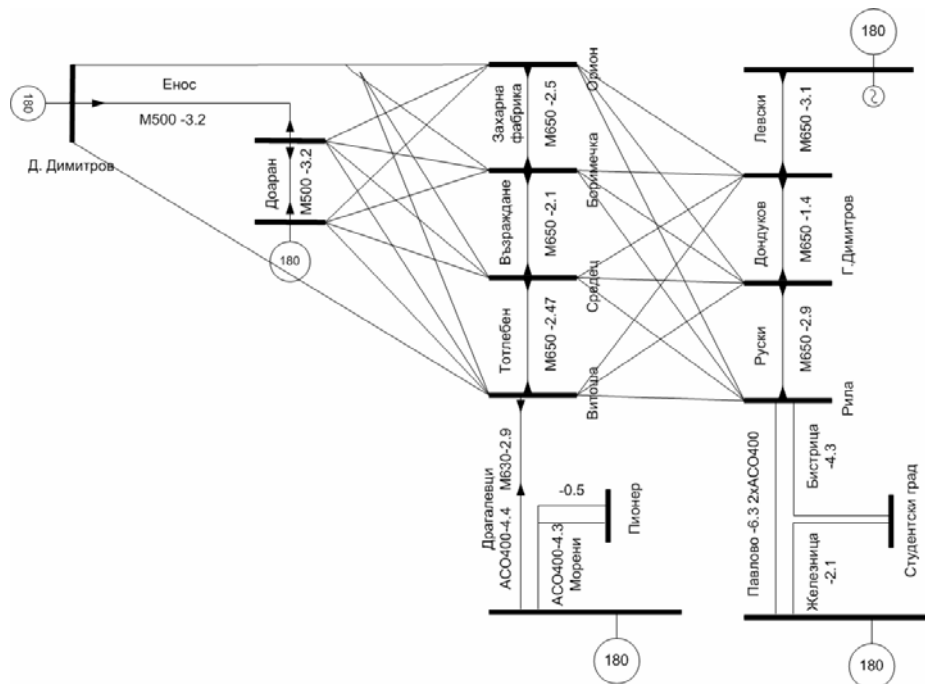


Fig. 5. The grid with some of the possible solutions

The best solution is to have a fulfillment of infrastructure endurance on peak currents that are lesser than the maximal by cable specifications of the existing infrastructure while having the minimal distance in km between the new lines.

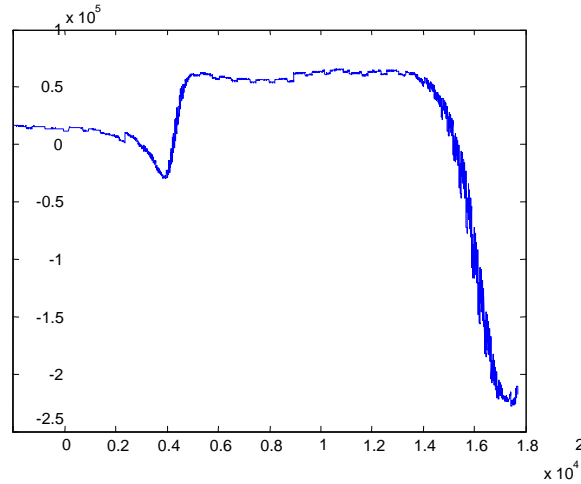


Fig. 6. Current variation trough one node for many grid stricture variations

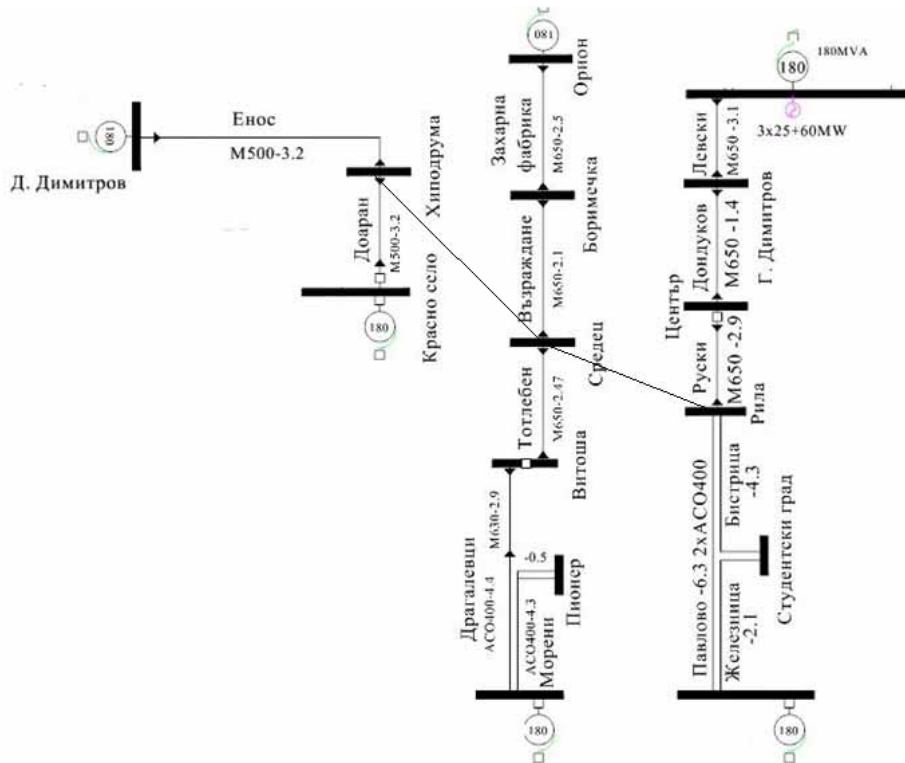


Fig. 7. The best solution for the parallel lines

3. CONCLUSION

With computational algorithms the optimal places for placement of parallel lines in existing electric grids can easily be determined with respect to minimal line costs and acceptable minimal peak power transfer from the infrastructure.

References

- [1] Zhiyu Zeng, Zhiyu Zeng; Peng Li, Peng Li, Locality-Driven Parallel Power Grid Optimization, *Computer-Aided Design of Integrated Circuits and Systems*, IEEE Transactions on, Volume 28 (8)
- [2] Bo Yu, Jun Xiao, Li Guo, Multi-scenario, multi-objective optimization of grid-parallel Microgrid, *Electric Utility Deregulation and Restructuring and Power Technologies (DRPT)*, 2011 4th International Conference, pp.1638 - 1646
- [3] R. K. Ahuja, T. L. Magnanti, and J. B. Orlin. *Network Flows: Theory, Algorithms, and Applications*. Prentice Hall, NJ (1993).
- [4] J. Salmeron, K. Wood, and R. Baldick, Analysis of Electric Grid Security Under Terrorist Threat, *IEEE Trans. Power Systems* 19 (2004), 905-912.
- [5] J. Arroyo and F. Galiana, On the Solution of the Bilevel Programming Formulation of the Terrorist Threat Problem, *IEEE Trans. Power Systems*, Vol. 20 (2005), 789-797.
- [6] D. Bienstock and S. Mattia, Using mixed-integer programming to solve power grid blackout problems, *Discrete Optimization* 4 (2007), 115-141.

ИНВАРИАНТИ НА ЧУВСТВИТЕЛНОСТТА НА ЧЕСТОТНО СЕЛЕКТИВНИ КОМУНИКАЦИОННИ ВЕРИГИ

Антонио Андонов, Силвия Андонова, Марияна Михова

Катедра "СОТС", Висше транспортно училище "Тодор Каблешков",
ул. Гео Милев 158, София 1574, България, тел: +359 29709426,
e-mail: andonov@vtu.bg, sss5@abv.bg

Резюме. *Едно от съвременните направления в решаването на проблема за повишаване на шумоустойчивостта и ефективността на комуникационните канали е синтезът на адаптивни предизкривяващи филтри, компенсирани изменящата се активност на канала. При синтеза на такива филтри е от особено значение определянето на зависимостта на техните свойства от изменението на параметрите им, задавани с т.н. функции на чувствителност. Настоящата статия разглежда определянето на специални функционални зависимости между тези функции, наричани инварианти на чувствителността. Те са от голямо практическо значение, защото определят ограниченията за независимо изменение на функциите на чувствителност при синтеза на оптимални нискочувствителни адаптивни филтри*

Ключови думи: *Инварианти на чувствителността, нискочувствителни адаптивни филтри*

1. ВЪВЕДЕНИЕ

Повишаването на шумоустойчивостта и ефективността на комуникационните системи заема важно място в съвременната теория и техника на предаването на информация. Един от подходите в това направление е свързан със синтеза на т.н. предизкривяващи филтри в предавателя, които биха реализирали такова изменение на формата на предавания сигнал, което би обусловило неизкривена форма на сигнала в точката на приемане, т.е. би осигурило компенсация на реакция на комуникационния канал. При синтеза на такива филтри от особено значение е определянето на зависимостта на техните свойства от изменението на параметрите им, известно като проблем за чувствителността. Неговата същност се определя чрез численото изследване на параметричния модел на веригата в целия обхват на изменение на определящата съвкупност от параметри. Основен метод за изследване в теорията на чувствителността е използването на т.н. функции на чувствителността. Нека $\{\alpha_i\}_{i=1}^m$ е множество от параметрите на веригата, образуващо пълна съвкупност на α . При това променливата на състоянието $Y_i(t, \alpha)$ и показателите за качество $J_i(\alpha)$ са еднозначни функции на параметрите α_i . Тогава частните производни

$$\frac{\partial Y_i(t, \alpha)}{\partial \alpha_k}, \frac{\partial J_i(\alpha)}{\partial \alpha_k} \quad (1)$$

се наричат функции на чувствителността по отношение на съответните параметри.

Ако входните $X = X(t)$ и изходните $Y = Y(t)$ сигнали са векторни функции на времето, то конволюцията, определяща връзката между входа и изхода се представя аналитично чрез линеен оператор от вида [2-3],

$$Y(t) = L(x) = \int_{-\infty}^{\infty} H(t, \tau) X(\tau) d\tau = \int_{-\infty}^{\infty} H(t, t - \tau) X(t - \tau) d\tau \quad (2)$$

Тук ядрото на интегралния оператор $H(t, \tau)$ е известно и пълно изследвано, като матрична функция на Грин [2,3]. Ако функцията на Грин $H(t, \tau)$ удовлетворява условието

$$H(t, \tau) = 0 \text{ за } t < \tau \quad (3)$$

то операторът (2) е физически реализуем. Функциите на Грин в този случай се наричат тегловни функции. Равенство (2) за физически реализуем оператор приема вида

$$Y(t) = L(x) = \int_{-\infty}^t H(t, \tau) X(\tau) d\tau = \int_0^{\infty} H(t, t - \tau) X(t - \tau) d\tau. \quad (4)$$

2. ОПРЕДЕЛЯНЕ НА ИНВАРИАНТИ НА ЧУВСТВИТЕЛНОСТТА НА ПРЕДАВАТЕЛНИ ФУНКЦИИ НА КОМУНИКАЦИОННИ ВЕРИГИ

Както е известно, предавателната функция $W(p)$ на линеен пасивен четири-полюсник представлява дробнорационална функция [1], т.е. отношение на полиноми на Хурвиц от вида:

$$W(p) = \frac{B(p)}{A(p)} = \frac{\sum_{i=0}^s b_i p^{s-1}}{\sum_{i=0}^n a_i p^{n-1}}, \quad s \leq n,$$

коэффициентите на които a_i и b_i зависят от параметрите $\alpha_1, \dots, \alpha_n$. Може да се покаже, че ако е изпълнено условие (2), то съществува инвариант във вида

$$W(p) = \sum_{k=1}^m \frac{\partial \ln W(p)}{\partial \ln \alpha_k} = const. \quad (5)$$

За тази цел да определим най-напред кореновите инварианти на чувствителността на предавателната функция. Да разгледаме многочлена

$$D(p) = \sum_{k=0}^n a_k p^{n-k} \text{ за } a_0 \neq 0,$$

корените на който са нули или полюси на предавателната функция на веригата и зависят от параметрите $\alpha_1, \dots, \alpha_m$: $p_i = p_i(\alpha_1, \dots, \alpha_m)$, $i \in (1, n)$. Сумата от корените на многочлена $D(p)$ е равна на :

$$\sum_{i=1}^n p_i = \frac{a_1}{a_0} \quad (6)$$

Ако се диференцира това отношение по параметъра α_k , се получава

$$\sum_{i=1}^n \frac{\partial p_i}{\partial \alpha_k} = -\frac{\frac{\partial a_1}{\partial \alpha_k} a_0 - \frac{\partial a_0}{\partial \alpha_k} a_1}{a_0^2}. \quad (7)$$

Ако коефициентите a_0 и a_1 не зависят от параметъра α_k , т.е. $\frac{\partial a_1}{\partial \alpha_k} = 0$ и

$\frac{\partial a_0}{\partial \alpha_k} = 0$, то

$$\sum_{i=1}^n \frac{\partial p_i}{\partial \alpha_k} = 0 \quad \text{или} \quad \sum_{i=1}^n \frac{\partial p_i}{\partial \ln \alpha_k} = 0. \quad (8)$$

Следователно сумата от коефициентите на полинома $D(p)$ по отношение на изменението на параметъра α_k е равна на нула, т.е това е инвариант.

Нека коефициентите a_0, a_1, \dots, a_n са полилинейни функции на параметрите $\alpha_1, \dots, \alpha_m$. Тогава са в сила зависимости от тип (2):

$$\sum_{k=1}^m \alpha_k \frac{\partial a_i}{\partial \alpha_k} = q a_i, \quad i \in (0, n). \quad (9)$$

Ако умножим с α_k и сумираме по k лявата и дясна част на равенството (7), като отчетем (9) можем да получим, че:

$$\sum_{k=1}^m \sum_{i=1}^n \frac{\partial p_i}{\partial \ln \alpha_k} = -\frac{1}{a_0^2} (a_0 a_1 - a_1 a_0) = 0$$

Следователно, получава се инвариант

$$\sum_{k=1}^m \sum_{i=1}^n \frac{\partial p_i}{\partial \ln \alpha_k} = 0 \quad (10)$$

Да разгледаме сумата

$$\sum_{k=1}^m \frac{\partial p_i}{\partial \ln \alpha_k}$$

за случай на комплексно спрегнати корени. Като диференцираме тъждеството $D(p_i) = 0$ по параметъра α_k , получаваме

$$\frac{\partial D}{\partial p_i} \frac{\partial p_i}{\partial \alpha_k} + \sum_{j=0}^n \frac{\partial D}{\partial a_j} \frac{\partial a_j}{\partial \alpha_k} = 0,$$

откъдето

$$\frac{\partial p_i}{\partial \ln \alpha_k} = - \frac{\sum_{j=0}^n p_i^{n-j} \frac{\partial a_j}{\partial \ln \alpha_k}}{\frac{\partial D}{\partial p_i}} \quad (11)$$

Тогава, като се отчете равенство (10) се получава

$$\sum_{k=1}^m \frac{\partial p_i}{\partial \ln \alpha_k} = - \frac{q \sum_{j=0}^n p_i^{n-j} a_j}{\frac{\partial D}{\partial p_i}} = - \frac{q D(p_i)}{\frac{\partial D}{\partial p_i}}. \quad (12)$$

В резултат получаваме инвариант

$$\sum_{k=1}^m \frac{\partial p_i}{\partial \ln \alpha_k} = 0. \quad (13)$$

Съответно, за предавателната функция $W(p)$ на веригата може да се запише:

$$\begin{aligned} \frac{\partial \ln W(p)}{\partial \ln \alpha_k} &= \frac{\alpha_k}{W(p)} \left[\sum_{i=0}^n \frac{\partial W(p)}{\partial a_j} \frac{\partial a_i}{\partial \alpha_k} + \sum_{i=0}^s \frac{\partial W(p)}{\partial b_j} \frac{\partial b_i}{\partial \alpha_k} \right] = \\ &= \frac{\alpha_k}{W(p)} \left[\frac{1}{A(p)} \sum_{i=0}^s p^{s-i} \frac{\partial b_i}{\partial \alpha_k} - \frac{B(p)}{A^2(p)} \sum_{i=0}^n p^{n-i} \frac{\partial a_i}{\partial \alpha_k} \right] = \\ &= \frac{\alpha_k}{B(p)} \sum_{i=0}^s p^{s-i} \frac{\partial b_i}{\partial \alpha_k} - \frac{\alpha_k}{A(p)} \sum_{i=0}^n p^{n-i} \frac{\partial a_i}{\partial \alpha_k} \end{aligned}$$

Като се отчете (8) и израза за инвариант (13) след редица преобразувания се получава

$$\sum_{j=1}^m \frac{\partial \ln W(p)}{\partial \ln \alpha_j} = \sum_{j=1}^m \frac{\partial \ln k}{\partial \ln \alpha_j} = \text{const} \quad (14)$$

3. ОПРЕДЕЛЯНЕ ИНВАРИАНТИТЕ НА ЧУВСТВИТЕЛНОСТТА НА ПАСИВНИ И АКТИВНИ ФИЛТРИ

Да разгледаме предавателната функция на елементарен пасивен RC филтър [1]

$$W(p) = \frac{1}{1 + Tp}, \quad T = RC.$$

Тази предавателна функция може да се представи във вида

$$W(p) = \frac{g}{g + Cp}, \quad g = \frac{1}{R},$$

където g е проводимостта.

Да разгледаме сумата

$$S(p) = \frac{\partial \ln W(p)}{\partial \ln C} + \frac{\partial \ln W(p)}{\partial \ln g}$$

Тъй като

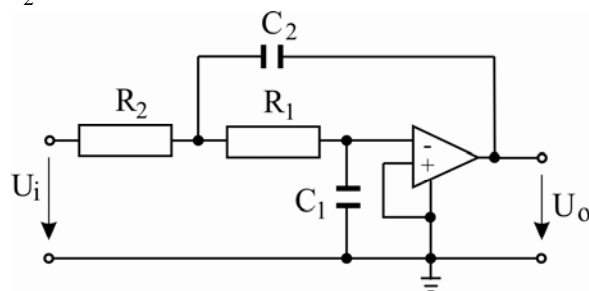
$$\frac{\partial \ln W(p)}{\partial \ln C} = -\frac{Cp}{g + Cp}, \quad \frac{\partial \ln W(p)}{\partial \ln g} = -\frac{Cp}{g + Cp},$$

то следва, че $S(p) = 0$.

Нека е дадена схемата на активен филтър (фиг. 1) с предавателна функция [1]:

$$W(p) = \frac{k}{1 + [C_1(R_1 + R_2) - (k-1)C_2R_2][p + R_1]R_2C_1C_2p^2} = \frac{g_1g_2k}{g_1g_2 + [C_1(g_1 + g_2) - (k-1)C_2g_1]p + C_1C_2p^2},$$

където $g_1 = \frac{1}{R_1}$, $g_2 = \frac{1}{R_2}$.



Фиг. 1. Активен филтър

Появилият се параметър k , който е безразмерен за получаването на инварианти, не е необходимо да се отчете при сумирането, тъй като не е необходимо да се отчита чувствителност по този параметър. Тогава се получава

$$\frac{\partial \ln W(p)}{\partial \ln g_1} = \frac{C_1(g_2 + C_2 p)p}{lp}$$

$$\frac{\partial \ln W(p)}{\partial \ln g_2} = \frac{[(C_1 - k - 1)C_2]g_1 p + C_1 C_2 p^2 + C_1 g_2 p}{l(p)}$$

$$\frac{\partial \ln W(p)}{\partial \ln C_1} = -\frac{C_1(g_1 + g_2)p + C_2 p^2}{l(p)}$$

$$\frac{\partial \ln W(p)}{\partial \ln C_2} = -\frac{C_2(1-k)g_1 p + C_2 p^2}{l(p)},$$

където

$$l(p) = g_1 g_2 + [C_1(g_1 + g_2) - (k-1)C_2 g_1]p + C_1 C_2 p^2$$

и съответно

$$\frac{\partial \ln W(p)}{\partial \ln g_1} + \frac{\partial \ln W(p)}{\partial \ln g_2} + \frac{\partial \ln W(p)}{\partial \ln C_1} + \frac{\partial \ln W(p)}{\partial \ln C_2} = 0.$$

4. ЗАКЛЮЧЕНИЕ

Пред изкривяващите и коригиращи филтри, използвани за реализиране на линейни операции на сместа сигнал-шум с цел при неизменна средна мощност на сигнала на входния комуникационен канал да се увеличи отношението сигнал-шум на входа на приемника, представляват минимално-фазови пасивни и активни четириполусници. Анализът на параметричната чувствителност на такива филтри, особено при реализация на адаптивно предизкривяване по отношение на изменящата се активност на канала изисква определяне на различни ограничения и взаимни връзки между функциите на чувствителността. Определенето на инвариантите на чувствителността на такива филтри са от изключителна актуалност, защото показват ограниченията за независимо изменение на функциите на чувствителност при синтеза на нискочувствителни оптимални филтри и облекчават анализа на тяхната чувствителност.

Литература

- [1] Андонов А., Г. Д. Ненов, Комуникационни вериги и сигнали, София, ВТУ, 2006, 320 стр.
- [2] Lange F. H., Signale und systeme, VEB Verlunng Technik, Berlin, 1970
- [3] Read R., The Essence of Communication Theory, Berlin Heidelberg, 2005.

УНИВЕРСАЛЕН УЛТРАВИОЛЕТОВ ОПТИЧЕН МИКРОСКОП И RIFE BEAM RAY (RBR) – ДВЕ ОТКРИТИЯ БЕЗ АВТОРСТВО

*Валентина Танева Танева-Тончева¹, Иван Танев Иванов²,
Радостина Пенева Ташева³*

⁽¹⁾Департамент по приложна физика, Технически Университет, адрес, uraa@dir.bg,

⁽²⁾ Dept. of Physics, Biophysics, Roentgenology and Radiology; Medical Faculty;
Thracian University, Stara Zagora 6000, Bulgaria, ivanov_it@gbg.bg,

⁽³⁾ Департамент по приложна физика, Технически Университет, rpt@tu-sofia.bg

Abstract. *This paper presents two of doctor's Royal Remand Rife discoveries: 1) Universal heterodyne UV optical microscope, which gives 60 000X magnifications. This device enables its user to find so called. Mortal Oscillatory Rate (MOR) for a wide spectrum of pathogen microorganisms; 2) The Rife Beam Ray (RBR) – a device for electromagnetic therapy.*

Ключови думи: *оптика, микроскоп, резонанс, амплитудна модулация, патогенни микроорганизми, честоти на д-р Райф.*

1. УВОД

Човешкото око е естествена оптическа система, която се характеризира с определена разделителна способност $d=0,176 \text{ mm}$ от разстояние на най-добро виждане – 250 mm [1, 3, 8]. Размерите на микроорганизмите, голяма част от растителните и животински клетки, малките кристали, детайлите от микроструктурата на кристалите и сплавите и т.н., са значително по-малки от тази стойност.

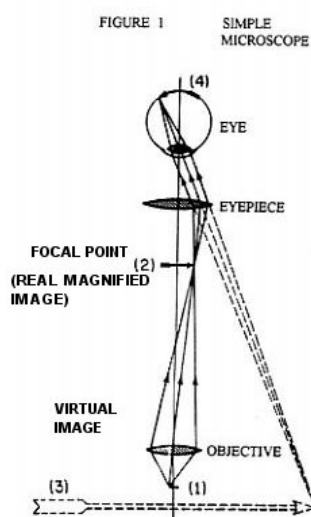
За наблюдението и изучаването на подобни малки обекти са създадени микроскопите от различен тип: оптичен – на близкото поле, конфокален, двуфотонен лазерен; електронен – просветващ, растерен; сканиращ електронен – атомно-силов, тунелен; рентгенов микроскоп – отражателен, проекционен, лазерен; диференциален интерференчно контрастен микроскоп.

До средата на XX век се работи само с видимо – оптично, излъчване в диапазона 400-700nm и близката UV област.

2. ОПТИЧЕН МИКРОСКОП

Основно предимство на оптичния микроскоп е, че през системата от лещи преминава видима светлина и дава увеличен образ. Така могат да се наблюдават невидими с просто око малки обекти.

Оптическата част на микроскопа включва *обектив* и *окуляр* [1, 2]. При работата с него светлината пада върху огледало, отразява се и преминавайки през кондензор, се концентрира върху образеца (1), фиксиран върху предметната масичка. Обективът дава увеличен действителен образ (2), който се наблюдава с око през окуляра, подреден в оптичната система като лупа непосредствено – образ (3) – фиг. 1.



Фиг. 1: Оптичен микроскоп:

- (1) – обект;
- (2) – образ от обектива
- (3) – образ от окуляра;
- (4) – око.

От гледна точка на геометричната оптика, подходяща комбинация обектив-окуляр би могла да даде неограничено увеличение, но – на практика – увеличението на микроскопа се получава като произведение от увеличението на обектива и окуляра, съответно

$$V = W_{obj} \cdot W_{oc}. \quad (1)$$

Всяко от тях се пресмята по формулата:

$$W = f/(a-f), \quad (2)$$

където f е фокусното разстояние на съответната леща, a е разстоянието от обекта до равнината на лещата.

Максималното увеличение за комбинацията обектив-окуляр е 10×100 , което дава окончателно **1000x** за жълта светлина (светлина, разделителната способност на която е около $0,2 \mu\text{m}$). При използване на

светлина от UV-областта увеличението може да достигне $2000\text{--}3000x$ (разделителна способност $0,1 \mu\text{m}$). В бактериологията се използва полезно увеличение $900x$ (обектив – $90x$, окуляр – $10x$). На практика се приема, че разделителната способност е равна на половината дължина на вълната на използваната за наблюдение светлина.

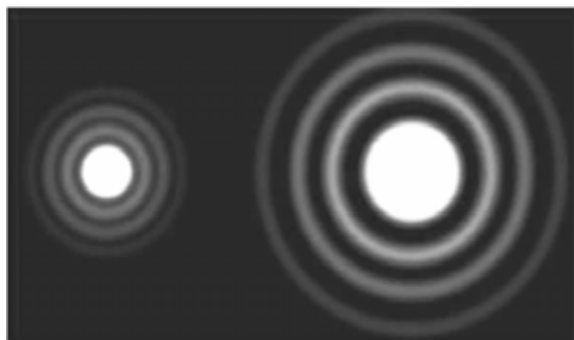
За изучаване на обекти, по-малки от посочените, се използват микроскопи, работещи с отразена светлина, като за целта се подбират кондензори на тъмно поле с параболична или кардиоидна форма.

Осветяването на образците е важно за получаване на висококачествени изображения в микроскопията. Август Келер през 1893 година разработва метод за осветяване, при който върху образа на обекта вече не се наслагва образът на осветяващата лампа с нажежаема жичка. През 1953 година Фриц Церник получава Нобелова награда за разработения от него метод на фазовия контраст, с помощта на който могат да се наблюдават и прозрачни обекти. Този метод отстранява нуждата от предварително оцветяване на живите клетки, нещо, което обикновено ги умъртвява.

За да се разбере причината за ограниченията, наложени от природата върху оптичните микроскопи, да разгледаме проблемите, поставящи предел на полезното увеличение.

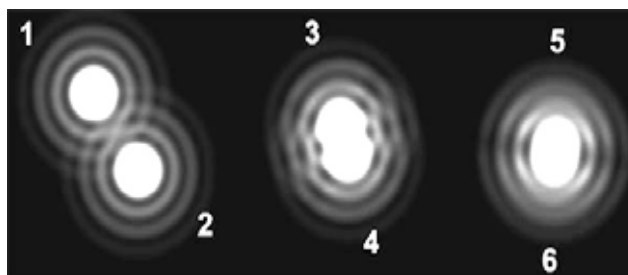
2.1. Фраунхоферова дифракция

Заради дифракционните явления в оптичните прибори точков обект, наблюдаван чрез единична двойно изпъкнала леща, не е точка, а система от концентрични светли и тъмни пръстени, съгласно принципите на Хюйгенс-Френел – фиг. 2.



Фиг. 2. Светеща точка, наблюдавана през обективи с нулева сферична aberация и различна числова апертура $A = n \sin i$ – вляво с два пъти по-голяма апертура от тази на дясното. Интензивността на централния максимум е приблизително 85% от сумарната интензивност на всички останали части на изображението. Снимка: „Квант“.

Ако наблюдаваме не един, а два точкови обекта, всеки от техните образи, поради Фраунhoferовата дифракция, представлява система от концентрични тъмни и светли пръстени. – фиг. 3.



Фиг. 3. Изображение на група точкови източници: 1 и 2 са на разстояние, значително по-голямо от $d = 0,61\lambda / (n \sin i)$; 3 и 4 — на разстояние $d/2$; 5 и 6 — на разстояние, значително по-малко от $d/2$. Снимка: «Квант»

Ако разстоянието d между обектите стане достатъчно малко, образите им ще започнат да се припокриват. Това означава, че върху поставения за наблюдение образец не всеки две самостоятелно светещи точки ще могат да бъдат наблюдавани отделно една от друга, защото светлите центрове на техните Фраунhoferови образи ще се припокриват забележимо.

В оптиката, за разделение на изображенията, се използва критерий на Релей, когато първият тъмен пръстен на едното съвпада със светлия център на другото:

$$d = \frac{0,61\lambda}{n \sin i} \quad (3)$$

където d е минималното възможно за наблюдаване разстояние между двата обекта (разделителна способност), λ е дължината на вълната на използваната светлина, n е относителният показател на пречупване между средата, в която са обектите и лещата, а i е апертурен ъгъл на оптичната система за наблюдение.

Произведението $A=nsini$ се нарича *числова апертура* и тя определя разделителната сила на микроскопа.

Критерият на Релей, съгласно с Теорията на Аббе за микроскопа, е приложим както за осветявани обекти, така и за самосветещи. Замествайки съответстващите стойности за λ , n и i , уравнение (3) дава минимална стойност за d около $0,2 \mu m$, както бе споменато по-горе, която стойност е на порядък по-голяма от средния радиус на вирусите. Тези $0,2$ микрона са разделителна способност, получена без да се отчетат другите, влошаващи качествата на оптичния уред ефекти.

2.2. Аберации на оптичните системи

Аберация на оптическа система наричаме всяко нарушаване на *подобие* между обекта и наблюдаваното изображение, дължаща се на отклонението на лъчите от онова направление, което биха имали в *идеална* оптическа система. Аберациите водят до това, че образът на точка е размита фигура (*фигура на разсейването*), което влияе на контраста и рязкостта на изображението, а оттам и на липсата на подобие.

Аберациите в една оптична система могат да се разделят основно на два вида: 1) Сферични аберации – кома, астигматизъм, дисторсия, кривина на полето на образа и 2) Хроматична аберация.

Сферичните аберации са геометрични нарушения, при които образът на точка може да е деформиран, да има светеща опашка, да се наблюдават два образа един зад друг и т.н.

Хроматичната аберация се дължи на дисперсията на светлината, която в оптическите каталози се отразява чрез *коэффициент на дисперсия* или *число на Аббе*:

$$\nu = \frac{n_D - 1}{n_F - n_C}, \quad (4)$$

където n_D се отнася за показателя на пречупване на линията $589,3 \text{ nm}$ n_F и n_C – за линиите $486,1 \text{ nm}$ и $656,3 \text{ nm}$ съответно.

Голямата стойност на числото на Аббе говори за вещество с малка дисперсия и обратно – например, флуоритът има $\nu = 95$, а тежките стъкла – $\nu = 20$.

Фокусното разстояние на лещата, от своя страна, се определя от съотношението:

$$\frac{1}{f} = (N - 1) \left(\frac{1}{R_1} - \frac{1}{R_2} \right) \quad (5)$$

където N е относителният показател на пречупване, а R_1 и R_2 са радиусите на предната и задна сферични повърхности на лещата. В същото време, увеличителната сила D на оптичната система зависи от фокусното ѝ разстояние f по формулата:

$$D = \frac{1}{f} \quad (6)$$

Когато през оптичната система се пропуска бяла светлина, различните спектрални компоненти (дължини на вълната) ще имат различно задно фокусно разстояние. Така възниква *надлъжна хроматична aberация* – даже за параксиалните лъчи съществува последователност от фокуси, отговарящи за различните дължини на вълната, разположени надлъжно върху оптичната ос, по дължина на отрязъка VR(виолет-червено). В съответствие с казаното по-горе, точка от оста се изобразява като цветни кръгчета, наредени едно зад друго, ако се проектират на екран, като най-близкото до оптичния център – и най-малко – съответно, е виолетовото, а най-далеч и най-голямо – червеното.

За да се отстрани хроматичната aberация, се конструират комбинирани лещи – дублети *ахромати* и триелементни *апохромати*. Двueleментният ахромат се състои от двойка лещи – събирателна и разсейваща, изработени съответно от кронглас (обикновено, калиево или бариево стъкло с малък показател на пречупване) и флинтглас (оловно стъкло с голям показател на пречупване). Корекцията на хроматичната aberация става за сметка на корекцията на дисперсията от различните видове стъкла.

На практика, обаче, при апохроматите в един общ фокус се събират само сините и жълтите лъчи, докато червените се фокусират по-далеч – получава се т.нар. *остатъчен (вторичен) хроматизъм*. За да бъде дефекта напълно отстранен, едната леща на дублета трябва да се изработи от по-специален материал – да е флуоритен или лантанов елемент, или да се добави трета леща, отстраняваща остатъчния хроматизъм на първите две. Усъвършенстваните по този начин обективи се наричат *апохромати*.

3. ЕЛЕКТРОНЕН МИКРОСКОП

Появата на електронния микроскоп става възможно след цяла поредица открития в областта на физиката в края на XIX и началото на XX век. Това са откритието на електрона от Дж. Томсън през 1897 г. и експерименталното откритие на вълновите му свойства през 1926 г. от Дейвисън и Джермер, което потвърждава предложената през 1924 г. от де Бройл хипотеза за корпускулярно-вълновия дуализъм на всички видове материя. През 1926г. немският физик Г. Буш създава първата магнитна леща, с помощта на която могат да се фокусират електронни снопове, което е предпоставка за конструиране на първия електронен микроскоп през 1931-1932 г. от Р. Рутенберг, М. Кнол и Ъ. Руска.

Оптичната система на електронния микроскоп вместо от стъклени, е съставена от магнитни лещи, които се произват не от видима или UV светлина, от електронни снопове с енергии до няколко *MeV* и ускоряващо напрежение – няколко *MV* в условията на дълбок вакуум. Разделителната способност на електронните микроскопи надвишават тази на оптичните от 1 000 – 10 000 пъти и за

най-добрите съвременни електронни микроскопи достига до $10^{-10} m$ и по-малко, а увеличението е от порядъка на 10^6 x [3, 4, 5]. Голямото увеличение в този тип микроскопи се достига благодарение на изключително малката дължина на вълната на де Бройл за електроните – по-малка от $10^{-12} m$.

Основен проблем, който се появява в микроскопията, е как да се направят малките обекти **видими**. За целта се прилагат няколко технологии – оцветяване с минерални бои, с метални пари, термична обработка, химично третиране с определени реагенти. В практическата бактериология най-разпространеният метод за фиксация на пробата е чрез термична обработка с горелка – груб метод, който съхранява морфологията и свързването на бактерията с оцветителя. За свето-оптичката микроскопия се използва формалин, спирт, глутаралдехид, течност на Карнуа, ацетон, пари на осмиевата киселина и др.

За съжаление, всички изброени техники за визуализация, приложени върху микроорганизми – клетки, бактерии и вируси – безкомпромисно ги умъртвяват.

Казано накратко, ако искаме да наблюдаваме и изучаваме живи микроорганизми, работим с обикновен оптичен микроскоп [7]. Но минималният размер на обектите е ограничен – да са не по-малки от $0,1 \mu m$.

От друга страна, размерът на вируса на тютюневата мозайка е $\sim 0,28 \mu m$ в дължина и $0,015 \mu m$ в диаметър. Дребните вируси – на полиомиелита, на жълтата треска и др. – са с диаметър $\sim 0,020-0,025 \mu m$. Това е доста под минималната разделителна способност на обикновените оптични микроскопи.

Електронните микроскопи имат достатъчно голямо увеличение. Но живи клетки, поставени във вакуум, неизбежно се дехидратират и умират. От друга страна, срезове на клетките, подготвени за наблюдение с електронен микроскоп, трябва да са много тънки, поради което електроните минават през материала без промени, а това довежда до сливане на образа с фона. За да се избегне този проблем, върху пробата се прави покритие с метални пари, които да дадат сянка и да оформят някакъв видим образ. Този образ е сив, без никакви цветове, а това пък води до артефакт – загуба или изкривяване някои компоненти на пробата.

Има ли изход?

4. УНИВЕРСАЛЕН УЛТРАВИОЛЕТОВ ХЕТЕРОДИНЕН ОПТИЧЕН МИКРОСКОП НА Д-Р РОЯЛ РЕЙМЪНД РАЙФ

Роял Реймънд Райф е блестящ учен, създал и развил технологии, които и до днес все още се използват в различни области на оптиката, електрониката, радиохимията, биохимията, балистиката, авиацията. Райф, фактически, е родоначалник на биоелектронната медицина. За конкретни изобретения и научни достижения Райф получава почетното звание *Doctorate by the University of Heidelberg*. В течение на почти 66-те години, които Райф посвещава на проектирането и създаването на уникални медицински прибори и инструменти, той работи за

такава известна корпорация като Цайс (Zeiss Optics), както и за Правителството на Съединените Щати.



Роял Реймънд Райф
(1888-1971)

Целият живот на този скромен и трудолюбив човек е посветен на търсене лечението на най-тежките заболявания на човека – туберкулозата, антракса, рака. Изследванията на този скромен, но трудолюбив човек, можем да групираме в две направления:

1) Създава на Универсален хетеродинен ултравиолетов оптичен микроскоп, който дава увеличение над **60 000 X**, с което неколkokратно надвишава максималното за обикновен оптичен микроскоп.

2) Конструира и прилага в медицината **Rife Beam Ray (RBR)** (Излъчвател на Райф) – прибор за електромагнитна терапия, работещ на резонансен принцип. Уредът произвежда широк спектър специфични за всеки тип патогенен микроорганизъм резонансни терапевтични честоти – **Mortal Oscillatory Rate (MOR)**.

Съгласно доклада, представен в журнала на Института Франклин [6], микроскопът на Роял Райф дава увеличение 60000 X. Окулярът на този инструмент е бинокъл, но по-надолу върху статива е монтиран и монокулярен сегмент с увеличение 1800X.

Микроскопът на д-р Райф [8, 9, 10, 11] има две съществени характеристики, които обединяват само предимствата на разгледаните по-горе сродни апарати:

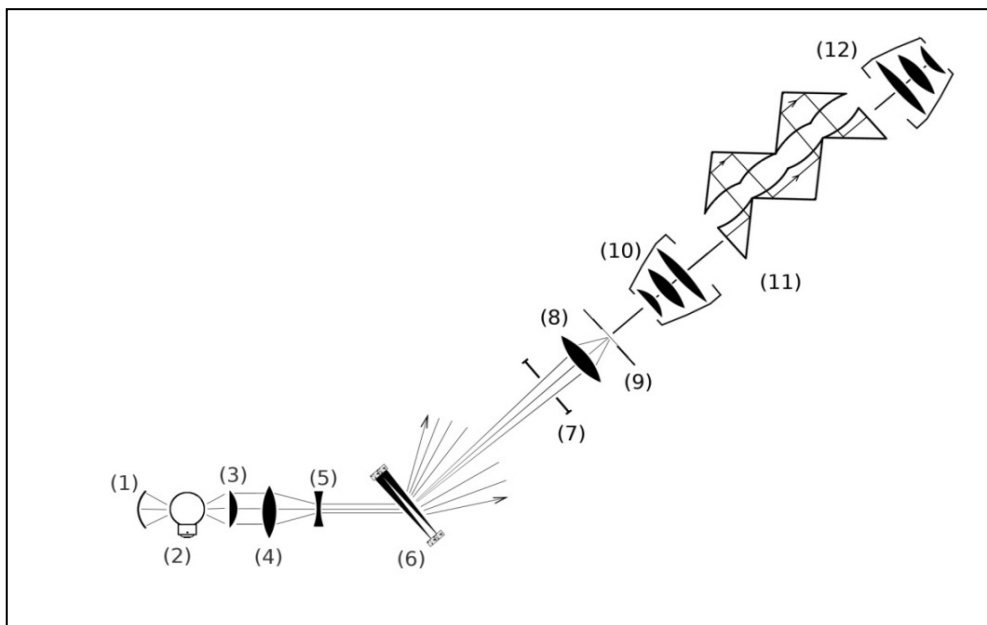
– Работи със светлина – това означава, че микроорганизмите – бактерии и вируси – не се умъртвяват по никакъв начин по време на наблюдението;

– Дава увеличение близо до стойностите на електронните микроскопи – т.е., може да даде образи на живи вируси, причинители на редица заболявания.

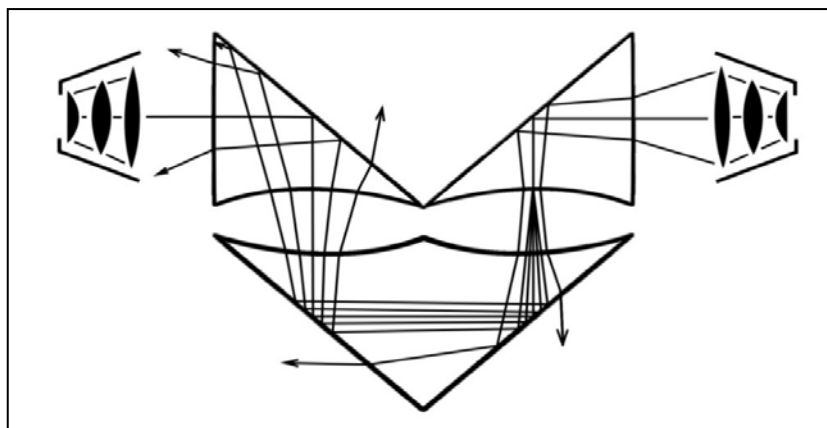
Как Райф съчетава само предимствата на двата вида микроскопия – оптичката и електронната? Как, като се използва светлина в микроскопа, се избягват съпътстващите оптиката дифракция и aberации, та да се получава толкова голямо увеличение?

Светлината от дъгова живачна лампа – фиг. 4 – през колимиращото устройство (5) се насочва към система клиновидни призми на Райсли (6). Тези призми дават спектрално ветрило в целия видим и в широк **ултравиолетов** диапазон. Диафрагма (7) с променливо по диаметър кръгло отверстие отделя и насочва тесен монохроматичен светлинен сноп през събирателна леща (8), която го стеснява допълнително в интензивно светло петно под образаца, разположен върху кварцова пластинка на предметното столче (9) на микроскопа. Между обектива и окуляра (12) светлината преминава през няколко призмени блока, изработени от чист кварц, между които са оформени четири на брой сферични въздушни лещи – фиг. 5.

4.1. Устройство и работа на микроскопа на д-р Р. Р. Райф



Фиг. 4. Устройство на микроскопа на Райф: Осветяваща система – (1) до (4); монохроматор – призми на Райсли (6); микроскоп – (9) до (12).



Фиг. 5. Лъчева диаграма, поясняваща действието на един от двата призмени блока, разположени между обектива и окуляра на микроскопа на Райф

Микрообективът (10) действа като обектив на обичаен микроскоп, но сходността на снопа зад него е само 1^0 и по-малко заради специалния подбор на лещите в него – с намаляваща оптична сила. Поради това, пречупването на първата призмена стена слабо влияе на степента на сходност.

В Универсалния микроскоп са постигнати два основни ефекта, които позволяват голямото увеличение – 60 000X, постигнато по оптичен път – 1) корекция дифракцията на светлината; 2) корекция на сферичните аберации; 3) избягване на хроматичната аберация.

Райф избягва ограниченията, налагани от дифракцията на Фраунхофер, като умело прилага **принципа за обратимост на светлинните лъчи**, посредством

обектив (10) и окуляр (12), аналогични по устройство, но противоположно ориентирани. Остатъчната Фраунхоферова дифракция от разходимостта на светлинния сноп в обектива, напълно се компенсира от окуляра и остава само оригиналната картина на ясния образ на обекта. От друга страна, въздушните лещи, оформени от всеки две противоположно ориентирани сферични повърхности между стъклените призми взаимно изключат ефектите, свързани с Фраунхоферовата дифракция, тъй като разстоянието между последната стена на призмения блок и първата сферична повърхност на лещите на окуляра е правилно избрано.

От оптиката е известно, че всички видове сферични аберации на лещите могат да се избегнат, ако се работи само с параксиални лъчи – такива, които са успоредни на оптичната ос на системата и се разпространяват много близо до нея.

В микроскопа на д-р Райф това се постига на няколко етапа. Снопът лъчи, идващ от обектива (вдясно – виж фиг. 5) преминава през призмите и се разширява по такъв начин, че само тесен сноп лъчи достигат до окуляра. Трябва да се отбележи, че още преди сходящият сноп зад обектива да сформира образ, той влиза в първата въздушна леща и се превръща във вече разходящ сноп. След преминаване през четирите въздушни лещи на призмения блок, снопът още се разширява, лъчите, които могат да доведат до възникване на сферични аберации напускат оптичната система, т.е., действително само параксиални лъчи, идващи от обекта, достигат окуляра, и създават изображение.

В Универсалния ултравиолетов микроскоп на д-р Райф не се налагат корекции за евентуална хроматична аберация, тъй като в него се използва не бяла, а много тясна ивица ултравиолетова светлина, получена чрез системата клиновидни призми на Райсли – фиг. 4, с която се осветяват наблюдаваните образци.

От многобройните наблюдения над различни видове микроорганизми, д-р Райф открива, че всеки от тях притежава поне по една **специфична** дължина на вълната, която ги кара да флуоресцират. Тази спектрална честота – луминесцентна или флуоресцентна – има резонансен характер. Дългогодишните изследванията на д-р Райф довеждат до създаване на каталози за идентифициране на микроорганизмите по характерната честота на флуоресценция.

Този подход решава два основни проблема на конвенционалната оптична микроскопия и на електронната микроскопия.

Най-напред – тъй като се работи с много тясна спектрална ивица светлина, хроматичната аберация се изключва от процеса на наблюдение. Отпада и нуждата от нейната корекция, защото не се използва бяла, а чисто монохроматична светлина. Затова в микроскопа на д-р Райф виждаме само единични двойноизпъкнали лещи от чист стопен кварц.

По време на работа самите обекти стават светещи, поради което отпада нуждата от оцветители, от други видове обработка – фиксиране с химикали и органични разтворители, загряване, изсушаване и др. Т.е., Универсалният ултравиолетов микроскоп дава възможност за наблюдение с увеличение от порядъка на няколко десетки хиляди пъти на живи микроорганизми в процеса на тяхното нарастване, размножаване, взаимодействие с други микрообекти.

Но 75% от обектите, които д-р Райф наблюдава чрез Универсалния микроскоп, флуоресцират в ултравиолетовия диапазон на електромагнитния спектър, което е извън обсега на човешкото зрение. За преодоляването на този проблем се използва **ултравиолетова хетеродинна микроскопия** – техника, която се основава на обединяване на две, специфични за микроорганизма късовълнови ултравиолетови честоти и получаване на трета – вече във видимия диапазон (*днес това се постига чрез луминесцентни екрани*).

4.2. Постижения на ултравиолетовата хетеродинна микроскопия

Още през 1920 г. Райф успява за пръв път да изолира и фотографира бактериите, причиняващи туберкулоза, които гледани в микроскопа на Райф светят изумруденозелено, на *E. Coli* – в махагонов цвят, на *лепрозата* – рубиненочервени.

По-късно през 1931 г. Райф изолира още един микроорганизъм, много по-малък от бактериите и характерен с неговото специфично пурпурно-червено излъчване. Този обект той нарича вирус *Cryptocides primordiales: Bacillus X – ВХ*. Процесът бива също така надлежно филмиран от Райф и неговите сътрудници. Това пурпурно-червено светене Райф вижда при всеки случай рак, който изследва.

С техниката на хетеродинната микроскопия Райф постига следното:

1) провежда наблюдения над живи организми – живи вируси в движение; вируси, променящи формата си, за да се нагодят към средата; вируси преди, по време на атака на жива клетка и процеса на размножаване и преобразуване на здрави клетки в туморни;

2) създава каталог с индивидуалните спектроскопични „подписи” на всички наблюдавани от него патогенни микроорганизми, причинители на над 500 вида заболявания.

5. РЕЗОНАНСЕН RIFE BEAM RAY (RBR) (Излъчвател на Райф)

Още през 1917 г., работейки с протозои и големи бактерии, д-р Роял Реймънд Райф открива, че краткотраен силен електрически импулс ги убива.

Като начин за окончателно разрушаване на болестотворни микроорганизми – бактерии и вируси – д-р Райф разработва нов, революционен метод, който се основава на **Резонансният принцип**, който той използва за наблюдението им. Д-р Райф предполага, че за всеки патоген съществува специфична **честота във високочестотния електромагнитен спектър**, която увеличава многократно амплитудата на собствените им колебания. Това води до разрушаване на обвивката (пръскане, лизиране) и смърт на обекта [12, 13, 14, 15].

Щастливото обстоятелство е, че чувствителността на нормална здрава клетка към тези честоти е около 2000 пъти по-ниска в сравнение с чувствителността на микроорганизмите, заради чувствителната разлика в размерите. Т.е., трети-

рането на заразен тъкан със специфичната за патогенния организъм резонансна честота, води до цялостна смърт на микробите, без ни най-малко здравата тъкан да пострада. Впоследствие, Райф нарича тази специфична за всеки болестотворен микроорганизъм летална честота **Mortal Oscillatory Rate (MOR)** (Смъртоносна честота на вибрации – терапевтични честоти).

В конструкцията на апаратурата, която д-р Райф първоначално използва за въздействие върху малките бактерии и вируси е включен радиопредавател с променлива носеща честота на изхода, към който, вместо антена, се свързва газов диод **Phanotron** (газова тръба пълна с хелий). Терапевтичната **висока честота** амплитудно се модулира върху носещата аудио честота, в резултат на което се получават високочестотни импулси с назъбена форма, следващи един след друг с аудио честота, които са в състояние да навлязат и вътре, в организма. С така модулираното лъчение се третира всяко едно вътрешно заболяване, независимо дали причинителят е бактерия или вирус.

Когато атакуваните микроорганизми са върху предметно стъкло или по кожата на болния, аудио честотата не е необходима. Осцилаторът на Излъчвателя **RBR** се настройва на съответната терапевтична честота за патогена, който ще се атакува, **Phanotron** – тръбата излъчва ВЧ изходен импулс и микроорганизмите от дадения вид умират.

В резултат на дълги изследвания и експерименти Райф създава каталог за специфичните терапевтични честоти за всички известни по онова време микроорганизми.

През живота си д-р Райф създава общо пет типа излъчвателни машини. Най-добрата от тях – под №3 – е конструирана и произведена от работещият за д-р Райф инженер Филип Хойлънд, наречена **Резонансен Rife Beam Ray (RBR)** (Излъчвател на Райф), с помощта на който патогенните микроорганизми биват атакувани и унищожавани директно в организма на човека. За лечебните си цели д-р Райф дори отделя **Phanotron**-тръбата от останалото оборудване и я поставя на 20-40см от пациента.

Първоначално този инструмент е посрещнат в медицинските среди много ентузиазирани. Използван е от много лекуващи лекари по онова време, а получените резултати са невероятни!

В клиниката на д-р Милбанк Джонсън през **1934** г. с помощта на **Излъчвател № 3** се провежда контролен експеримент над 16, т.н. „безнадеждно” болни от рак хора, под наблюдението на медицинска комисия, назначена от Университета в Южна Калифорния. Лечението, провеждано над болните, представлява три минутни процедури на облъчване с **RBR**-излъчвателя на д-р Райф, настроен на терапевтичната за ВХ (раков вирус) честота веднъж на три дни. Между две последователни лъчеви процедури на болните се дава перорално сиропи и чайове за прочистване на организма от остатъчните, получени от умъртвените вируси, вредни вещества. Без тридневната почивка между процедурите пациентите се чувствали зле. След три месеца 14 от тях са били изписани от комисията наблюдаващи лекари, ръководени от д-р Елвин Фоорд, доктор на медицинските науки и патологоанатом на групата, като **клинически здрави**.

Неоспоримата ефективност за лечение с **RBR**-излъчвателя на д-р Райф събира три години по-рано на организирана от д-р Милбанк Джонсън знаменателна среща, на четиридесет и четирима лекари, които честват д-р Райф, неговия универсален микроскоп и обявяват „края на всички болести”.

В хода на срещата бива направена демонстрация, фотографиране и филмиране процеса унищожаване на микроорганизми от поразени болни тъкани.

Д-р Милбанк Джонсън по-късно експериментира с **Излъчвател №4**, модифициран да работи без амплитудно-модулиран с аудио честота сигнал, но със значително по-висока изходна мощност. Терапевтичното действие на този уред е значително по-недвусмислено и има граници на въздействие в радиус до 300 м.

6. ЗАКЛЮЧЕНИЕ

Плазмените устройства на д-р Райф бързо стават легендарни и започват да се произвеждат още през 30-те години на 20 век. През 1938-39 г. се основава „**Beam Rays Corporation instrument**” за производство на Райф-излъчватели.

Първоначалните възторзи на медиците, обаче, бързо утихват и през 1939 г. почти всички лекари и учени, присъствали на срещата, организирана осем години по-рано от д-р Милбанк Джонсън, отричат, че са познавали Райф. Какво се е случило?

Големите американски корпорации виждат в работата на д-р Райф конкуренция и заплаха за своите печалби. Върху Райф и неговите сътрудници започват атаки на всяко ниво. Триумфът и наздравниците траят цели петнадесет минути, след които настъпва тъмнина и забрава.

Д-р Райф е блестящ учен, развил и внедрил технологии, които се използват и днес в различни области на оптиката, електрониката, радиохимията, биохимията, балистиката, авиацията. Идеите на д-р Райф намират приложение в биоелектронната медицина. Широко се използват уреди за електромагнитна терапия и усилване на имунната система. Някои резонансни честоти се прилагат за подтискане на вредните, други – за подобряване растежа на полезните микроорганизми.

Без Флуоресцентният микроскоп, разработен върху идеите на д-р Райф, работата на нито една съвременна болница е невъзможна.

За конкретни изобретения и научни достижения Райф получава 14 отделни награди и почетното звание **Doctorate by the University of Heidelberg**.

Може би някога името на д-р Райф ще изгрее отново и ще заеме своето законно място в съвременната медицина. До тогава, неговата технология ще е достъпна само за онези хора, които се стремят да я открият, опознаят и използват.

Литература

- [1] Ландсберг, Г. С., „Оптика”, Издательство „Наука”, 1976 г.
- [2] Ежов, А.: Как рассмотреть нанообъект в оптический микроскоп, «Квант» № 2, 2010.
- [3] Стоянов П. А., Мосеев В. В., Розоренова К. М., Ренский И. О., Электронный микроскоп предельного разрешения ЭМВ-100Л, "Изв. АН СССР. Сер. физическая", т. 34, 1970.
- [4] Хокс П., Электронная оптика и электронная микроскопия, пер. с англ., М., 1974.
- [5] Вуколов Н. И., Гербин А. И., Котовщиков Г. С. Приёмные электронно-лучевые трубки: Справочник. — М.: Радио и связь, 1993.
- [6] Journal of the Franklin Institute Volume 237(2):103-130 (1944), Page 117, Feb., 1944.
- [7] Словарь терминов микробиологии
- [8] <http://www.rifetechnologies.com/>
- [9] <http://www.rife.org/>
- [10] <http://www.rense.com/general31/rife.htm>
- [11] http://www.rife.de/what_has_become_of_the_rife_microscope.html
- [12] http://www.rife.de/rife_related_videos.html
- [13] http://www.youtube.com/watch?v=AysfKyl8O9k&feature=player_embedded
- [14] <http://www.youtube.com/watch?v=jSYcN5A1qJE&NR=1>
- [15] <http://www.youtube.com/watch?v=NJhz4Gfz-Bc&feature=related>

REAL EIGENVALUE RANGE DETERMINATION FOR THE INTERVAL GENERALIZED EIGENVALUE PROBLEM

Lubomir Kolev

Department of Theoretical Electrical Engineering, Technical University of Sofia,
bd. Kl. Ohridski 8, 1000 Sofia, Bulgaria, e-mail: lkolev@tu-sofia.bg

Abstract. *There exist uncertain parameters problems in circuit theory and electromagnetism that lead to interval generalized eigenvalue problems. In this paper, a new method of polynomial complexity for determining the range of a real eigenvalue is suggested. It employs only linear operations which accounts for its improved numerical efficiency over other known methods.*

Keywords: *Real eigenvalue ranges, Electromagnetism, Numerical analysis*

1. INTRODUCTION

Consider the generalized eigenvalue problem

$$Ax = \lambda Bx \quad (1)$$

where A and B are known $n \times n$ real matrices. Let A be an $n \times n$ interval matrix. In a recent paper [1], the following interval generalized eigenvalue problem

$$Ax = \lambda Bx, \quad A \in \mathbf{A}, B \in \mathbf{B} \quad (2)$$

where \mathbf{A} and \mathbf{B} are given interval matrices, has been considered. The relation (2) defines each eigenvalue λ_k as an implicit function of A and B , i.e. $\lambda_k = \lambda_k(A, B)$. In case of real eigenvalues, the range $\lambda_k^* = [\underline{\lambda}_k^*, \overline{\lambda}_k^*]$ is given by the real set

$$\lambda_k^* = \{\lambda_k : Ax = \lambda Bx, A \in \mathbf{A}, B \in \mathbf{B}\}. \quad (3)$$

As is well known, determining the real range λ_k^* is an NP-hard problem (exponential numerical complexity in n). In [1], a method for determining λ_k^* (further referred to as method M0) has been suggested whose numerical complexity is only polynomial in the size n of A and B . The method is applicable if certain sufficient, computationally verifiable conditions are satisfied.

In the present paper, a new method of polynomial complexity for determining the range λ_k^* of a real eigenvalue of the generalized eigenproblem (2) is suggested. The method is based on the following ideas. The original problem (3) of determining the

interval $\lambda_k^* = [\underline{\lambda}_k^*, \overline{\lambda}_k^*]$ is equated to that of determining its left end-point $\underline{\lambda}_k^*$ and right end-point $\overline{\lambda}_k^*$ separately. Each end-point is found as the global solution of a respective optimization problem:

$$\underline{\lambda}_k^* = \min\{\lambda_k(A, B), A \in \mathbf{A}, B \in \mathbf{B}\}, \quad (4a)$$

$$\overline{\lambda}_k^* = \max\{\lambda_k(A, B), A \in \mathbf{A}, B \in \mathbf{B}\}. \quad (4b)$$

The global solution of (4) is reached in two stages.

Stage 1. Using a specific local optimization technique, we find an inner (upper) bound $\underline{\lambda}_k$ on $\underline{\lambda}_k^*$, having the property

$$\underline{\lambda}_k \geq \underline{\lambda}_k^*; \quad (5a)$$

In a similar way, an inner (lower) bound $\overline{\lambda}_k$ on $\overline{\lambda}_k^*$ is computed such that

$$\overline{\lambda}_k \leq \overline{\lambda}_k^*. \quad (5b)$$

Stage 2. Using an appropriate check, we verify if the respective local solution is, in fact, global, i.e. if

$$\underline{\lambda}_k = \underline{\lambda}_k^* \quad (6a)$$

and

$$\overline{\lambda}_k = \overline{\lambda}_k^*. \quad (6b)$$

In this paper, we assume that conditions (6) are satisfied.

It should be stressed that unlike the previous method M0, the present method (referred to as method M1) employs only linear operations. This feature of method M1 accounts for its improved numerical efficiency as compared to method M0.

2. MAIN RESULTS

2.1. Globality of the upper bound $\underline{\lambda}_k$

An interval matrix $\mathbf{A} = [\underline{\mathbf{A}}, \overline{\mathbf{A}}] := \{A : \underline{A} \leq A \leq \overline{A}\}$ is called regular if each $A \in \mathbf{A}$ is non-singular; otherwise, it is called singular. The regularity radius of \mathbf{A} is defined as [2]

$$r^*(\mathbf{A}) = \min\{r \geq 0 : [A^c - rR, A^c + rR] \text{ is singular}\}. \quad (7)$$

Evidently, \mathbf{A} is regular if and only if

$$r^*(\mathbf{A}) > 1. \quad (8)$$

Conversely, A is singular if and only if

$$r^*(A) \leq 1. \quad (9)$$

An interval matrix A will be referred to as minimally singular if

$$r^*(A) = 1. \quad (10)$$

The following result will be needed in the sequel.

Lemma 1. A real number α is an eigenvalue of the bundle (A, B) if and only if

$$C = A - \alpha B \text{ is singular.} \quad (11)$$

We now introduce the notation

$$A(r) = A_c + rR, \quad R = [-R, R] \quad (12)$$

to represent equivalently the interval matrix $[A_c - rR, A_c + rR]$ in (7). Let A^* be the short notation for $A(r^*)$. Obviously, the regularity radius $r^*(A^*)$ of A^* is

$$r^*(A^*) = 1. \quad (13)$$

Thus, on account of (13) A^* is minimally singular.

We also introduce the interval matrix

$$C = A - \underline{\lambda}_k B. \quad (14)$$

Now the following result is valid.

Theorem 1: The upper bound $\underline{\lambda}_k$ on the left end-point $\underline{\lambda}_k^*$ of the real eigenvalue range λ_k^* determines $\underline{\lambda}_k^*$ itself, i.e.

$$\underline{\lambda}_k = \underline{\lambda}_k^* \quad (15)$$

if and only if

$$r^*(C) = 1 \quad (16)$$

where $r^*(C)$ is the regularity radius of C defined in (14).

Proof. Necessity. If $\underline{\lambda}_k = \underline{\lambda}_k^*$, then using (14) let

$$C^* = A - \underline{\lambda}_k^* B. \quad (17a)$$

Thus, each $C \in C^*$ is of the form

$$C = A - \underline{\lambda}_k^* B. \quad (17b)$$

By the definition (4a), the global minimum $\underline{\lambda}_k^*$ is reached for some pair of matrices A^* and B^* so by (17b)

$$C^* = A^* - \underline{\lambda}_k^* B^* . \tag{18}$$

But $\underline{\lambda}_k^*$ is the eigenvalue of the bundle (A^*, B^*) so by (18) and Lemma 1 C^* is singular. On the other hand, all C defined by (17b) and distinct from C^* in (18) are non-singular ($\underline{\lambda}_k^*$ is an eigenvalue only of the bundle A^* and B^*). Thus, C^* in (17a) is an interval matrix that is minimally singular. Hence, the regularity radius $r^*(C) = 1$.

Sufficiency. If

$$r^*(A - \underline{\lambda}_k B) = 1 \tag{19}$$

then there exists such a pair A' and B' that

$$\det(A' - \underline{\lambda}_k B') = 0. \tag{20}$$

According to Lemma 1, the real number $\underline{\lambda}_k$ is the k th eigenvalue of the bundle (A', B') . At the same time, it follows from (19) that the interval matrix

$$C = A - \underline{\lambda}_k B \tag{21}$$

is minimally singular. Hence, all pairs (A, B) with $A \neq A'$ and $B \neq B'$ yield

$$\lambda_k(A, B) \neq \underline{\lambda}_k(A', B'). \tag{22}$$

In fact, it will be shown that

$$\lambda_k(A, B) > \underline{\lambda}_k(A', B'), \quad A' \neq B', \quad A' \neq B'. \tag{23}$$

To prove (23), assume to the contrary that $\underline{\lambda}_k$ is only a local minimum of (4a) and that another $\hat{\lambda}_k$ is the global minimum of (4a). Thus, $\hat{\lambda}_k$ is reached for a pair (\hat{A}, \hat{B}) such that

$$\hat{\lambda}_k = \lambda_k(\hat{A}, \hat{B}) < \lambda_k \tag{24}$$

In that case, the pair (\hat{A}, \hat{B}) and $\hat{\lambda}_k$ should be associated with a singular matrix

$$\hat{C} = \hat{A} - \hat{\lambda}_k \hat{B} , \tag{25}$$

giving rise to minimally singular interval matrix

$$C = A - \hat{\lambda}_k B . \tag{26}$$

Hence,

$$r^*(A - \hat{\lambda}_k B) = 1. \tag{27}$$

However, (27) is in contradiction with (19). Indeed, let

$$\alpha = \underline{\lambda}_k / \hat{\lambda}_k \quad (28a)$$

so

$$\hat{r} = (1/\alpha) \neq 1. \quad (28b)$$

Using (28), we transform (19) into the form

$$r^*(\hat{r}A - \hat{\lambda}_k B) = 1 \quad (29)$$

which is a contradiction with (27) in view of (28b).

Thus, we have proved the validity of (23) and, hence, the globality of $\underline{\lambda}_k$, which completes the proof of the theorem.

Theorem 1 provides a simple global optimality check for $\underline{\lambda}_k$: if condition (16) is fulfilled, then $\underline{\lambda}_k$ is, in fact, equal to $\underline{\lambda}_k^*$.

The following result is a direct consequence of Theorem 1.

Corollary 1. Let $\alpha \in R$. If

$$r^*(A - \alpha B) > 1. \quad (30a)$$

then

$$\alpha > \underline{\lambda}_k^*, \quad (30b)$$

i.e. α is strictly an upper bound on $\underline{\lambda}_k^*$. Similarly, if

$$r^*(A - \alpha B) < 1. \quad (31a)$$

then

$$\alpha < \underline{\lambda}_k^*, \quad (31b)$$

i.e. α is strictly a lower bound on $\underline{\lambda}_k^*$.

2.2. Globality of the lower bound $\bar{\lambda}_k$

Similar results are obtained for the case of the right end-point $\bar{\lambda}_k^*$ of the range λ_k^* .

3. COMPUTATIONAL ASPECTS

3.1. Inner solutions

Consider the real eigenvalue λ_k of (2) for a fixed pair (A, B) . Let x and y denote the right and left eigenvectors associated with λ_k . To express the dependence of λ_k , x and y on A and B , we shall use, whenever necessary, the notation $\lambda_k(A, B)$, $x(A, B)$ and $y(A, B)$. As shown in [1]

$$\underline{\lambda}_k^* = \min\{y^T(A, B)Ax(A, B) / y^T(A, B)Bx(A, B), A \in \mathbf{A}, B \in \mathbf{B}\}. \quad (32)$$

Procedure 1 (for finding $\underline{\lambda}_k$). To simplify the presentation (without loss of generality), it is assumed that $\underline{\lambda}_k > 0$.

Step 0 (initialization). Set $n_i = 0$ (n_i is the iteration number) and $\lambda^0 = 0$. Let $A = A_c$ and $B = B_c$.

Step 1. Let $n_i = n_i + 1$. Find the k th real eigenvalue λ_k^i of $Ax = \lambda Bx$ and the corresponding right eigenvector x , using some generalized eigenvalue problem solver.

Step 2. Find the left eigenvector y associated with λ_k^i using the efficient technique suggested in [3].

Step 3. Compute the sign vector z^x of the eigenvector x using

$$z_i^x = (\text{sgn } x)_i := \begin{cases} 1, & \text{if } x_i \geq 0 \\ -1, & \text{if } x_i < 0 \end{cases} \quad (33)$$

In the same way, find the sign vector z^y of the eigenvector y . Form the sign vector $z = (z^x; z^y)$. Introduce the real matrices A^z and B^z with components

$$a_{ij}^z = \begin{cases} a_{ij}, & \text{if } z_i^y z_j^x = 1 \\ \bar{a}_{ij}, & \text{if } z_i^y z_j^x = -1 \end{cases} \quad (34a)$$

$$b_{ij}^z = \begin{cases} b_{ij}, & \text{if } z_i^y z_j^x = -1 \\ \bar{b}_{ij}, & \text{if } z_i^y z_j^x = 1 \end{cases} \quad (34b)$$

Step 4. Let $\lambda_k^0 = \lambda_k^i$, $A = A^z$, $B = B^z$ and start a cycle from Step 1 until the sign vector z remains unchanged (the current z is equal to z' of the previous iteration).

Step 5. A bound from above $\underline{\lambda}_k$ equal to λ_k^i of the last iteration has been found.

Procedure 2 (for finding $\bar{\lambda}_k$). It has the same structure as Procedure 1.

3.2. Determining the regularity radius $r^*(C)$

The regularity radius $r^*(C)$ is determined using the recent method in [3]. This is an efficient polynomial complexity iterative method.

3.3. Comparison with a previous method

In this section, it is shown theoretically that the present method (method M1) is more efficient computationwise than the previous method in [1] (method M0). Indeed, both methods have polynomial-time numerical complexity provided they are applicable. Therefore, the comparison will be based on two features:

- (i) Numerical efficiency: volume of computations needed;
- (ii) Domain of applicability: capacity to solve problems of increased uncertainty intervals.

As shown in the previous section, method M1 is based entirely on linear operations. In particular, the outer solution $\mathbf{x}^{(k)}(\underline{\mu})$ or $\mathbf{y}^{(k)}(\underline{\mu})$ is determined solving a corresponding linear interval system of size $n-1$. Conversely, method M0 resorts to solving a nonlinear (quadratic) algebraic system of n equations in n unknowns to compute the outer solutions λ_k , $\mathbf{x}^{(k)}$ and $\mathbf{y}^{(k)}$ needed to compute the range λ_k^* [1,Sect.2]. Thus, method M1 requires less computation than method M0 (at each iteration) of the respective method. Also, method M1 will converge in a smaller number of iterations than method M0. The joint influence of these two factors, lesser amount of computation at each iteration and smaller number of iterations, accounts for the expected improved numerical efficiency and larger domain of applicability of method M1 as compared to method M0. Several numerical examples solved by methods M1 and M0 (using INTLAB [6] to implement the interval computations) seem to confirm the above theoretical expectations.

4. CONCLUSION

The analysis of many electrical and electronic devices whose physical parameters are not known exactly can be performed using the “perturbed” generalized eigenvalue problem (2). A method for determining the range $\lambda_k^* = [\underline{\lambda}_k^*, \overline{\lambda}_k^*]$ of a real eigenvalue for the above interval eigenvalue problem has been suggested. The original problem (3) of determining the interval λ_k^* is equated to that of separately determining its left end-point $\underline{\lambda}_k^*$ and right end-point $\overline{\lambda}_k^*$. It has been shown that the problem of determining each end-point reduces to the problem of determining the regularity radius $r^*(C)$ of a related interval matrix C (Theorems 1). The latter problem is solved using the efficient method of [3] whose numerical complexity is polynomial in the size n of the matrices involved.

The method suggested seems to be an improvement as regards the numerical efficiency as well as the domain of applicability over other known methods of polynomial complexity [1], [4], [5].

References

- [1] L. Kolev, “Determining the range of real eigenvalues for the interval generalized eigenvalue problem”, *COMPEL (The international journal for computation and mathematics in electrical and electronic engineering)*, vol. 27, pp. 1463 –1480, 2008.
- [2] S. Poljak, and J. Rohn, “Radius of non-singularity”, Research Report, KAM Series 88-117, Faculty of Mathematics and Physics, Charles University, Prague, 1988.
- [3] L. Kolev, “A method for determining the regularity radius of interval matrices”, *Reliable Computing*, vol. 16, pp. 1–26, 2011.
- [4] L. Kolev, “Determining the positive definiteness margin of interval matrices”, *Reliable Computing*, vol. 13, pp. 445 – 466, 2007.
- [5] L. Kolev, “Eigenvalue range determination for interval and parametric matrices”, *International Journal of Circuit Theory and Applications*, vol. 38, pp.1027–1061, 2010.
- [6] S. Rump, “INTLAB – INTerval LABoratory”, in *Developments in Reliable Computing*, Tibor Csendes, Ed. Netherlands: Kluwer, 1999.

RELATIONS BETWEEN MARGIN OF STABILITY, STABILITY RADIUS AND REGULARITY RADIUS

Lubomir Kolev

Department of Theoretical Electrical Engineering, Technical University of Sofia,
bd. Kl. Ohridski 8, 1000 Sofia, Bulgaria, e-mail: lkolev@tu-sofia.bg

Abstract. *The margin of stability $M(\mathbf{A})$ and stability radius $r^*(\mathbf{A})$ are well-known quantitative measures for the degree of stability robustness for linear continuous time-invariant dynamic systems whose parameter uncertainties are modeled by an interval matrix \mathbf{A} . At the same time, an alternative robustness measure, the so-called regularity radius $\rho^*(\mathbf{A})$ of \mathbf{A} , is used in applied mathematics. In this paper, useful relations between $M(\mathbf{A})$, $r^*(\mathbf{A})$ and $\rho^*(\mathbf{A})$ are revealed.*

Keywords: *Margin of stability, stability radius, regularity radius*

1. INTRODUCTION

As is well-known (e.g., [1], [2]), robust stability properties of linear continuous time-invariant dynamic systems whose parameters uncertainties are modeled by an interval matrix \mathbf{A} can be assessed quantitatively using the following two measures: (i) margin of stability $M(\mathbf{A})$ of \mathbf{A} and (ii) stability radius $r^*(\mathbf{A})$ of \mathbf{A} . The former measure (chronologically introduced earlier than $r^*(\mathbf{A})$) is defined as follows:

$$M(\mathbf{A}) = -\max\{\operatorname{Re}[\lambda_k(\mathbf{A})]: Ax = \lambda x, k = 1, \dots, n, A \in \mathbf{A}\} \quad (1)$$

where $\operatorname{Re}[\lambda_k(\mathbf{A})]$ is the real part of the k th eigenvalue of \mathbf{A} . The stability radius $r^*(\mathbf{A})$ of \mathbf{A} is defined as:

$$r^*(\mathbf{A}) = \min\{r \geq 0: [A_c - rR, A_c + rR] \text{ is critically stable}\} \quad (2)$$

where the real matrices A_c and R are the center and radius of \mathbf{A} .

It should be stressed that the problem of determining $M(\mathbf{A})$ or $r^*(\mathbf{A})$ is NP-hard ([2]). Therefore, all known methods for exact (within round-off errors) evaluation of these stability measures require a volume of computation that grows exponentially with the size n of \mathbf{A} . This justifies any attempt to develop methods of better numerical complexity. Such an improvement, however, is possible only at the cost of introducing suitably chosen restricting conditions on the class of dynamic systems considered.

On the other hand, another robustness characteristic of interval matrices, the so-called regularity radius $\rho^*(\mathbf{A})$ of \mathbf{A} , has been used in computational mathematics (cf., e.g. [3] and the references there). It is defined as follows:

$$\rho^*(\mathbf{A}) = \min\{r \geq 0: [A_c - rR, A_c + rR] \text{ is singular}\}. \quad (3)$$

Determining $\rho^*(A)$ is, in the general case, also a NP-hard problem. However, there exist a number of approaches to approximately assess the regularity radius. Also, a polynomial complexity method for computing $\rho^*(A)$ has been recently suggested [4], which imposes a minimum of restrictions and seems to be rather efficient as compared to previously known methods [3]. Thus, the following natural question arises: is there any link between the stability radius $r^*(A)$ of an interval matrix A and its regularity radius $\rho^*(A)$. If the answer is positive, this would permit to enlarge the arsenal of methods for tackling the robust stability problem by appealing to (or adapting) methods that have originally been developed for exact or approximate determination of $\rho^*(A)$.

In the present paper, we reveal a connection between the quantitative stability measures $r^*(A)$ and $\rho^*(A)$ for the general case of non-symmetric matrices provided certain relatively mild conditions (encountered most often in practice) are additionally imposed on A . More specifically, we establish (Section 2) that computing $r^*(A)$ can be equated to computing $\rho^*(A)$ for a large class of interval matrices when the robust stability is governed by a real eigenvalue (a rigorous definition of this requirement will be given later in the text). It is also shown (Section 3) that for the same class of interval matrices a useful relation between the stability radius and the stability margin exists: the problem of determining $M(A)$ of A can be tackled by solving a corresponding stability radius problem.

2. EQUIVALENCE BETWEEN $r^*(A)$ AND $\rho^*(A)$

We first need several preliminary facts. On account of (1) and (2), A is (asymptotically) stable if and only if

$$r^*(A) > 1 \quad (4a)$$

or

$$M(A) < 0. \quad (4b)$$

Hence

$$r^*(A) = 1 \quad (5a)$$

or

$$M(A) = 0 \quad (5b)$$

are two equivalent conditions for A to be critically stable, i.e. to contain a real matrix A which is critically stable.

We now introduce the notation

$$A(r) = A_c + rB, \quad B = [-R, R] \quad (6)$$

to represent equivalently the interval matrix $[A_c - rR, A_c + rR]$ in (3). Let A^* be the short notation for $A(r^*)$. Obviously, the stability radius $r^*(A^*)$ of A^* is

$$r^*(A^*) = 1. \quad (7)$$

Thus, on account of (5a) A^* is critically stable. We also make the natural assumption that the nominal system corresponding to $A = A_c$ is (asymptotically) stable, i.e. all its eigenvalues $\lambda_k^0 = \lambda_k(A_c)$ have negative real parts $\text{Re}[\lambda_k^0]$ and that λ_k^0 have been ordered in decreasing value of $\text{Re}[\lambda_k^0]$.

Let the class of linear continuous time-invariant systems considered be denoted C_0 . We now introduce a sub-class C_1 of C_0 which has the following property.

Property 1: The first eigenvalue λ_1^0 of the centre A_c of A is real and dominant, i.e.

$$\lambda_1^0 > \text{Re}[\lambda_2^0]. \quad (8)$$

Moreover, the relation (8) is robust in A^* , i.e.

$$\lambda_1(A) \geq \text{Re}[\lambda_2(A)], \quad A \in A^*. \quad (9)$$

At this point, definition (3) is written equivalently in the form

$$\rho^*(A) = \min\{r \geq 0: \det(A^c + rB) = 0, B \in B\}. \quad (10)$$

We have the following result.

Theorem 1: Definition (2) is equivalent to definition (3) and, hence,

$$r^*(A) = \rho^*(A) \quad (11)$$

if and only if Property 1 is valid.

Corollary 1: Definition (3) is equivalent to definition (2), if all eigenvalues $\lambda_k(A)$ of each $A \in A$ are real.

On account of Corollary 1, the equivalence between (2) and (3) is guaranteed for the following two large classes of interval matrices:

Class 1: robustly aperiodic matrices [2];

Class 2: symmetric interval matrices. In the latter case, it is of interest to determine the maximum singular value of an associated matrix [5], [6].

Checking Property 1 can be done in various ways (cf. [7], [8] and the references therein). Another possibility to check Property 1 is to appeal to the notion of the D-stability [1, Ch. 4] and the corresponding sufficient conditions for D-stability.

From a computational point of view, the reduction of the problem of determining the stability radius $r^*(A)$ of the interval matrix A to that of determining the regularity radius $\rho^*(A)$ of A is attractive since an efficient method for computing $\rho^*(A)$ has been recently suggested in [4]. It is based on an equivalent transformation of the original problem (3) to the problem of determining the real maximum magnitude (rmm) eigenvalue μ^* of an associated interval generalized eigenvalue problem

$$Bx = \mu A^0 x, \quad B \in \mathbf{B}, \quad \mathbf{B} = [-R, R], \quad A^0 = -A_c \quad (12)$$

where by definition $\mu^* = \max \{|\mu| : Bx = \mu A^0 x, \quad B \in \mathbf{B}\}$. The value μ^* is found by an efficient iterative method of polynomial complexity [4]. As shown in [4], the regularity radius $\rho^*(A)$ is then determined by the formula

$$\rho^* = 1/|\mu^*|. \quad (13)$$

In view of (11) (under the validity of Property 1), formula (22) becomes

$$r^* = 1/|\mu^*|. \quad (14)$$

Thus, for systems from class C_1 the stability radius can be determine in polynomial time using the method from [4] for computing μ^* .

Remark. A method (dedenoted here as method M0) for computing $r^*(A)$ based on formula (14) was suggested for the first time in [9]. However, due to papers' length limits the validity of equivalence of (2) and (10) and, hence, of the validity of the method itself was not presented there. The present Theorem 1 and Corollary 1 provide the missing theoretical foundation of method M0. Without the explicit statement of Property 1, method M0 does not guarantee determination of $r^*(A)$ since, in the form presented in [9], it is only based on a necessary condition. Hence, in the general case, method M0 only yields a lower bound $\underline{r}(A)$ on $r^*(A)$.

The above results can be useful in solving various qualitative robust analysis problems also. Thus, the following theorem suggests a new necessary and sufficient condition for a system from class C_1 to be stable.

Theorem 2: A system pertaining to class C_1 is robustly stable if and only if the rmm solution μ^* of the associated interval generalized eigenvalue problem (12) satisfies the inequality.

$$\mu^* < 1. \quad (15)$$

Corollary 2: A system pertaining to class C_1 is instable if a lower bound $\underline{\mu}$ on μ^* of the associated interval generalized eigenvalue problem (12) satisfies the inequality $\underline{\mu} \geq 1$.

3. A RELATION BETWEEN STABILITY RADIUS AND STABILITY MARGIN

In this section, it is shown that if Property 1 is valid the problem of determining the stability margin $M(A)$ of an interval matrix A can be tackled by solving a corresponding stability radius problem.

Property 2: The first eigenvalue λ_1 of A is real and robustly dominant in A , i.e.

$$\lambda_1(A) \geq \text{Re}[\lambda_2(A)], \quad A \in \mathbf{A}. \quad (16)$$

It is seen that Property 2 is easier to satisfy than Property 1 since $\mathbf{A} \subset \mathbf{A}^*$. Its validity can be verified using the methods for validating Property 1.

Let $\bar{\lambda}_1^*$ be the right end-point of the range of the first eigenvalue over \mathbf{A} . Further, let $\bar{\lambda}_1$ be a lower bound on $\bar{\lambda}_1^*$. We also introduce the interval matrix

$$\mathbf{C} = \mathbf{A} - \bar{\lambda}_1 I. \quad (17)$$

Now the following result is valid.

Theorem 3: The lower bound $\bar{\lambda}_1$ on the right end-point $\bar{\lambda}_1^*$ of the range $\lambda_1(\mathbf{A})$ of the real eigenvalue $\lambda_1(\mathbf{A})$ determines $\bar{\lambda}_1^*$, i.e.

$$\bar{\lambda} = \bar{\lambda}_1^*, \quad (18)$$

if and only if

$$r^*(\mathbf{C}) = 1 \quad (19)$$

where $r^*(\mathbf{C})$ is the stability radius of \mathbf{C} defined in (17).

Thus, if (18) is valid, then by Theorem 3 and (1)

$$M = -\bar{\lambda}_1. \quad (20)$$

4. CONCLUSION

For linear uncertain systems described by a corresponding interval matrix \mathbf{A} , a class \mathbf{C}_1 has been introduced which is characterised by Property 1 (the dominant eigenvalue of a related matrix \mathbf{A}^* is real). For systems from this class, it has been shown that:

(i) The problem of determining the stability radius $r^*(\mathbf{A})$ reduces to the problem of determining the regularity radius $\rho^*(\mathbf{A})$ (Theorem 1).

(ii) There exists a link between the problem of determining the stability margin $M(\mathbf{A})$ of the original interval matrix \mathbf{A} and the problem of determining the stability radius $r^*(\mathbf{C})$ of an associated matrix \mathbf{C} (17) (Theorem 3).

The above relations may be used as a starting point for developing efficient methods capable of solving various quantitative and qualitative robust stability analysis problems in polynomial time for systems pertaining to class \mathbf{C}_1 .

References

- [1] L. Kolev, "Interval Methods for Circuit Analysis," World Scientific: Singapore, New Jersey, London, 1993.
- [2] B. Polyak, "Robust linear algebra and robust aperiodicity", in Directions in Mathematical Systems Theory and Optimization, A. Rantzer, C. Byrnes, Ed. LNCIS, 2003, pp.249-260.
- [3] C. Jansson and J. Rohn, "An algorithm for checking regularity of interval matrices," SIAM J. Matrix Anal. Appl., vol. 20 (3), pp.756-776, 1999.
- [4] L. V. Kolev, "A method for determining the regularity radius of interval matrices", Reliable Computing, vol. 16, pp. 1-26, July, 2011.
- [5] H. Ahn, and Y. Chen, "Exact maximum singular value calculation of an interval matrix", IEEE Trans. on Automatic Control, vol. 52, pp. 510–514, 2007.
- [6] L. Kolev, "Strong stability radius of linear interval parameter circuits," Proceedings of the Summer School "Advanced aspects of theoretical electrical engineering", (TU-Sofia), 20 – 23 Sept. 2009, Sozopol, Bulgaria, pp. 87-90, 2009.
- [7] L. Kolev, "Eigenvalue range determination for interval and parametric matrices," International Journal of Circuit Theory and Applications, vol. 38, pp. 1027–1061, 2010.
- [8] L. Kolev, and S. Petrakieva, "Assessing the stability of linear time-invariant continuous interval dynamic systems," IEEE Trans. on Automatic Control, vol. 50, pp. 393 – 397, 2005.
- [9] L. Kolev, "Stability radius of linear interval parameter circuits", Proceedings of the XXV International Symposium on Theoretical Electrical Engineering (ISTET-09), June 22-24, 2009, Luebeck, Germany, pp. 87-91, 2009.

HARDWARE AUTHENTICATION MODULE USING FEIGE-FIAT-SHAMIR ZERO-KNOWLEDGE ALGORITHM

Valentin S. Mollov, Yancho Z. Kolev

Technical University of Sofia, Dept. of Computer Systems,
1000 Sofia, Bulgaria, 8 Kl.Ochridsky Blvd., e-mail: mollov@tu-sofia.bg

Abstract. *This paper focuses on a sample hardware application of the Feige-Fiat-Shamir (FFS) cryptographic identification protocol to implement as an essential part of user-software protection mechanism. The implemented algorithm has shown itself as a powerful tool when implemented as a separate hardware module which participates into the overall authentication mechanism of commercial software packets, like CAD systems, multimedia applications, web-server applications, etc. Such hardware unit based protection schemes are definitely a step beyond the conventional software protection algorithms, as they offer a secure storage of the secret keys and reliable execution of the required crypto-operations. The FFS algorithm is based on interactive, dynamic randomized challenge and response message exchanges between two sides - prover of identity and verifier - and has the so called “zero-knowledge” property. It means that during the entire identification process the prover of identity does not reveal any information about its secret keys to the verifier or to any other prospective malicious participant.*

Keywords: *Feige-Fiat-Shamir, zero-knowledge identification, cryptography*

1. INTRODUCTION

Nowadays there is a wide range of techniques involved in the authentication and identification process. The focus of this contribution is on the implementation of the Feige-Fiat-Shamir algorithm – a representative of the group of more advanced strong cryptographic identification protocols. This kind of identification mechanisms apply dynamically changing information which increases the difficulty for any prospective adversary to carry out a successful attack against the cryptographic protocol. The authentication/identification process involves interactive challenge and response protocol between two sides – claimant (hardware unit) and verifier (software application). Challenge-response mechanisms require the claimant and the verifier to interact but generally do not require them to be synchronized. The interaction generally consists of a random single or multiple challenges sent by the verifier to the claimant who must compute and provide a valid response. This process can be executed repeatedly in time, with an acceptable speed, so it will not have a negative influence on the overall execution time of the software application.

There is a special class of challenge-response mechanisms and identification protocols that have a property called “zero-knowledge”. It is possible and very likely that the zero-knowledge authentication protocols will become important and more widely deployed in the future. Using such a protocol, a claimant can prove knowledge of a

secret (e.g., a cryptographic key) while revealing no information about the secret key during carrying out of the protocol and particularly no information about the private key stored in the hardware module is sent or disclosed to the verifier [1]. Nevertheless, the verification process can be accomplished by using the authentic public parameters that are function of the secret ones. Besides, to find the private key knowing the public one is considered to be computationally infeasible because of the one-way arithmetic function used for computing the public key. All strong identification and authentication protocols are synthesized using and applying in practice the asymmetric cryptographic techniques. The increased security of these techniques is based on some mathematical assumptions and number-theoretic unsolvable problems like: (1) difficulty of factorizing large integers; (2) extracting square roots modulo large integer, (3) finding discrete logarithms, and so on. These problems remain difficult to solve for acceptable time only if the integers are big enough. The latest standards about the size of parameters in respect to the security require the parameters' length to be at least 1024 bits. It is highly recommended that this length to be above 2048 bits [1].

2. FEIGE-FIAT-SHAMIR IDENTIFICATION ALGORITHM

The algorithm ensures the identification of entity P (prover of identity) by entity V (verifier). Here, “prover of identity” means that the entity which has its secret keys proves their possession to the verifier V without revealing the actual secret values. There is no leak of useful information about the secret parameters of the prover P during execution of the protocol. In general, the Feige-Fiat-Shamir (FFS) identification protocol guarantees that the entity P proves its identity to the entity V by set of t executions of a 3-step message exchange mechanism.

2.1. Selection of security parameters

After the generation of two secret prime numbers p and q , the public modulus of all computations $n=p.q$ is calculated. In our current implementation n is 1024 bits long. Each of the prime numbers p and q must be congruent to 3 mod 4 according to the FFS protocol. The integer numbers k and t define the overall security of the protocol and will be discussed later.

2.2. Selection of per-entity keys

At first, we generate k random integers $s_1, s_2, s_3, \dots, s_k$ in the range $1 \leq s_i \leq n-1$, and k random bits $b_1, b_2, b_3, \dots, b_k$. The greatest common divisor of s_i and n must be equal to 1. The second step is to compute:

$$v_i = (-1)^{b_i} \cdot (s_i^2)^{-1} \bmod n, \text{ where } 1 \leq i \leq k.$$

So, the as-called pre-keys of P are as follows: public key – $(v_1, v_2, v_3, \dots, v_k, n)$; secret key – $(s_1, s_2, s_3, \dots, s_k)$.

2.3. Messages of the protocol

Each execution-consists of three successive messages between the prover and the verifier that have the following description:

$$(1) P: [x = \pm r^2 \bmod n] \rightarrow V$$

$$(2) V: [(e_1, e_2, e_3, \dots, e_k), e_i \in \{0,1\}] \rightarrow P$$

$$(3) P: [y = r \cdot \prod_{j=1}^k s_j^{e_j} \bmod n] \rightarrow V$$

2.4. Actions of the protocol

The entity V accepts the identity of entity P if all t executions are successful. We assume that the verifier V has the authentic public key of the prover P. An execution is successful if the verification is confirmed by the verifier V and the following actions are carried out.

(1) P selects random integer r , $1 \leq r \leq n-1$, and a random bit b . Then P computes

$$x = (-1)^b \cdot r^2 \bmod n$$

and sends x to V. Here x is called “commitment”;

(2) when entity V has received x , it sends to P the “challenge” – a random sequence of k bits $(e_1, e_2, e_3, \dots, e_k)$;

(3) upon obtaining the “challenge”, P calculates the “response”, according to the following relationships:

$$y = r \cdot \prod_{j=1}^k s_j^{e_j} \bmod n$$

and sends y to the verifier V;

(4) finally, after receiving the “response”, V starts a verification process by checking the correctness of the equation:

$$\pm x = y^2 \cdot \prod_{j=1}^k v_j^{e_j} \bmod n.$$

If it is correct, the execution is successful, otherwise it is unsuccessful.

2.5. Security of the protocol

The integer numbers k and t are called security parameters. The probability of impersonation, i.e. to break the algorithm, is given by the formula:

$$P = \frac{1}{2^{k \cdot t}}$$

Some appropriate values of the security parameters can be $k=6$, $t=5$, so we have $P=2^{-30}$. Originally, it was suggested k to be an integer number in the range $1 \leq k \leq 20$.

The security also relies on the difficulty of extracting square roots modulo a large composite integer n which has unknown prime factors. The task is equivalent of finding the prime factors.

2.6. A numerical example of the FFS protocol with small integer numbers

According to 2.1, we choose $p=7$, $q=11$, and $n=77$. We also select $k=3$ and $t=1$. Afterwards, we calculate the per-entity keys as described in 2.2:

(a) we select $k=3$ secret random integers: $s_1=12$, $s_2=39$, $s_3=61$, and $k=3$ secret random bits $b_1=1$, $b_2=0$, $b_3=1$.

(b) then, the computation of the public v_i follows as:

$$\begin{aligned} v_1 &= (-1)^{b_1} \cdot (12^2)^{-1} \bmod 77 = 54; \\ v_2 &= (-1)^{b_2} \cdot (39^2)^{-1} \bmod 77 = 4; \\ v_3 &= (-1)^{b_3} \cdot (61^2)^{-1} \bmod 77 = 40. \end{aligned}$$

After the above calculations, we can summarize that the secret key of the prover P is (12, 39, 61) and the public key is (54, 4, 40, 77). In accordance to 2.4, P and V will execute the following exchange steps in order to carry out the FFS protocol.

- (1) P: $r=35$, $b=1$; $[x = (-1)^{b_1} \cdot 35^2 \bmod 77 = 7] \rightarrow V$;
- (2) V: $[e=(110)] \rightarrow P$;
- (3) P: $[y=35 \cdot 12 \cdot 39 \bmod 77 = 56] \rightarrow V$;
- (4) V: $z=56^2 \cdot 54 \cdot 4 \bmod 77 = 7$. The execution of the protocol is successful, because z is equal to the received x after the first step (1).

3. HARDWARE AUTHENTICATION MODULE PROTOTYPING

The developed hardware prototype implements the functionalities related only to the prover P, as described in sec.2. For this application, the verifier V is a separate computer program running on a PC. The overall structure of the implemented prototype is shown in Fig. 2. We used Cypress CY7C68013A high-speed USB peripheral controller and the XC3S1200E FPGA device, both available over the Digilent Nexys 2 Development Kit.

Here, the multiplier block– **montgomery_multiplier_i1** realizes the Montgomery algorithm [2] for fast modular multiplication of large integers, as it is shown in Fig. 1.

The Montgomery multiplier is necessary in order to compute the “commitment” and “response” messages of the FFS protocol. Complying with the requirement for at

least 1024-bit computing, the **montgomery_multiplier_i1** module uses 1024-bit adders. Therefore, we have long carry chains, which affect negatively the clock frequency of the design. To resolve this issue, a lot of research has been done in this sense. Some practical results and approaches are published in [2,3].

```

MP (a , b):
(1) p = 0
(2) for i = 0 to k - 1 do
    d = p + ai · b
    if (d mod 2 = 0) then
        p = d / 2
    else
        p = (d + n) / 2
    end if
end for
(3) if (p ≥ n) then
    MP = p - n
else
    MP = p
end if

```

Fig. 1. Montgomery Product algorithm

Following [4], we implemented a pseudo-random bit generator **prbg_i1**, which is used when the message “commitment” is computed. Three linear feedback shift registers of different length are involved, where the most significant bit of the first shift register controls the work of the other two shift registers and the generated pseudo-random bit is the *xor* of the most significant bits of the slave registers.

To make use the onboard USB controller available, we designed a separate module **usb_fpga_bridge_i1**. It has two important functions: (1) byte-wise writing of the two computed messages “commitment” and “response” into the upload-buffer of the USB controller, and (2) byte-wise reading of the message “challenge” from the download-buffer of the USB controller. The bridge itself has 128B dual-port memory block (**dual_port_ram_i1**). One port is used by the data stream FSM (**data_stream_ctrl_i1**) synchronously (at 48MHz) with the USB controller, and the other memory port is dedicated to the rest of the computational structure of the prototyped device.

The secret keys are stored in the module **tkrom_i1**, which in our case is 16Kx1 memory, functioning as a ROM. The sequence of all operations is managed by a FSM module: **control_unit_i1**. Modules, not described here, are shown in grey color.

Several simulations using the Xilinx ISim simulator have been run during the design process in order to debug and verify the functionality of the prototype. Here, in Fig. 3, we show simulation of the module **montgomery_multiplier_i1** for very small 8-bit integers and the modulus is 239.

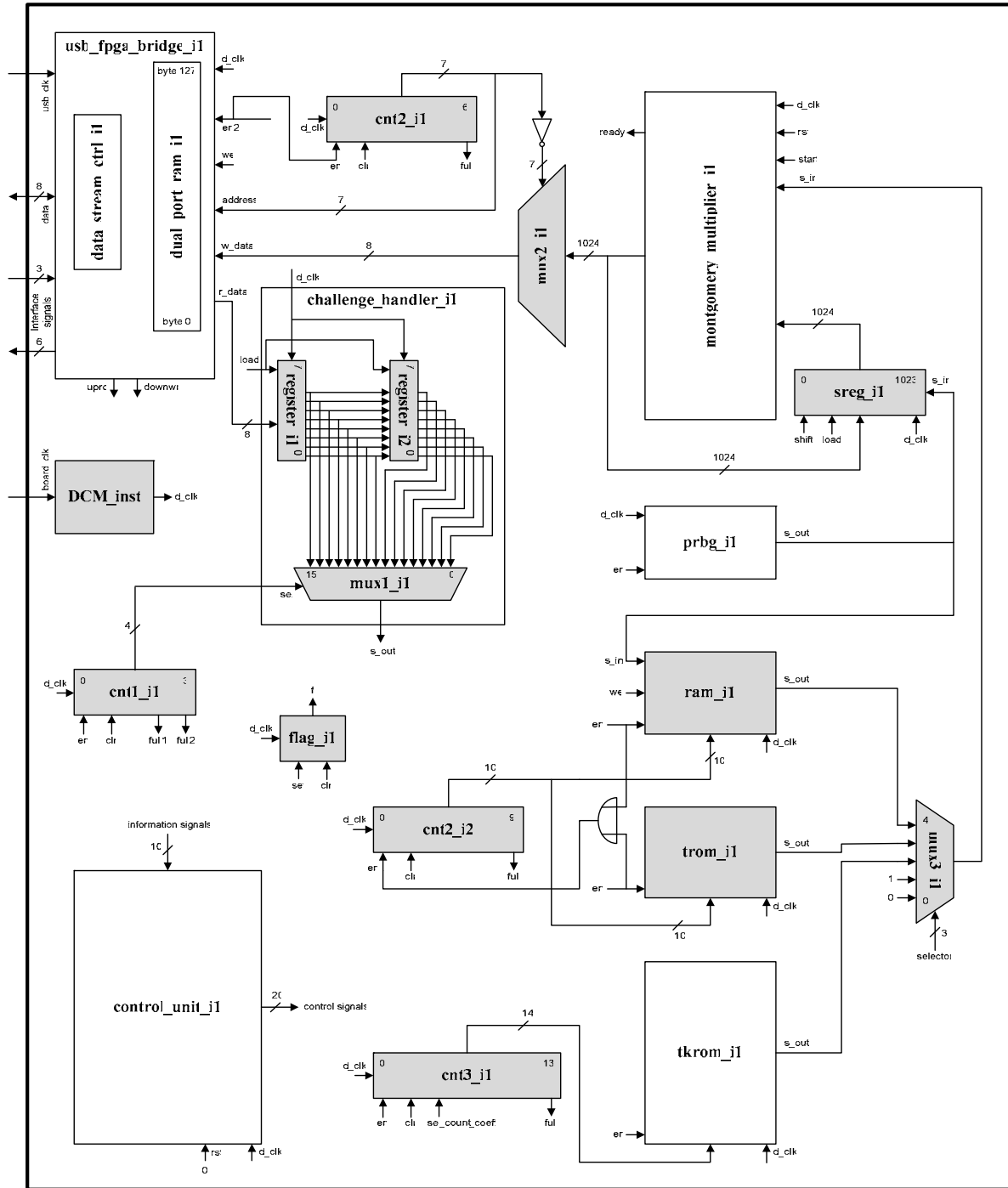


Fig. 2. Simplified block diagram of the designed prototype using Verilog hardware description language

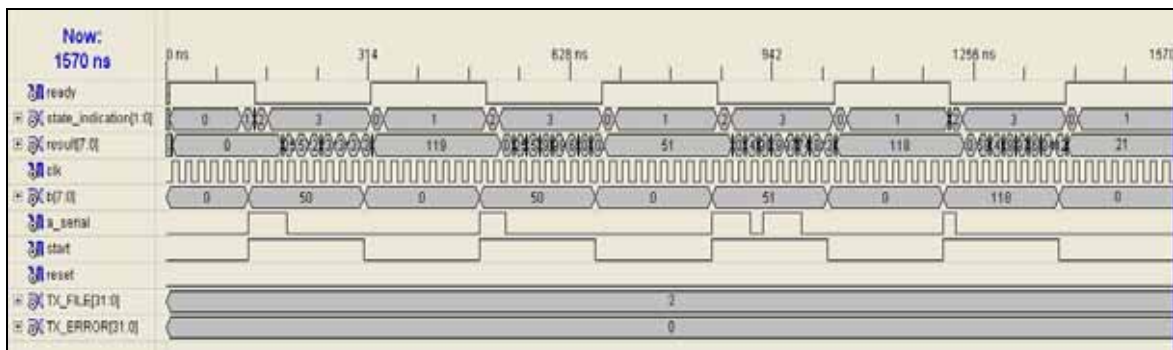


Fig. 3. Simulation results from the modular multiplication block

4. CONCLUSIONS AND RESULTS

Our prototype fully implements the functions of the prover, participating in the Feige-Fiat-Shamir identification protocol. In our implementation, the “commitment” is computed in 0.294ms, the “response” – in 1.613ms. The prototype operates at 11.11 MHz. Assuming the relatively limited logic resources and low clock speed of the target FPGA device the reported results are quite encouraging, as we have complied with the main security requirement for computation with at least 1024-bits long integers. There is no limitation for the type of data exchange interface as the required speed of information transfer is not critical for the protocol itself. Assuming the current advances in wireless communications, the prototyped identification module can be adapted for application in mobile user devices since it does not require substantial hardware resources.

References

- [1] Mao, W., *Modern Cryptography: Theory and Practice*, Prentice Hall, 2003.
- [2] Rodriguez-Henriquez, F., Saqib, N., Diaz-Perez, A., Koc, C., *Cryptographic Algorithms on Reconfigurable Hardware*, Springer, 2006.
- [3] Huang, M., Gaj, K., El-Ghazawi, T., *New Hardware Architectures for Montgomery Modular Multiplication Algorithm*, *IEEE Trans.on Comp.*, vol.60,no.7, 2011, pp. 923-936.
- [4] Gunther C.G., *Alternating step generators controlled by De Bruijn sequences*, *EURO-CRYPT'87 Proc.6th annual int. conf. on Theory and application of cryptographic techniques*, pp.5-14, Springer-Verlag Berlin, Heidelberg 1988.

ELECTRICAL LOSSES IN SEMI-CONDUCTIVE DEVICES

Jordan Shopov, Galia Georgieva-Taskova, Simona Filipova-Petrakieva

Theory of Electrical Engineering, Technical University of Sofia,
8, Kl. Ohridsku, blvd., 1000 Sofia, Bulgaria,
e-mails: shopov@tu-sofia.bg, gvgt@tu-sofia.bg, petrakievas-te@tu-sofia.bg

Abstract: *Electrical losses take an essential part in switching on state of the semi-conductive devices (including diodes, transistors and thyristors). In the paper, working process of semi-conductive device in control mode of the current passed through the consumer, switched on in the network with considerable varying parameters is studied. This working mode arises when it controls the consumers in outlying rural regions and villages, where the voltage varies in wide intervals.*

Keywords: *electrical losses in semi-conductor's devices, average and RMS value of the current, coefficient of the form*

1. INTRODUCTION

Very often in the real energy systems arises the situation when the consumers are remote from the supply network, which parameters vary in wide intervals. Typical example for this is consumers in outlying rural regions, villages and etc. In this case, a stabilization of the voltage, respectively of the current passed through the consumers, is needed. It realizes by switching on the devices with semi-conductive elements as a diodes, transistors, thyristors and etc., which ensure half- or full-wave voltage control (see Fig. 1). One possible way to obtain this is using phase control, where it varies with the angle of phase control for the semi-conductive device – α [1, 2, 3].

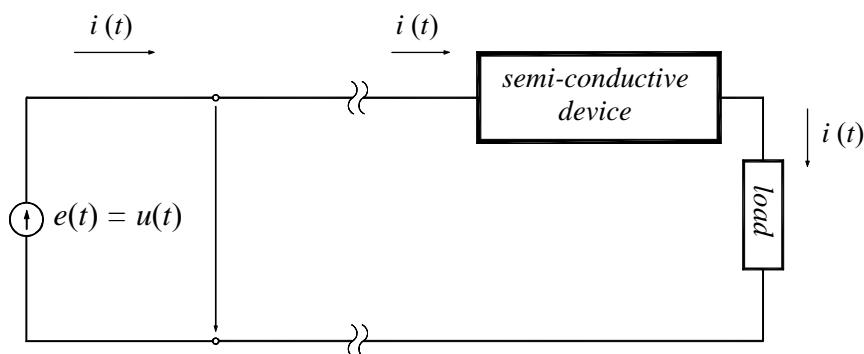


Fig. 1. Electric circuit for half- and full-wave voltage control

In this control the evolved power and the heating of the semi-conductive devices significantly depend on the average value of the current I_{av} (given in the manuals). The maximum possible value of this current $I_{av \max}$ defines in full sine wave voltage ($\alpha = 0$). In this maximum threshold the admissible parameters of the semi-conductive device don't increase and the latter keeps its working capacity.

2. PROBLEM STATEMENT

When the phase control on the current, passed through the load, makes, the electric losses evolved in semi-conductive device as a heat determine as an average value of the power for one half-period $T/2=\pi$.

$$P_{av} = \frac{1}{T/2} \int_0^{T/2} u(t).i(t)dt = \frac{1}{\pi} \int_0^{\pi} u(t).i(t)dt \quad (1)$$

In general volt-ampere (V-A) characteristic of these devices (diodes, thyristors) in working state is following:

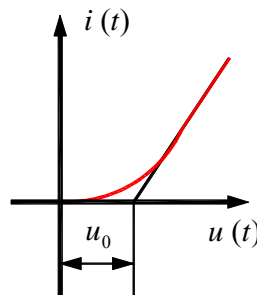


Fig. 2. V-A characteristic of semi-conductive device (in general form)

With sufficient practical accuracy it can be approximated with linear one as:

$$u(t) = u_0 + R_d.i(t), \quad (2)$$

where: $u_0 = const.$ – rapid voltage;

R_d – differential resistance, taking into account the slope of the graphic $(\Delta U/\Delta I)$.

After substituting (2) in (1) it gets:

$$\begin{aligned} P_{av} &= \frac{1}{\pi} \int_0^{\pi} u(t).i(t)dt = \frac{1}{\pi} \int_0^{\pi} (u_0 + R_d.i(t)).i(t)dt = \frac{1}{\pi} \int_0^{\pi} u_0.i(t)dt + \frac{1}{\pi} \int_0^{\pi} R_d.i(t).i(t)dt = \\ &= u_0 \cdot \frac{1}{\pi} \int_0^{\pi} i(t)dt + R_d \cdot \frac{1}{\pi} \int_0^{\pi} i^2(t)dt = u_0 \cdot I_{av} + R_d \cdot I_{RMS}^2 = u_0 \cdot I_{av} + R_d \cdot k_f^2 \cdot I_{av}^2 \end{aligned} \quad (3)$$

3. DELAY (TRIGGERING) ANGLE INFLUENCE OVER THE AVERAGE AND THE RMS VALUE OF THE CURRENT THROUGH THE SEMI-CONDUCTIVE DEVICE IN PHASE CONTROL

In phase control devices the delay (triggering) angle α changes. This angle defines from the beginning (zero point) of the sine wave. Without lost of generality it

assumes $\psi_u = 0$. Beside of the fact that the average power P_{av} relates from the average and the RMS value of the current, calculated for half-period $T/2 = \pi$, it will be analyzes the supplying voltage only for this interval (Fig. 3).

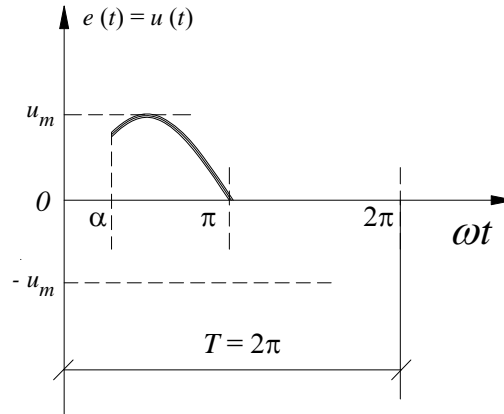


Fig. 3. Phase control of the voltage

Then the average value of the current as a function of delay angle α determines as follows:

$$I_{av}(\alpha) = \frac{1}{\pi} \int_{\alpha}^{\pi} i(t).dt = \frac{1}{\pi} \int_{\alpha}^{\pi} i_m \cdot \sin(\omega t + \psi_i).dt$$

To simplify the analysis without loss of generality it makes the assumption $\psi_i = 0$. Then giving an account of the fact $\omega = 2\pi f = 2\pi / T = 2\pi / 2\pi = 1$ it gets the following expression about the average value of the current:

$$I_{av}(\alpha) = \frac{1}{\pi} \int_{\alpha}^{\pi} i_m \cdot \sin t . dt = \frac{i_m}{\pi} (-\cos t) \Big|_{\alpha}^{\pi} = \frac{i_m}{\pi} (\cos \alpha - \cos \pi) = \frac{i_m}{\pi} (\cos \alpha + 1)$$

$$I_{av}(\alpha) = \frac{i_m}{\pi} (1 + \cos \alpha) \quad (4)$$

The respective expression for the RMS value of the current is following:

$$I_{RMS}^2(\alpha) = \frac{1}{\pi} \int_{\alpha}^{\pi} i^2(t).dt = \frac{1}{\pi} \int_{\alpha}^{\pi} i_m^2 \cdot \sin^2(\omega t + \psi_i).dt$$

To simplify the analysis without loss of generality it makes the assumption $\psi_i = 0$. Then giving an account of the fact $\omega = 2\pi f = 2\pi / T = 2\pi / 2\pi = 1$ it gets the following expression about the RMS value of the current:

$$\begin{aligned}
I_{RMS}^2(\alpha) &= \frac{1}{\pi} \int_{\alpha}^{\pi} i_m^2 \cdot \sin^2 t \cdot dt = \frac{i_m^2}{\pi} \int_{\alpha}^{\pi} \frac{(1 - \cos 2t)}{2} \cdot dt = \frac{i_m^2}{2\pi} \int_{\alpha}^{\pi} dt - \frac{i_m^2}{2\pi \cdot 2} \int_{\alpha}^{\pi} \cos 2t \cdot d(t \cdot 2) = \\
&= \frac{i_m^2}{2\pi} \cdot \left[t \Big|_{\alpha}^{\pi} - \frac{1}{2} \sin 2t \Big|_{\alpha}^{\pi} \right] = \frac{i_m^2}{2\pi} \cdot \left[\pi - \alpha - \frac{1}{2} (\sin 2\pi - \sin 2\alpha) \right] = \frac{i_m^2}{2\pi} \cdot \left[\pi - \alpha + \frac{\sin \alpha}{2} \right] = \\
&= \frac{i_m^2}{4\pi} \cdot [2\pi - 2\alpha + \sin \alpha] \\
I_{RMS}(\alpha) &= \frac{i_m}{2} \cdot \sqrt{\frac{2\pi - 2\alpha + \sin \alpha}{\pi}} \quad (5)
\end{aligned}$$

After division of (5) to (4) the following formulae about the coefficient of the form k_f as function of delay α , is obtained:

$$k_f(\alpha) = \frac{I_{RMS}(\alpha)}{I_{av}(\alpha)} = \frac{i_m}{2} \cdot \sqrt{\frac{2\pi - 2\alpha + \sin \alpha}{\pi}} \cdot \frac{\pi}{i_m \cdot (1 + \cos \alpha)} = \frac{\sqrt{\pi \cdot (2\pi - 2\alpha + \sin \alpha)}}{2 \cdot (1 + \cos \alpha)} \quad (6)$$

4. CRITERION FOR DETERMINING THE MAXIMUM ADMISSIBLE ANGLE OF PHASE CONTROL - α_{max}

In general, electric losses in semi-conductive devices mainly depend on the average value of the current, passed through them and more slightly depend on the respective RMS value of this current in terms of formulae (3). In phase control they are a function of delay α (see (4, 5, 6)). Then the final expression for the average power as a function of α is:

$$P_{av}(\alpha) = u_0 \cdot I_{av}(\alpha) + R_d \cdot k_f^2(\alpha) \cdot I_{av}^2(\alpha) = u_0 \cdot I_{av}(\alpha) + R_d \cdot I_{av}^2(\alpha) \cdot \frac{\pi \cdot (2\pi - 2\alpha + \sin \alpha)}{4 \cdot (1 + \cos \alpha)^2} \quad (7)$$

The maximum admissible power, evolved in semi-conductive device (i.e. maximum possible electric losses in it), calculates in average value of the current equal of the nominal one and delay $\alpha = 0^0$, i.e.

$$\left| \begin{array}{l} I_{av} = I_{nom} \\ \alpha = 0 \end{array} \right. \Rightarrow P_{av}^{max} = u_0 \cdot I_{nom} + R_d \cdot I_{nom}^2 \cdot \frac{\pi^2}{8} \quad (8)$$

If the device works in average value of the current then these losses depend on the delay as follows:

$$I_{av} = s I_{nom} = const., \quad 0 < s \leq 1 \Rightarrow P_{av}(\alpha, s) = u_0 \cdot s I_{nom} + R_d \cdot s^2 I_{nom}^2 \cdot \frac{\pi (2\pi - 2\alpha + \sin \alpha)}{4(1 + \cos \alpha)^2} \quad (9)$$

Giving an account of this fact, the condition for normal working of the semi-conductive device (without overheating and damaging) is:

$$P_{av}(\alpha, s) < P_{av}^{\max}. \quad (10)$$

Then substituting in (10) expressions (8) and (9) it gets the following inequality:

$$\underbrace{u_0 \cdot s I_{nom}}_{c_1 = const.} + \underbrace{R_d \cdot s^2 I_{nom}^2 \cdot \frac{\pi}{4}}_{c_2 = const.} \cdot \frac{(2\pi - 2\alpha + \sin \alpha)}{(1 + \cos \alpha)^2} < \underbrace{u_0 \cdot I_{nom} + R_d \cdot I_{nom}^2 \cdot \frac{\pi^2}{8}}_{c_3 = const.}$$

$$c_1 + c_2 \cdot \frac{(2\pi - 2\alpha + \sin \alpha)}{(1 + \cos \alpha)^2} < c_3$$

$$\frac{(2\pi - 2\alpha + \sin \alpha)}{(1 + \cos \alpha)^2} < \frac{c_3 - c_1}{c_2} = c = const. \quad (11)$$

The maximum possible delay α_{\max} determines as a solution of (11). It is different for each chosen average value of the current $I_{av} = s I_{nom} = const.$, $0 < s \leq 1$. When this angle is exceeded the semi-conductive devices can damage.

The dependence on the power evolved in the semi-conductive device as function of the delay angle α in different constant values of the average current, passed through the device, is shown on Fig. 4.

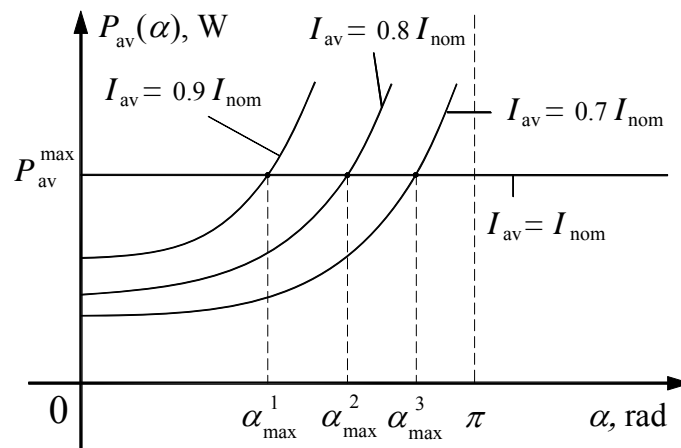


Fig. 4. Characteristics $P_{av}(\alpha)$, $0 < \alpha < \pi$ when $I_{av} = const.$

5. CONCLUSION

When the consumers are remote from the network supply with considerable varying parameters, it is necessary to use stabling devices, including non-linear semi-

conductive elements. Electric losses of the respective device can be defined more simple when approximate this characteristics with linear ones. These losses depend on mainly of the average value of the current and more slightly depend on its RMS value (in terms of the coefficient of the form). The values of the latter quantities are a function of the delay (triggering) angle α when makes phase control.

In stabilization, based on phase control of the average value of the current, which is multiple of the nominal one ($I_{av} = sI_{nom} = const.$, $0 < s \leq 1$), when exceeds the delay angel α_{max} (determined according to (11)), the electric losses in semi-conductive device will evolves the maximum admissible (when $I_{av} = I_{nom}$ and $\alpha = 0$) and the latter can damages.

References

- [1] М. Минчев, Й. Шопов, Е. Рац, “Преобразувателна техника“, Авангард Прима, София 2008, 160 стр.
- [2] М. Минчев, П. Пенчев, “Безконтактни апарати“, Техника, София 1976.
- [3] Ст. Табаков, “Тиристорна техника“, Техника, София 1982, 354 стр.
- [4] К. Брандиски, Ж. Георгиев, В. Младенов, Р. Станчева, “Теоретична електротехника – част 1“, КИНГ, София, 2004, 384 стр.

MATLAB ORIENTED MODEL OF PHOTOVOLTAIC MODULE CONSIDERING THE ENVIRONMENTAL FACTORS

Stoyan Hristov Bozhkov

Department of "Electrical Engineering, Electronics and Automatics"
Technical University of Sofia,
Bul. "Burgasko chose" № 59, Sliven 8800, Bulgaria, phone:+359895586485 ,
e-mail: s_bozhkov@abv.bg

Abstract. *The paper presents a possible option to create a simulation model of photovoltaic module. For creating a simulation model were used theoretical relationships describing electric processes in photo conversion using an one diode replacement scheme. In a model input data are dynamically changing environmental parameters, namely the intensity of solar radiation, air temperature and the temperature of the cell. Output data is electric current generated by photo voltaic module. Is used the product Matlab & Simulink, providing an easy upgrade, further development of the model and create an overall complete photo voltaic simulation power plant*

Keywords: *photovoltaic cell, one diode replacement scheme, photo-generated electricity*

1. INTRODUCTION

The rapid penetration of renewable energy sources globally as well as locally in Bulgaria led to a number of positive effects such as generation of electricity without the use of traditional fuel and consequently no pollution; getting called. "free electricity" and using the connected photovoltaic system through its "auxiliary functions" [1]

Along with these positive effects in the foreground appeared a number of operational nature of the difficulties associated with inspection and adjustment of the traffic capacity of the transmission grid, control stress levels in the nodes and consideration of short-circuit capacity of the existing traditional defense [4].

It is necessary to predicted and respectively modeled PV system performance depending on the factors of the environment, and to explore the behavior of future PV system released in different modes, by using virtual simulations.

2. GENERALITIES

Photovoltaic source is a compilation of interconnected solar cells, electrical connections, safety components and support facilities. Solar cells are made of semiconductor material that for the most part is mainly silicon. In the absence of light, volt-ampere (V-A) characteristic of the solar cell is exponential in the form similar to the semiconductor diode. The principle of operation is based on the photovoltaic

effect, which is used for making different photoelectric semiconductor devices. The structure of the photo elements, also called photovoltaics, is no different from that of the photodiodes, which is why when studying the operation of photovoltaics have been applied mainly one and two-diode replacement schemes.

The most common replacement scheme of photovoltaic cell is called one diode scheme representing current source connected in parallel with the diode on it

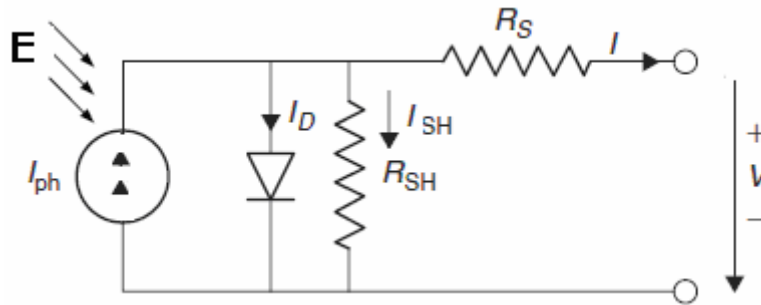


Fig. 1

Shown in Figure 1., I_{ph} is generated photo electricity; I_D - dark current; R_{SH} - internal diode shunt resistance reporting leakage currents due to structural and construction defects; R_S - series resistance representing the resistance of a cell

Current source generates the so-called photocurrent I_{ph} , determined according to Kirchoff's first law is:

$$I_{ph} = I_D + I_{SH} + I \tag{1}$$

Transferred by the photovoltaic cell current will be:

$$I = I_{ph} - I_D - I_{SH} \tag{2}$$

The equation by Second Kirchoff's law for output circuit of Figure 1 is:

$$IR_S + U - I_{SH} R_{SH} = 0 ; I_{SH} = \frac{U + IR_S}{R_{SH}} \tag{3}$$

Replace the equation (3) in (2) in which:

$$I = I_{ph} - I_D - \frac{U + IR_S}{R_{SH}} \tag{4}$$

Is recorded dark photocurrent in the diode in which equation(2) mining the type [2]:

$$I = I_{ph} - I_S \left[\exp\left(\frac{q}{kT_C A} (U + IR)\right) - 1 \right] - \frac{U + IR_S}{R_{SH}} \tag{5}$$

Where: I_s -dark current of the cell; q -charge ($=1.6 \times 10^{-19} [^{\circ}C]$); k -the Boltzmann's constant ($=1.38 \times 10^{-23} [J/K]$), T_c - cell temperature $[K]$; A -coefficient depending on the type of PV technology.

Generated by the photocell current, depending on solar intensity and cell temperature is [2]:

$$I_{ph} = [I_{SC} + K_I (T_C - T_{REF})] \lambda, \quad (6)$$

Where: I_{SC} - is short circuit current of the cell at temperature $T = 25^{\circ}C$ and solar activity $1kW/m^2$; K_I - cell temperature coefficient for short circuit; T_{REF} - reference cell temperature; λ - solar activity $[kW/m^2]$

The cell temperature and current saturation are determined by:

$$T_c = T_A + \left(\frac{NOCT - 20}{0.8} \right) * \frac{E}{800}, \quad (7)$$

$$I_S = I_{RS} \left(\frac{T_c}{T_{REF}} \right)^3 \exp \left[\frac{qE_G}{kA} \left(\frac{1}{T_{REF}} - \frac{1}{T_c} \right) \right] \quad (8)$$

Here T_A - is ambient temperature; $NOCT$ - normal operating cell temperature ($=49C$); I_{RS} - reverse satisfy current of the cell

$$I_{RS} = \frac{I_{SC}}{\exp \left(\frac{qU_{oc}}{kAT_{REF}} \right) - 1}, \quad (9)$$

in (9) U_{oc} - is a load voltage of PV cell.

In an ideal photovoltaic cell(unit) $R_s = 0$ and $R_{SH} = \infty$, then the equivalent circuit of PV cell (unit) described by equation (5) and presented in Figure 1, is to modify the equivalent circuit of figure 2, described by equation (10):

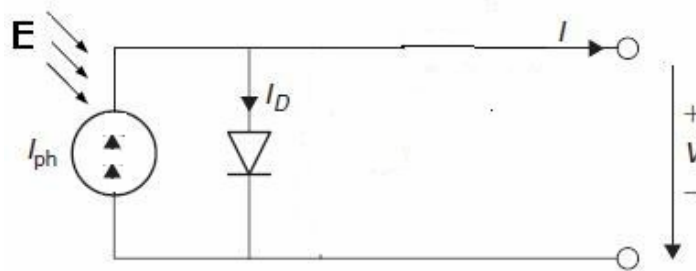


Fig. 2

$$I = I_{ph} - I_S \left[\exp \left(\frac{qU}{kT_c A} \right) - 1 \right] \quad (10)$$

Solar unit consisting of N_p connected parallel cells and N_s connected cellular elements [3] is shown in Figure 3

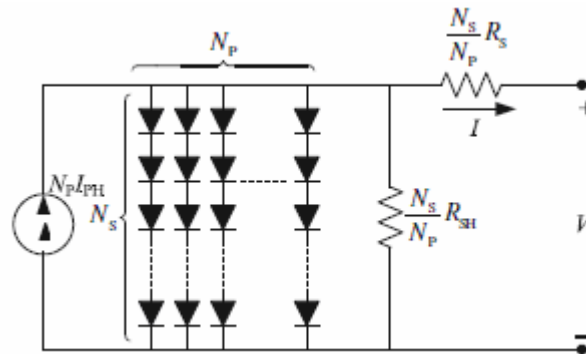


Fig. 3

3. CREATE A PV MODEL IN SIMULINK ENVIRONMENT

For compiling MATLAB based model in SIMULINK environment taking account the solar radiation, ambient temperature and the type of material used in PV cell is used shown in [3] converted model presented in Figure 4

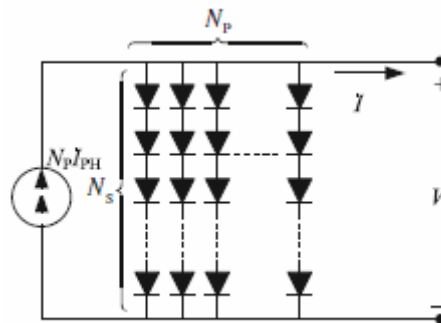


Fig. 4

Equation (10), applied to shown Fig.4 has the form (11):

$$I = N_p I_{ph} - N_p I_s \left[\exp\left(\frac{qU}{N_s k T_c A}\right) - 1 \right] \tag{11}$$

Based on mathematical equations given in section 2, describing processes in photovoltaic cell with surrounding figures, is constructed mathematical model of photovoltaic unit in Simulink environment with the general form shown in Figure 5.

Input data for compiled model are solar radiation, ambient temperature, the parameters of the photovoltaic module and the type of technology for making photovoltaics

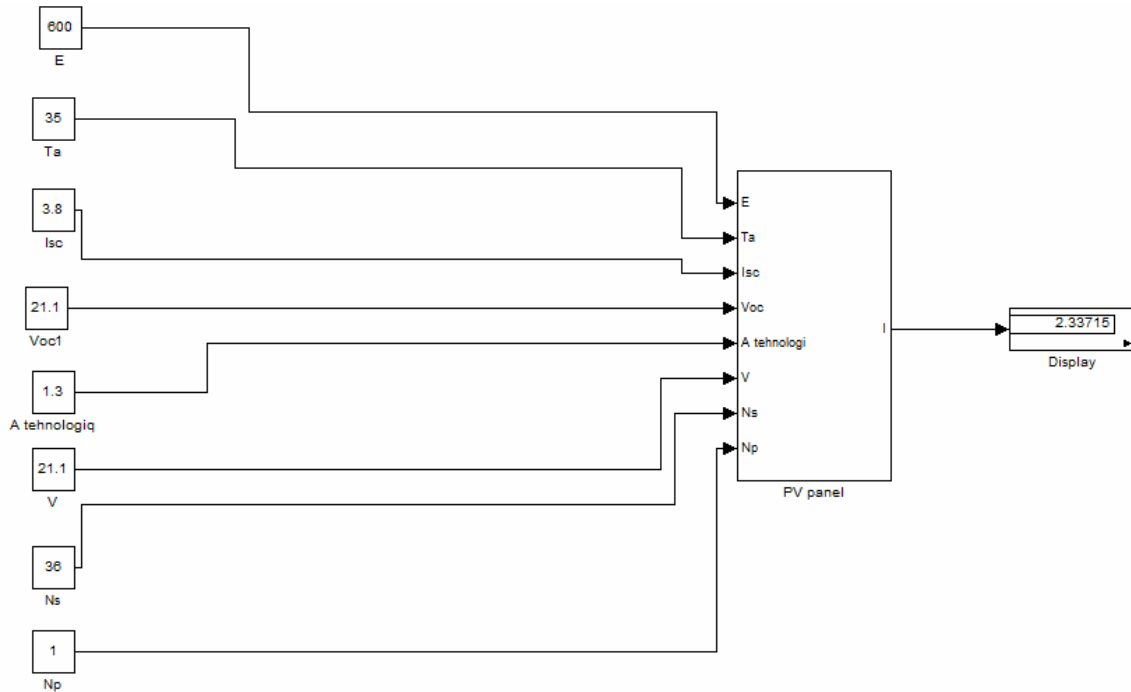


Fig. 5

The internal structure of the constructed module, developed using equations (1)-(11) and described using various mathematical modules has the form;

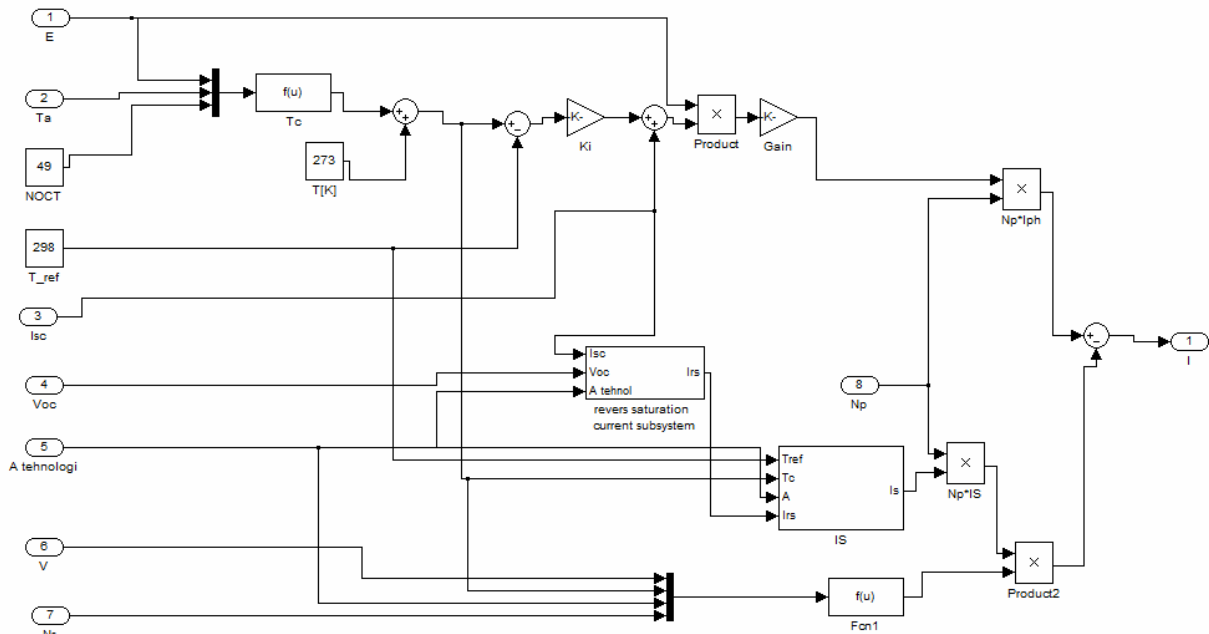


Fig. 6

4. CONCLUSIONS

- The model is adaptable to different types of PV units and enables making variance analysis to measure the impact of various environmental factors
- In comparison made with the effects of model tabular results, observed error to 5%, which is within the tolerance research
- A model could be used for training students from "Renewable Energy Sources"

References

- [1] IEEE 1547.3 Guide for Monitoring, Information Exchange, and Control of Distributed Resources Interconnected with Electric Power Systems, 2007.
- [2] Kalogirou S. Solar energy engineering: processes and systems: chapter 9. Academic Press; 2009. p. 469–517.
- [3] Tsai, Huan –Liang, Insolation-oriented model of fotovoltaic using Matlab/Simulink; Solar Energi, 2010.
- [4] Неделчева С. Електрически мрежи, София, 2005 г.
- [5] Chervenкова Т, А. Chervenkov, St. Bozhkov „Computer simulation of higt frequensy signal propagation in medium voltage power cables“, TU – Sofia; 2009

FACTORS INFLUENCING ELECTRICAL PERFORMANCE OF PHOTOVOLTAIC SYSTEMS

Stoyan Hristov Bozhkov

Department of "Electrical Engineering, Electronics and Automatics"
Technical University of Sofia,
Bul. "Burgasko cheso" № 59, Sliven 8800, Bulgaria, phone:+359895586485 ,
e-mail: s_bozhkov@abv.bg

Abstract *The expansion in Bulgaria in the last years of renewable energy sources and in particular the so-called photovoltaics necessitate examination critically assessed and consideration both during the design and in service with a number of factors affecting the production of electricity from "solar" sources. This publication was made possible review as one of the effects of species photovoltaic technologies used in production of photovoltaics, and some of the major environmental factors that have an important impact on their operation.*

Keywords: *renewable energy sources, photovoltaic technologies, environmental factors.*

1. INTRODUCTION

Solar photovoltaic energy is becoming an increasingly important part of the renewable energy sources in the world [1]. The main advantage of these sources is to generate electricity without emitting pollutants and without being required any kind of fuel. There are many factors that affecting the operation and efficiency of photovoltaic based electricity generation systems such as photovoltaic cell technology, environmental conditions and the selection of required equipment [2]. The efficiency, defined as the proportion of energy output and accidental solar radiation on photovoltaic panel is an important factor direct effect on optimal design of each "solar system".

For these characteristics this paper is focused on main global factors that should be taken into account when modeling the efficiency of PV systems, their design and maintenance

2. GENERAL TYPES OF FACTORS

The factors that significantly affecting the operation and efficiency of photovoltaic based electricity generation systems are: photovoltaic cell technology, environmental conditions and the selection of required equipment

2.1. Influence of species photovoltaic technology

➤ *Monocrystalline silicon cells* – these cells are made from pure monocrystalline silicon. In these cells, silicon is a single continuous structure of the crystal lattice, with almost no defects or impurities. The main advantage of monocrystalline cells is

their high efficiency, which is usually around 15%. The disadvantage of these cells is complicated production process required to obtain monocrystalline silicon, which results in slightly higher costs than those of others technologies [7]. Crystalline silicon technology is well established for photovoltaic modules and have a long run time /20 years and over/ [9].

➤ *Polycrystalline silicon cells* – less expensive polycrystalline silicon material passes through the expensive and energy-consuming process of improving the crystal. Polycrystalline cells are manufactured by many grains of monocrystalline silicon.

In manufacturing process molten polycrystalline silicon is cast into ingots, which are then processed into very thin layers and assembled into complete cells Polycrystalline. Cells are cheaper to produce than monocrystalline cells because as their production requires simpler manufacturing process. But they are, however, slightly less effective, with an average efficiency being around 12% [7, 9].

➤ *Amorphous silicon cells* – generally the main difference between these cells and the above is that instead of crystalline, amorphous cells are composed of silicon atoms in homogeneous thin layer. Additionally that amorphous silicon absorbs light more effectively than crystalline silicon which leads to thinner cells known as thin film photovoltaic technology. The biggest advantage of these cells is that amorphous silicon can be placed in a wider range of substances, said flexible. For these reasons, thin film solar is approximately 15% market share, while the remaining 85% for crystalline silicon [10]. Their disadvantage is low efficiency, which is on the order of 6% [7].

➤ *Photovoltaic cells from Cadmium sulfide* – the material silicon which then attracts a lot of attention is cadmium sulfide. Transducers of cadmium sulphide are considered particularly promising for the production of cheaper photo cells required for large-scale photo electric conversion of solar energy. For their production using a minimum amount of material as the layer is very thin, making them typical of thin film photovoltaic cells. Moreover, they come from a polycrystalline material which is initially at a low cost of monocrystalline silicon.

Voltage at idle of cells from cadmium sulfide is less than that of silicon is in the order of 400-500 mV. Short circuit current is an order of magnitude to that of silicon. The maximum electrical efficiency is between 8%÷8.5%. Theoretical calculations show that the maximum efficiency of photovoltaic thin cadmiumsulfidereaches 11-14% [3].

➤ *Photovoltaic cells from Gallium Arsenide* – photo cells from Gallium Arsenide have - higher efficiency than polycrystalline thin-film photo cells. There has been an electrical efficiency of 13%, and according to various sources and 15%. The maximum theoretical efficiency is higher than that of silicon and amount 27%, Due to its physical properties, this type of material is closest to optimal material used to make photovoltaic cells. Furthermore, the voltage is significantly greater and at room temperature reaches 1V. Since the reduction of voltage with increasing temperature is a percentage of the initial voltage, it follows that in this type of photo cells that decline will be considerably smaller. Although of these advantages, a major disad-

vantage is that arsenic is a rare and expensive material and expendable materials unit appears to make more than cadmium sulfide photovoltaic cells [3].

➤ *New directions photovoltaic* – PV cell composed of a material can convert only about 15% of the available energy to useful electricity. To improve performance, you can use several cells with different band gaps that the technology is more complex and therefore more - expensive. The latest trend in this direction in technology is the productions of photovoltaic cells .Triple connected cells are significantly more complex, respectively. More expensive, but with them to achieve 40% efficiency. Photovoltaic cell consists of three layers of photovoltaic material found on one another; each of them different in range captures sunlight.

2.2. Effect of environmental conditions

There are many different types of conditions and environmental factors that directly or indirectly affect the efficiency of the photovoltaic system, and from there directly on its attaching electrical system or node from the mains. Some of these factors are:

➤ *Temperature variations* – Temperature is a parameter that has a great influence in the behavior of the PV system, as it changes the efficiency of the system and its output energy. With increasing ambient temperature respectively. Cell, its effectiveness reduces significantly Fig. 1

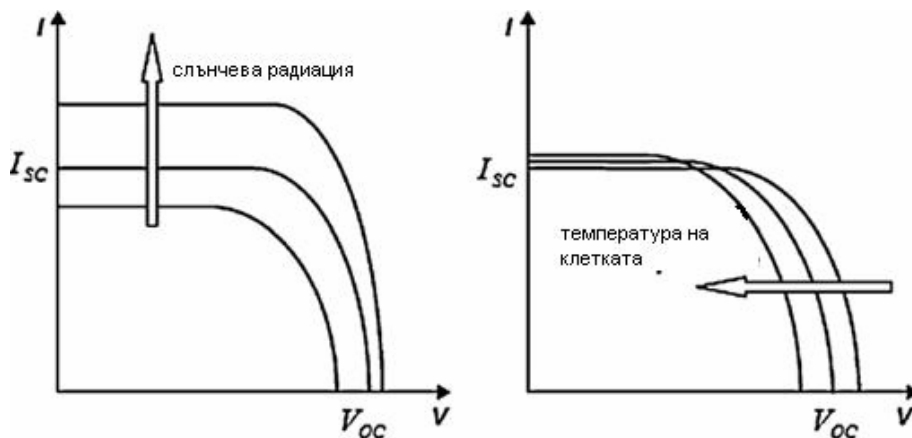


Fig. 1

With increasing solar radiation, the voltage at idle and the current increase while an increase in temperature of the cell, the voltage at idle decreases. Therefore photovoltaic cells work much better in cold weather than in warm.

The calculation of the normal operating temperature of photovoltaic modules using EU standards [4,5] is based on the calculation of the temperature of the module through the application of "normal operating cell temperature" /NOCT/:

$$T_M = T_a + (NOCT - 20) * \frac{E}{800} \quad (1)$$

where: T – The temperature of the environment $^{\circ}\text{C}$; E - Solar irradiation $\left[\frac{\text{W}}{\text{m}^2}\right]$;
NOCT – 49 [$^{\circ}\text{C}$]

Introduced is the indicator "*energy efficiency of the photovoltaic cell*" - ...[5], which is calculated using the point of maximum power- P_{max} of photocell divided the product of the surface area of the cell and the intensity of sunlight falling on it, under standard conditions test:

$$\eta = \frac{P_{\text{max}}}{E S_c} \quad (2)$$

By increasing the temperature of the cell reduces efficiency of the module.

➤ *Irregularity of the incident light* – The power of solar power systems depend on the intensity of solar radiation. Equability of sunshine the solar panels determined their high efficiency. If a photocell included in the composition of the solar panel is illuminated with a low intensity of neighbor elements, it forms called "*parasitic load*" and reduces the total power generation of the panel. To ensure maximum performance and high efficiency, the solar panel must be exactly navigate to the sun so that the sunlight falling is angled 90 degrees to the photovoltaic panel. Therefore, system an automatic monitoring position of the sun are widely used. For the latitude of Bulgaria according voltaic orientation of experimental studies must be within 32 to 35 degrees, which provides maximum electricity during the summer months.

➤ *Wether conditions* – dust and dirt that accumulates on the surface of PV modules of the block sunlight as a result of reaching a reduction of the total amount produced by the solar power plant. Although typical dirt /dust/ clean during rainy days and months, it is a realistic assessment of the performance of the system must take into account the accumulation of dust during dry no rain days. Studies conducted Indicating modules dust accumulation show that 100W unit, working with some accumulated dirt /dust like/ can spend an average of 79W [6]. The attempts made for a period of six months in the territory of Sliven reported a drop in total electricity of stationary photovoltaic park built by 3MW, with 1.5% as a result of contamination by dust.

2.3. Influence of system facilities

The main facilities in important influence on the efficiency of photovoltaic systems as a whole are: inverters and batteries.

➤ *Inverters* are used to convert DC electricity produced AC. Depending on their structure , they are single-phase and three-phase. Each of them is characterized by an energy conversion efficiency [7]. The main task is to invert also maintain constant AC voltage of invert part as possible – efficiency:

$$\eta_{\text{inv}} = \frac{P_{\text{out}}}{P_{\text{in}}} = \frac{V_{\text{AC}} I_{\text{AC}} \cos(\varphi)}{V_{\text{DC}} I_{\text{DC}}} \quad (3)$$

where: $\cos(\varphi)$ is the power factor;

I_{DC} and V_{DC} are current respectively voltage of input side of the inverter. The efficiency of the inverter, thus the photovoltaic system as a whole, have a significant effect: the temperature of the environment, requirements for dust and moisture resistance, and electromagnetic compatibility standards [8]. Photovoltaic inverter manages the park, setting the hours of turning the system set up, respectively accession to the electric grid. When batteries are used in conjunction with a photovoltaic system, they must be located in an area with no sudden extreme temperature changes and adequately ventilated [2]. Energy produced during the day is not consumed by the loads is stored in batteries and thus saved electricity could be used at night, on days with bad weather, or to cover the peak load peaks. For these features to work, the batteries operate under frequent charging and discharging, which is on the requirements placed on them are higher than conventional batteries. Controllers control charge and discharge the battery, working with photovoltaic systems "dosed" exchange flow of energy to be so that there is optimum voltage of the photovoltaic system at any point in time.

However, in many cases, the voltage at the terminals of the batteries may not be the optimum operating voltage for photovoltaics, which property is mainly due to the presence of controllers optimize the performance of photovoltaic module, so that it always works in the point of maximum power independently of battery voltage [7].

3. CONCLUSIONS

From these representations could be summarized the following conclusions:

- The main problem of the photovoltaic cells is that they are less effective if their position is not selected properly.
- With the increase in sunlight and avoiding shading increases their efficiency, while it is necessary to take measures to reduce the temperature of the cells using forced cooling and greening of the area under the photovoltaic array.
- Knowledge of different factors influencing photovoltaic plants contribute to the creation of photovoltaic simulation tools through which could be a detailed analysis of system performance in real field work.

References

- [1] Global trends in sustainable energy investment 2007. United Nations Environment, Programme/New Energy Finance Ltd; 2007.
- [2] Mehmet Emin Meral, Furkan Dincer „A review of the factors affecting operation and efficiency of photovoltaic based electricity generation systems” *Renewable and Sustainable Energy Reviews* 15 (2011), pp.2176–2184.
- [3] Р. Младенчева „Фотоволтаични електросистеми”, Ековат технологии. 2009.
- [4] IEC 61215: Crystalline silicon terrestrial photovoltaic (PV) modules—design qualification and type approval; 2005.

- [5] Yamaguchi T, Kawakami M, Kitano K, Nakagawa S, Tokoro T, Nakano T, et al. Data analysis on performance of PV system installed in south and north directions. In: 3rd world conference on photovoltaic energy conversion. 2003. p. 2239–42.
- [6] Endecon Engineering: Energy technology development division, consultant report, a guide to photovoltaic (PV) system design and installation. California Energy Commission; 2001. p. 1–40.
- [7] Kalogirou S. Solar energy engineering: processes and systems: chapter 9. Academic Press; 2009. p. 469–517.
- [8] Ishikawa T. Grid connected photovoltaic power systems: survey of inverter and related protection equipments. Task V Grid Interconnection of Building Integrated And Other Dispersed Photovoltaic Power Systems; 2002, p.1–64
- [9] C. apar S. Photovoltaic power generation for polycrystalline solar cells and turning sunlight into electricity. M.Sc. thesis, Engineering Physics University of Gaziantep; July 2005.
- [10] http://en.wikipedia.org/wiki/Solar_cell#Thin-film_solar_cells; 2010 [accessed February 2010].

AUTOMATING DETERMINATION OF THE OPTIMUM POWER AND NUMBER OF TRANSFORMATION STATION IN THE RESIDENTIAL PART OF SETTLEMENTS

Atanas Chervenkov

Department of Theoretical Electrical Engineering, Technical University of Sofia,
8, Kliment Ohridski, 1000 Sofia, Bulgaria, phone: +35929653319, e-mail: acher@tu-sofia.bg

Abstract. *The automated determination of power for medium voltage transformers, their number and their optimal placement in residential settlements - small and medium-sized cities, villages and resorts are considered. A computer-aided design program running under operating system WINDOS 32 bit is developed. The programme was written in Turbo Pascal. It was developed multivariate to determine the optimal number of transformer stations and optimal power of transformers. The program determines the electrical load center, where it is recommended to have transformer stations and the power supply substation HV / MV. The program aims to improve the education of students in "Electrical Engineering" in Faculty of Engineering and Pedagogy of TU - Sofia in the subjects "Electric power supply of settlements" and "Electrical networks and systems". The program can be used of designers, working in the field of electrical supply of cities and resorts for developing and modernization of electrical networks for MV. A methodological guide for the automated determination of optimal power of transformer and the number of transformer stations is developed. The software product requires minimal computer resources and knowledge to work with Windows, as well as basic knowledge in "Electrical Engineering", "Electrical Networks" and "Electric power supply of settlements."*

Keywords: *CAD, power, substation, transformer, settlements.*

1. INTRODUCTION

Need to improve the training courses "Electrical Engineering", "Electrical settlements" and "Electric Networks and Systems" requires the use of modern technical equipment, computer systems and programs for engineering automation [2, 3]. The use of computers in engineering education has proven its benefits in recent years.

The use of a computer design of electrical networks and systems, and in particular the automation of the process of determining the number and location of power transformer stations available to power supply with electricity of customers in settlements is discussed.

This article discusses a computer program to automate the process of designing electrical distribution networks for medium voltage in the training of students. It improves the level of understanding of the material in the conduct of exercises and development of project assignments.

2. DESCRIPTION OF THE PROGRAMME

The computer program includes: main program, process control and corrections; help procedure; procedure for displaying the results and input-output procedure of connections with WINDOWS.

The primary program code is written of the language PASCAL [4]. It was developed in the 32 bit version. The program has the opportunity to develop and introduce new units or replace existing procedures.

Software product requires minimal computer resources and knowledge to work with Windows, as well as basic knowledge in "Electrical Engineering", "Electrical Networks" and "Electric power supply of settlements".

The main program contains a module for calculating. It liaises with the various procedures and ensures their successful completion.

After launching the program menu is displayed on the computer screen. The first option on this menu is a procedure to help how work the program - Fig. 1.

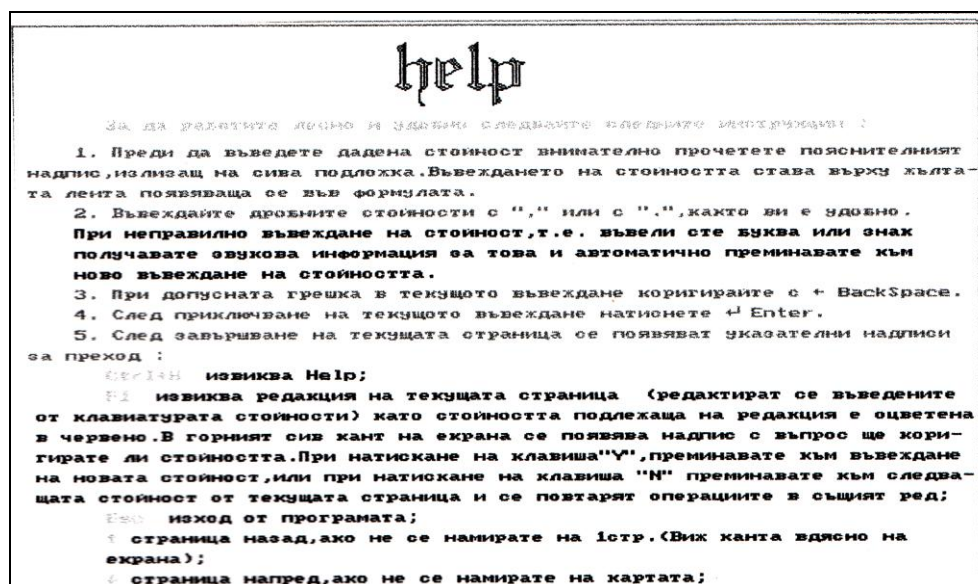


Fig. 1

On the basis of the procedure for help was developed and methodological guide for preliminary information about the program.

To determine the locations of transformer stations shall be assumed the city plan of the settlement and construction features of buildings. Also be considered and the condition they are located in the basements of public buildings (shops, kiosks and etc.) and individual buildings (if this is possible and costly implementation) or completed transformer substation (externally available).

On the first stage determines the calculation load of the unit power substation. The computing load in accordance with the other probably-statistical method is determined. Finally it is defined as the average load of the two methods.

The maximum active and reactive power of the power substations HV / MV is determined by the expression [1]

$$P_{\max TP} = \frac{P_{\max}}{K_{e3}K_{e2}}, kW \quad (1)$$

$$Q_{\max TP} = \frac{Q_{\max}}{K_{e3}K_{e2}}, kVAr, \quad (2)$$

where: K_{e3} and K_{e2} are coefficients of simultaneity of loads network level MV / Power substation and level power substation / MV network, their values are set in the range 0.90-0.95 and 0.85-0.9, respectively.

Then the module of the full maximum power is determined

$$S_{\max TP} = P_{\max TP} + jQ_{\max TP} \quad (3)$$

$$|S_{\max TP}| = \sqrt{P_{\max TP}^2 + Q_{\max TP}^2}, kVA$$

Optimal power transformer station S_T be determined for the case of a uniformly distributed load, as is the normal load in the settlements.

$$S_T = k_{TP} \sqrt{\delta \alpha}, \quad (4)$$

where: α is the number of LV terminals (380V) of a transformer station;

δ is installed power of transformer station per unit length (1 km);

k_{TP} is a factor, depending on the power of transformer stations, investment and operating costs for the terminals of the power substation.

Terminals of the power substations are recommended to have LV cable (380 V). The cables are laid on both pavements of the streets in four directions and taking $\alpha = 8$.

Power δ depends of power of transformer substations $S_{\max TP}$, the length of the streets in town and the average distance between power substations (in the opinion of NEC accepts this distance to 600 m).

The coefficient k_{TP} is determined for two types of nominal power of transformers in a power substation and five types of cross-sections of LV cables. Calculations are performed with two types of transformers - with power 630 kVA and 400 kVA for example. LV cable lines are calculated for the section of the cores of 50 mm^2 to 150 mm^2 .

The calculated optimum power of transformer station S_T is rounded of the program to the nearest standard value – 160 kVA, 250 kVA, 400 kVA или 630 kVA.

Then the optimal number of power substations n in the settlement is determined

$$n = \frac{|S_{\max TP}|}{S_T} \quad (5)$$

The optimal number of power substations is rounded to an integer.

The program performs multivariate design. The determination of optimum power S_T and number n of power substations are done in two ways in the implementation of two additional optimization criteria.

The first additional criterion is admissible loss of voltage in low voltage network. It provides quality of delivered electrical energy.

Optimal power of transformer station S_T in this case is determined by the expression

$$S_T = k_{TP}^{1/3} \sqrt[3]{\delta^2 \alpha^2} \quad (6)$$

The coefficient k_{TP} is defined similarly, but taking account of permissible voltage loss in LV networks, specific electrical resistance of the wires and the power factor of the network.

The second optimization criterion is permissible heating of wires in grid to low voltage. It ensures reliable power supply.

Optimal power of transformer station S_T in this case is determined by the expression

$$S_T = k_{TP}^{1/3} \sqrt[3]{\delta \alpha^2} \quad (7)$$

The coefficient k_{TP} is defined similarly, but takes into account investments in low-voltage power lines and the number of terminals of a transformer station.

Finally are selected, the optimum power and the number of power substations of one of three criteria.

The calculation procedure includes determining locations of power substations. A total area of the regulatory settlement S_{NM} is inserted. The area supplied by a transformer station is determined as

$$F = \frac{S_{NM}}{n} \quad (8)$$

For uniformly distributed electric load, the area of electricity from a transformer station is assumed to be a circle with radius

$$R = \sqrt{\frac{F}{\pi}}, \text{ km} \quad (9)$$

With adequate scale M (the default is set of 1:5000 scale) are plotted on the map numbers n of circles of radius r

$$r = \frac{R}{M} \quad (10)$$

When the center of the circle is on regulated area, power substations are located on the street.

The density of power substations in the central parts of the town is increased, because there is expected a higher growth of load.

Finally the location of the substation HV / MV is determined. It is situated in the village near HV power transmission line 110 kV.

The procedure for displaying the results performs the visualization of the described above computational process. The performance of the procedure during the execution of the program is shown in Fig. 2 and Figure 3.

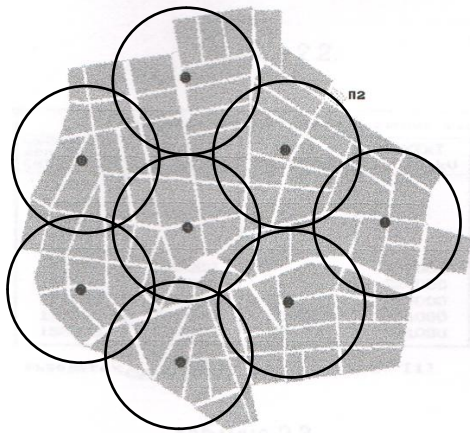


Fig. 2

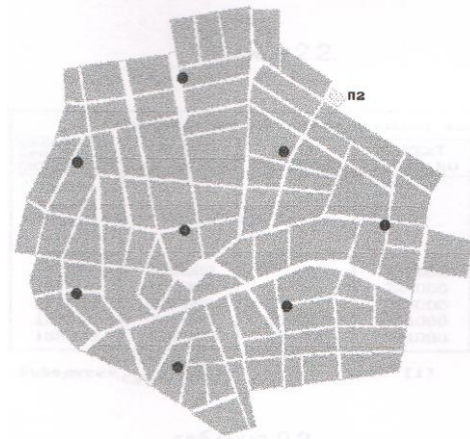


Fig. 3

The procedure for reviewing and correcting data entry purposes editing entries. The students can make changes to entered data, using the information for help and after having ensured that the data are in acceptable for the design. If some of the data are faulty, program invites students to correct them. The numerical values of the data is entered in point – "." or comma – ",". Thus are removed the system settings for data format depending on the language – English or Bulgarian.

4. CONCLUSION

The CAD programme is developed. The programme determine the power for transformers of medium voltage, their number and optimal placement in residential settlements – small and medium-sized cities, villages and resorts.

It was developed for multivariate design, using three optimum criterions.

The program improves the education of students in "Electrical Engineering" in Faculty of Engineering and Pedagogy of TU - Sofia in the subjects "Electric supply of settlements "and" Electrical networks and systems".

A methodological guide for the automated determination of the optimal power of transformers and the number of transformer stations is developed.

References

- [1] Genkov N. and others, "Guidelines for the design of electrical networks and systems", Technika, Sofia, 1993 (in Bulgarian).
- [2] Todorka Chervenкова and Stoyan Bozhkov, "Program to support the education of students in the study of resonance in serial circuit", Proceedings of summer school "Advanced aspects of theoretical electrical engineering" Sozopol 2005, pp. 181-186.
- [3] Todorka Chervenкова, Stoyan Bozhkov, "Computer program for processing of experimental data by investigation of two-port devices", Proceedings of summer school "Advanced aspects of theoretical electrical engineering Sozopol 2007", vol. II, pp. 99-103.
- [4] <http://www.lazarus.freepascal.org/>.

A NEW METHOD FOR A REAL STATE OF POWER TRANSFORMERS BASED ON THE AREA OF PARTIAL DISCHARGE

Nikolina Petkova

Department of Theoretical Electrical Engineering, Technical University of Sofia,
8 Kliment Ohridski blvd., 1000 Sofia, Bulgaria, phone: +3599652498,
e-mail: npetkova@tu-sofia.bg

Abstract. There are many methods to diagnose the current state of the power transformers. The electrical method of measuring of partial discharges in the volume of the power transformer gives the maximum information that can be desired. In this paper, a new method, based on the determining algorithm for analyzing the signals measured as well as on preparing the necessary recommendations by the expert monitoring system, is suggested.

1. INTRODUCTION

This new method determines the state of the power transformer based on the area of partial discharge appearance. The most important parameters regarding the final software decision about the actual transformer state are the location of the partial discharge, the partial discharge case and the transformer oil conditions.

The possible cases of partial discharge occurrence are A, B, C, D, E, F, G, H, J, K, L, M and N. The possible locations of partial discharges are in the tank, windings, leads, tap changer and the other. Only two cases of oil conditions are considered—good and bad oil.

Failures are usually triggered by severe conditions, such as lightning strikes, switching transients, short-circuits, or other incidents. When the transformer is new, it has sufficient electrical and mechanical strength to withstand unusual system conditions. As transformers age, their insulation strength can degrade to the point that they cannot withstand system events such as short-circuit faults or transient overvoltage [1, 2].

To prevent these failures and to maintain transformers in good operating condition is a very important issue for utility companies. Traditionally, preventive routine maintenance programs combined with regular testing are used. With deregulation, it has become increasingly necessary to reduce maintenance costs and equipment inventories. This has led to reductions in routine maintenance. The need to reduce costs has also resulted in reductions in spare transformer capacity and increases in average loading. There is also a trend in the industry to move from traditional time-based maintenance programs to condition-based maintenance [1, 2].

These changes occur at a time when the average age of the transformers in service is increasing and approaching the end of nominal design life. The change to condition-based maintenance has resulted in the reduction, or even elimination, of routine

time-based maintenance. Instead of doing maintenance at a regular interval, maintenance is only carried out if the condition of the equipment requires this. Hence, there is an increasing need for better nonintrusive diagnostic and monitoring tools to assess the internal condition of the transformers. If there is a problem, the transformer can then be repaired or replaced before it fails [1, 2].

In a substation, the condition of the oil can be examined using Dissolved Gas Analysis (DGA). It has only been performed in a lab, where at first the oil sample is degassed followed by a gas-chromatographic analysis of the extracted gas sample. Then, the composition of the gas mixture and the total amount of extracted gases is analyzed. This method gives precise and reproducible results, thus reliable results are achieved. The result of such a transformer examination is nevertheless influenced by the quality of the oil sample that is used for DGA [3].

The gasses that are dissolved in the insulating oil are energy generated due to a fault, thus resulting in the partial or complete destruction of the Hydrocarbon molecular chains of the insulating oil. The fractions consist of:

- Hydrogen H_2
- Methane CH_4
- Ethane C_2H_6
- Ethene C_2H_4
- Ethine C_2H_2
- Propane C_3H_8 and
- Propene C_3H_6 ,

Due to the de-polymerization of the solid paper insulation additionally:

- Carbon Dioxide CO_2 and
- Carbon Monoxide CO

are generated.

The atmospheric gases:

- Oxygen O_2 and
- Nitrogen N_2

are dissolved in the insulating liquid as well if the transformer is of breathing type and is exposed to the environment [3].

As long as the concentrations of the dissolved gasses do not exceed certain limits or changes in oil solubility, the composition of the dissolved gases can be used for analysis if the ratio of their content is evaluated.

This relation is dominated by the form and amount of energy that has been applied in the transformer failure, thus thermal faults and electrical faults can be distinguished. A more precise distinction between the sizes of the failures and the level of concentration of gases is also specified in the standard IEC 60599.

In our case, the results from the chemical conditions of the oil could be summarized as GOOD OIL (if the concentrations of the gases are in compliance to standard

IEC 60599) or BAD OIL (if the concentrations of the gases are not in compliance to standard IEC 60599). These results are used in the decision module where the operator takes the final decision regarding the emergency of the partial discharge that is detected. In substations, information for the condition of the oil is provided by technical labs in six month intervals.

2. SOFTWARE SYSTEM RUNNING

The software program responsible for the decision regarding the status of the transformer is developed in Visual Studio.

It has to be set the settings for the next parameters: case of PD occurrence, partial discharge location and oil condition. The software determines the level of criticality of the power transformer state.

➤ *Step 1* – Press the button “START DECISION MODULE” and the following window will appear:

Step 1 is common for all tests.

➤ *Step 2* – Depending on the input data, we will have the following situations:

- Status **WORK** – Input data:
 - Case of PD occurrence: A
 - Partial discharge location: TANK
 - Oil condition: Good

Output data:

Status message: WORK

- Status **ATTENTION** – Input data:
 - Case of PD occurrence: C
 - Partial discharge location: WNDG
 - Oil condition: Good

Output data:

Status message: ATTENTION

- Status **DANGER** - Input data:
 - Case of PD occurrence: C
 - Partial discharge location: LEADS
 - Oil condition : Bad

Output data:

Status message: DANGER



Fig. 1. Conclusion Module– screenshot



Fig. 2. Conclusion Module– case A (work state-tank)

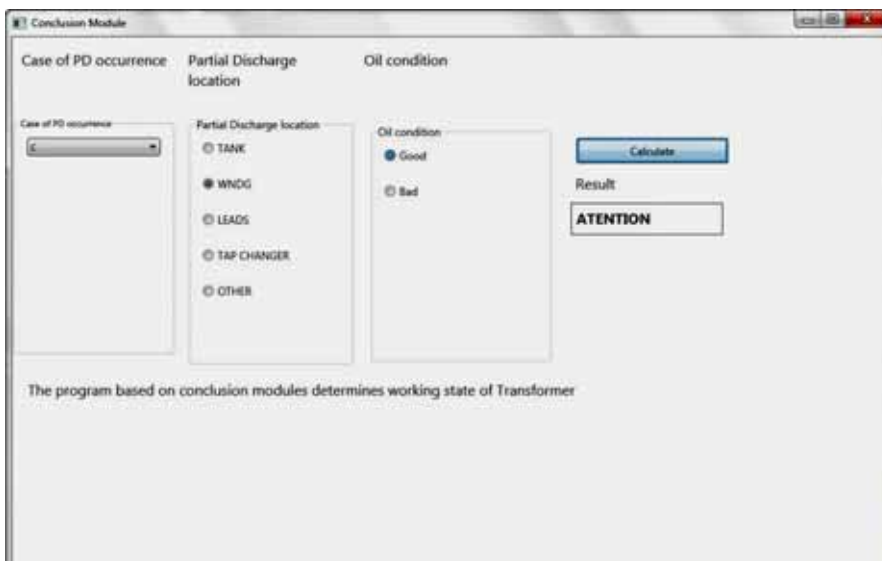


Fig. 3. Conclusion Module– case C (attention state - WNDG)

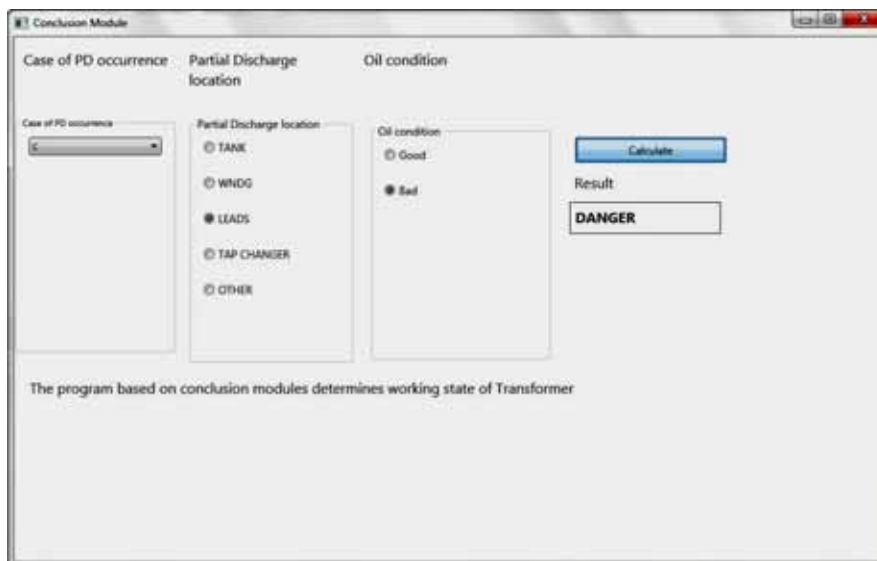


Fig. 4. Conclusion Module – case C (danger state - LEADS)

3. CONCLUSION

In this paper a new PD methodology were described. This kind of logic is approximately new and in progress. This new way provides meaningful and additional information for PD analysis. The software based on the prescribed algorithm for analyzing the signals measured as well as on preparing the necessary recommendations by the expert monitoring system.

Acknowledgement. The work was supported by FP7 project South–East European TSO Challenges (SEETSOC), R&DS of the Technical University - Sofia contract № 4149-M.

References

- [1] IEC 60270:2000 - High-voltage test techniques - Partial discharge measurements.
- [2] IEC 60076-3:2000-03 - Power transformers – Insulation levels, dielectric tests and external clearances in air
- [3] Online gas analysis of transformers, Energy Support, http://energy-support.de/3_trafo/analytik-schadgas.php

A SIMULINK MODEL OF A DC/DC BUCK CONVERTER CONTROLLER BASED ON THE GENERAL SLIDING MODE CONTROL

Ivan Mitkov Trushev

Department of Theoretical Electrical Engineering, Faculty of Automatics
Technical University of Sofia 8, Kliment Ohridski St, Sofia-1000
BULGARIA, phone: 9653319, e-mail: ivant@tu-sofia.bg

Abstract: *The considered DC/DC buck converter controller is based on the classical (general) sliding mode control (SMC). The simulations are made for two different α called convergence factor. It is shown that the controller with higher α has faster dynamic response and the speed of voltage response is proportional to the magnitude of the coefficient α .*

Keywords: *DC/DC buck converter, general sliding mode control (SMC)*

1. INTRODUCTION

Switched Mode DC/DC converters are essential for efficient conversion of the battery voltage to various supply voltages, needed to perform every function with minimum power drain. With a DC/DC converter a variable battery supply voltage can be converted to an optimal supply voltage for an application.

It is known that the switching DC/DC converters are highly nonlinear plants with uncertain parameters and inevitable and significant perturbations during operation. The control in high performance DC/DC converters requires not only to ensure system stability but also to achieve a rapid response to sudden changes of the load, to achieve good regulation.

In this contribution a DC/DC buck converter controller based on conventional sliding mode control (SMC) is considered [1] – [3].

The paper is organized as follows. In the next section we consider the analytical model of buck DC/DC converter. In section 3 we consider the basics of the general (conventional) sliding mode control for buck DC/DC converters. We present a Simulink model of a buck DC/DC converter controller based on the general SMC in section 4 and the simulation results in section 5. The concluding remarks are given in section 6.

2. ANALYTICAL MODEL OF THE CONVERTER

Figure 1 shows a sliding mode controlled buck DC/DC converter.

We sense the output voltage v_0 multiplied by appropriate coefficient $\beta = R_2 / (R_1 + R_2)$ that is subtracted from the reference voltage V_{ref} (voltage error). That forms our first state variable x_1 (voltage error).

$$x_1 = V_{ref} - \beta v_0 \tag{1}$$

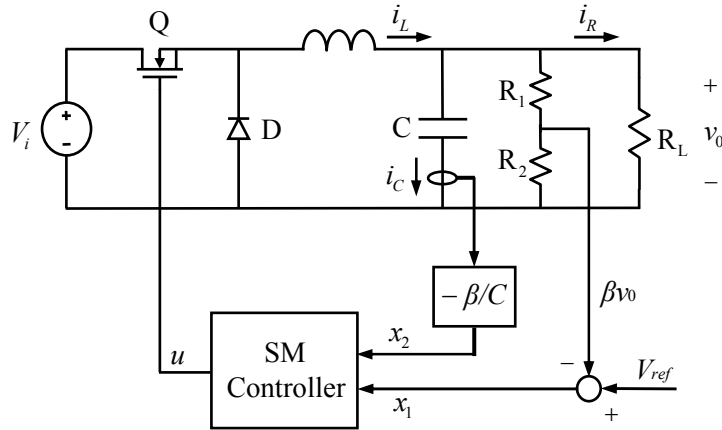


Fig. 1. Sliding Mode Controlled Buck DC/DC Converter

The rate of change of the voltage error x_2 is our second state variable:

$$x_2 = \dot{x}_1 = -\beta \frac{dv_0}{dt} = -\beta \frac{i_c}{C} \tag{2}$$

The differentiation of equation (2) with respect to time gives

$$\dot{x}_2 = -\frac{\beta}{C} \frac{di_L}{dt} + \frac{\beta}{R_L C} \frac{dv_0}{dt} \tag{3}$$

Based on the state space averaging method [4], [5] and [6] we can write $v_L = uV_i - v_0$. Taking into account that $v_L = L(di_L/dt)$ we obtain

$$\frac{di_L}{dt} = \frac{v_L}{L} = \frac{uV_i - v_0}{L} \tag{4}$$

where u is the control input that can be 1 (switch Q is ‘ON’) or 0 (switch Q is ‘OFF’).

When we substitute (4) in (3), we get

$$\dot{x}_2 = -\frac{\beta}{LC} (uV_i) - \frac{1}{LC} x_1 - \frac{1}{R_L C} x_2 + \frac{V_{ref}}{LC} \tag{5}$$

3. SLIDING MODE CONTROL FOR BUCK DC/DC CONVERTER

In sliding mode control the controller employs a sliding surface or line to decide its control input states u , which corresponds the turning on and off the power converter’s switch, to the system:

$$S = \alpha x_1 + x_2 \tag{6}$$

where α is a positive quantity in some literature called a convergence factor and is taken to be

$$\alpha = \frac{1}{R_L C} \quad (7)$$

Graphically the sliding line is a straight line on the state plane with gradient α that determines the dynamic response of the system in sliding mode with a first order time constant $\tau = 1/\alpha$.

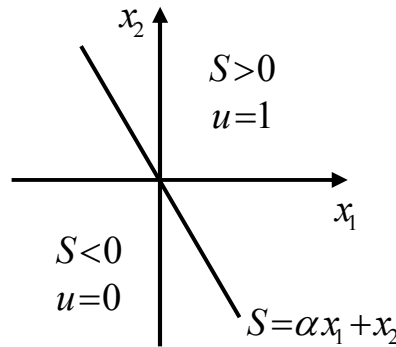


Fig. 2. A diagram of sliding mode control

To ensure that a system follows its sliding surface, a control law must be imposed:

$$u = \begin{cases} 1 = 'ON' & \text{when } S > 0 \\ 0 = 'OFF' & \text{when } S < 0 \end{cases} \quad (8)$$

The existing condition for sliding mode [2], [6] is:

$$\dot{S} = \begin{cases} \dot{S} < 0 & \text{for } S > 0 \\ \dot{S} > 0 & \text{for } S < 0 \end{cases} \quad (9)$$

Based on this we get the following expression for \dot{S} :

$$\dot{S} = \alpha \dot{x}_1 + \dot{x}_2 = \alpha x_2 + \dot{x}_2 = \alpha x_2 - \frac{\beta}{LC} (uV_i) - \frac{1}{LC} x_1 - \frac{1}{R_L C} x_2 + \frac{V_{ref}}{LC} \quad (10)$$

Depending on S and u the state space is divided into two regions
region 1: $S > 0$ and $u = 1$

$$\dot{S}_1 = \left(\alpha - \frac{1}{R_L C} \right) x_2 - \frac{\beta}{LC} (uV_i) - \frac{1}{LC} x_1 + \frac{V_{ref}}{LC} < 0 \quad (11)$$

region 2: $S < 0$ and $u = 0$

$$\dot{S}_2 = \left(\alpha - \frac{1}{R_L C} \right) x_2 - \frac{1}{LC} x_1 + \frac{V_{ref}}{LC} > 0 \tag{12}$$

Sliding mode will only exist on the portion of the sliding line that covers both of the region 1 ($\dot{S}_1 < 0$) and region 2 ($\dot{S}_2 > 0$) [6].

From one side the speed of the system increases with increasing of α (sliding line become steeper), but from other side the existing region of the sliding mode decreases that can cause an overshoot in the voltage response ($\alpha \gg 1/R_L C$) [6].

4. A SIMULINK MODEL OF A DC/DC BUCK CONVERTER CONTROLLER BASED ON THE GENERAL SLIDING MODE CONTROL

Based on the general sliding mode control law and on the above calculations it is designed a Simulink model of a buck DC/DC converter controller shown in Figure 3. The parameters of the converter are: $V_i = 3.7V$; $L = 10\mu H$; $C = 50\mu F$; $R_{L(nom)} = 10\Omega$.

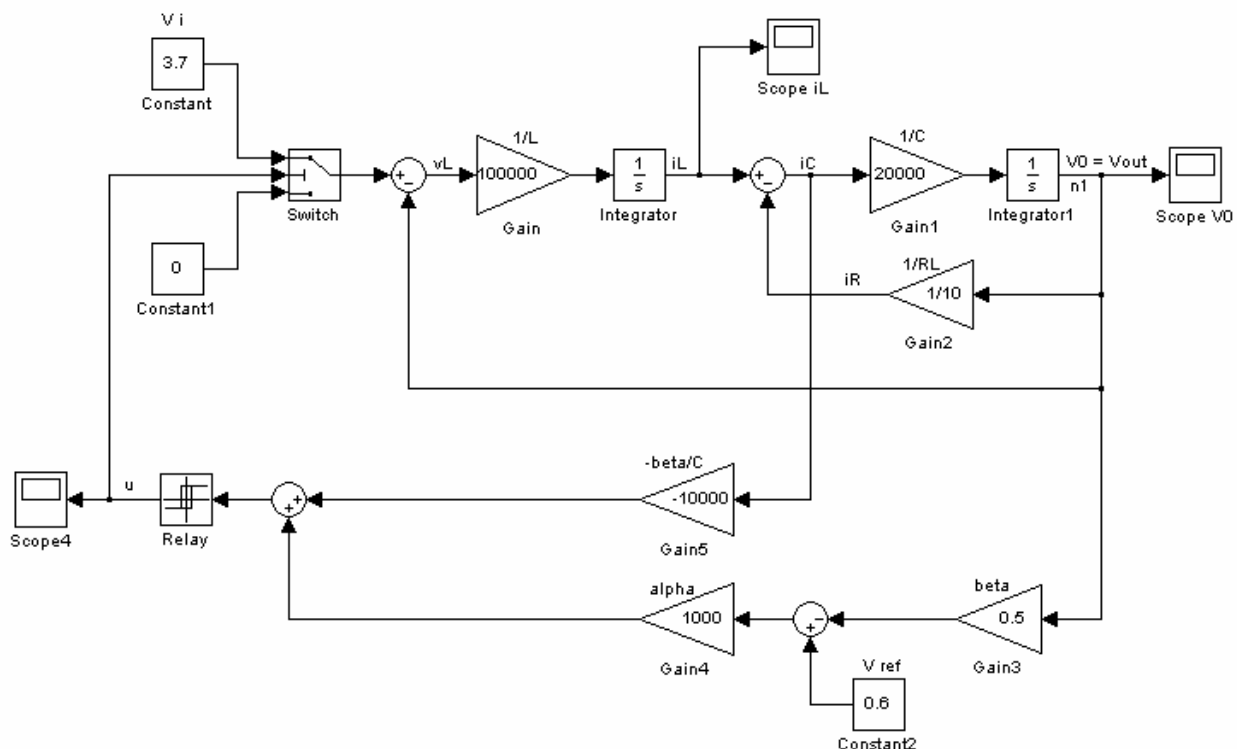


Fig. 3. A Simulink model of a buck DC/DC converter controller. The parameters of the converter are: $V_i = 3.7V$; $L = 10\mu H$; $C = 50\mu F$; $R_{L(nom)} = 10\Omega$.

5. SIMULATION RESULTS

The simulations are made for two different cases: when $\alpha = 6000$ and when $\alpha = 2000$.

Figure 4 shows the output voltage response in the case when $\alpha = 6000$. The other parameters of the controller are: $V_{ref} = 0.6V$, $\beta = 0.5$.

We start the simulation with a nominal load of 10Ω , then apply a step load change to 2Ω at time $t = 5$ ms and step load change to 20Ω at time $t = 8$ ms.

Figure 5 shows the changes in the inductor current.

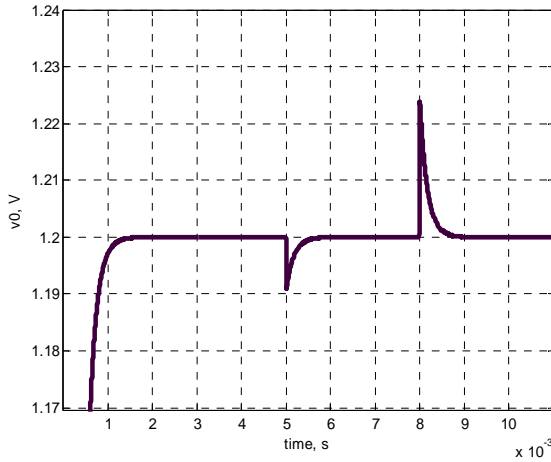


Fig. 4. Output voltage response in the case when $\alpha=6000$

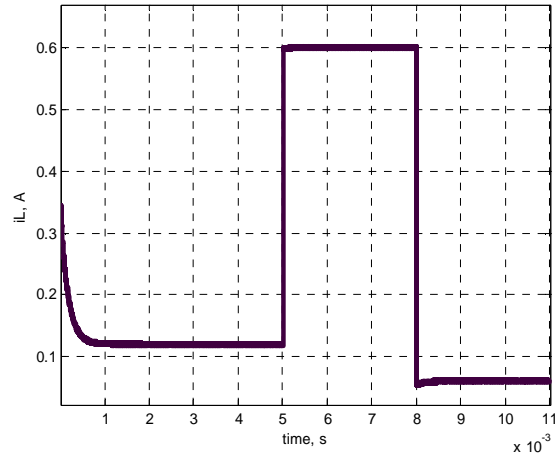


Fig. 5. Inductor current changes in the case when $\alpha=6000$

The next two graphs are related to the case when $\alpha=2000$, $V_{ref}=0.6V$, $\beta=0.5$. The output voltage response is shown on Figure 6. We start the simulation with a nominal load of 10Ω , then apply a step load change to 2Ω (over-loaded condition) at time $t=5$ ms and step load change to 20Ω (under-loaded condition) at time $t = 8$ ms.

Figure 7 shows the changes in the inductor current in that case.

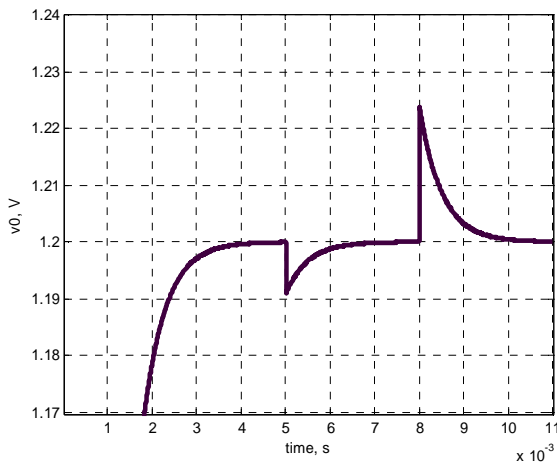


Fig. 6. Output voltage response in the case when $\alpha=2000$

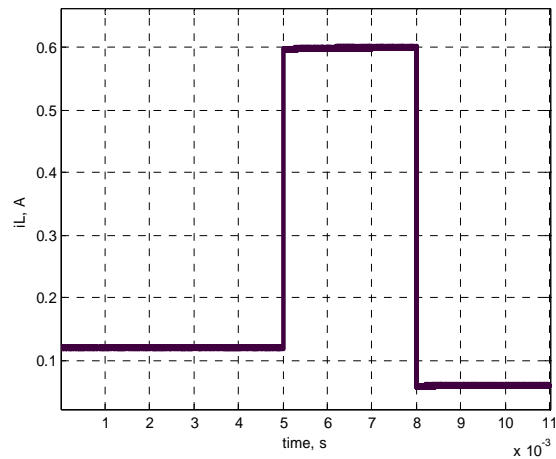


Fig. 7. Inductor current changes in the case when $\alpha=2000$

6. CONCLUSIONS

Simulation results show that the controller with higher α has faster dynamic response and the speed of voltage response is proportional to the magnitude of the coefficient α . The objective for further research is to design a scheme in PSpice based on the presented Simulink model.

References

- [1] Utkin V. I., "Sliding modes and their application in variable structure systems", MIR, Moscow, Russia, 1974 (in Russian).
- [2] P. Mattavelli, L. Rossetto, G. Spiazzi, P. Tenti, "General-purpose sliding-mode controller for DC/DC converter applications", Proc. of IEEE Power Electronics Specialists Conf. (PESC), Seattle, June 1993, pp.609-615.
- [3] P. Mattavelli, L. Rossetto, G. Spiazzi, "Small-Signal Analysis of DC/DC Converters with Sliding Mode Control", in IEEE Trans. on Power Electronics, Vol. 12, No. 1, 1997, pp. 96-102.
- [4] Sanders S. R., J. M. Noworoski, X. Z. Liu, G. C. Verghese, "Generalized averaging method for power conversion circuits", IEEE Trans. on Power Electronics, vol. 6, No. 2, April 1991.
- [5] Mahdavi J., A. Emadi, H. A. Toliyat, Application of State Space Averaging Method to Sliding mode control of PWM DC/DC Converters, IEEE Industry Application Society Annual Meeting, New Orleans, Louisiana, Oct. 5-9, 1997.
- [6] Siew-Chong Tan, Y. M. Lai, Chi K. Tse, and Martin K. H. Cheung, "An adaptive sliding mode controller for buck converter in continuous conduction mode", Proceedings, Applied Power Electronics Conference and Exposition (APEC 2004), February 2004, California, U.S.A.

СИНТЕЗ И АНАЛИЗ НА НИСКОЧЕСТОТНИ И ВИСОКОЧЕСТОТНИ АКТИВНИ БИКВАДРАТНИ ФИЛТРОВИ ЗВЕНА С ИЗПОЛЗВАНЕТО НА MATLAB И MICROCAP

Таня Методиева Стоянова¹, Адриана Найденова Бороджиева²

¹Катедра „Теоретична и измервателна електротехника”, ²Катедра „Телекомуникации”, Русенски университет „Ангел Кънчев”, България, 7017 Русе, ул. „Студентска” № 8, тел.: ¹(00359 82) 888 502, ²(00359 82) 888 734, e-mail: ¹tstoyanova@uni-ruse.bg, ²aborodjieva@ecs.uni-ruse.bg

Резюме: В тази публикация се синтезират и анализират нискочестотни и високочестотни активни биквадратни филтрови звена. Това се извършва по зададена нормализирана предавателна функция по напрежение и при известни нормиращо съпротивление и гранична честота. Синтезът се реализира чрез програмата MATLAB, а анализът на проектираните филтри след избора на стандартни стойности на съпротивленията на резисторите и на капацитетите на кондензаторите в синтезираните вериги се извършва чрез програмата MicroCAP, използвана за симулация на аналогови и цифрови вериги. Резултатите ще бъдат използвани в процеса на обучение по дисциплината „Комуникационни вериги”, изучавана от студентите от специалност „Телекомуникационни системи” от образователно-квалификационната степен „Бакалавър”.

Ключови думи: Анализ, синтез, активни биквадратни филтрови звена.

1. ВЪВЕДЕНИЕ

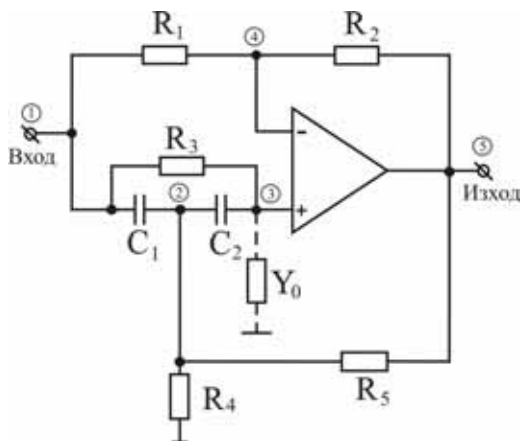
Разглежданите активни филтрови биквадратни звена [2, 3, 4] са изградени от един операционен усилвател, резистори и кондензатори.

В табл. 1 са дадени нормализираните предавателни функции по напрежение на активни нискочестотни и високочестотни филтри от втори ред, както и тяхната предавателна функция, записана чрез коефициента на усилване в лентата на пропускане k_0 , кръговата гранична честота ω_c и полюсния качествен фактор Q на тези филтри [2, 3, 4].

Табл. 1. Предавателни функции по напрежение на НЧФ и ВЧФ от втори ред

Активни филтри от втори ред		
Нискочестотен филтър (НЧФ)	$T(p) = \frac{H \cdot (p^2 + a)}{p^2 + b_1 p + b_0}$	$T(p) = \frac{k_0 (p^2 + \omega_\infty^2)}{p^2 + \frac{\omega_c}{Q} p + \omega_c^2}$
Високочестотен филтър (ВЧФ)	$T(p) = \frac{ap^2}{p^2 + b_1 p + b_0}$	$T(p) = \frac{k_0 p^2}{p^2 + \frac{\omega_c}{Q} p + \omega_c^2}$

2. СЪСТОЯНИЕ НА ПРОБЛЕМА – АНАЛИЗ И СИНТЕЗ НА НИСКОЧЕСТОТНИ И ВИСОКОЧЕСТОТНИ АКТИВНИ ФИЛТРОВИ БИКВАДРАТНИ ЗВЕНА



Фиг. 1. Схема на биквадратни активни филтрови звена с един операционен усилвател

На фиг. 1 е дадена схемата на активно биквадратно филтрово звено. В публикацията се предлагат методики за синтез на нискочестотни и високочестотни филтри, като са посочени и условията за проектирането им. В [5] чрез теорията на сигналните графи [1] е изведен аналитичният израз за предавателната функция на проектираните биквадратни филтрови звена (БФЗ).

След отчитане на условието за реализиране на предавателна функция на нискочестотен полиномен филтър, за който $Y_0 = pC_3$ и на високочестотен полиномен

филтър, за който $Y_0 = G_6$, и след няколко преобразувания [5], се получават изразите за тези функции, показани в табл. 2.

Табл. 2. Предавателни функции на нискочестотен и високочестотен полиномни филтри, синтезирани по схемата на БФЗ от фиг. 1

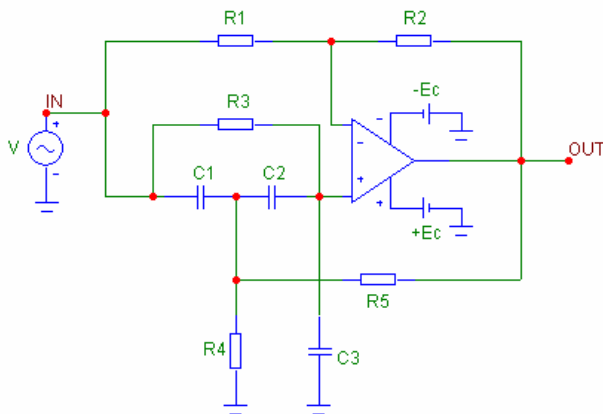
Предавателна функция на нискочестотен полиномен филтър
$T(p) = \frac{\frac{C_1 \cdot C_2 \cdot G_2 - G_1 \cdot C_3 \cdot (C_1 + C_2)}{G_2 \cdot (C_1 \cdot C_2 + C_1 \cdot C_3 + C_2 \cdot C_3)} \left[p^2 + \frac{G_2 \cdot G_3 \cdot (G_4 + G_5)}{C_1 \cdot C_2 \cdot G_2 - G_1 \cdot C_3 \cdot (C_1 + C_2)} \right]}{p^2 + p \cdot \left[\frac{G_3 \cdot (C_1 + C_2) + G_4 \cdot (C_2 + C_3) + C_3 \cdot G_5 - \frac{C_2 \cdot G_1 \cdot G_5}{G_2}}{C_1 \cdot C_2 + C_1 \cdot C_3 + C_2 \cdot C_3} \right] + \frac{G_3 \cdot (G_4 + G_5)}{C_1 \cdot C_2 + C_1 \cdot C_3 + C_2 \cdot C_3}}$
Предавателна функция на високочестотен полиномен филтър
$T(p) = \frac{p^2 + \frac{G_4 + G_5}{C_1 C_2} \left(G_3 - \frac{G_1 \cdot G_6}{G_2} \right)}{p^2 + p \cdot \left[\frac{G_4}{C_1} + (G_3 + G_6) \cdot \left(\frac{1}{C_1} + \frac{1}{C_2} \right) - \frac{G_1 \cdot G_5}{C_1 \cdot G_2} \right] + \frac{(G_4 + G_5) \cdot (G_3 + G_6)}{C_1 C_2}}$

3. РЕЗУЛТАТИ

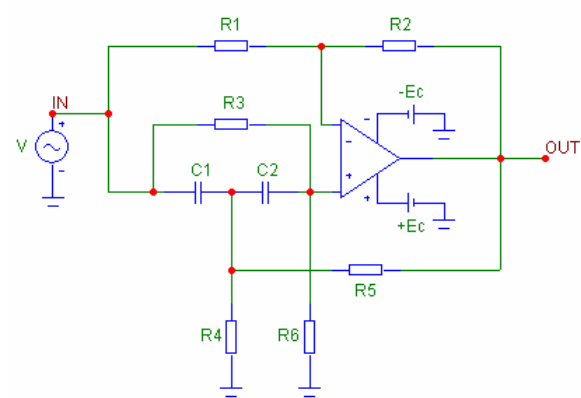
Алгоритъм за синтез и анализ на нискочестотните и високочестотните активни биквадратни филтрови звена

1. Въвеждане на коефициентите b_0 , a и b_1 в предавателната функция по напрежение $T(p)$ на синтезираните филтри (коефициентите трябва да са положителни числа, за да е изпълнено условието за устойчивост на системата). При предложените методики за синтез на НЧФ и ВЧФ по-долу (точка 2) са посочени по-конкретните условия, на които трябва да отговарят стойностите на коефициентите.

2. Изчисляване на нормираните стойности на елементите на синтезираните филтри. Схемите на синтезираните НЧФ и ВЧФ са показани на фиг. 2 и фиг. 3.



Фиг. 2. Нискочестотен полиномен филтър



Фиг. 3. Високочестотен полиномен филтър

Параметрите на елементите в схемата се получават от решението на системи уравнения (за НЧФ – система от 5 уравнения с 8 неизвестни, а за ВЧФ – система от 4 уравнения с 8 неизвестни).

При решаването на системите се приема следното условие за проектиране: еднакви капацитети в схемата (като нормирани стойности) и/или еднакви проводимости в схемата, а именно:

- за НЧФ – $C_1 = C_2 = C_3 = C$; избират се нормирани стойности за C и G_1 ;
- за ВЧФ – $C_1 = C_2 = C$ и $G_1 = G_2 = G$; избират се нормирани стойности за C и G .

При спазване на условията за коефициентите на нормализираните предавателни функции (табл. 1), дадени в табл. 3, от решенията на системите се получават изразите за параметрите на елементите в схемата (табл. 4).

1. Въвеждане на стойността на нормиращото съпротивление R_N .

2. Въвеждане на срязващата честота f_c за НЧФ или ВЧФ и изчисляване на нормиращата кръгова честота $\omega_N = 2\pi f_c$.

3. Изчисляване на денормираните стойности на елементите на двуполусниците:

- за резисторите – получените стойности за съпротивления $R_k = 1/G_k$ за $k = 1..6$ се умножават с нормиращото съпротивление R_N ;
- за кондензаторите – получените стойности за капацитети се разделят на произведението $\omega_N \cdot R_N$.

Табл. 3. Условия, на които трябва да отговарят коефициентите на нормализираните предавателни функции от табл. 1

За НЧФ	$a > 3b_0; \frac{a-b_0}{2a} \sqrt{\frac{6ab_0}{a-3b_0}} < b_1 < \frac{a-b_0}{a} \sqrt{\frac{6ab_0}{a-3b_0}}; H = \frac{b_0}{a} < \frac{1}{3}.$
За ВЧФ	$a < b_0; (b_0 - a) \sqrt{\frac{2}{a}} < b_1 < (a + b_0) \sqrt{\frac{2}{a}}; H = 1.$

Табл. 4. Изрази за параметрите на елементите на синтезираните биквадратни звена на НЧФ и ВЧФ

За НЧФ	$G_2 = \frac{2aG_1}{a-3b_0}, G_3 = C \sqrt{\frac{3b_0(a-3b_0)}{2a}},$ $G_4 = C \left(\frac{2ab_1}{a-b_0} - \sqrt{\frac{6ab_0}{a-3b_0}} \right), G_5 = C \left(2 \sqrt{\frac{6ab_0}{a-3b_0}} - \frac{2ab_1}{a-b_0} \right).$
За ВЧФ	$G_3 = C \sqrt{\frac{a}{2}} \cdot \frac{b_0+a}{2a}, G_4 = \frac{C}{2} \left(b_1 + 2 \sqrt{\frac{a}{2}} \cdot \frac{a-b_0}{a} \right),$ $G_5 = \frac{C}{2} \left(2 \sqrt{\frac{a}{2}} \cdot \frac{a+b_0}{a} - b_1 \right), G_6 = C \sqrt{\frac{a}{2}} \cdot \frac{b_0-a}{2a}.$

4. Избор на стандартни стойности на елементите на филтъра.

5. Извеждане на предавателните функции по напрежение $T(p)$ на НЧФ и ВЧФ съответно от фиг. 2 и фиг. 3 (ще се получат изразите, дадени в табл. 2).

6. Изчисляване на коефициента на усилване H в лентата на пропускане, на полюсния качествен фактор Q , на сръзващата честота f_c и на честотата с безкрайно голямо затихване f_∞ за НЧФ и ВЧФ, след избора на стандартни стойности на елементите (изразите са показани в табл. 5).

7. Симулационно изследване на синтезираните филтри с използване на програмния продукт MicroCAP – изчертаване на амплитудно-честотната характеристика, определяне на параметрите H, Q, f_c и f_∞ от снетата амплитудно-честотна характеристика и сравнение с получените от изчисляването в точка 8.

Разработени са скриптове на MATLAB [6] за изчисляване на нормализираните и денормализираните стойности на компонентите за НЧФ и ВЧФ при зададена нормирана предавателна функция по напрежение.

Пример: Проектиране на нискочестотни и високочестотни биквадратни активни филтрови звена от втори ред с гранична честота $f_c = 1 \text{ kHz}$ и нормирана

предавателна функция по напрежение $T(p)$. Денормализирането по честота и по съпротивление се извършва с нормиращо съпротивление $R_N = 10\text{ k}\Omega$. Резултатите са показани в табл. 6. След това е извършен избор на стандартни стойности по скалата E-24, които се използват при симулацията с MicroCAP [7] за изчертаване на амплитудно-честотните характеристики (в dB) на проектираните филтри (табл. 7).

Табл. 5. Изрази за параметрите H , Q , f_c и f_∞ на синтезираните биквадратни звена на НЧФ и ВЧФ

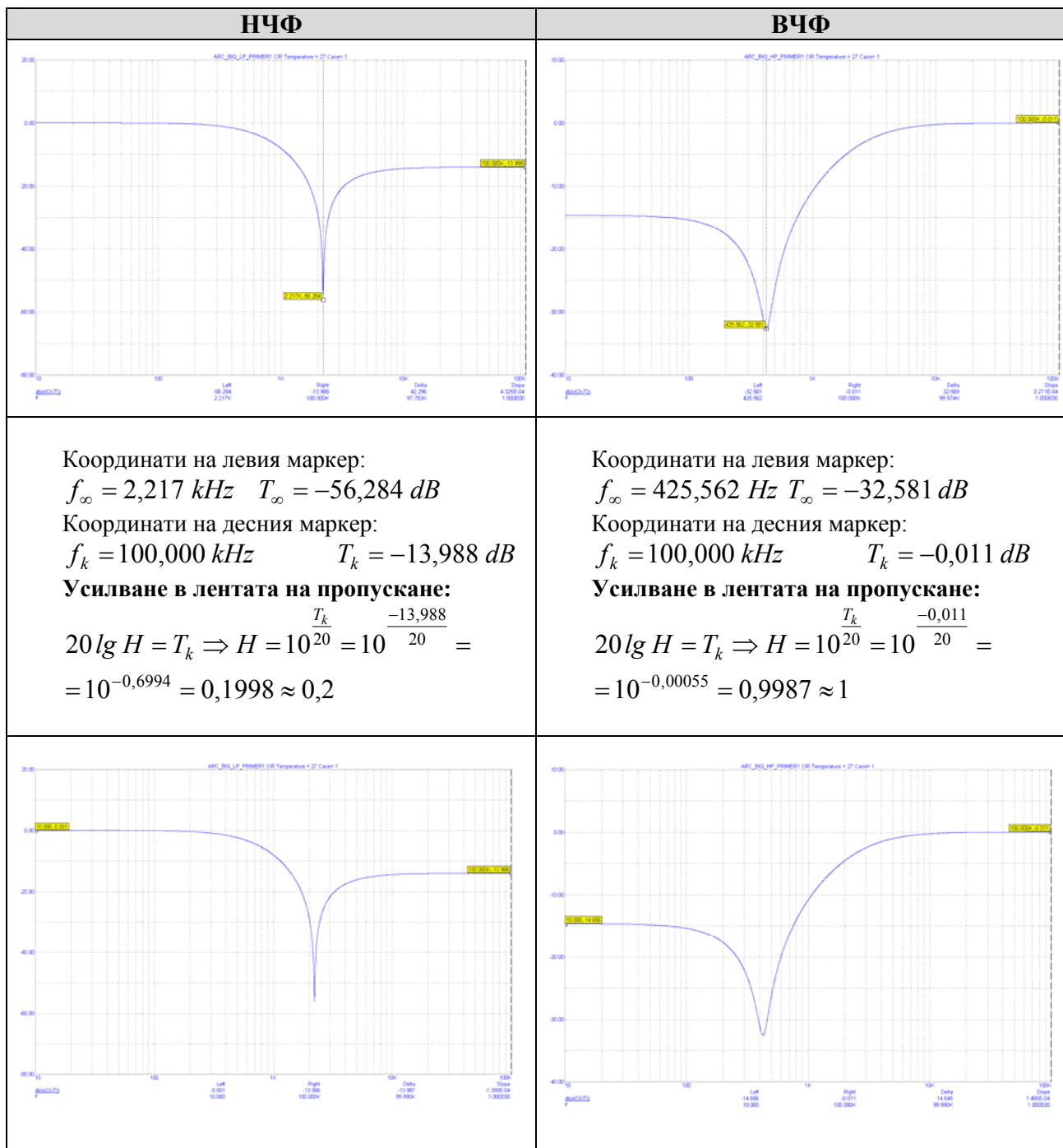
3а НЧФ	$\omega_c = \sqrt{\frac{G_3 \cdot (G_4 + G_5)}{C_1 \cdot C_2 + C_1 \cdot C_3 + C_2 \cdot C_3}}, \text{ rad/s},$ $\omega_\infty = \sqrt{\frac{G_2 \cdot G_3 \cdot (G_4 + G_5)}{C_1 \cdot C_2 \cdot G_2 - G_1 \cdot C_3 \cdot (C_1 + C_2)}}, \text{ rad/s},$ $Q = \frac{\omega_c (C_1 \cdot C_2 + C_1 \cdot C_3 + C_2 \cdot C_3)}{G_3 \cdot (C_1 + C_2) + G_4 \cdot (C_2 + C_3) + C_3 \cdot G_5 - \frac{C_2 \cdot G_1 \cdot G_5}{G_2}};$ $H = \frac{C_1 \cdot C_2 \cdot G_2 - G_1 \cdot C_3 \cdot (C_1 + C_2)}{G_2 \cdot (C_1 \cdot C_2 + C_1 \cdot C_3 + C_2 \cdot C_3)}.$	$f_c = \frac{\omega_c}{2\pi}, \text{ Hz};$ $f_\infty = \frac{\omega_\infty}{2\pi}, \text{ Hz};$
3а ВЧФ	$\omega_c = \sqrt{\frac{(G_4 + G_5) \cdot (G_3 + G_6)}{C_1 C_2}}, \text{ rad/s},$ $\omega_\infty = \sqrt{\frac{G_4 + G_5}{C_1 C_2} \left(G_3 - \frac{G_1 \cdot G_6}{G_2} \right)}, \text{ rad/s},$ $Q = \frac{\omega_c}{\frac{G_4}{C_1} + (G_3 + G_6) \left(\frac{1}{C_1} + \frac{1}{C_2} \right) - \frac{G_1 \cdot G_5}{C_1 \cdot G_2}};$	$f_c = \frac{\omega_c}{2\pi}, \text{ Hz};$ $f_\infty = \frac{\omega_\infty}{2\pi}, \text{ Hz};$ $H = 1.$

Табл. 6. Резултати от проектирането на НЧФ и ВЧФ с MATLAB

Тип на филтъра	Нормализирани стойности	Денормализирани стойности	Стандартни стойности (E-24)	Забележка
НЧФ	$R_1 = 1$	$R_1 = 10\text{ k}\Omega$	$R_1 = 10\text{ k}\Omega$	$T(p) = \frac{0,2 \cdot (p^2 + 5)}{p^2 + 2p + 1}$ $H = 0,2, Q = 0,5$
	$R_2 = 0,2000$	$R_2 = 2\text{ k}\Omega$	$R_2 = 2\text{ k}\Omega$	
	$R_3 = 1,2910$	$R_3 = 12,9099\text{ k}\Omega$	$R_3 = 13\text{ k}\Omega$	$H = 0,2$ $f_c = 991,7398\text{ Hz}$ $f_\infty = 2,2176\text{ kHz}$ $Q = 0,5020$
	$R_4 = 0,8873$	$R_4 = 8,8730\text{ k}\Omega$	$R_4 = 9,1\text{ k}\Omega$	
	$R_5 = 0,3642$	$R_5 = 3,6417\text{ k}\Omega$	$R_5 = 3,6\text{ k}\Omega$	
	$C_1 = 1$	$C_1 = 15,9155\text{ nF}$	$C_1 = 16\text{ nF}$	
	$C_2 = 1$	$C_2 = 15,9155\text{ nF}$	$C_2 = 16\text{ nF}$	
	$C_3 = 1$	$C_3 = 15,9155\text{ nF}$	$C_3 = 16\text{ nF}$	

ВЧФ	$R_1 = 1$ $R_2 = 1$ $R_3 = 1,0541$ $R_4 = 4,2537$ $R_5 = 2,5166$ $R_6 = 1,5811$ $C_1 = 1$ $C_2 = 1$	$R_1 = 10\text{ k}\Omega$ $R_2 = 10\text{ k}\Omega$ $R_3 = 10,5409\text{ k}\Omega$ $R_4 = 42,5371\text{ k}\Omega$ $R_5 = 25,1657\text{ k}\Omega$ $R_6 = 15,8114\text{ k}\Omega$ $C_1 = 15,9155\text{ nF}$ $C_2 = 15,9155\text{ nF}$	$R_1 = 10\text{ k}\Omega$ $R_2 = 10\text{ k}\Omega$ $R_3 = 11\text{ k}\Omega$ $R_4 = 43\text{ k}\Omega$ $R_5 = 24\text{ k}\Omega$ $R_6 = 16\text{ k}\Omega$ $C_1 = 16\text{ nF}$ $C_2 = 16\text{ nF}$	$T(p) = \frac{p^2 + 0,2}{p^2 + 3p + 1}$ $H = 1, Q = 0,3333$ <hr/> $H = 1$ $f_c = 992,7120\text{ Hz}$ $f_\infty = 427,1952\text{ Hz}$ $Q = 0,3460$
-----	--	--	--	--

Табл. 7. Резултати от изследването на НЧФ и ВЧФ с MicroCAP



<p>Координати на левия маркер: $f_s = 10,000 \text{ Hz}$ $T_s = -0,001 \text{ dB}$</p> <p>Гранична честота на филтъра:</p> $20 \lg H \frac{\omega_\infty^2}{\omega_c^2} = T_s \Rightarrow 20 \lg H \frac{f_\infty^2}{f_c^2} = T_s$ $H \frac{f_\infty^2}{f_c^2} = 10^{\frac{T_s}{20}} \Rightarrow f_c = f_\infty \sqrt{\frac{H}{10^{\frac{T_s}{20}}}}$ $= 2,217 \cdot 10^3 \cdot \sqrt{\frac{0,1998}{10^{\frac{-0,001}{20}}}} = 991,0337 \text{ Hz}$	<p>Координати на левия маркер: $f_s = 10,000 \text{ Hz}$ $T_s = -14,656 \text{ dB}$</p> <p>Гранична честота на филтъра:</p> $20 \lg H \frac{\omega_\infty^2}{\omega_c^2} = T_s \Rightarrow 20 \lg H \frac{f_\infty^2}{f_c^2} = T_s$ $H \frac{f_\infty^2}{f_c^2} = 10^{\frac{T_s}{20}} \Rightarrow f_c = f_\infty \sqrt{\frac{H}{10^{\frac{T_s}{20}}}}$ $= 425,562 \sqrt{\frac{0,9987}{10^{\frac{-14,656}{20}}}} = 988,7360 \text{ Hz}$
--	---

4. ИЗВОДИ

1. В публикацията е описан алгоритъм, заложен в програмен модул, с използване на MATLAB, създаден за синтез и анализ на нискочестотни и високочестотни активни биквадратни филтрови звена от втори ред с един операционен усилвател.

2. Изведени са изрази за предавателните функции по напрежение на синтезираните филтри. Представени са и получените изрази за срязващата честота и за честотата, при която затихването е безкрайно голямо, за коефициента на усилване в лентата на пропускане и за полюсния качествен фактор на синтезираните филтри.

3. Програмният модул е приложен за синтез на конкретни нискочестотно и високочестотно биквадратни звена. Те са симулирани на MicroCAP и техните характеристики и параметри са показани в публикацията.

4. Разработеният програмен модул може да послужи и за автоматизиране на процеса на генериране на варианти на задания за курсови задачи по дисциплината „3110 Комуникационни вериги”, включена като задължителна в учебния план на специалността „Телекомуникационни системи” за образователно-квалификационна степен „Бакалавър”.

Литература

- [1] Боянов, Й., Е. Шойкова. Теория на електронните схеми. София, Техника, 1995.
- [2] Манукова, А., А. Бороджиева. Комуникационни вериги – ръководство за упражнения. 104 стр., Русе, 2002.
- [3] Стоянов, Г. Теоретични основи на съобщителната техника. София, Техника, 1993.
- [4] Стоянова, Т., А. Бороджиева. Синтез и анализ на заграждащи активни биквадратни филтрови звена с използването на MATLAB и MicroCAP. 8th Summer School, Advanced Aspects of Theoretical Electrical Engineering, Sozopol '2010, 19.09. – 22.09.2010, Sozopol, Bulgaria, Regular papers, Part 2, pp. 53 – 62.
- [5] Стоянова, Т., А. Бороджиева. Приложение на теорията на сигналните графи при анализа на активни биквадратни филтрови звена. 8th Summer School, Advanced Aspects of Theoretical Electrical Engineering, Sozopol '2010, 19.09. – 22.09.2010, Sozopol, Bulgaria, Regular papers, Part 2, pp. 71 – 77.
- [6] <http://www.mathworks.com>.
- [7] <http://www.spectrum-soft.com/index.shtm>

СИНТЕЗ И АНАЛИЗ НА РЕАКТИВНИ (LC) ФИЛТРИ С ИЗПОЛЗВАНЕТО НА МАТЛАВ И MICROCAP

Таня Методиева Стоянова¹, Адриана Найденова Бороджиева²

¹Катедра „Теоретична и измервателна електротехника”,

²Катедра „Телекомуникации”, Русенски университет „Ангел Кънчев”,

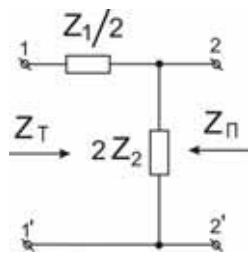
България, 7017 Русе, ул. „Студентска” № 8, тел.: ¹(00359 82) 888 502, ²(00359 82) 888 734,

e-mail: ¹tstoyanova@uni-ruse.bg, ²aborodjieva@ecs.uni-ruse.bg

Резюме: В тази публикация се синтезират и анализират нискочестотни, високочестотни, лентови и заграждащи филтри – тип „К” (прототипи) и тип “m” (последователно-производни и паралелно-производни). Това се извършва при известни номинално характеристично съпротивление, гранична (средна) честота и коефициент m (само за производните филтри). Синтезът се реализира чрез програмата MATLAB, а анализът на проектираните филтри след избора на стандартни стойности на капацитетите на кондензаторите в синтезираните вериги се извършва чрез програмата MicroCAP, използвана за симулация на аналогови и цифрови вериги. Резултатите ще бъдат използвани в процеса на обучение по дисциплината „Комуникационни вериги”, изучавана от студентите от специалност „Телекомуникационни системи” от образователно-квалификационната степен „Бакалавър”.

Ключови думи: Синтез, анализ, реактивни (LC) филтри.

1. ВЪВЕДЕНИЕ



Фиг. 1. Схема на Г-образно полузвено на реактивен LC-филтър

Обект на публикацията са реактивните (LC) филтри – тип „К” и тип „m” (последователно-производни и паралелно-производни). Прилага се класическата теория на LC-филтрите, изградена на базата на основното филтрово полузвено – Г-образен четириполусник (Г-образно полузвено) с Т-вход с импеданс Z_T и П-вход с импеданс Z_{II} (фиг. 1) и образуваните с него сложни верижни съединения, които се съгласуват характеристично [1, 2].

2. СЪСТОЯНИЕ НА ПРОБЛЕМА

Реактивните филтри тип „К”, наречени „прототипи”, и производните филтри тип „m” имат:

- еднакви номинални характеристични съпротивления R ;
- еднаква гранична честота ω_c (за нискочестотния и високочестотния филтри) и една и съща средна честота ω_0 (за лентовия и заграждащия филтри);

– еднакви входни съпротивления откъм T -вход за последователно-производните филтри тип „ m ” $Z_T^m = Z_T^K$, както и изпълнението на условията:

$$Z_1^m = mZ_1; \quad Z_2^m = \frac{1}{m} \cdot Z_2 + \frac{1-m^2}{4m} \cdot Z_1; \tag{1}$$

– еднакви входни съпротивления $Z_{II}^m = Z_{II}^K$ откъм II -вход за паралелно-производните филтри тип „ m ”, както и условията:

$$Z_2^m = \frac{1}{m} Z_2; \quad \frac{1}{Z_1^m} = \frac{1}{m \cdot Z_1} + \frac{1-m^2}{4m} \cdot \frac{1}{Z_2}. \tag{2}$$

Въз основа на тези характеристики на прототипа и производните филтри, както и на зависимостите (1) и (2), се получават схемите и параметрите на елементите на съответните „ m ” производни нискочестотни и високочестотни филтри, показани в табл. 1 [1, 2].

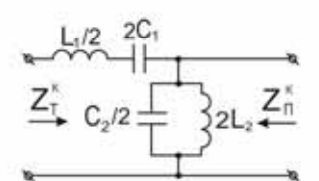
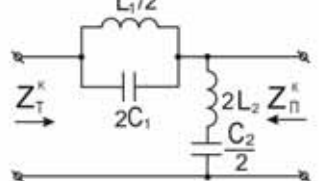
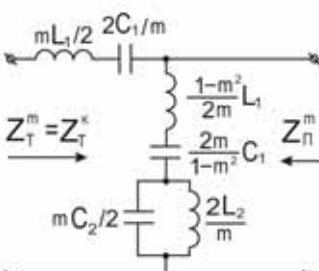
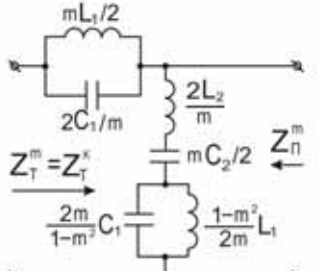
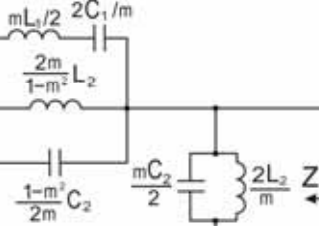
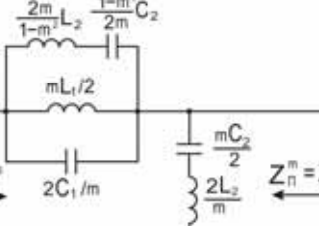
Табл. 1. Нискочестотни и високочестотни LC -филтри тип „ K ” и тип „ m ”

Нискочестотни реактивни филтри	Високочестотни реактивни филтри
Тип „ K ”	Тип „ K ”
Последователно производни тип „ m ”	Последователно производни тип „ m ”
Паралелно производни тип „ m ”	Паралелно производни тип „ m ”

3. РЕЗУЛТАТИ

По аналогия на проектирането на „m” производни нискочестотни и високочестотни филтри, са проектирани схемите [1, 2] и получени параметрите на елементите за лентовите и режекторните (заграждащи) „m” производни филтри. Те са показани в табл. 2.

Табл. 2. Лентови и режекторни реактивни филтри тип „К” и тип „m”

Лентови реактивни филтри	Режекторни реактивни филтри
Тип "к"	Тип "к"
	
Последователно производни тип "m"	Последователно производни тип "m"
	
Паралелно производни тип "m"	Паралелно производни тип "m"
	

Разработен е скрипт на MATLAB с название *LC_m.m*, който позволява проектирането на последователно-производни и паралелно-производни реактивни (*LC*) филтри: нискочестотни, високочестотни, лентови и заграждащи.

По-долу са показани снимки на екрана при изпълнение на разработения скрипт, след избора на проектиране на последователно-производен НЧФ.

Алгоритъм на скрипта

1. Извежда се меню за избор на решаваната задача, т.е. избор на филтъра, който ще се оразмерява (фиг. 2).

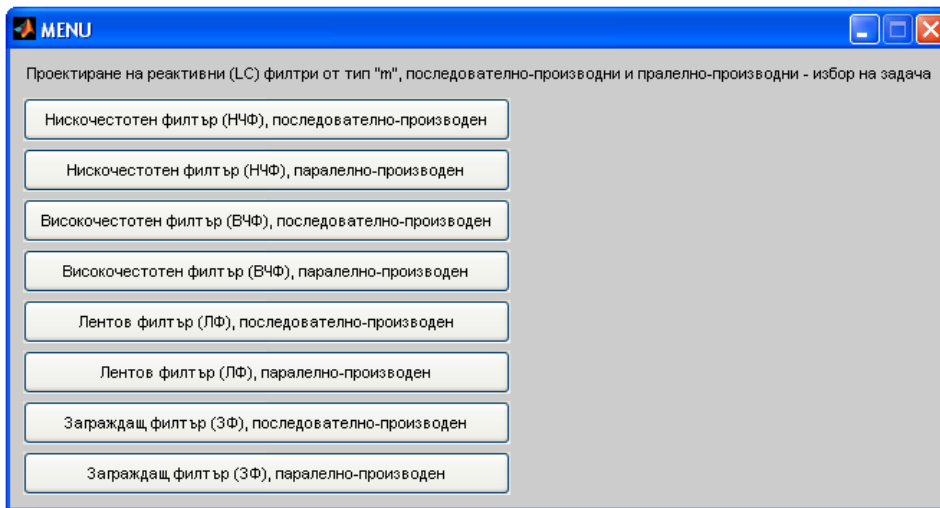
2. Въвеждат се стойностите за:

– номиналното характеристично съпротивление R ;

– граничната честота ω_c (за нискочестотния и високочестотния филтри) и

за средната честота ω_0 (за лентовия и заграждащия филтри);

– коефициента m за производните филтри (фиг. 3а, блок 1).



Фиг. 2. Меню за избор на филтъра, който ще се оразмерява

3. Проверка за коректността на въведените числени стойности на величините и при необходимост извеждане на съобщение за ново въвеждане на данни.

4. Оразмеряване на LC -филтър, тип „К”, като се определят параметрите на G -полузвено, без и с отчитане на коефициентите в схемата (фиг. 3а, блок 2).

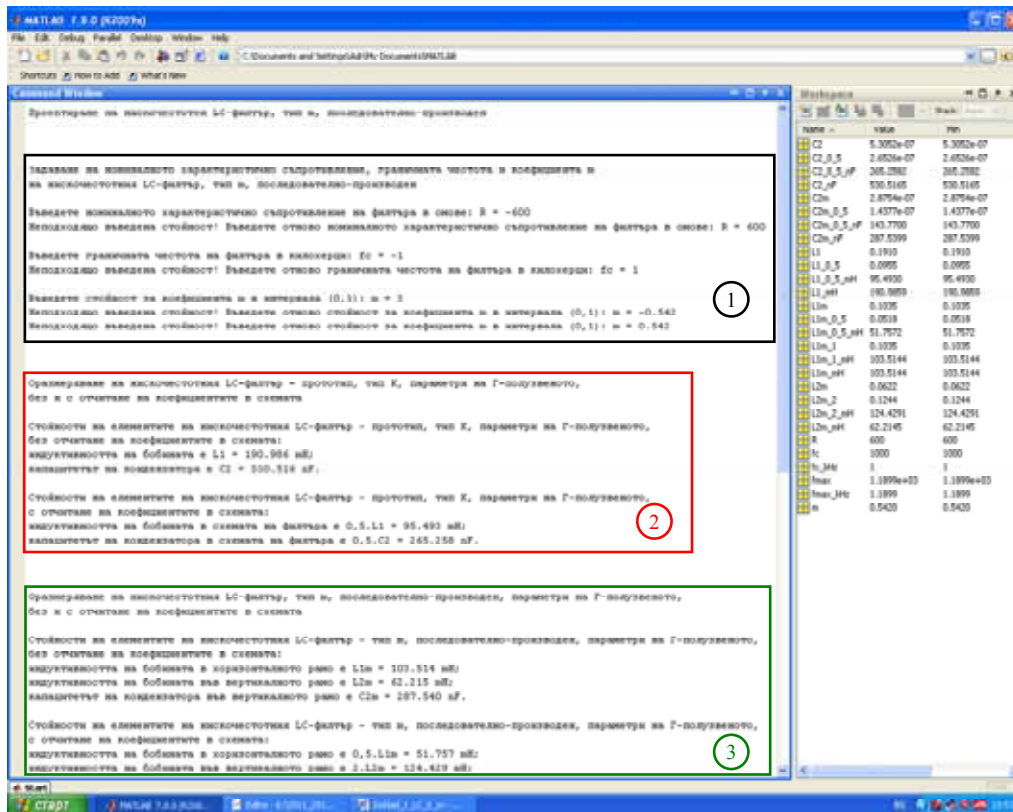
5. Оразмеряване на съответния избран LC -филтър, тип „m”, последователно-произведен или паралелно-произведен, като се определят параметрите на G -полузвено, без и с отчитане на коефициентите в схемата (фиг. 3а, блок 3).

6. Определяне на честотата ω_∞ , при която затихването става безкрайно голямо, за LC -филтъра, тип „m”, последователно- или паралелно-произведен (само за нискочестотни и високочестотни производни филтри) (фиг. 3б, блок 3).

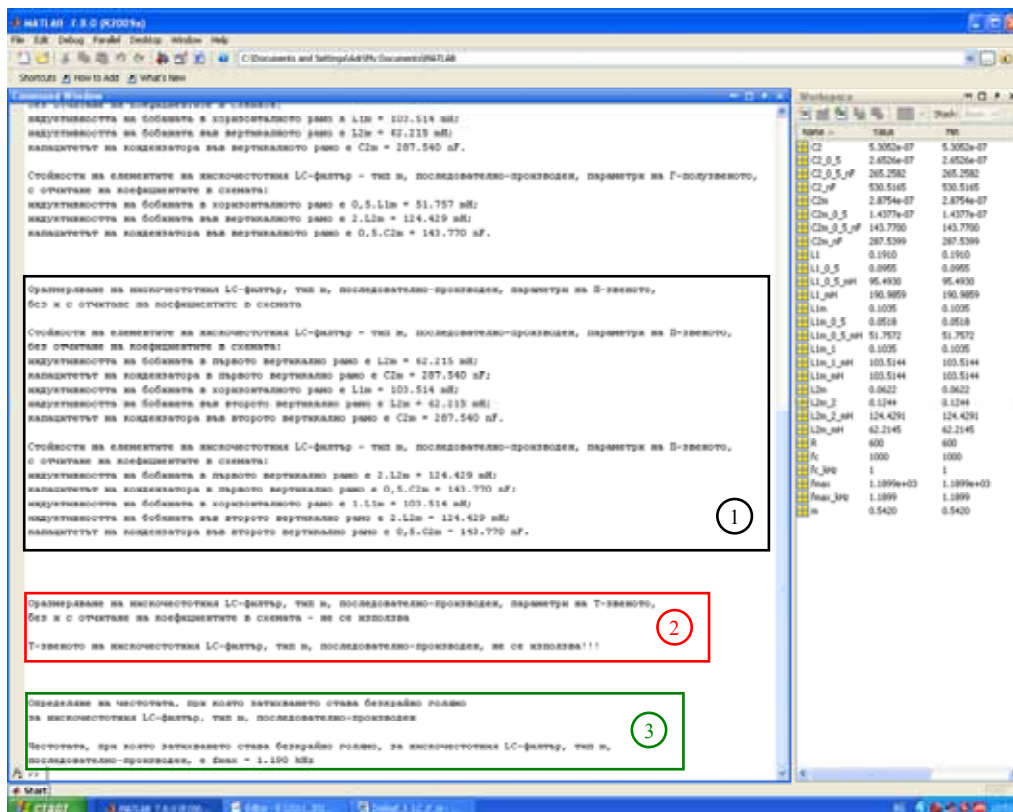
Програмата позволява оразмеряването на T -звено (паралелно-производно) и на L -звено (последователно-производно) (фиг. 3б, блок 1 и блок 2).

Всички изчислени стойности се извеждат с 3 знака след десетичната запетая. Стойностите на индуктивностите на бобините са в милихенри, а на капацитетите на кондензаторите са в нанофаради.

След избор на стандартни стойности на капацитетите на кондензаторите (в случая е използвана скалата E-96) се извършва симулационно изследване на оразмерения производен филтър чрез програмата MicroCAP, като по този начин се осъществява анализ на проектираната схема (фиг. 4). Графиката на фиг. 4 потвърждава получените стойности за честотите f_c и f_∞ .



a)



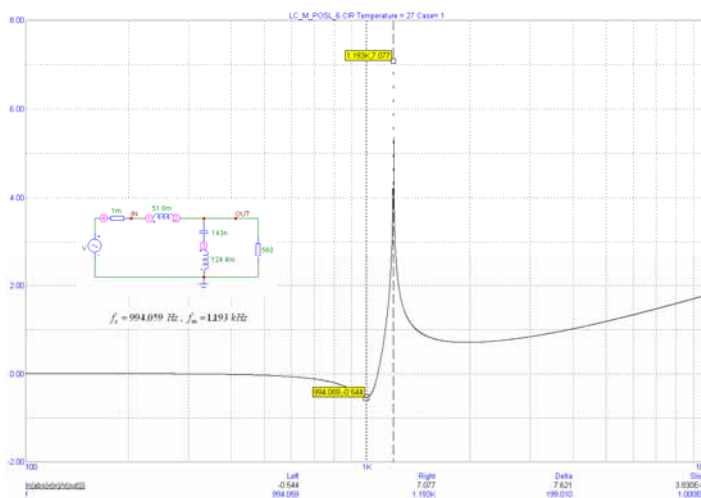
b)

Фиг. 3. Снимка от изпълнение на програмата, при избор на проектиране на НЧФ, последователно-производен, при следните входни данни:

$$R = 600 \Omega, f_c = 1 \text{ kHz} \text{ и } m = 0,542$$

Разработеният скрипт може да бъде разширен, с цел извеждане в графични прозорци предварително на: **1)** схемата на проектирания филтър (включително и на съответния прототип, на базата на който се извършва проектирането на производния филтър – на Γ -полузвеното, Π -звеното и T -звеното); **2)** формулите, по които се извършва оразмеряването на прототипа и на съответния производен филтър; **3)** формулата за изчисляване на честотата, при която затихването става безкрайно голямо (за нискочестотни и високочестотни филтри); **4)** честотната зависимост на затихването и на характеристичните импеданси за „m” филтрите, както и на прототипите (така ще се виждат предимствата на производните филтри спрямо прототипите).

Разработеното приложение може да се модифицира за обучението на студенти, като вместо да извежда изчислените стойности на пресмятаните параметри на елементите, студентите да въвеждат стойностите за съответния параметър от клавиатурата (след като са изчислили такива, знаейки формулите за пресмятане), до въвеждане на подходящи стойности, най-близки до изчислените от програмата (при допустимо отклонение).



Фиг. 4. Симуляционно изследване на проектирания последователно-производен НЧФ, след избор на стандартна стойност на кондензатора (чрез MicroCAP)
 $f_c = 994,059 \text{ Hz}$; $f_\infty = 1,193 \text{ kHz}$

4. ИЗВОДИ

1. Синтезират се и се анализират чрез MATLAB нискочестотни, високочестотни, лентови и заграждащи (режекторни) филтри – тип „K” (прототипи) и тип „m” (последователно-производни и паралелно-производни) при известни номинално характеристично съпротивление, гранична (средна) честота и коефициент m (само за производните филтри).

2. Анализират се чрез програмата MicroCAP проектираните филтри след избора на стандартни стойности на капацитетите на кондензаторите.

3. Резултатите ще бъдат използвани в процеса на обучение по дисциплината „Комуникационни вериги”, изучавана от студентите от специалност „Телекомуникационни системи” от образователно-квалификационната степен „Бакалавър”.

Литература

- [1] Манукова, А., А. Бороджиева. Комуникационни вериги – ръководство за упражнения. 104 стр., Русе, 2002.
- [2] <http://ecet.ecs.uni-ruse.bg/else/>

СИНТЕЗ И АНАЛИЗ НА ТРЕПТЯЩИ КРЪГОВЕ С ИЗПОЛЗВАНЕТО НА МАТЛАВ И MICROCAP

Таня Методиева Стоянова¹, Адриана Найденова Бороджиева²

¹Катедра „Теоретична и измервателна електротехника”, ²Катедра „Телекомуникации”, Русенски университет „Ангел Кънчев”, България, 7017 Русе, ул. „Студентска” № 8, тел.: ¹(00359 82) 888 502, ²(00359 82) 888 734, e-mail: ¹tstoyanova@uni-ruse.bg, ²aborodjieva@ecs.uni-ruse.bg

Резюме: В тази публикация се синтезират и анализират секционирани трептящи кръгове с капацитивен и с индуктивен делител, както и трансформатори с настроен трептящ кръг. Синтезът се реализира чрез програмата MATLAB, а анализът на проектираните трептящи кръгове, след избора на стандартни стойности на капацитетите на кондензаторите в синтезираните вериги, се извършва чрез програмата MicroCAP, използвана за симулация на аналогови и цифрови вериги. Резултатите ще бъдат използвани в процеса на обучение по дисциплината „Комуникационни вериги”, изучавана от студентите от специалност „Телекомуникационни системи” от образователно-квалификационната степен „Бакалавър”.

Ключови думи: Синтез, анализ, секционирани трептящи кръгове с капацитивен и с индуктивен делител, трансформатори с настроен трептящ кръг.

1. ВЪВЕДЕНИЕ

Обект на изследване в тази публикация са секционирани трептящи кръгове с капацитивен и/или с индуктивен делител, както и трансформаторите с един настроен трептящ кръг. При тези вериги могат да се променят техните параметри – ширина на честотната лента B и качествен фактор Q , при определени стойности на съпротивлението на товара R и на входното им съпротивление R_i при резонанс. Това дава допълнителна степен на свобода за независимо избиране на честотната лента и коефициента на трансформация на импеданси. Секционирани трептящи кръгове се използват широко при генераторите и теснолентовите високочестотни усилватели, генератори на Колпитц [1, 3].

2. СЪСТОЯНИЕ НА ПРОБЛЕМА

Проектирането на секционирани трептящи кръгове е извършено за случая, когато общият качествен фактор Q на кръга, измерен на изводите на R_i (схемите са дадени в табл. 1), е по-голям от десет – $Q \approx f_0/B \geq 10$, при предварително зададени стойности на R_2 , R_i , на резонансната честота f_0 и на пропускателната честотна лента B , като се определят стойностите на:

- L , C_1 и C_2 – на трептящ кръг с капацитивен делител;
- C , L_1 и L_2 – на трептящ кръг с индуктивен делител;

– L_1 и L_2 , взаимната индуктивност M , коефициента на връзката k и капацитета на кондензатора C – на трансформатор с един настроен трептящ кръг. При проектиране на трептящите кръгове може да се направи произволен избор на Q_p , но тогава е задължително да се изчисли k [1, 3].

Табл. 1. Схеми на секционирани трептящи кръгове с капацитивен и с индуктивен делител и на трансформатор с един настроен трептящ кръг

Секционирани трептящи кръгове	
Схеми	Заместващи схеми
С капацитивен делител	
С индуктивен делител	
Трансформатор с един настроен трептящ кръг	

При проектирането се пренебрегват активните загуби в бобината. В този случай могат да се използват точните или приблизителните формули, поместени в табл. 2. При проектирането им се използват и формулите за преобразуване на паралелно в последователно свързване на два двуполюсника [1, 3].

3. РЕЗУЛТАТИ

Разработена е софтуерна система, базирана на MATLAB, предназначена за синтез (оразмеряване) на секционирани трептящи кръгове с капацитивен и/или индуктивен делител, както и на трансформатори с настроен трептящ кръг. В

публикацията са приложени снимки от екраните при изпълнение на разработеното приложение. Алгоритмите за синтез на разглежданите комуникационни вериги са дадени в [1, 2, 3].

Табл. 2. Проектиране на трептящ кръг с капацитивен делител, с индуктивен делител и трансформатор с един настроен трептящ кръг за $Q \approx f_0/B \geq 10$

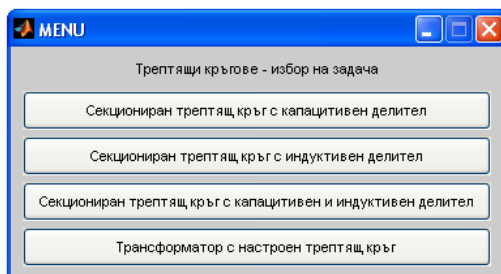
$Q \approx \frac{f_0}{B}; \rho = \frac{R_t}{Q}; L = \frac{\rho}{2\pi f_0}; C = \frac{1}{2\pi f_0 \rho}; N = \sqrt{\frac{R_t}{R_2}}; Q_p \approx \frac{Q}{N};$	
Точни формули при $Q_p < 10$	Приблизителни формули при $Q_p \geq 10$
Формули за изчисление на трептящ кръг с капацитивен делител	
$Q_p = \sqrt{\frac{Q^2 + 1}{N^2} - 1}; C_2 = \frac{Q_p}{\omega_0 R_2}; C_{se} = \frac{C_2(Q_p^2 + 1)}{Q_p^2};$ $C_1 = \frac{C_{se} \cdot C}{C_{se} - C}.$	$Q_p \approx \frac{Q}{N}; C_2 \approx NC;$ $C_1 \approx \frac{C_2}{N-1}.$
Формули за изчисление на трептящ кръг с индуктивен делител	
$Q_p = \sqrt{\frac{Q^2 + 1}{N^2} - 1}; L_2 = \frac{R_2}{\omega_0 Q_p}; L_{se} = \frac{L_2 Q_p^2}{Q_p^2 + 1}; L_1 = L - L_{se}.$	$Q_p \approx \frac{Q}{N}; L_2 \approx \frac{L}{N};$ $L_1 \approx (N-1)L_2 = L - L_2$
Трансформатор с един настроен трептящ кръг	
$R_{se} = \frac{\left(\frac{M}{L_2}\right)^2 R_2}{Q_p^2 + 1}; L_0 = L_1 \left(\frac{Q_p^2 + 1 - k^2}{Q_p^2 + 1}\right); M = k\sqrt{L_1 L_2}; L_2 = \frac{R_2}{\omega_0 Q_p};$ $L_1 = L_0 \left(\frac{Q_p^2 + 1}{Q_p^2 + 1 - k^2}\right); Q = \frac{Q_p^2 + 1 - k^2}{Q_p \cdot k^2}; k^2 = \frac{Q_p^2 + 1^2}{Q_p \cdot Q + 1};$ $Q_p = Q \left[\frac{k^2}{2} + \sqrt{\frac{k^4}{4} + \frac{k^2 - 1}{Q^2}} \right]; Q_{p \min} = \frac{1}{Q} [\sqrt{Q^2 + 1} - 1]; k_{\min} = \frac{\sqrt{2}}{Q} \sqrt{\sqrt{Q^2 + 1} - 1}$	

Алгоритъм на програмата за синтезиране на секционирани трептящи кръгове с капацитивен и/или с индуктивен делител и на трансформатор с един настроен трептящ кръг – скрипт с название *menu_STK_TNTK.m*

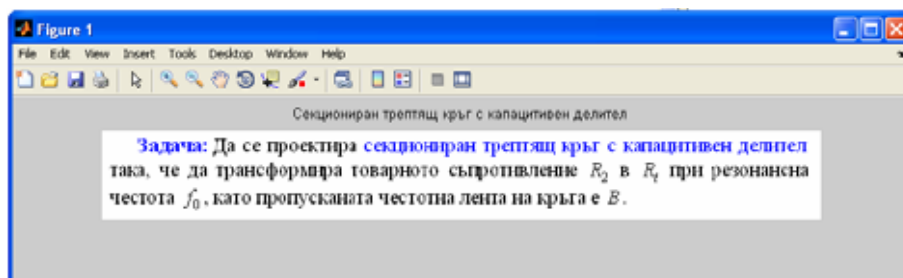
1. Извеждане на меню за избор на решаваната задача (фиг. 1).
2. Извеждане в отделни графични прозорци на етапите на решаване на задачата: 1) условието на задачата, която ще се решава (фиг. 2 а); 2) схемата на разглеждания трептящ кръг, който ще се оразмерява (фиг. 2 б);

3) формулите за изчисляване на търсените величини (фиг. 2 в).

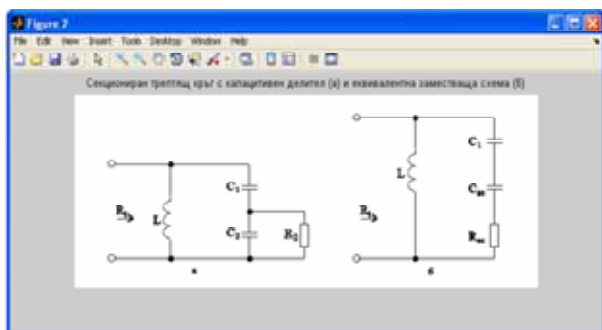
На фиг. 3 е показана снимка на екрана при изпълнение на разработения скрипт при проектирането на секционирания трептящ кръг с капацитивен делител.



Фиг. 1. Меню за избор на решаваната задача



а)



б)

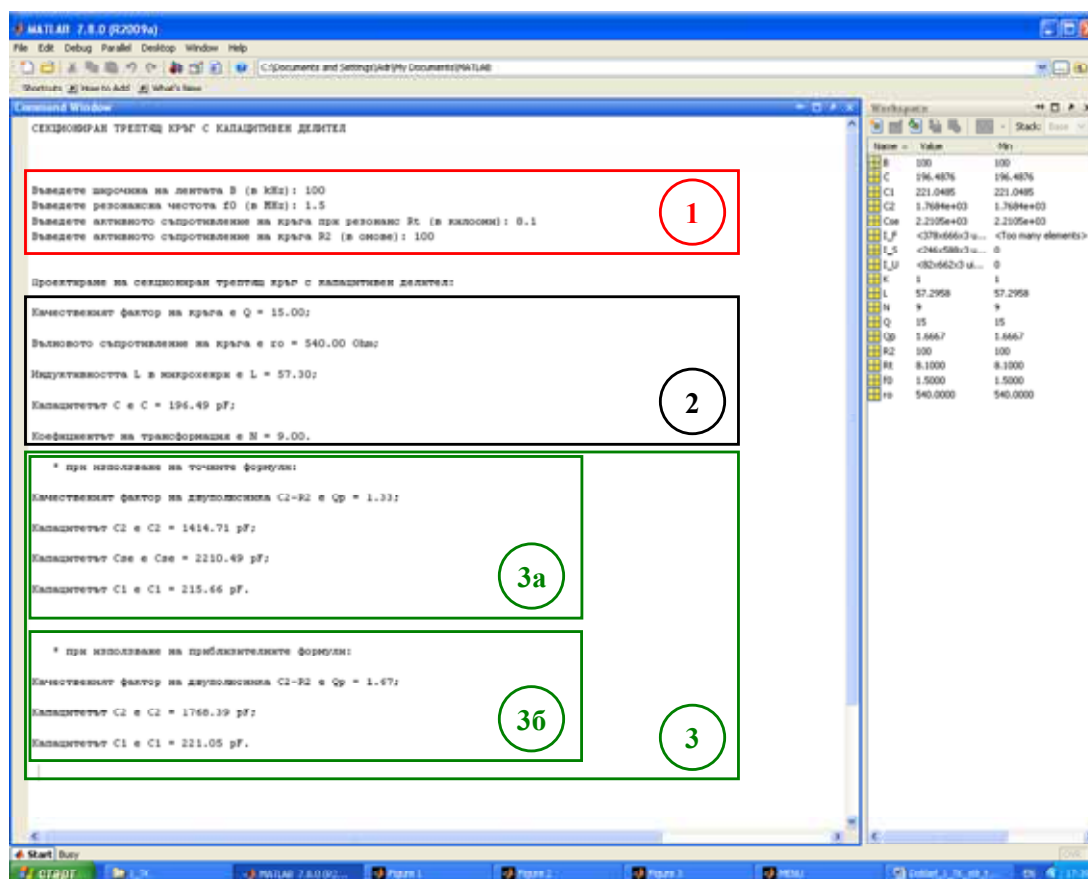
Формули за изчисляване на трептящ кръг с капацитивен делител	
За $Q = f_0/B \geq 10$	
$Q = \frac{f_0}{B}, \rho = \frac{R_1}{\omega L}, L = \frac{\rho}{2\pi f_0}, C = \frac{1}{2\pi f_0 \rho}, N = \sqrt{\frac{R_1}{R_2}}, Q_0 = \frac{Q}{N}$	
Точни формули при $Q_0 \geq 10$	Приблизителни формули при $Q_0 \geq 10$
$Q_0 = \sqrt{\frac{Q^2 + 1}{N^2 - 1}}$	$Q_0 = \frac{Q}{N}$
$C_2 = \frac{C_0}{\omega_0 R_2}$	$C_2 = NC$
$C_n = \frac{C_2(Q_0^2 + 1)}{Q_0^2}$	$C_1 = \frac{C_2}{N - 1}$
$C_1 = \frac{C_2 C_n}{C_n - C}$	

в)

Фиг. 2. Графични прозорци при решаването на задачата за проектиране на секционирания трептящ кръг с капацитивен делител: а) условие на поставената задача; б) схема и еквивалентна заместваща схема на секционирания трептящ кръг с капацитивен делител; в) формули за оразмеряване на секционирания трептящ кръг с капацитивен делител

- Въвеждане на входните данни: широчината на пропусканата лента B (в kHz); резонансната честота f_0 (в MHz); активното съпротивление на кръга при резонанс R_1 (в килооми) и активното съпротивление на кръга R_2 (в оме) (фиг. 3, блок 1). Програмата проверява коректността на въведените данни. Ако въведените стойности не са положителни числа, тогава на екрана се извежда съобщение „Неподходящо въведена стойност!“ и потребителят се подканва за повторното въвеждане на исканата величина.

- Определяне на търсените в задачата величини – качественият фактор на кръга Q ; вълновото съпротивление на кръга ρ в омове; индуктивността L в микрохенри; капацитетът C в пикофаради и коефициентът на трансформация N (фиг. 3, блок 2). Следва изчисление на параметрите на елементите на избраната синтезирана верига по точните (фиг. 3, блок 3а) и по приблизителните формули (фиг. 3, блок 3б), които за съответните вериги са дадени в табл. 2. За конкретния случай са показани и на фиг. 2 в.



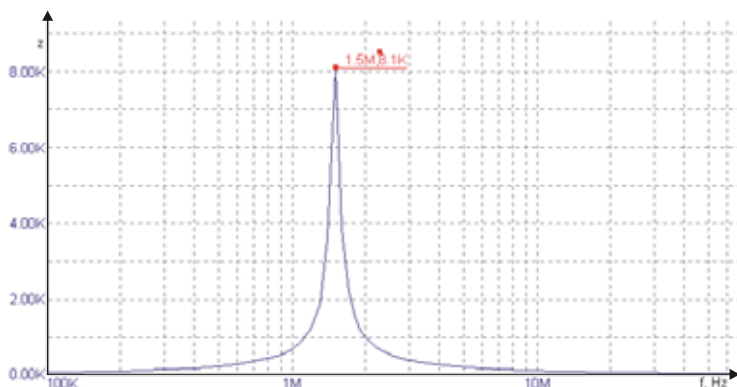
Фиг. 3. Снимка на екрана при изпълнение на разработения скрипт при проектирането на секциониран трептящ кръг с капацитивен делител

3. Оразмеряване на трептящия кръг и извеждане на резултатите за числените стойности на параметрите на елементите (фиг. 3, блок 3, за конкретния случай).

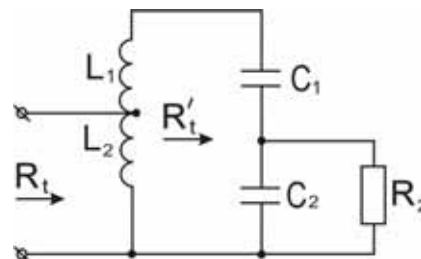
Анализът на синтезираните вериги се осъществява с програмата MicroCAP, използвана за симулация на аналогови и цифрови вериги. При симулационното изследване на проектирания секциониран трептящ кръг с капацитивен делител се получава показаната на фиг. 4 характеристика за $z(f)$. След подбор на стандартни по стойност елементи (капацитети на кондензатори) се донастройва кръга, за да изпълнява поставеното условие за трансформация на импеданси.

Интерес представлява третият тип трептящ кръг за оразмеряване: секциониран трептящ кръг с капацитивен и с индуктивен делител, при който товарното

съпротивление R_2 се трансформира чрез капацитивен делител до по-голяма стойност R'_t , която впоследствие се трансформира чрез индуктивен делител до по-малка стойност R_t (двойно трансформиране) (фиг. 5).



Фиг. 4. Характеристика $z(f)$ на проектирания и симулиран секционирания трептящ кръг с капацитивен делител: $f_0 = 1,5 \text{ MHz}$, $R_t = 8,1 \text{ k}\Omega$



Фиг. 5. Секционирания трептящ кръг с капацитивен и с индуктивен делител

4. ИЗВОДИ

1. Разработено е приложение, базирано на MATLAB, което дава възможност за синтез/оразмеряване на секционирани трептящи кръгове с капацитивен и/или индуктивен делител, както и на трансформатори с настроен трептящ кръг.

2. Чрез анализа на синтезираните вериги, който се осъществява с програмата MicroCAP, се потвърждават желаните качества на тези вериги.

3. Резултатите могат да се използват в процеса на обучение по дисциплината „Комуникационни вериги”, изучавана от студентите от специалност „Телекомуникационни системи” от образователно-квалификационната степен „Бакалавър”.

Литература

- [1] Краус, Х., Ч. Бостиян, Ф. Рааб. Полупроводникова радиотехника. София, Техника, 1985.
- [2] Стоянов, Г. Теоретични основи на съобщителната техника. София, Техника, 1993.
- [3] Манукова, А., А. Бороджиева. Комуникационни вериги – ръководство за упражнения. 104 стр., Русе, 2002.

ОЦЕНЯВАНЕ НА РОЛЯТА НА МЯСТОТО И ГОЛЕМИНАТА НА КАПАЦИТЕТА НА КОНДЕНЗАТОРА В ПАРАМЕТРИЧНИТЕ ИНДУКТИВНО-КАПАЦИТИВНИ СТАБИЛИЗАТОРИ НА ТОК И НАПРЕЖЕНИЕ

*Георги Рашков Георгиев¹, Таня Методиева Стоянова²,
Надежда Лиозовна Евстатиева³, Димчо Василев Киряков⁴*

Катедра “Теоретична и измервателна електротехника”,
Русенски университет “Ангел Кънчев”,
ул. „Студентска” № 8 , 7017 гр. Русе, България,
тел.: 035982 888 412¹, 035982 888 502², 035982 888 638³, 035982 888 371⁴
e-mail: grashkov@uni-ruse.bg¹, tstoyanova@uni-ruse.bg²,
nevstatieva@uni-ruse.bg³, kiriakov@uni-ruse.bg⁴

Резюме. В тази публикация е направена съпоставка и сравнителна оценка на качествата на работа на трите възможни вида на индуктивно-капацитивните стабилизатори на ток (в някои случаи и на напрежение), с различни качества на стабилизацията. Те са представители на така наречените параметрични източници на ток. При изследваните видове, техният основен елемент кондензаторът, е свързан към първичната, към вторичната или към шунтовата намотки на съгласуващия трансформатор.

Ключови думи: Кондензатор, намотки (вторична, първична, шунтова), стабилизация на ток и напрежение, условия за резонанс, индуктивно-капацитивни стабилизатори, параметрични източници на ток (ПИТ)

1. ВЪВЕДЕНИЕ

Параметричните източници на ток (ПИТ) са разновидност на голямата група на индуктивно-капацитивните стабилизатори на ток (ИКСТ). Характерните им особености са свързани с ферорезонансните явления (наред с резонанса между дросел и кондензатор, на който се основават ИКСТ), както и наличието на съгласуващ трансформатор. Последният при това е обединен с дросела и така се постига сериозно подобряване на масогабаритните показатели на системата. Освен това този трансформатор позволява използването на ПИТ за хранване на по-мощни консуматори (например, заваръчни токоизточници, лазерни установки и пр.), в сравнение с електронните стабилизиращи схеми.

2. СЪСТОЯНИЕ НА ПРОБЛЕМА

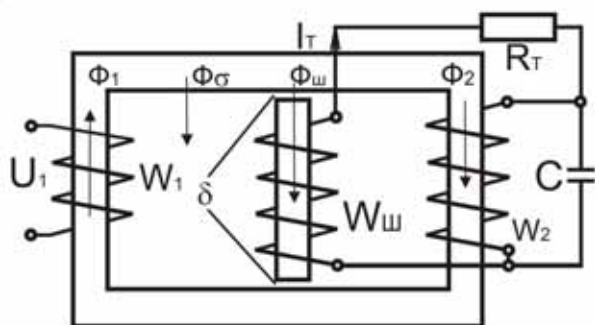
А. Основните изследвания и анализи на параметричните източници на ток са проведени при кондензатор, свързан към вторичната намотка (директно, или през добавъчни навивки) [2] и в резултат на тях са установени най-пълно техните качества. На фиг. 1 е показано едно такова схемно решение.

3. РЕЗУЛТАТИ

Макар и не така задълбочено, са проведени и изследвания за схеми, при които кондензаторът е включен към някоя от другите намотки на системата.

Поставя се цел да се анализират сравнително всички възможни позиции на кондензатора и се определят техните качества.

Ролята на капацитета на кондензатора, в основния схемен вариант (нека тук го наречем условно 1А) от фиг. 1, е да осъществява резонанс с индуктивностите, внасяни във веригата, основно от въздушната междина δ и донякъде от разсеяния магнитен поток Φ_δ .



Фиг. 1

След комплексно решаване на електромагнитната верига, при приемане на почти задължителните при анализ на такива вериги опростяващи допускания, с цел получаване удобни за ползване (но и с достатъчна точност)

резултати, условието за този резонанс се определя от [2]:

$$X_C = X_\delta + X_\sigma . \quad (1)$$

Това условие осигурява стабилизацията на тока на изхода на системата. Големината му се определя [2] :

$$I_T = \frac{U_1 \cdot W_2}{W_1} \cdot \frac{1}{(m+1) \cdot X_\delta + X_\sigma} \neq f(R_T) , \quad (2)$$

където

$$m = \frac{W_2}{W_{ш}} .$$

Вижда се независимостта на тока от големината на товарното съпротивление, без значение на големината му. Тук трябва да се отбележи (това се отнася и за всички следващи по-надолу случаи и изследвания), че в някои режими, е възможно да се появят наситени участъци в магнитопровода на системата. Тогава техните съпротивления вече стават осезаеми, не могат да се пренебрегнат, което води до известни отклонения от стабилизиращите свойства на системата. Практиката показва, че те не са големи.

Установена е възможност кондензаторът да се включва не директно към вторичната намотка, а през добавъчни навивки към нея. Това само намалява големината на необходимия капацитет, без да променя нищо в работата на системата. Основното качество на решението кондензатор към вторичната намотка, е

осигуряване на много добра стабилизация на тока. Видно е, че (макар и след допустима идеализация на електромагнитната верига) той не зависи от товара - $I_T \neq f(R_T)$. При това (за разлика от известните електронни стабилизатори на ток) става въпрос за много големи товари – от порядъка на стотици ампера.

Други изследвания показват, че за стабилизацията на тока е от значение съпосочността на включване на вторичната и шунтовата намотки. Изложеното до тук се отнася за задължително противоположно включване на двете намотки. Решаването на електромагнитната верига при отразяване съпосочност на двете намотки [1] (наричаме го вариант 1Б) дава за тока израза:

$$I_T = \frac{U_1 \cdot W_2}{W_1} \cdot \frac{m \cdot (X_2 + X_C) X_{III} \cdot X_\delta + X_2 \cdot X_C (X_{III} + X_\delta)}{R_T [X_\delta (X_{III} + X_\delta) (X_2 + X_C) + X_{III} X_\delta (X_2 + X_C) + X_2 \cdot X_C (X_{III} + X_\delta)]}. \quad (3)$$

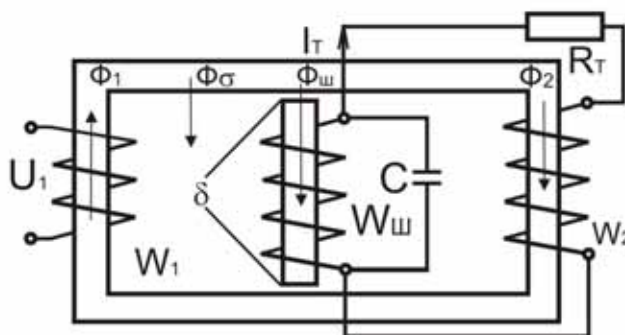
Като се отчетат незначителните (при ненаситен магнитопровод) стойности на съпротивленията X_2 , X_δ и X_{III} , за по-голяма отчетливост насоката на анализа, тук те могат да се пренебрегнат. Тогава се получава:

$$I_T = \frac{U_1 \cdot W_2}{W_1} \cdot \frac{(m+1)}{3R_T} = f(R_T), \quad (4)$$

а

$$U_T = R_T \cdot I_T = \frac{U_1 \cdot W_2}{W_1} \cdot \frac{(m+1)}{3R_T} \neq f(R_T). \quad (5)$$

Видно е (3), че при съпосочно свързване на вторичната (W_2) и шунтовата (W_{III}) намотки, системата не е стабилизатор на ток. Тя се превръща в стабилизатор на напрежение (5). При това стабилизацията му не се влияе от кондензатора. Той има значение само за по-добър фактор на мощността $\cos \varphi$.



Фиг. 2

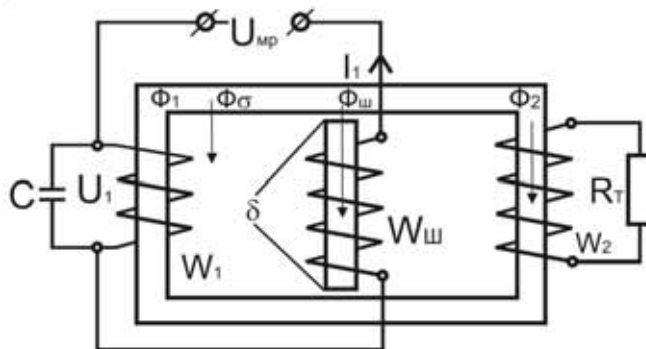
Б. Освен към вторичната намотка, кондензаторът по принцип може да се свърже и към шунтовата намотка, която играе ролята на дросел. Основното

схемно решение за този случай (нека го наречем вариант 2А) е показано на фиг.2, но са възможни и варианти, когато шунтовата намотка (с кондензатора към нея) се свързва последователно с първичната намотка (вариант 2Б), вместо с вторичната такава, или пък е независима от двете намотки (вариант 2В). Подробно тези три възможности са анализирани в [3]. Основното заключение, което се налага след анализите е, че когато кондензаторът е свързан към шунтовата намотка, не са възможни режими на стабилизация на тока. Всъщност то потвърждава предварителните очаквания, защото в този случай кондензаторът остава изолиран, отделен от индуктивността, внасяна в системата от разсейването и въздушната междина.

В общ случай не е възможна и стабилизация на напрежението. Само при вариант 2Б и то единствено при противоположно свързване на намотките W_2 и $W_{ш}$ и е налице частен случай, когато системата може да прояви свойства на стабилизатор на напрежение. Но това е възможно само в определен диапазон на изменение на товарното съпротивление. Аналитичните изследвания сочат, че това е възможно, само ако е изпълнено следното условие:

$$Z_T \gg \frac{j\omega W_2}{R_{\mu}}. \quad (6)$$

Казаното определя вариантите с кондензатор към шунтовата намотка като такива с най-слаби възможности по отношение стабилизация на тока, или напрежението, поради което те не се препоръчват за практическо приложение като стабилизатори.



Фиг. 3

В. Установена е трета възможност за свързване на кондензатора и тя е към първичната намотка [4]. Принципно схемно решение за такава възможност е показано на фиг. 3. Изследването на тази схема посредством комплексния метод (след полагане на съответните опростяващи допускания) води до получаване на следния израз за тока през товара (основната величина в работата на стабилизатора):

$$I_T = \frac{U_1 \cdot W_2^2 \cdot \frac{R_{\mu III}}{\omega^2 \cdot C} \left(\frac{1}{W_{III}} + \frac{1}{W_2} \right) + W_{III} \left(1 - \frac{R_{\mu III} \cdot X_C}{\omega \cdot W_{III}^2} \right)}{W_2 \cdot \frac{1}{\omega \cdot C} (W_1 + W_{III})^2 - W_1^2 \cdot W_{III}^2 \left(\frac{R_T}{W_2^2} + \frac{\omega}{R_{\mu \sigma}} \right) \cdot \left(1 - \frac{R_{\mu III} \cdot X_C}{\omega \cdot W_{III}^2} \right)}. \quad (7)$$

Анализите, проведени по аналогични методи на първите два варианта (кондензатор към вторичната и към шунтовата намотки), показват следващите поважни резултати. Условието за получаване на феромагнитен резонанс тук се отличава от (1) и е:

$$X_{III} = X_{\delta} = X_C = \frac{1}{\omega C} = X. \quad (8)$$

При неговото изпълнение изразът за тока през товарното съпротивление (7) добива вида:

$$I_T = \frac{U_1 \cdot W_2}{W_1} \cdot \frac{1}{X(m+1)} \neq f(R_T), \quad (9)$$

като тук

$$m = \frac{W_1}{W_{III}}.$$

Известни са и изследвания на влиянието на елементите на ПИТ върху неговата работа [5]. С тяхна помощ е установено, че стойността на капацитета на кондензатора в системата пряко осигурява условието за резонанс, оттам и стабилизацията на тока и нейното самостоятелно изменение не се препоръчва. По принцип е възможно такова изменение да става, но задължително и само в съчетание (съгласно с (1) и (9)), с изменението на някои от останалите параметри (въздушна междина δ , брой навивки W_2), като се следи за изпълнението на условията (1) и (7), които осигуряват стабилизацията на тока. При стабилизация на напрежението (която се явява неосновна функция на ПИТ), ролята на кондензатора е преди всичко количествена и там свободата за неговото вариране е малко по-голяма.

В заключение може да се каже, че проведеният сравнителен анализ върху различните схемни решения на ПИТ и различните им работни режими и формулираните въз основа на него изводи, позволяват да се прави избор в зависимост от конкретните нужди на потребителя на стабилизирани ток (напрежение). И когато се търсят възможности за получаване на максимални товарни токове (вече бе споменато, че тази възможност, заедно с подобрените масогабаритни показатели, вследствие обединяването на съгласуващия трансформатор и дросела), е най-ценното качество на ПИТ) трябва да се избира схемно решение с кондензатор към вторичната намотка.

4. ИЗВОДИ

Наблюдаваното сходство между резултатите за първия и третия варианти, позволява да се проведе сравнителен анализ между тях. Той води до следните основни изводи:

1. И в двата случая системата осигурява много добра стабилизация на товарния ток - $I_T \neq f(R_T)$. Тази стабилизация се нарушава само в случаите на поява наситени участъци в магнитопроводите, което прави техните магнитни съпротивления неподходящо големи, за да бъдат пренебрегвани в аналитичните изрази.
2. Главно предвид съотношението между първичната и вторичната намотки (обикновено $W_1 \gg W_2$), то големината на товарния ток е в пъти по-голяма, когато кондензаторът е включен към вторичната намотка.
3. Необходимият за настъпването на резонанс капацитет в първия случай, е по-малък, в сравнение с третия. Предвид неголемите стойности на реактивното съпротивление от разсеян магнитен поток (X_σ), то съгласно (1) и (9) разликата не е значителна.
4. Липсата на намотка, която да е последователно включена към първичната, не позволява на системата с кондензатор на входа (към W_1) да се използва и като стабилизатор на напрежение. За разлика от случая, когато кондензаторът е към вторичната намотка.

Литература

- [1] Georgiev G.R. Working along the lines of MET in linking secondary and shunt coils. Report YUNS with international participation VTU "A. Kanchev", 1994.
- [2] Georgiev G.R. Single-phase current source parametric. Working conditions of arc welding. Candia. Thesis, VMEI - Sofia University "A. Kanchev" Rouse, 1982.
- [3] Georgiev G.R. Operation of a transformer with magnetic shunt capacitor and shunt to the coil. Report on international. Summer School of the Technical University - Sofia, Sozopol, 2005.
- [4] Trifonov NT, G.R.Georgiev, H.A.Yosifov Single-phase parametric source current with a capacitor to the primary side for manual arc welding. Varna, 1993, LG "Zh.Kyuri", 1993.
- [5] Georgiev G.R. Summary study the influence of the main parametric current source on quality. Scientific works of the RU "Rousse", 1990.

OPTIMIZATION OF 4-POLE SMALL DC MACHINE USING FEM AND EVOLUTION STRATEGY

Kostadin Brandisky

Department Theoretical Electrical Engineering, Technical University of Sofia,
blv. Kliment Ohridski 8, 1000 Sofia, Bulgaria,
phone: +359 2 965 3809, e-mail: kbran@tu-sofia.bg

Abstract: *In this paper 2D Finite Element Method and optimization by (1+1) evolution strategy are used to maximize the average running torque of a small 4-pole PM DC machine. The cogging torque value is used as constraint and is maintained below a specified level. The FEM program is controlled by a specially developed parameterized Visual Basic script, which creates the model of the machine depending of the 7 geometric parameters which values are supplied by the optimization program. The optimization allowed the average torque to be increased by 24.5% and the cogging torque to be diminished by 80.5%.*

Keywords: *PM DC machine, FEA, optimization, evolution strategy*

1. INTRODUCTION

The Permanent Magnet Direct Current (PM DC) machines are widely used in the automotive industry, automation, robotics, home appliances, etc. They are produced in large quantities and even small improvement in the construction can lead to considerable savings in the production process [1].

In this paper, the Finite Element Method (FEM) [2] and optimization by evolution strategy [3,4] are used to maximize the average running torque of a small 4-pole PM DC machine. In the same time, the cogging torque is maintained below a certain level. This improves the machine performance and reduces the noise.

2. PROBLEM DESCRIPTION

2.1. The optimized PM DC motor

The PM DC machine which is optimized (Fig. 1) is a small 4-pole permanent magnet DC machine having rated power output of 170 W at 18000 rpm, supply voltage 18 V and rated current 3 A. The ferrite permanent magnets have segmental shape. The rotor has 10 slots. One of the main tasks before the designer of such devices is to increase the torque of the machine. The torque can be increased by increasing the current loading (number of conductors in a slot and the current in a conductor). This is not always possible, because the slots can accommodate limited number of conductors, and also there are limitations on the current density in a conductor. Increasing the current density above a certain level can lead to overheating and low reliability of the motor. Increasing the flux in the air gap can also increase the torque, but this will

require larger stator or bigger/stronger permanent magnets. In many cases this cannot be allowed because of limited space and constraints on the prices. Reducing the air gap thickness also can increase the magnetic flux across the air gap, but there are physical limits.

In this work we investigate the case when the outer diameter of the stator and the shaft diameter are fixed. It is possible to vary the dimensions of the rotor yoke, rotor slots and teeth, PM sizes and the stator yoke thickness. This could be done effectively using optimization program and FEM analysis of the machine. FEM is used to compute accurately the magnetic flux density, torque and the cogging torque of the machine under consideration. In the last years FEM is preferred to compute the distribution of the magnetic field in electrical machines, because of its accuracy, possibilities to model complex geometries and to take into account the nonlinearity of the ferromagnetic materials.

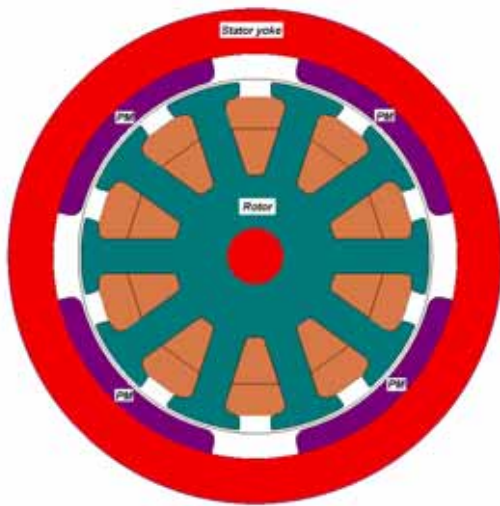


Fig. 1. Outline of the machine

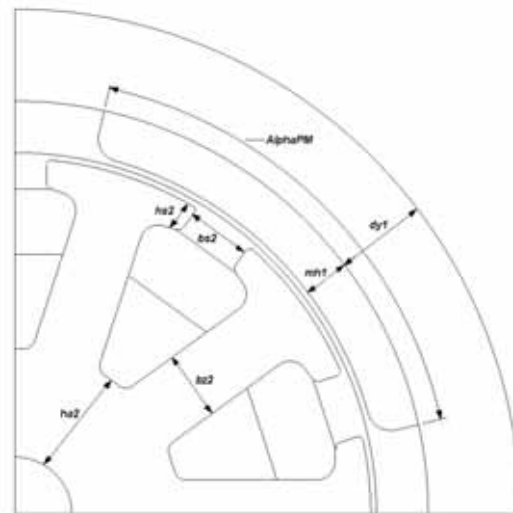


Fig. 2. Design parameters

2.2. Statement of the optimization problem

The optimization problem for the permanent magnet machine under investigation can be stated as follows:

$$\text{Maximize AverageTorque}(\mathbf{x}) = AT \quad (1)$$

where

$\mathbf{x} = \{dy1, mh1, \text{AlphaPM}, bz2, ha2, bs2, hs2\}^t$ is the vector of design variables:

- dy1 – stator yoke thickness [mm]
- mh1 – PM height [mm]
- AlphaPM – PM angle [degrees]
- bz2 – tooth width [mm]
- ha2 – rotor yoke height [mm]
- bs2 – slot opening width [mm]
- hs2 – slot opening height [mm],

Subject to the constraints:

$$\text{Cogging Torque } CT(\mathbf{x}) < 0.03 \text{ N.m} \quad (2)$$

Slot fill-factor $K_{fill} = S_{wires} / S_{slot} < 0.8$ and three geometrical constraints used to ensure valid model.

The design variables (see Fig. 2) and their limits are shown in Table 1:

Table 1. Design variable limits

Design variable	Description	Initial value	Minimum value	Maximum value
dy1	stator yoke thickness [mm]	4	2	6
mh1	PM height [mm]	2	1	4
AlphaPM	PM angle [degrees]	65	50	80
bz2	tooth width [mm]	3	2	4
ha2	rotor yoke height [mm]	4.7	3	6
bs2	slot opening width [mm]	2.8	1	4
hs2	slot opening height [mm]	1.2	0.5	2

The FEM program [2] is controlled by a specially developed parameterized Visual Basic script, which creates the model of the machine depending of the 7 geometric parameters which values are supplied by the optimization program. As a whole, the model is described by 25 parameters, most of them preserved constant because of physical constraints.

Since the running torque period is 36^0 (360 divided by 10 rotor slots), the simulation for rotor positions from 0^0 to 36^0 with step of 1^0 is considered when computing the average torque. The average torque is computed using excitation current equal to the rated current of the machine 3A. The torque at specific position of the rotor against stator is computed by post-processing the results from the FEM analysis, by using the Maxwell stress formula. Special measures are taken to compute accurately the torque in two layers of elements in the air gap that are not touching the rotor outer surface and the stator inner surface. Thus, the higher numerical errors at the interface elements between air and iron are avoided. This is done by using four layers of elements in the air gap.

The cogging torque period T_c is given by the formula

$$T_c = 360 / N_a \quad (3)$$

where

$$N_a = N_p \times N_s / \text{GCD}(N_p, N_s) \quad (4)$$

N_p and N_s are respectively the number of poles and number of slots.

$\text{GCD}(N_p, N_s)$ is the *Greatest Common Divisor* of N_p and N_s .

The cogging torque period for $N_p=4$ and $N_s = 10$ is $T_c = 18^0$. In order to compute accurately the cogging torque, the FEM simulation is performed for rotor positions

from 0° to 18° with step of 1° . The cogging torque computation is done with zero current in the coils, thus leaving only the torque pulsations caused by the changing magnetic flux created by the permanent magnets when the rotor rotates.

In addition, there exists a potential possibility the torque computations at different rotor positions to be performed in parallel, instead serially, on several CPU cores, if they are available.

2.3. The (1+1) evolution strategy

In this work a simple (1+1) evolution strategy is used for optimization of the PM DC motor. Evolution strategies copy some of the principles of nature, though in very simplified form.

In general, the evolution strategy methods have the following properties:

- General purpose optimization methods
- Robust, global-search oriented and derivative-free
- Relies on the idea that each design variable can be represented as a random value rather than a deterministic one
- Consists of random walk of the design variables through the design space
- Guaranties that there is a non-zero probability to find the global minimum

In order to be robust, global-search oriented and derivative-free, the optimization uses zeroth-order evolutionary strategy, consisting of random walk of the design variables through the design space subject to constraints, and in which the movement of the design variables is governed by *Gaussian* statistics with variable metrics.

The operation of the optimizer relies on the idea that each design variable can be represented as a random value. The *Gauss* probability density function is used to vary the design variables in the search space.

The algorithm starts from a guess solution (the starting point x_0 supplied by the user) and iteratively applies three basic operators:

generation(mutation)
selection
annealing

which are repeated until the termination test is satisfied.

The accuracy threshold (i.e. *search tolerance*) may be prescribed by the user.

In the *generation* step a new value of the i -th design variable is computed

$$x(i) = m(i) + u \cdot d(i) \quad i = 1, n \quad (5)$$

perturbing parameters $m(i)$ and $d(i)$ by means of a random sample u (u fulfils *Gauss probability density function*). Here, n is the number of design variables, x is the vector of design variables, m is the vector of the mean values, and d is the vector of deviations.

In the *selection* step, if the new design vector does not violate constraints and bounds, a choice is made between values $m(i)$ and $x(i)$, $i=1,n$, depending on the better value of the objective function.

In the *annealing* step, the vector d is updated by multiplication or division by coefficient $q < 1$, in order to keep the probability of successful iteration around a prescribed optimal value p (an iteration is successful if x is feasible and improves the objective function). The heuristic values for q and p are: $q=0.8-0.9$ and $p=0.1-0.2$ [3].

In practice, the effect of annealing is to control the width of *Gauss* bell: the wider the bell is, the larger the search region around the current design point is. When a better point is found, the width of the bell is increased around the new point to search for further improvements; if no improvement is found, the width of the bell is gradually decreased up to convergence.

The search process stops when the size of the current search region is small enough, i.e., if $d/d_0 < ST$, where ST is a prescribed search tolerance. The smaller is the search tolerance, the longer it will take to reach an optimum.

The algorithm is also referred to as (1+1) evolution strategy (or zero-th order evolution strategy). Higher-order ES are obtained by generating multiple vectors m and d and then selecting the best pair at each iteration; in that case the drawback would be the increase of the computational cost. If the computer in use has several cores or CPUs, several evolutions from different starting points can be run in parallel.

All the procedure is truly derivative-free which is very suitable for difficult non-differentiable objective functions. Additional potential advantage of the evolution strategies is that the higher-order evolution strategy methods are inherently parallelizable, which could decrease considerably the computing time when run on computers having multi-core CPUs or many-core GPUs.

3. RESULTS

3.1. Results from torque optimization

Using the simple (1+1) evolution strategy, after 13 hours computation and 139 generations on PC having AMD Athlon 64x2 CPU, 2.21GHz, 3GB RAM, the following optimum results, shown in Table 2, were obtained. The optimization was run 3 times with different initial points and the best results were retained and shown.

Table 2. Objectives, initial and optimized values

Objectives and constraints	Unit	Goal	Initial value	Optimized value	Improvement %
Average torque	N.m	maximum	0.0784	0.0976	+ 24.5
Cogging torque	N.m	< 0.03	0.0286	0.00556	- 80.5

It is seen that the average torque is increased by 24.5% compared to the initial design. The cogging torque is also improved – diminished by 80.5%.

The optimized values of the design parameters can be seen in Table 3, in the column “End”.

3.2. Sensitivity analysis

The sensitivities of the design variables could give the designer insight on which variables are most important and have the most significant impact on the design, so that he knows what should be changed first in order to improve the design. In Table 3 the sensitivities of the design variables in regard to the torque value are shown.

Table 3. Variation of the design variables

Design variable	Description	Start	End	Variation, %
dy1	stator yoke thickness [mm]	4	4.683	+ 17
mh1	PM height [mm]	2	3.212	+ 60.6
AlphaPM	PM angle [degrees]	65	74.7	+ 14.9
bz2	tooth width [mm]	3	3.999	+ 33.3
ha2	rotor yoke height [mm]	4.7	4.581	- 2.53
bs2	slot opening width [mm]	2.8	2.732	- 2.42
hs2	slot opening height [mm]	1.2	0.8705	- 27.4

In this design the permanent magnet height, the tooth width and the stator yoke thickness have the most significant impact on the torque value. The increase of the permanent magnet height increases the generated magnetic flux. The increase of the tooth width and the stator yoke thickness diminishes the magnetic reluctance of the magnetic path and increases the magnetic flux. Both factors increase the torque produced by the machine.

4. CONCLUSIONS

In this paper the Finite Element Method and optimization by (1+1) evolution strategy are used to maximize the average running torque of a small 4-pole PM DC machine. The optimization allowed the average torque to be increased by 24.5% and the cogging torque to be diminished by 80.5%.

The optimization of this PM DC machine could be complicated by introducing more objective functions and more constraints (e.g., price, efficiency, demagnetization, etc.), which will require multiresponse optimization.

The results of the optimization have confirmed the good potential of the evolution strategies in optimization of electrical machines.

References

- [1] K. Brandisky, R. Belmans and U. Pahner, "Optimization of a Segmental PM DC Motor using FEA, Statistical Experiment Design Method and Evolution Strategy", Proceedings of the Symposium on Power Electronics, Electrical Drives, Advanced Electrical Motors - SPEEDAM 1994, 7-9 June, Taormina, Italy, pp. 7-12.
- [2] Infolytica Corp., MagNet v. 7.3, 2D & 3D Tutorials, Montreal, Canada, 2012.
- [3] Infolytica Corp., OptiNet v. 7.3, Minimizing cogging torque in a brushless motor Tutorial, Montreal, Canada, 2012.
- [4] H.-P. Schwefel, Numerical Optimization of Computer Models, John Wiley & Sons, 1981.

AN APPLICATION OF MATLAB AND ORCAD PSPICE FOR THE EDUCATION ON THE SUBJECT “CIRCUITS AND SIGNALS” PART I

Snejana Terzieva, Ivan Tabahnev, Simeon Vladov

Department Theoretical Electrical Engineering, Technical University of Sofia,
8, Kliment Ohridski Str., Sofia 1000, Bulgaria,
phone: +0359 965 23 94, e-mail: ster19@tu-sofia.bg

Abstract: *An approach for education on the subject “Circuits and Signals” for the MSc students of Electrical engineering, Electronics and Automation in this paper has been proposed. The examined analogue circuits are investigated first analytically and then they are simulated using both OrCad PSpice and MATLAB in order to visualize the output results. Finally, on the base of the mathematical models of the analogue prototypes difference equations are formed. Using these equations digital circuits are synthesized in the MATLAB environment. OrCad PSpice and MATLAB are of the great help for the students to understand principles, laws and methods of the circuits and signals theory. Visualization of analytical and numerical results is important that the students better understand the subject of interest.*

Keywords: *electrical engineering education, analogue and digital circuits, OrCad PSpice, MATLAB.*

1. INTRODUCTION

The subject “Circuits and Signals” is intended for the MSc students of Electrical engineering, Electronics and Automation concerning their profound and extended education. The syllabus includes topics of analysis and synthesis of analogue and digital circuits.

An undeniable fact is that during last years digital circuits and systems enter everywhere in our life and without any “conflict” they replace their analogue predecessors. In addition for analysis and synthesis of digital circuits the mathematical models and techniques inherent in them any are used.

The natural world we live in, as well as most artificial sources, produce signals we are accustomed to consider mainly of the analogue type. (This means that the signal $f(t)$ is defined, somehow, for all values of the continuous variable t .) Present-day engineer should be familiar with digital signals and systems and their mathematical processing [1]. This is because nowadays almost all measuring instruments (electrometers, wattmeters, voltmeters, oscilloscopes, etc.) are digital, i.e. they operate with digital signals. The same concerns definitely the relay protection of electrical objects.

This paper proposes a way that given circuits to be analyzed:

- 1) Analytically – through theoretical results obtained during lectures and seminars.
- 2) Numerically – through simulating models which to visualize the results obtained.

2. THEORY

From the pedagogical viewpoint it is a good idea the process of sampling the signals to be visualized, i.e. the process of presenting an analogue signal by its digital equivalent

$$x(t) \Rightarrow x(nT),$$

where T is the sampling period, and n is an integer ($n = 0, 1, 2, \dots$). When a continuous time (analogue) signal is to be sampled the choice of a sampling frequency for the signal must be determined by the highest frequency component of the Fourier spectrum of the signal. In practice, the sampling frequency should be at least two times higher than the highest frequency component of the analogue signal [2]. As a relative scale coefficient for time we put $T = 1$.

The most important class of digital systems is that for which excitation $x(n)$ and the response $y(n)$ are related by a linear difference equation with constant coefficients of the form

$$y(n) = \sum_{k=0}^p a_k x(n-k) - \sum_{k=1}^q b_k y(n-k), \quad p \leq q, \quad (1)$$

where a_k and b_k are constants.

These equations provide a very accurate description of practical digital processing systems.

If the present value of the output signal (response) $y(n)$ depends on the past response values $y(n)$ as well as the past and present excitation values $x(n)$ then the corresponding digital system (filter) is recursive. This means that at least one coefficient $b_k \neq 0$.

If the output signal $y(n)$ does not depend on the present and past values of $y(n)$ then the corresponding filter is nonrecursive, i.e. $b_k = 0$ for all k .

An example of a nonrecursive difference equation is

$$y(n) = a_0 x(n) + a_1 x(n-1) + a_2 x(n-2), \quad (2)$$

and a recursive difference equation is

$$y(n) = a_0 x(n) + a_1 x(n-1) + a_2 x(n-2) - b_1 y(n-1) - b_2 y(n-2). \quad (3)$$

There are different ways for solving these equations [3]. When a classical method is used one finds the solutions of the homogeneous equation and partial solutions separately. Another method consists of a creation of a table that contains values of the input and output signals and solving the difference equation for each value of n . This method could be used in cases when we are interested in only few values of the output signal.

The description of the discrete linear circuits and their analysis can be conveniently accomplish using Z -transform:

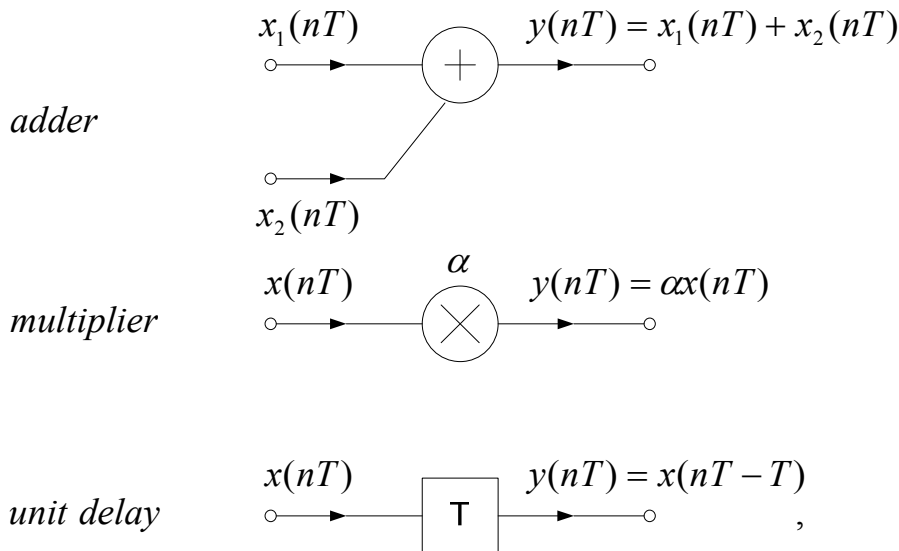
$$x(nT) \Rightarrow X(z) = \sum_{n=0}^{\infty} x(nT)z^{-n} . \tag{4}$$

The digital systems are described by a transfer function defined as a ratio between the output and input signal. In Z -domain the transfer function is

$$H(z) = \frac{Y(z)}{X(z)}, \tag{5}$$

where $Y(z) \Rightarrow y(nT)$.

For realization of specific digital circuits, in particular digital filters, with a given transfer function the following blocks are used [2]:



where α is a weight coefficient.

Nonrecursive equation (2) in Z -domain is

$$Y(z) = a_0X(z) + a_1z^{-1}X(z) + a_2z^{-2}X(z), \tag{6}$$

and corresponding transfer function of the digital filter is

$$H(z) = \frac{Y(z)}{X(z)} = a_0 + a_1z^{-1} + a_2z^{-2}. \tag{7}$$

Recursive equation (3) in Z -domain and the corresponding transfer function of the digital filter are:

$$Y(z) = a_0X(z) + a_1z^{-1}X(z) + a_2z^{-2}X(z) - b_1z^{-1}Y(z) - b_2z^{-2}Y(z), \tag{8}$$

$$H(z) = \frac{Y(z)}{X(z)} = \frac{a_0 + a_1 z^{-1} + a_2 z^{-2}}{1 + b_1 z^{-1} + b_2 z^{-2}}. \quad (9)$$

3. SIMULATING MODEL OF FIRST-ORDER LOW-PASS FILTER

A passive low-pass filter of first order is shown in Fig. 1.

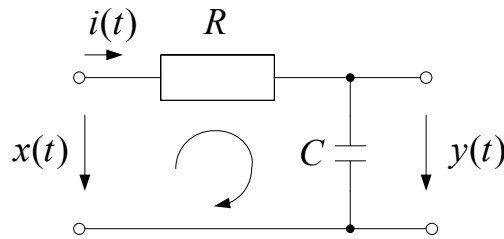


Fig. 1

For the circuit analysis Ohm's Law and Kirchhoff's Voltage Law are used:

$$i(t) = C \frac{du_c(t)}{dt} = C \frac{dy(t)}{dt},$$

$$RC \frac{dy(t)}{dt} + y(t) = x(t). \quad (10)$$

When the input voltage is a sine-wave $x(t) = u(t) = u_m \sin \omega t$ the phasor method [4] is used in order to find analytical solution of the equation (10). Given the circuit parameters $R = 1 \text{ k}\Omega$, $C = 1 \mu\text{F}$, $U = 1 \text{ V}$, $f = 500 \text{ Hz}$ the solution for the output voltage is

$$y(t) = u_c(t) = 0.303\sqrt{2} \sin(3140t - 1.263) \text{ V}.$$

For modeling, simulating and visualization of circuits, signals and processes OrCad PSpice and MATLAB packages are used [5, 6, 7]. The simulation results of the circuit through PSpice are given in Fig. 2a, b.

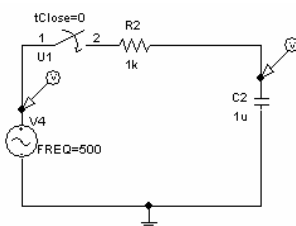


Fig. 2a

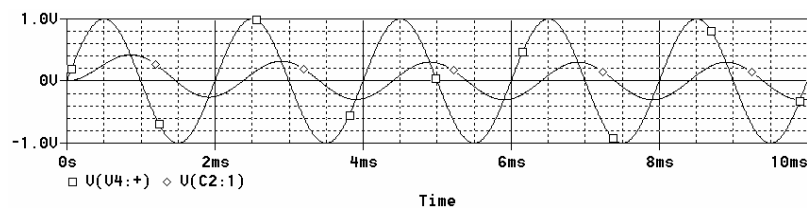


Fig. 2b

Similar results are observed when a simulating model in the graphical environment MATLAB (Simulink) is created. In this case ready graphical functional blocks from standard Simulink library are used. (See Fig. 3a.)

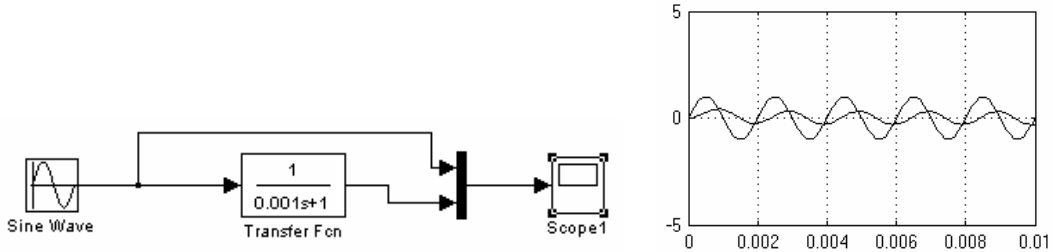


Fig. 3a

Fig. 3b

The Laplace transform of the circuit transfer function is used

$$T(s) = \frac{1}{RCs + 1}.$$

The input and output voltages for these particular data are shown in Fig. 3b.

In the case of a rectangular input impulse with the amplitude of 1V and duration of 5 ms the result of PSpice and Simulink for the input and output voltages are shown in Fig. 4a, b and Fig. 5a, b.

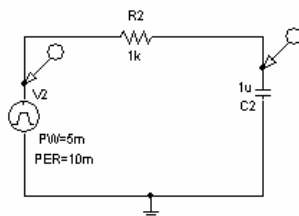


Fig. 4a

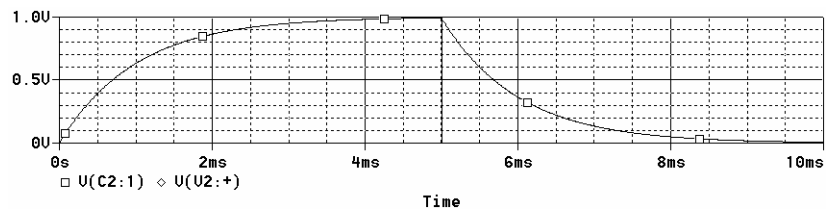


Fig. 4b

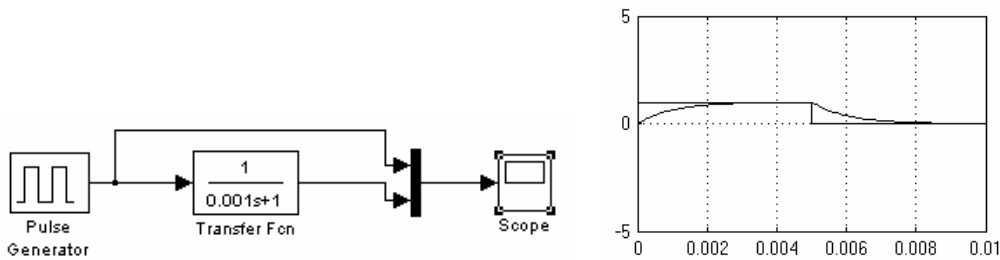


Fig. 5a

Fig. 5b

After sampling the analogue signals the differential equation (10) is transformed in a difference equation:

$$\frac{dy(t)}{dt} = \frac{\Delta y(t)}{\Delta t} \Rightarrow \frac{y(n) - y(n-1)}{T}$$

$$RC \frac{y(n) - y(n-1)}{T} + y(n) = x(n)$$

$$\left(\frac{RC}{T} + 1 \right) y(n) = x(n) + \frac{RC}{T} y(n-1)$$

$$(RC + T)y(n) = Tx(n) + RCy(n-1)$$

$$y(n) = \frac{T}{RC + T} x(n) + \frac{RC}{RC + T} y(n-1),$$

or in general form

$$y(n) = a_0 x(n) + b_1 y(n-1), \quad (11)$$

where $a_0 = \frac{T}{RC + T}$, $b_1 = \frac{RC}{RC + T}$.

A recursive digital filter that is described by equation (11) is shown in Fig. 6.

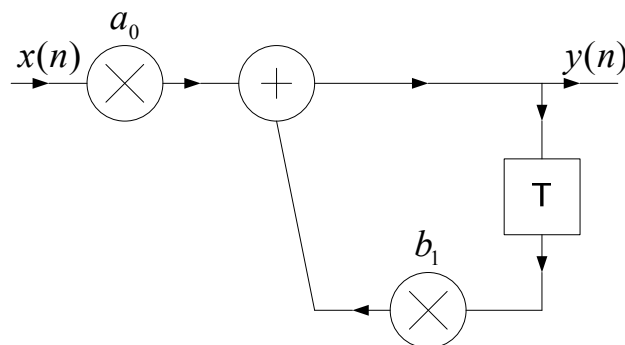


Fig. 6

Equation (11) in Z-domain is

$$Y(z) = a_0 X(z) + b_1 z^{-1} Y(z), \quad (12)$$

and then the transfer function of this digital filter is

$$H(z) = \frac{Y(z)}{X(z)} = \frac{a_0}{1 - b_1 z^{-1}}. \quad (13)$$

The transfer function (13) of the synthesized digital filter is realized through MATLAB by the function *filter* with the following syntax [6]:

$$y = \text{filter}(Nz, Dz, x),$$

where y is the wanted discrete output signal $y(n)$, x is the input discrete signal $x(n)$, $Nz = [a_0]$ and $Dz = [1 - b_1]$ are vectors with elements the coefficients of the transfer function of the filter. The simulation results are given in Fig. 7 and Fig. 8.

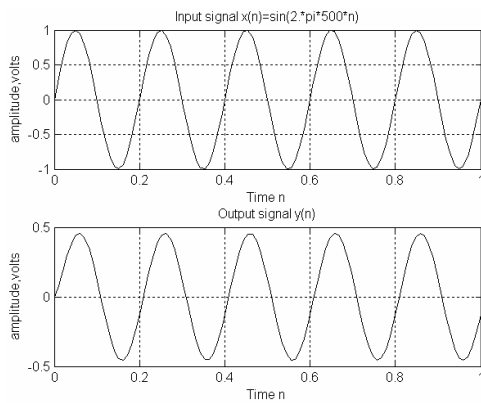


Fig. 7

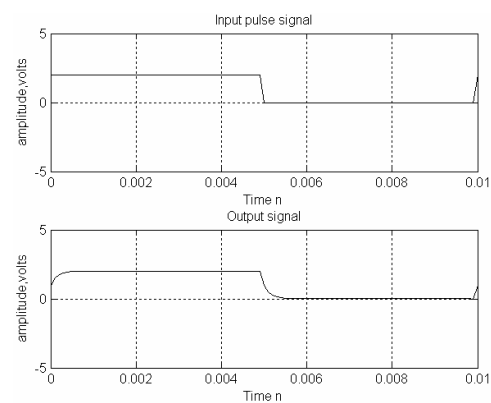


Fig. 8

4. CONCLUSION

The use of PSpice and MATLAB for education on the subject “Circuits and Signals” will result in:

- better clearness for learning the subject taught;
- connection of the “dull” theory with practical skills for simulating of mathematical models and visualization of both input and output signals;
- making students familiar with the possibilities of PSpice and MATLAB for visualization the results of circuits considered.

References

- [1] H. Baher, Analog and digital signal processing, John Wiley&Sons, 1992.
- [2] R. Penev, Manual for laboratory practice and seminars on signals and systems, TU-Sofia, 1999, in Bulgarian.
- [3] B. Donevsky, Mathematical methods for digital processing, TU-Sofia, 2006, in Bulgarian.
- [4] K. Brandisky et al, Textbook on Theory of electrical engineering, part II, Sofia, 2005, in Bulgarian.
- [5] F. J. Monssen, OrCAD Pspice with Circuit Analysis, Third edition, Prentice Hall, New Jersey, Columbus, Ohio, 2001.
- [6] U. Lazarev, MATLAB processes and systems modeling, Piter, Kiev, 2005, in Russian.
- [7] K. Brandisky et al, Textbook on solving electrical engineering problems with PSpice, Siela, Sofia, 2002, in Bulgarian.

AN APPLICATION OF MATLAB AND ORCAD PSPICE FOR THE EDUCATION ON THE SUBJECT “CIRCUITS AND SIGNALS” PART II

Snejana Terzieva, Ivan Tabahnev, Simeon Vladov

Department Theoretical Electrical Engineering, Technical University of Sofia,
8, Kliment Ohridski Str., Sofia 1000, Bulgaria,
phone: +0359 965 23 94, e-mail: ster19@tu-sofia.bg

Abstract. *The idea of introducing MATLAB and PSpice for the education on the subject “Circuits and Signals” for the MSc students of Electrical engineering, Electronics and Automation has been continued in this paper. An example for synthesis of a second-order band-pass filter has been considered. A method for analysis that includes first obtaining the mathematical model and then the synthesis of a band-pass filter has been presented. The simulations with specific data and visualization the results obtained help better understanding the considered subject.*

Keywords: *electrical engineering education, analogue and digital circuits, OrCad PSpice, MATLAB.*

1. INTRODUCTION

The subject “Circuits and Signals” is intended for the MSc students of Electrical engineering, Electronics and Automation concerning their profound and extended education. The syllabus includes topics of analysis and synthesis of analogue and digital circuits and especially digital filters [1].

The necessity for learning digital filters is engendered of their high application in digital signal processing and communication. It is known that analogue and digital filters affect both amplitude-frequency response and phase-frequency response as well [2].

The aim of this paper is to help students better understand the subject taught and get a visual idea of the signal processing in the subject “Circuits and Signals”.

2. THEORY

It is possible to synthesize a digital filter by its analogue prototype using some basic characteristics concerning the process of the circuit. The characteristics can be a differential equation, a transfer response or an impulse response.

Some of the methods of synthesis are named after their basic characteristic [3]:

- method of sampling the differential equation;
- method of the invariant frequency response;
- method of the invariant impulse response.

Each of the methods has its own special characteristics connected with a different accuracy of reproduction of amplitude-frequency response, differences in their structure, etc.

The differential equation is sampled and this necessitates the analogue circuits to be replaced by digital ones and the differential equation to be replaced by a corresponding difference equation. The analogue quantity time t is replaced by the discrete time nT and the result is

$$t \Rightarrow nT; \quad x(t) \Rightarrow x(nT); \quad y(t) \Rightarrow y(nT),$$

where T is the sampling period, n is an integer ($n = 0, 1, 2, \dots$). Since a relative scale for the time is frequently used, we put $T = 1$. The digital equivalent $x(nT)$ corresponds to the input analogue signal $x(t)$ and the digital equivalent $y(nT)$ corresponds to the output analogue signal $y(t)$.

The differential increment of the argument is

$$dt \Rightarrow T; \quad dt^2 \Rightarrow T^2,$$

and the function increments corresponding to the first- and second-order finite differences are [2]:

$$\begin{aligned} dx(t) &= x(n) - x(n-1); & dy(t) &= y(n) - y(n-1); \\ d^2x(t) &= x(n) - x(n-1) - [x(n-1) - x(n-2)] = x(n) - 2x(n-1) + x(n-2); \\ d^2y(t) &= y(n) - y(n-1) - [y(n-1) - y(n-2)] = y(n) - 2y(n-1) + y(n-2). \end{aligned}$$

The accuracy of the transform becomes higher if the finite increments have been determined by the Runge-Kutta method.

The solution of difference equations is frequently found in the Z -domain:

$$x(nT) \Rightarrow X(z) = \sum_{n=0}^{\infty} x(nT)z^{-n}. \quad (1)$$

The transfer function defined as the ratio between the output and input signal in the Z -domain is

$$H(z) = \frac{Y(z)}{X(z)}, \quad (2)$$

where $Y(z) \Rightarrow y(nT)$.

In order to realize digital filters with a known transfer function the following basic blocs are used: adder, multiplier and unit delay.

A digital second-order filter and its transfer function in the Z -domain are:

$$Y(z) = a_0X(z) + a_1z^{-1}X(z) + a_2z^{-2}X(z) - b_1z^{-1}Y(z) - b_2z^{-2}Y(z), \quad (3)$$

$$H(z) = \frac{Y(z)}{X(z)} = \frac{a_0 + a_1z^{-1} + a_2z^{-2}}{1 + b_1z^{-1} + b_2z^{-2}}. \quad (4)$$

3. SIMULATING MODEL OF A SECOND-ORDER BAND-PASS FILTER

The circuit of a passive second-order band-pass filter is given in Fig. 1.

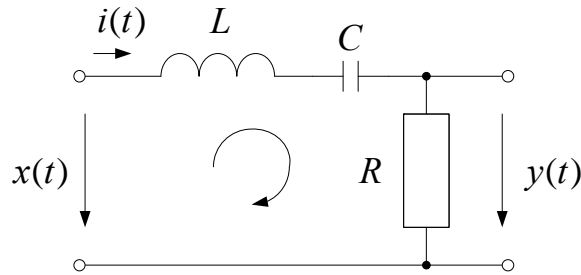


Fig. 1

For the analysis of the circuit Ohm's Law and Kirchhoff's Voltage Law are used. As a result the basic differential equation is found [4]:

$$L \frac{di(t)}{dt} + \frac{1}{C} \int i(t) dt + y(t) = x(t)$$

$$L \frac{d^2 i(t)}{dt^2} + \frac{1}{C} i(t) + \frac{dy(t)}{dt} = \frac{dx(t)}{dt} \quad i(t) = \frac{y(t)}{R}$$

$$\frac{L}{R} \frac{d^2 y(t)}{dt^2} + \frac{1}{RC} y(t) + \frac{dy(t)}{dt} = \frac{dx(t)}{dt} \quad \left| \times \frac{R}{L} \right.$$

$$\frac{d^2 y(t)}{dt^2} + \frac{1}{LC} y(t) + \frac{R}{L} \frac{dy(t)}{dt} = \frac{R}{L} \frac{dx(t)}{dt} \quad (5)$$

The quantities connected with the filter operation – the resonance frequency ω_0 , the characteristic impedance ρ and the quality factor Q , are introduced

$$\omega_0 = \frac{1}{\sqrt{LC}}, \quad \rho = \sqrt{\frac{L}{C}}, \quad Q = \frac{\rho}{R}, \quad \frac{R}{L} = \frac{\omega_0}{Q},$$

and the equation (5) takes the form:

$$\frac{d^2 y(t)}{dt^2} + \frac{\omega_0}{Q} \frac{dy(t)}{dt} + \omega_0^2 y(t) = \frac{\omega_0}{Q} \frac{dx(t)}{dt}. \quad (6)$$

When the input voltage is a sine-wave $x(t) = u(t) = u_m \sin \omega t$ and the circuit parameters are $R = 20 \Omega$, $L = 10 \text{ mH}$, $C = 100 \mu\text{F}$, $U = 1 \text{ V}$, $\omega = \omega_0 = 10^3 \text{ rad/s}$, $f = f_0 = 159.15 \text{ Hz}$, the circuit is in a resonance state and after the transients the output voltage repeats the input one. The value of the quality factor is $Q = 0.5$.

The amplitude-frequency response (AFR) and the phase-frequency response (PFR) of the circuit after simulating by PSpice [5, 6] are given in Fig. 2. The resonance frequency $f_0 = 158.489 \text{ Hz}$ and the band-pass $\Delta f = 317.506 \text{ Hz}$ can be easily found by the AFR. The value of the Q -factor of the RLC -circuit is

$$Q = \frac{f_0}{\Delta f} = 0.4991$$

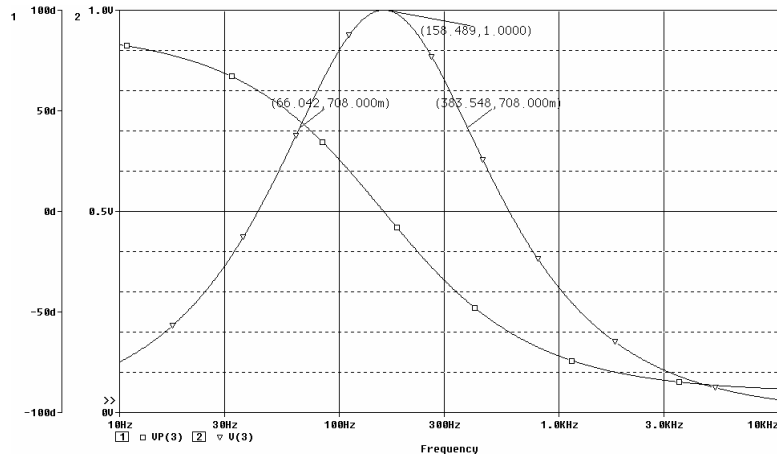


Fig. 2

The quality factor could be found by macros that uses objective function for determining resonance frequency and the frequency band-pass and the result is $Q = 0.500645$.

Using MATLAB [7] graphs of the AFR and the PFR are given in Fig. 3a, b.

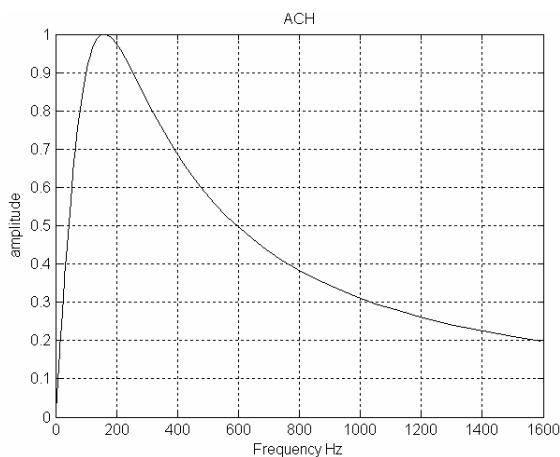


Fig. 3a

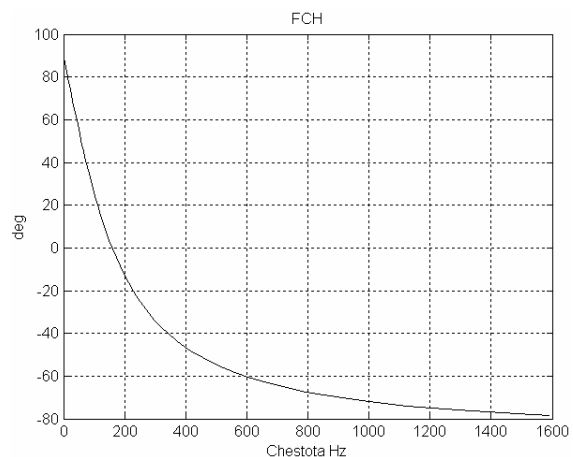


Fig. 3b

The graphs of the input and output voltage as a function of time are given in Fig. 4. The PSpice simulations and the values of the quantities taken from the graphs confirmed the theoretical results.

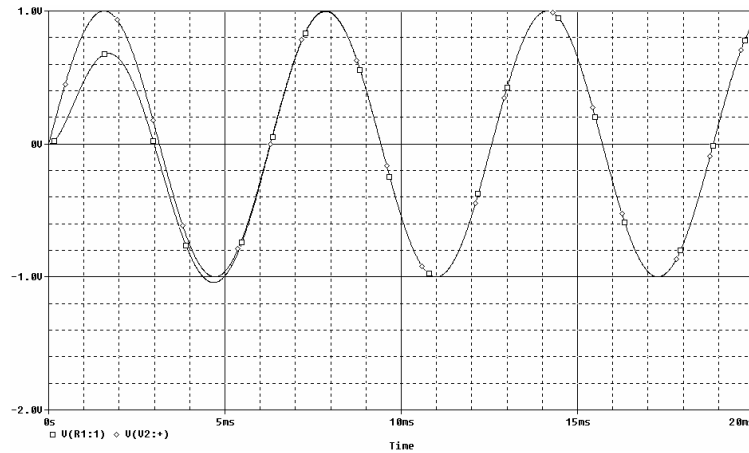


Fig. 4

Similar results are observed when a simulating model in the graphical environment Simulink of MATLAB has been created. In this case ready graphical functional blocks from standard Simulink library are used (see Fig. 5a). The Laplace transform of the circuit transfer function is used

$$T(s) = \frac{RCs}{LCs^2 + RCs + 1}.$$

The input and output voltages for these particular data are shown in Fig. 5b.

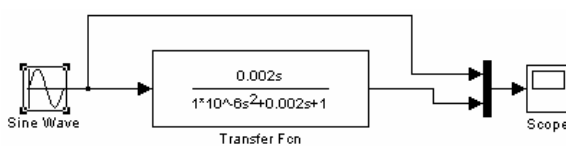


Fig. 5a

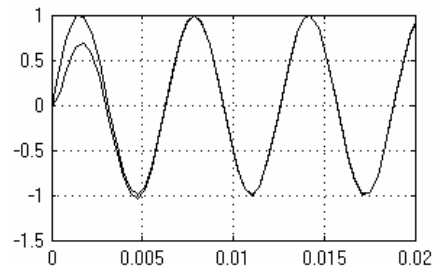


Fig. 5b

After sampling, the analogue signals the differential equation (6) is transformed in a difference equation:

$$\frac{y(n) - y(n - 1) - [y(n - 1) - y(n - 2)]}{T^2} + \frac{\omega_0}{Q} \frac{y(n) - y(n - 1)}{T} + \omega_0^2 y(n) = \frac{\omega_0}{Q} \frac{x(n) - x(n - 1)}{T}$$

$$Q[y(n) - 2y(n - 1) + y(n - 2)] + \omega_0 T[y(n) - y(n - 1)] + \omega_0^2 Q T^2 y(n) = \omega_0 T[x(n) - x(n - 1)]$$

$$[Q + \omega_0 T + \omega_0^2 Q T^2]y(n) = \omega_0 T x(n) - \omega_0 T x(n - 1) + (2Q + \omega_0 T)y(n - 1) - Qy(n - 2).$$

The general form of the difference equation that describes the operation of the digital filter of Fig. 6 is

$$y(n) = a_0x(n) - a_1x(n - 1) + b_1y(n - 1) - b_2y(n - 2), \tag{8}$$

where
$$a_0 = a_1 = \frac{\omega_0 T}{Q + \omega_0 T + Q\omega_0^2 T^2},$$

$$b_1 = \frac{2Q + \omega_0 T}{Q + \omega_0 T + Q\omega_0^2 T^2},$$

$$b_2 = \frac{Q}{Q + \omega_0 T + Q\omega_0^2 T^2}.$$

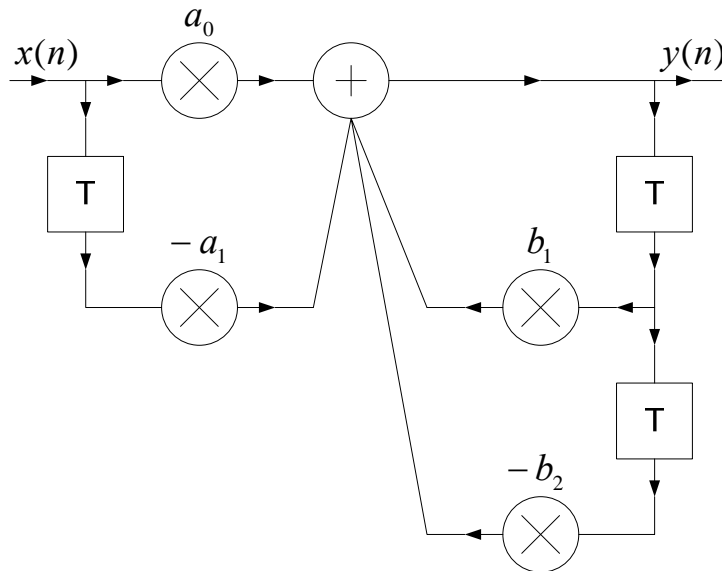


Fig. 6

The equation and the transfer function in the Z -domain are

$$Y(z) = a_0X(z) - a_1z^{-1}X(z) + b_1z^{-1}Y(z) - b_2z^{-2}Y(z) \tag{9}$$

$$H(z) = \frac{Y(z)}{X(z)} = \frac{a_0 - a_1z^{-1}}{1 - b_1z^{-1} + b_2z^{-2}}. \tag{10}$$

The transfer function (10) of the synthesized digital filter is realized through MATLAB by the function *filter* with the following syntax [7,8]:

$$y = filter(Nz, Dz, x),$$

where y is the wanted discrete output signal $y(n)$, x is the input discrete signal $x(n)$, $Nz = [a_0 \ a_1]$ and $Dz = [1 \ -b_1 \ b_2]$ are vectors with elements the coefficients of the transfer function of the filter. The results of the simulation are shown in Fig. 7 and Fig. 8.

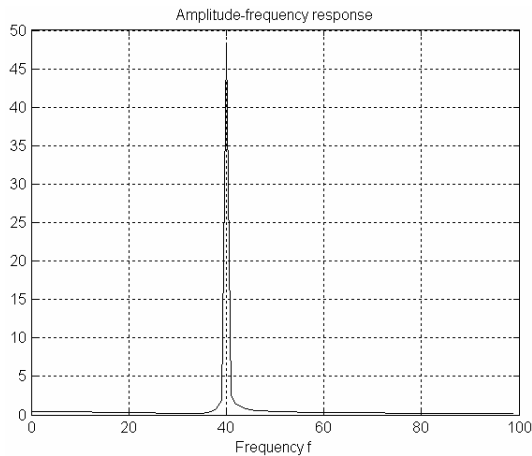


Fig. 7

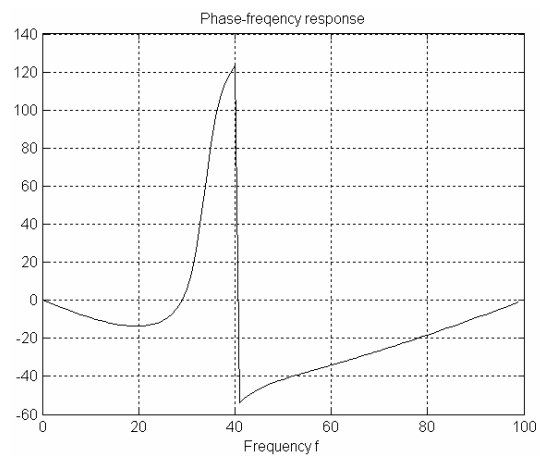


Fig. 8

4. CONCLUSION

The application of PSpice and MATLAB result in better understanding and better learning the filters considered. The subject "Circuits and Signals" becomes more attractive to the students. Based on this application it is possible to think about introducing these topics in laboratory practice.

The IT advance makes possible mathematical models to be used. These models can simulate corresponding processes and operative models of different circuits. The adequacy of the models of the real physical objects could be proved in the real output functions with the simulated ones.

References

- [1] H. Baher, Analog and digital signal processing, John Wiley&Sons, 1992.
- [2] R. Penev, Manual for laboratory practice and seminars on signals and systems, TU-Sofia, 1999, in Bulgarian.
- [3] B. Donevsky, Mathematical methods for digital processing, TU-Sofia, 2006, in Bulgarian.
- [4] K. Brandisky et al, Textbook on Theory of electrical engineering, part II, Sofia, 2005, in Bulgarian.
- [5] F. J. Monssen, OrCAD Pspice with Circuit Analysis, Third edition, Prentice Hall, New Jersey, Columbus, Ohio, 2001.
- [6] K. Brandisky et al, Textbook on solving electrical engineering problems with PSpice, Siela, Sofia, 2002, in Bulgarian.
- [7] U. Lazarev, MATLAB processes and systems modeling, Piter, Kiev, 2005, in Russian.
- [8] Z. Nikolova, K. Ivanova, Manual for laboratory practice on communication circuits with MATLAB, "King – 2001", Sofia, 2004, in Bulgarian.

TRANSFORMER WINDINGS WITH BIG SECTION, HIGH CURRENT AND LOW VOLTAGE

Kiril Stoyanov Stoykov

Technical University of Sofia, 8, Kliment Ohridski, blvd., 1000, Sofia, Bulgaria,
phone: +359 2 965 3665, e-mail: k_stoykov@tu-sofia.bg

Abstract: *In the paper, the advantages and disadvantages of the coils used in transformers supplying electric furnaces (electric furnace transformers). Technique for automatic calculation of the eddy-current coefficient in laps' coils is proposed. These coils are used usually when the currents are over than 100 kA. The possible boundary values of the laps' widths are given in table form.*

Keywords: *low-voltage winding, screw-winding, disc-winding, lap-winding.*

1. INTRODUCTION

The windings of the transformers for high current and low voltage are the most important constructive elements of the transformers supplying electric furnaces (electric furnace transformers). These windings have small number of windings (up to 5 and very rarely more than 5) and they are made from a conductor with very big section. They are manufactured for voltages from 50–60 V to 1000 V. The main parameters of the electric furnace transformers, produced in Republic Bulgaria, are shown in Table 1.

Table 1

№	Power, MVA	Number of windings w_{HH} , -	Section of the conductor, mm^2	Current through the w_{HH} , A	Secondary voltage, V	Type of the coil
1	1,6 with reactor	6	1120	2000	63 ÷ 113	rimmed
2	2,0 with reactor	6	1585,28	3401	100 ÷ 225	double disks
4	7,5 with reactor	8	1000	10040	101 ÷ 290	double disks
5	13,3	8	1200	12703	132 ÷ 390	double disks
6	50,0	5	10124,8	32052	229 ÷ 825	double disks
7	50,0	2	12000	65000	188-590	lap

It is obvious that the windings for high current have very big section of the conductor, which insists on applying some additional actions with respect to their fixture in order to ensure electro-dynamic stability of the transformer.

The requirements, defined about the windings for high current and low voltage, are following: low overhead losses; sufficient electro-dynamic stability; admissible heating stability (according to the standard); low price and easily and simple production.

The made investigations show that the mentioned above requirements satisfy the transformer with screw-winding, disk-winding and lap winding.

2. PROBLEM STATEMENT

2.1. Screw windings

These coils apply in transformers with power smaller than 6300 kVA and secondary currents up to 5000 A [1]. They produce as one-walk or multiple-walk, when it is necessary to increase the section of the conductor (resp. coil). As a rule the section of the coil determines according to the number of the parallel conductors, put in the radial direction of one walk.

One-walk screw coils use for the transformers with middle power and smaller sections of the conductor (up to 4-6 parallel conductors). When the number of parallel conductors is bigger (from 8 to 20) it uses duplex screw windings. When it studied power transformers and the supplying voltages are upper than 35 kV, the number of parallel conductors can reach 40. Then it applies tree- and four-walk screw coils.

In practices the screw coils produces as short ones, which manufactures as a normal screw coils. The litters put axially each other and they are connected in parallel.

The short screw coils realizes on the common isolative cylinder and each coil begin right after the end of the previous one in order to minimize the empty space. There is a loop between the coils and she uses for taking off the respective coil's terminals. The loop cuts and one terminal uses as an end of current short screw coil, but the other terminal is the beginning for the next screw coil. The practice shows than screw coils consist of big number parallel conductors. It means that the conductors are in diffuse fields with different intensity, which leads to arising of the circulation currents. The losses, caused from these currents, decreases by changing the order of the conductors in their manufacturing, so called transposition. Usually in practice applies Hobert's transposition, which is considered as the best one. Unfortunately, it is very sophisticated – the investigations shows, that the transpositions in one short screw coils are 100-200 [1, 2], but sometimes still more. This considers as a serious disadvantage of these type coils.

Other its disadvantage consists of some difficulties in taking off terminals to the rimmed system, which is as a result of the large number of conductors (resp. big section).

There disadvantages compensate with the advantages of the short screw coils, which have very good heating and electro-dynamic stability and have low overhead losses [5], [8].

2.2. Coil with disc windings

2.2.1. Coil with continuous disc windings

In practice [8] there are electric furnace transformers with low voltage coil produced as continuous disk coil. Its construction is based on the loops between the separately disks. These loops cut and its terminals solder on the respective rims. These coils require splitting of the rims in several groups, which can be combined either in serial or in parallel connection each other. In first way, the secondary voltage is a sum of the voltages for each pair of disks and the current is equal of the current passed through the one pair of rims. In second way, the voltage is equal of the voltage of one pair of rims and the current increases as times as the numbers of pairs of rims. This enables to use the rims with different sections, i.e. bigger and smaller sections for rims with bigger and smaller loads, respectively [6]. The research shows that the current distribution on the rims (resp. through the coils) is uneven [6], which is as result of the respective resistance of the coils. It is different during the coils, which lead to increasing of the current in the beginning and in the end sections up to 2 times [6, 8]. This causes serious heating and dynamic inconveniences. The solution of these problems needs of applying of the specifically actions as interweaving of the beginning and the end sections; increasing of the conductor's section in the beginning and the end sections; increasing of the cooling channels in axial direction and etc. These coils use in transformers with small number of windings of the secondary side and not big powers.

2.2.2 Double discs coils

This coil includes two disks. The number of windings in the disk is divisible of the number of the disks. This show that each disk have integer number of windings. It produces as the continuous disk coil. When there is a parallel conductors the transposition is made. Usually it applies the common transposition [1, 2]. However, it is imperfect and lead to bigger overhead losses. If the radial size of the conductor decrease and if increases the number of parallel conductors, then these losses decreases. The investigations show that double disks coil prefers from many companies, because it is suitable in constructive and technological sense, i.e. it is compact; it has high heating and electro-dynamic stability; it allows to realize a compensative rims' system without applying the additional constructive actions.

The mentioned above advantages of disks coils, give occasion for their widely using as low voltage coils in electric furnace transformers where the number of their windings is up to 3.

2.3. Lap coils

These coils uses in electric furnace transformers with very small number of windings in the secondary side (from 1 to 9) [9]. Usually it uses the sheets from cooper or aluminum with suitable height and width according to the power of the transformer.

The sheets divide in axial direction in separately bands, which connect in parallel to the rims' system.

An important feature of these coils is their dependence on the eddy currents, which cause additional power losses.

It is well known, that the eddy currents are related to the quasi stationary phenomena [3]. They create uneven distribution of the current density on the coils section, which causes other damaging phenomena (as skin effect, increasing of the respective resistance, decreasing on the inductance and etc.). Then the losses are as a result from the axial component as well as from the radial component of the diffusion field.

In practice, the losses from eddy currents estimate with so called eddy current coefficient K_B , which determines in percents from the main losses in the coil [2, 9]. The estimation makes separately for the axial and the radial components of the diffusion field. The problems concerned with influence of the radial component are discussed in details in [7].

The influence of the axial component can be analyzed by the following formula [2, 9]:

$$K_B = \frac{100}{9} \left(0,96 \cdot \Delta \cdot \sqrt{\frac{\sum I_{cu} \cdot K_R}{1}} \right)^4 \cdot (w^2 - 0,2), \% \quad (1)$$

where w – number of windings in the secondary side of the electric furnace transformer; Δ - width of the sheet, K_R - Rogovsky's coefficient, which in practice is 0,95 – 0,96; $\frac{\sum I_{cu}}{1}$ – ratio between the sum of all elementary bands and the main axial length of the coil.

The axial component of the eddy currents coefficient for different widths of the coil's sheets is calculated by software product MatLab and the results are given in Table 2.

The table helps the engineer to choose the width of the lap coil in terms of the numbers of its windings when it is imposed the restrictions on the additional losses from eddy currents. For example, in restriction for these losses to be smaller than 20 %, when the number of windings of the second side is given (see the marked half of the table 2) it can determine the maximum width of the lap coil. In addition easily can estimate the maximum current, which can passed through the lap coil.

Table 2

Laps width, cm	Number of windings in the secondary side of the transformer				
	$W_{HH}=1$	$W_{HH}=2$	$W_{HH}=3$	$W_{HH}=4$	$W_{HH}=5$
	K_B	K_B	K_B	K_B	K_B
0,1	0,006578	0,026521	0,064398	0,157432	0,262134
0,15	0,009456	0,039055	0,098762	0,178655	0,311505
0,2	0,010356	0,049025	0,113405	0,203440	0,320405
0,25	0,035642	0,153689	0,354378	0,864321	1,056743
0,3	0,052023	0,247441	0,572331	1,028330	1,610091
0,35	0,114567	0,632780	1,453673	2,202134	3,843290
0,4	0,164400	0,781320	1,809114	3,248015	5,101200
0,45	0,285341	1,239654	3,258621	5,894539	8,965231
0,5	0,401513	1,907115	4,416332	7,929012	12,453201
0,55	0,621453	2,943201	6,734520	12,002131	18,62378
0,6	0,832023	3,954552	9,157213	16,442453	25,810011
0,65	1,153687	5,432785	13,210045	23,456341	36,732109
0,7	1,542032	7,326096	16,965321	30,460213	47,812314
0,75	1,9503465	8,983457	19,073462	39,452371	75,521304
0,8	2,631024	12,498743	28,942116	51,963194	96,453120
0,85	3,321056	16,742356	37,345620	76,862345	133,345271
0,9	4,214034	20,019103	46,3592413	101,345621	153,813245
0,95	5,127345	24,987451	79,349201	153,452361	210,342156
1,0	6,424012	30,512345	112,432098	211,485678	267,835263
1,05	7,453627	38,523417	136,342567	241,674532	301,231567
1,1	9,405012	44,672345	180,123452	277,982346	330,174523
1,15	11,523456	52,234157	205,672345	320,324561	380,234151
1,2	13,301112	64,325671	234,234567	370,125678	401,235784
1,25	15,672340	58,934527	248,345261	398,673452	444,231314
1,3	18,346121	75,089045	272,098456	422,231562	480,123412
1,35	21,341264	79,784523	292,356743	436,253412	518,342617
1,4	24,6761212	88,213141	312,123141	450,123145	573,126735
1,45	28,342312	95,745362	332,845634	464,846352	650,123456
1,5	32,5182213	106,413121	360,231234	478,345621	737,213424
1,55	37,342516	224,524132	384,542132	493,441236	802,213242
1,6	42,096332	238,325607	408,112314	507,945321	867,321365
1,65	49,002134	298,121345	418,341267	557,876543	932,020345
1,7	56,127856	356,845362	448,213456	607,453426	967,564321
1,75	63,934526	415,453216	468,543216	657,452135	1017,364521
1,8	70,764321	474,563421	488,342165	707,317643	1067,453216
1,85	79,532156	533,325161	638,076543	847,634523	1200,213456
1,9	86,090876	599,314256	738,231567	987,654321	1333,020301
1,95	97,509876	661,534210	793,342109	1042,098762	1463,789064
2,0	109,102345	687,321345	848,098706	1097,543567	1593,098741

References

- [1] С. Фарбман, А. Ю. Бун, И. М. Райхлин. “Трансформаторы. Ремонт и модернизация трансформаторов”. Энергия. Москва, 1976.
- [2] А. Дачев, “Специални силови трансформатори”. Техника. София, 1967.
- [3] И. Ламмеранер, М. Штафль. “Вихревые токи”. Энергия. Москва – Ленинград, 1967.
- [4] Т. Тошков, “Изследвания върху трансформаторни намотки от фолио”. Дисертация, ВМЕИ “Ленин”. София, 1977.
- [5] А. Дачев, “Експериментално изследване на добавъчните загуби от вихрови токове”. Електропромишленост и приборостроене. №4, 1970.
- [6] К. Стойков, “Проблеми при проектиране на захранващи устройства за електрически пещи”. Дисертация. София, 2012.
- [7] А. Дачев, “Програма за определяне на добавъчните загуби от вихрови токове в трансформаторни намотки от радиалното поле на разсейванес помощта на ЕЦИМ”. Електропромишленост и приборостроене, №4, 1976.
- [8] В. Аншин, В. Т. Мейксон, “Новые серии электропечных трансформаторов”. Электротехника, №3, 1973.
- [9] А. Дачев, Р. Дачева, Я. Бехар, “Листова намотка”. Авторско свидетелство № 27034/15.08.1979 г., Н.Р.България.

EQUATIONS FOR ELECTROMAGNETIC INDUCTION IN ELECTROMAGNETISM

Ivan Stefanov Bozev

Department of "Fundamental Training", Higher Schoolm, "College of Telecommunications
and Post", 1700, Sofia, "Academic Stefan Mladenov" № 1, Bulgaria,
phone: +359 2 181 8062, e-mail: IBozev@hctp.acad.bg

Abstract. *This paper discusses some existing differences in equations for electromagnetic induction. In some literary sources mentioned difficulties in describing the phenomenon in some specific cases. To achieve uniformity in the description of electromagnetic induction has introduced an additional parameter to describe the magnetic field outside of Maxwell's equations. The introduction of the additional parameter allows an unambiguous description of the phenomenon. Examined the impact of the introduction of the new parameter to the existing equations in this area (the expressions describing electromagnetic induction, the Coulomb - Lorentz force, the magnetic vector potential and transmission of electromagnetic energy).*

Keywords: *electromagnetic induction, Maxwell equations, Coulomb-Lorentz force, magnetic vector potential, Poynting vector.*

1. INTRODUCTION

The description of a phenomenon used a mathematical model must be unambiguous and complete. This means that all specific situations should be described by equations of the model without problems and controversy. In several articles published controversial mathematical model to describe electromagnetic induction. In order to describe the electromagnetic field to eliminate controversial points need to be analyzed and to be completed mathematical model in such a way that the existing contradictions eliminated.

2. PROBLEM STATEMENT

The electromagnetic field is described by Maxwell's equations according to [1] (IEV 121-11-62), representing a set of equations relating the four vector quantities determining the electromagnetic field in a material medium or in vacuum and the two quantities electric current density and volumic electric charge set of equations relating the four vector quantities determining the electromagnetic field in a material medium or in vacuum and the two quantities electric current density and volumic electric charge

The Maxwell equations expressed in differential form are:

$$\operatorname{rot} \vec{E} = -\frac{\partial \vec{B}}{\partial t}; \quad \operatorname{div} \vec{D} = \rho; \quad (1a,b)$$

$$\operatorname{rot} \vec{H} = \vec{J} + \frac{\partial \vec{D}}{\partial t}; \quad \operatorname{div} \vec{B} = 0. \quad (2a,b)$$

Where rot and div denote the rotation and the divergence respectively, \vec{E} , \vec{D} , \vec{H} and \vec{B} are the four vector quantities determining the electromagnetic field, \vec{J} is the electric current density, ρ is the volumic electric charge and t is the time. The Maxwell equations completely define the electromagnetic field in a given medium only together with the relations characterizing the medium. In the case of linear medium these parameters are permeability- μ , permittivity- ε and conductivity - γ of the medium. The Maxwell equations expressed in integral form are:

$$\oint_C \vec{E} \cdot d\vec{l} = -\frac{d}{dt} \int_S \vec{B} \cdot d\vec{s}; \quad \oint_S \vec{D} \cdot d\vec{s} = Q; \quad (3a,b)$$

$$\oint_{\partial S} \vec{H} \cdot d\vec{l} = I_{encl} + \frac{d}{dt} \int_S \vec{D} \cdot d\vec{s}; \quad \oint_S \vec{B} \cdot d\vec{s} = 0. \quad (4a,b)$$

In these equations are respectively assigned: l is the contour limiting surface S and hence closed surface S .

Originally Maxwell's equations are 20 and include both integral and differential description. As used in the standard equations have been proposed by Heaviside later, they were divided into differential and integral.

It is considered that the differential and integral form of equations are equivalent, which means that each situation from equations in integral form can be described by differential quantities. Nevertheless, a number of publications showing the specific situations impossibility to describe certain cases with the specified variables and differential equations.

Subject of this report is the analysis of the equations relating to electromagnetic induction. In differential form we have

$$\operatorname{rot} \vec{E} = -\frac{d\vec{B}}{dt}. \quad (5)$$

In an integral form the dependence is

$$\oint_C \vec{E} \cdot d\vec{l} = -\frac{d}{dt} \oint_S \vec{B} \cdot d\vec{s} = -\frac{d\Phi_S}{dt} \quad (6)$$

and is known as the integral form of Faraday's law.

At the left side of (6) is usually valid only for closed loop.

When moving conductor in a magnetic field is also used the equation:

$$\vec{E} = (\vec{v} \times \vec{B}), \quad U_i = (\vec{v} \times \vec{B}) \cdot \vec{l}$$

for which is said to be a consequence from the integral form of Faraday's law.

The presence of a number of cases in which a formula is not an exact solution to a practical setting means that the mathematical model is limited, and in some situations you are unable to account for certain conditions. This is indicated in some of the literature [3], [4], [7]. In the other half think that these are two separate phenomena - driving electromagnetic induction and electromagnetic induction for amending covered magnetic flux [2], [5]. To make a complete mathematical model is needed for any specific situations to satisfy all dependencies used by the model.

In the literature cited most often seen combination of mobile and stationary parts of the loop in contact with each other through the brush in a constant magnetic field.

Individual cases considered can be grouped into four groups:

1. Contour of the fixed and movable part stationary magnetic field with brushes attached to the movable part (Fig. 1). In this case, the movable part is in the form of lead sheet to four cases may be displayed with similar figures. Loop formed by the way in wire between stationary brushes and the straight line between the brushes of wire in the form of sheet. The movement of the movable part of x_1 to x_2 with speed \vec{v} electromagnetic induction is given by the following relations

$$U_i = -\frac{d\Phi_o}{dt} = -\frac{d\Phi_k}{dt} = vBl \tag{7}$$

You can see that this is a classic case of a generator in which the rate of change of magnetic flux Φ_o covered from contour is equal to the speed of change of the truncated magnetic flux Φ_k from contour and thus is equal to vBl .

2. Contour of two fixed parts stationary magnetic field brushes moving from x_1 to x_2 with speed v (Fig. 2).

$$U_i = 0 = -\frac{d\Phi_k}{dt} = 0 \cdot B \cdot l \neq -\frac{d\Phi_o}{dt} \tag{8}$$

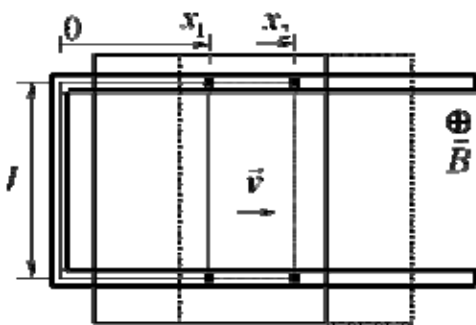


Fig.1

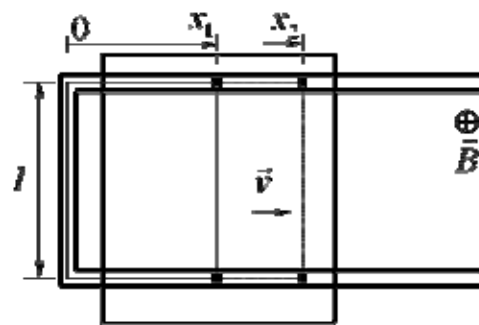


Fig.2

This case has no practical application, but it shows that there is a discrepancy between the induced voltage and the rate of change of magnetic flux covered.

3. Contour of the fixed and movable part stationary magnetic field with brushes attached to the fixed part (Fig. 3).

$$U_i = -\frac{d\Phi_k}{dt} = B \cdot v \cdot l \neq -\frac{d\Phi_o}{dt} = 0. \tag{9}$$

This is the case of the unipolar machine and is often cited as a paradox because no change of magnetic flux covered and there induced voltage. The case is a combination of the first two cases.

4. Contour of the fixed and movable part stationary magnetic field with varying brush position in mobile and fixed parts (Fig. 4).

$$U_i = -\frac{d\Phi_k}{dt} = v \cdot B \cdot l \neq -\frac{d\Phi_o}{dt} \neq 0 \tag{10}$$

This case is a combination of the above three cases.

From the analysis of the expressions for induced voltage in the above case shows that it is always proportional to the rate of change of magnetic flux truncated from the boundaries of the loop.

The rate of change of magnetic flux covered by the contour in the presence of movable contacts in it, do not generally correspond to the induced voltage in the circuit.

In literature there are many papers and analyzing complex situations, including modification of the magnetic field, but in this case there is no need to dwell on them.

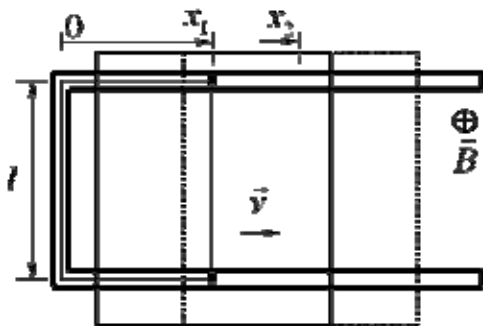


Fig.3

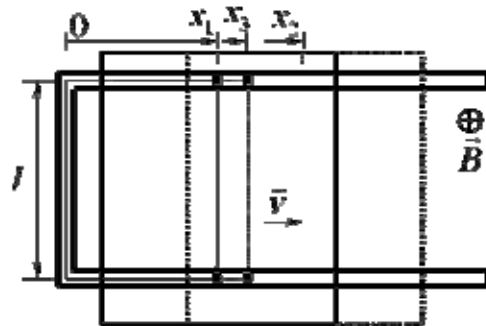


Fig.4

In references [6] and [7] described a paradoxical situation in which it is said that there is no logical description in the literature to date and concerns the induced tension in the conductors of classical generator placed in the channels of the rotor. On Figure 5 shows the main variables and parameters necessary to describe the induced voltage.

In engineering calculations to determine the induced voltage is used the expression

$$U_i = 2v_p B_0 l \tag{11}$$

Where B_0 is the magnetic flux density in the air gap, v_p is the peripheral speed of the rotor and l is the active length of the wires in the channel. Is multiplied by two, because it is reported that the turn is formed by two lengths. In the case working with induced voltage in a one turn.

Although the formula part of the magnetic flux density, which is the average of the differential type, the formula is an integral type, because it determines the magnetic flux covered by the loop

$$\frac{d\Phi}{dt} = 2v_p B_0 l.$$

The formula $U_i = 2v_p B_0 l$ will be differential type, if the parameters are differential parameters along the contour (wire), i.e.

$$U_i = 2v_c B_c l \tag{12}$$

Where B_c is the magnetic flux density in the wire, v_c is the wire speed in the case accept that matches the v_p .

Paradoxically, spoken of here is that the magnetic flux density in the conductor is B_c but is not B_0 . Value B_c is much less than that B_0 and does not match the value of the induced voltage.

$$U_i = 2v_p B_0 l \neq 2v_p B_c l \tag{13}$$

Let us analyze in more detail the expression for the value of the induced voltage in accordance with Fig. 5.

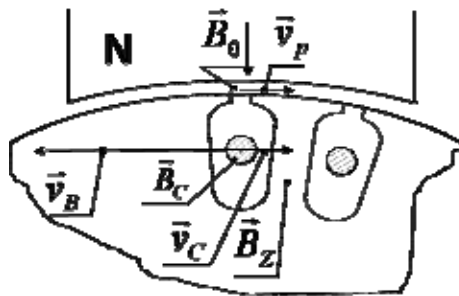


Fig.5.

When the relative permeability of the magnetic material of the rotor is μ_r , for the values of the magnetic flux density in the tooth B_z and in the channel (conductor) B_c we have:

$$B_z = \frac{2(\mu_r - 1)}{\mu_r} B_0; \quad B_c = \frac{2}{\mu_r} B_0. \tag{14}$$

Given the above dependencies and practical value of $\mu_r \cong 1000$ shows that there a big difference in determining the induced voltage with B_0 and B_c .

$$U_i = 2v_p B_0 l = 500(2v_p B_C l) \neq 2v_p B_C l \quad (15)$$

i.e. result is obtained, which is 500 times greater than that obtained from the classical formula for the induced voltage. This means that the formula is not a realistic mathematical model of the phenomenon described.

Let us consider a situation in which the conductor is stationary ($v_C = 0$) and the rotor moves in the space around the conductor in the channel with peripheral speed v_p . The example is practically realizable, despite being specific. In this case it appears that the value of the induced voltage should be zero in accordance with the formula for the induced voltage in differential form and reaffirms incorrect mathematical description.

There must be a mathematical model that provides an accurate relation between the differential parameters of the electromagnetic field and the value of the induced voltage.

Magnetic lines of force, in accordance with Faraday's ideas are uninterrupted lines. The rotor winding wires crossed them and covered them magnetic flux changes. When the rotor rotates, if we have to preserve the continuity of the magnetic lines of force is necessary in the mathematical model to introduce an additional speed v_B of transverse moving of the magnetic lines of force in the channel. In our sample case, the relationship between the peripheral speed of the rotor v_p and the transverse speed v_B of the magnetic lines of force in the channel is given by the equation:

$$\vec{v}_B = -\vec{v}_p (\mu_r - 1), \quad (16)$$

where assumed that the relative permeability in the channel (the material of the conductor and the insulation material) is equal to one.

Taking into account the expression (16), expression (13) gets the following form:

$$U_i = 2v_p B_0 l = 2(v_p - v_B) B_C l = 2\{v_p + v_p (\mu_r - 1)\} B_C l = 2\{v_C - v_p (\mu_r - 1)\} B_C l. \quad (17)$$

If we analyze the above relation is established:

1. Induced voltage is the sum of two composing, one of which is proportional to the speed of crossing of magnetic lines of force due to the movement of the conductor in the magnetic field. The second is proportional to the speed of crossing conductor of cross displacement of the lines of force $\{-\vec{v}_p (\mu_r - 1)\}$. Induced voltage is proportional to the rate of change of magnetic flux crossed by the contour.

2. Assuming $\mu_r = 1$, then $B_C = B_0$ and the analysis is restricted to rotation of a frame in the magnetic field in which there is no movement of flux of the magnetic field. Induced voltage is proportional to the rate of change of the crossed magnetic flux from the contour.

3. Assuming that $v_C = 0$, equation (17) determines the value of the induced voltage and it is again proportional to the rate of change of crossed magnetic flux from

the contour due to cross movement of the magnetic lines of force with speed $\{v_B = -v_p(\mu_r - 1)\}$.

Of the examples shown here that the induced voltage is always proportional to the rate of change of crossed magnetic flux from the contour.

For a more complete description of the electromagnetic induction phenomenon is necessary to introduce additional characteristic of the magnetic field, expressing velocity v_B of moving magnetic lines of force in the space.

According to IEV ref 121-11-19 magnetic flux density \vec{B} is defined as a vector field in which a moving charged particle with velocity v and with charge q acting force $\vec{F} = q\vec{v} \cdot \vec{B}$. In the so-defined vector field vectors \vec{B} have applied point, size and orientation in the space. They are not attributed to a transverse velocity v_B that reflects the possibility of transverse movement in the space of the magnetic lines of force (the expression is only valid for static magnetic field). In the scientific literature, the author has not encountered a description of the magnetic field to use v_B .

Using v_B for the characterization of time varying or space varying magnetic field can be justified with the help of Stokes' theorem used in the form of integral equations (3) of the Maxwell, known as the integral form of Faraday's law (6).

$$\oint_C \vec{E} \cdot d\vec{l} = -\frac{d}{dt} \oint_S \vec{B} \cdot d\vec{s} = -\frac{d\Phi_S}{dt}$$

The magnetic field is solenoidal field. The amendment to the flux Φ_S , piercing the surface S , bounded by the loop C at the expense of flux loop crossed.

Magnetic lines of force are closed lines may be inside the loop (covered by the contour), only cross it, or if there were to leave the loop to cross it. In other words, change the covered magnetic flux by the loop is equal to the truncated magnetic flux. In solenoidal field increases the density of the flux at a point in the expense ratio of the magnetic lines of force around it (movement of magnetic lines of force to it), a reduction of the magnetic flux density at a point at the expense of diluting the magnetic field lines around it (moving away the magnetic lines of force of it). In solenoidal field increases the density of the flux \vec{B} at a point in the expense compression ratio of the magnetic lines of force around it (movement of magnetic lines of force to it), a reduction of the magnetic flux density at a point at the expense of diluting the magnetic lines of force around it (moving away the magnetic lines of force of it).

Apparent from the above analysis shows that the transverse movement v_B of the magnetic lines of force is characteristic of any time-varying or space-varying magnetic field. Transverse motion v_B of magnetic lines of force is measurable (physical effects-rise- \vec{E}). Moving along the lines of force themselves is indistinguishable (not create a measurable physical effect).

Introducing v_B allows for a more complete description of the magnetic field in which most of the paradoxes discussed in the literature obtain unambiguous descrip-

tion of both differential and integral in kind.

If in (6) introduce the speed of transverse movement of the magnetic lines of force, we get differential description of the field strength \vec{E} along the loop C :

$$\oint_C \vec{E} \cdot d\vec{l} = \oint_C (\vec{v}_C - \vec{v}_B) \times \vec{B} \cdot d\vec{l} = -\frac{d}{dt} \oint_S \vec{B} \cdot d\vec{s} = -\frac{d\Phi_S}{dt}, \quad (18)$$

where \vec{B} , \vec{v}_C and \vec{v}_B are the values of the quantities at the point of the element $d\vec{l}$.

In case of a stationary loop we have:

$$\oint_C \vec{E} \cdot d\vec{l} = \oint_C (-\vec{v}_B) \times \vec{B} \cdot d\vec{l} = -\frac{d}{dt} \oint_S \vec{B} \cdot d\vec{s} = -\frac{d\Phi_S}{dt}$$

From the above expressions can be concluded that the generality law of electromagnetic induction in differential form is

$$\vec{E} = (\vec{v}_C - \vec{v}_B) \times \vec{B}. \quad (19)$$

If we take the left equality of (18)

$$\oint_C \vec{E} \cdot d\vec{l} = \oint_C (\vec{v}_C - \vec{v}_B) \times \vec{B} \cdot d\vec{l},$$

and because the right side of above equation is valid for any point of the circuit, we can write it in the form:

$$\int_{a(C)}^b \vec{E} \cdot d\vec{l} = \int_{a(C)}^b (\vec{v}_C - \vec{v}_B) \times \vec{B} \cdot d\vec{l}$$

IEV ref 121-11-20, Coulomb-Lorentz force \vec{F} exerted on a particle having electric charge q and velocity \vec{v} , given by the:

$$\vec{F} = q(\vec{E} + \vec{v} \times \vec{B}). \quad (20)$$

In this case, the expression is only valid for static magnetic field. If the magnetic field is variable over time, or moved in space, equation (20) yields the form:

$$\vec{F} = q(\vec{E}_Q + (\vec{v} - \vec{v}_B) \times \vec{B}), \quad (21)$$

where the electric field strength \vec{E}_Q is a result of charge Q . The compound $(\vec{v}_B \times \vec{B})$ is expressed as equivalent electric field.

The assumption that the magnetic field can be moved in space, this means that it carries its moving energy.

In (IEV ref 121-11-64) electromagnetic energy is given by:

$$\frac{1}{2} \int_V (\vec{E} \cdot \vec{D} + \vec{H} \cdot \vec{B}) dV$$

If in determining the flow of electromagnetic energy transfer approach analogous theorem of Umov [9], the transfer of energy only where there is movement (flow). Flows of energy transfer in the electromagnetic field in our sample case are two, total current and transverse displacement of the magnetic flux.

Electromagnetic power transmitted through the surface S can be defined as:

$$\vec{P}_S = \int_S \left\{ V \cdot \vec{j}_t + \vec{H} \cdot (\vec{v}_B \times \vec{B}) \right\} d\vec{s}. \quad (22)$$

where V is the electric potential, $\vec{j}_t = \vec{j} + \vec{j}_D$ - the total current density, \vec{j} - conduction current density and \vec{j}_D is the displacement current density.

In areas, where $\vec{j}_t = 0$, electromagnetic energy is transferred entirely magnetic way. In areas, where $\vec{v}_B = 0$, electromagnetic energy is transferred completely electrically.

Certainly the expression (22) differs from (IEV ref 121-11-66), where with the help of Poyting vector can be defined power passing through a closed surface.

If you convert the second term of the expression (22)

$$\vec{H} \cdot (\vec{v}_B \times \vec{B}) = \vec{H} \cdot \vec{E}_\mu,$$

shows that similar expression Poyting vector, but here \vec{E}_μ is the ingredient strength of the electric field due to transverse movement \vec{v}_B of the magnetic field.

According to 121-11-28 induced voltage is scalar quantity equal to the line integral of a vector quantity along a path C from point a to point b in which charge carriers can be displaced:

$$U_i = \int_{r_a(C)}^{r_b} \left(-\frac{\partial \vec{A}}{\partial t} + \vec{v} \times \vec{B} \right) \cdot d\vec{r}, \quad (23)$$

where \vec{A} and \vec{B} are respectively a magnetic vector potential and the magnetic flux density at a point $d\vec{r}$ of the path (C), \vec{v} is the velocity with which that point is moving, \vec{r} is position vector, and t is the time

The induced voltage is equal to the time derivative of the linked flux corresponding to the path.

The above formula does not account for transverse movement of the magnetic field. Taking into account equation (19), equation (23) yields species.

$$U_i = \int_{r_a(C)}^{r_b} \{(\vec{v} - \vec{v}_B) \times \vec{B}\} \cdot d\vec{r}. \quad (24)$$

On the other hand we know that the magnetic vector potential (IEV ref 121-11-23) is chosen so that $r\vec{\partial}t\vec{A} = \vec{B}$. To reflect the effects of transverse movement of the magnetic field is necessary to add a suitable compound that contains no rotation. Each time variable magnetic flux contains only one central line of force for which $\vec{v}_{BC} = 0$. For changing magnetic flux in time, other lines of force are concentrate (dilute) around it. With circular symmetry velocity at a point is proportional to a distance from this point to the fixed line of force and radially oriented. The transverse movement of the magnetic field in space is given by the speed of the central line of force $\vec{v}_{BC} \neq 0$. In this case, \vec{v}_B at a given point is the sum of the two speeds $\vec{v}_B = \vec{v}_{BC} + v_{BR}$.

The concept of "linked flux" in IEV ref 121-11-24 acquires the meaning of a truncated flow, and this truncated flow can be determined for each part of a curve, not only for loop.

In consideration of the quantity equations (1.2) can be represented in the following manner:

In consideration of the quantity \vec{v}_B to the equations (1), (2) can be represented in the following manner:

$$\vec{E} = (-\vec{v}_B \times \vec{B}), \quad \text{div}\vec{D} = \rho; \quad (25a)$$

$$r\vec{\partial}t\vec{H} = \vec{J} + \frac{\partial\vec{D}}{\partial t}; \quad \text{div}\vec{B} = 0; \quad (25b)$$

In this case, the component $\vec{E} = (-\vec{v}_B \times \vec{B})$ reflects the impact of the changing magnetic field (the phenomenon of electromagnetic induction). Expression (1a)

$r\vec{\partial}t\vec{E} = -\frac{\partial\vec{B}}{\partial t}$ is contained in equation (25a).

3. RESULTS

The article reviewed and systematized some problems from the literature to describe the phenomenon of electromagnetic induction. As a result, proposed an additional parameter describing the magnetic field. It is shown that any variable in space and time characterized magnetic field at any point in the magnetic flux density \vec{B} and an additional parameter \vec{v}_B – the rate of moving transverse to the magnetic lines of force. Additional characteristic allow for clear and complete description of the phenomenon of electromagnetic induction.

Examined the impact of the introduced feature in Maxwell's equations and expressions describing electromagnetic induction, the Coulomb-Lorentz force, magnetic vector potential and transmission of electromagnetic energy.

References

- [1] IEC 60050, International Electrotechnical Vocabulary (IEV): Area: 121: Electromagnetism, Section 121-11: Electromagnetic concepts and quantities.
- [2] Feynman R, Leighton R, and Sands M. *The Feynman Lectures on Physics* . 3 volumes 1964, 1966.
- [3] John David Jackson. *Classical Electrodynamics*. Third Edition. 1998.
- [4] G. Giuliani A general law for electromagnetic induction. *A Letters Journal Exploring the Frontiers of Physics*. 81 (2008) 60002.
- [5] E. Benedetto, M Capriolo, A Feoli and D Tucci. A little help for a better understanding and application of Faraday's law. 2012. *Eur. J. Phys.* **33**, L15 <http://stacks.iop.org/EJP/33/L15>
- [6] Bruce DePalma. *Where Electrical Science Went Wrong*. 1993. <http://depalma.pair.com/index.html>
- [7] Николаев Г. В. *Современная электродинамика и причины ее парадоксальности*. Томск. 2003 г.
- [8] Н. Умов. *Уравнения движения энергии в телах*. Одеса. 1874г.

BEHAVIORAL SPICE MODELING OF PHOTOVOLTAIC CELLS

*Elissaveta Dimitrova Gadjeva, Dimitar Yordanov Shikalanov**

Department of Electronics, Technical University of Sofia,
8 Kliment Ohridski Blvd., 1000 Sofia, Bulgaria,
phone +395 2 3725, e-mail: egadjeva@tu-sofia.bg

*Department of Informatics, New Bulgarian University,
Montevideo 21 Str., 1635 Sofia, Bulgaria, e-mail: dys@nbu.bg

Abstract. *In the present paper, behavioral computer SPICE model of photovoltaic cells is developed. The model parameters are automatically calculated using datasheet data. The temperature dependence of the model parameters is taken into account. The model is built as parameterized block. The input data are the short circuit current I_{sc} , the open circuit voltage V_{oc} and two remarkable points from the flat segments of the IV characteristic from the datasheet. A validation of the model is performed based on datasheet data of the PV cell and the accuracy of the model is investigated. The computer realization is performed in the Cadence Capture and Cadence PSpice environment.*

Keywords: *Photovoltaic cell, Behavioral model, PSpice simulator, Parameter determination, Temperature dependent parameters, Parameterized block*

1. INTRODUCTION

The photovoltaic cells and modules are of significant importance for the design of photovoltaic (PV) power systems. A number of computer models and parameter extraction procedures are proposed in [1-5].

In the present paper, behavioral computer SPICE models of photovoltaic cells are developed. The model parameters are automatically calculated using datasheet data. The temperature dependence of the model parameters is taken into account. The model is built as parameterized block. The input data are the short circuit current I_{sc} , the open circuit voltage V_{oc} and two remarkable points from the flat segments of the IV characteristic from the datasheet. A validation of the model is performed based on datasheet data of the PV cell and the accuracy of the model is investigated. The computer realization is performed in the *Cadence Capture* and *Cadence PSpice* environment.

2. PARAMETER EXTRACTION PROCEDURE

The equivalent circuit of the photovoltaic module consisting of N_s PV cells connected in series, is shown in Fig. 1.

The PV current I is described by the following equation:

$$I = I_{ph} - I_o \left(e^{\frac{V+IR_s}{A_1}} - 1 \right) - \frac{V + IR_s}{R_p} ; \quad A_1 = AN_s V_T ; \quad V_T = \frac{kT}{q}. \quad (1)$$

$G_p = 1/R_p$ is obtained for low voltages from the flat segment of IV characteristic (Fig. 2), where the diode current I_d and the voltage across R_s are neglected.

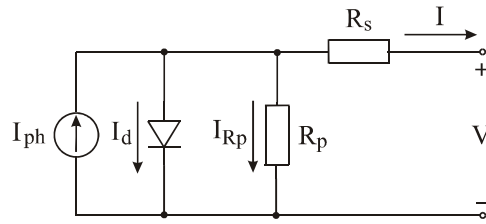


Fig. 1. Equivalent circuit of PV module

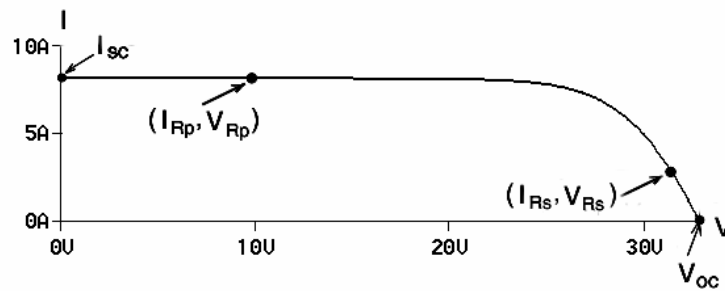


Fig. 2. Remarkable points of the IV characteristic for the model parameter determination

From (1)

$$I \approx I_{ph} - \frac{V}{R_p} ; \quad R_p = \frac{1}{G_p} ; \quad G_p = \left(\frac{dI}{dV} \right)_{V=0} . \tag{2}$$

The derivative G_p is calculated in the range $[0, V_{Rp}]$, which defines the flat part of the IV characteristic. As a result, the approximate value $R_{p,a}$ is obtained:

$$R_{p,a} = \frac{V_{Rp}}{I_{sc,dsh} - I_{Rp}} . \tag{3}$$

The description according to the input language of the *PSpice* simulator has the form:

$$Rp_a = \{VRp / (Isc_dsh - I_{Rp})\}$$

The approximate value $I_{o,a}$ is obtained from (1) for $I = 0$ and $V = V_{oc}$ in the form:

$$I_{o,a} = \frac{I_{ph} - \frac{V_{oc,dsh}}{R_p}}{e^{A_1} - 1} . \tag{4}$$

$I_{o,a}$ is calculated according to (4) using the following expressions according to the input language of the *PSpice* simulator:

$$A1 = \{A * N_s * 0.027\}$$

$$I_{o_a} = \{(I_{ph} - V_{oc_dsh} / R_{p_a}) / (\exp(V_{oc_dsh} / A1) - 1)\}$$

R_s is obtained using the slope of the IV characteristic near V_{oc} . The following equation is used:

$$V = R_s I + V_d, \tag{5}$$

where V_d is the diode voltage.

After differentiation of (5) with respect to I , the equation

$$R_s = R_{sV} - R_{sd} \tag{6}$$

is obtained, where

$$R_{sV} = \left. \frac{dV}{dI} \right|_{V=V_{oc}} = - \left(\left. \frac{dI}{dV} \right) \right|_{V=V_{oc}}^{-1}, \tag{7}$$

$$R_{sd} = \left. \frac{dV_d}{dI} \right|_{V=V_{oc}} = - \left(\left. \frac{dI}{dV_d} \right) \right|_{V=V_{oc}}^{-1} = \frac{A_1}{I_{oc} e^{A_1} \frac{V_{oc}}{A_1}}. \tag{8}$$

The approximate values $R_{sV,a}$, $R_{sd,a}$ and $R_{s,a}$ are obtained from the IV characteristic in the form:

$$R_{sV,a} = \frac{V_{oc,dsh} - V_{Rs}}{I_{Rs}}; \quad R_{sd,a} = \frac{A_1}{I_{o,a} e^{A_1} \frac{V_{oc,dsh}}{A_1}}; \quad R_{s,a} = R_{sV,a} - R_{sd,a} \tag{9}$$

The computer realization has the form:

$$RsV_a = \{(V_{oc_dsh} - V_{Rs}) / I_{Rs}\}$$

$$Rsd_a = \{A1 / (I_{o_a} * \exp(V_{oc_dsh} / A1))\}$$

$$Rs_a = \{RsV_a - Rsd_a\}$$

The parameterized model of the PV module consisting of N_s PV cells connected in series, is shown in Fig. 3.

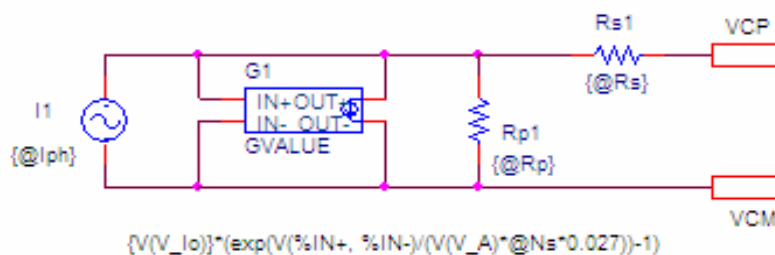


Fig. 3. Parameterized model of the PV module

The determination of the values of model parameters is realized using PARAMETERS statement (Fig. 4).

```

PARAMETERS:
Isc_dsh = 8.21A
VRp = 10V
IRp = 8.1856A
Rp_a = {VRp/(Isc_dsh-IRp)}
A1 = {A*Ns*0.027}
Voc_dsh = 32.9V
Io_a = {(Iph-Voc_dsh/Rp_a)/(exp(Voc_dsh/A1)-1)}

VRs = 32
IRs = 1.8516A
Vmpp_dsh = 26.2V
Impp_dsh = 7.5679
RsV_a = {(Voc_dsh-VRs)/IRs}
Rsd_a = {A1/(Io_a*exp(Voc_dsh/A1))}
Rs_a = {RsV_a-Rsd_a}

```

Fig. 4. The determination of the model parameters

The simulation result for the IV characteristic of the solar array KC200GT is shown in Fig. 5. The characteristic 1 (dashed line) corresponds to the datasheet data. The simulated characteristic 2 (solid line) is obtained by the calculated parameter values using remarkable points of the IV characteristic (Fig. 1). They match very closely the datasheet data.

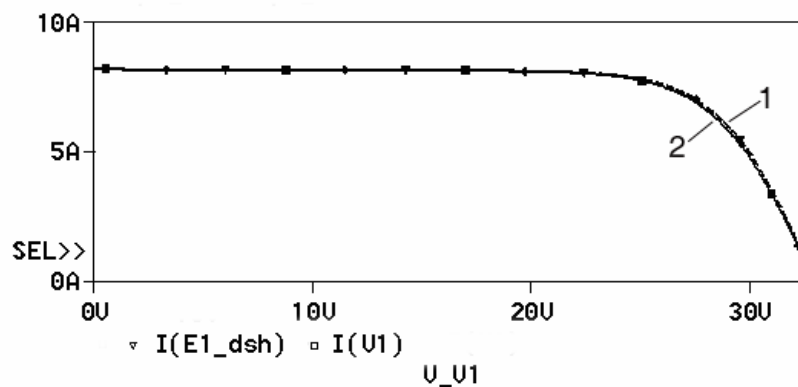


Fig. 5. Comparison of the simulation results with the datasheet characteristic

3. CONCLUSION

Behavioral SPICE models of photovoltaic cells have been developed. The model parameters are automatically calculated using four remarkable points data from the IV characteristic. The model is built in Capture as parameterized block. The input data are the short circuit current I_{sc} , the open circuit voltage V_{oc} and two points from the flat segments of the IV characteristic from the datasheet. A validation of the model is performed based on datasheet data of the PV cell and the accuracy of the model is investigated.

Acknowledgement

The investigations are supported by the project № DTK 02/50/17.12.2009.

References

- [1] H-L., Tsai, Ci-Siang Tu, Yi-Jie Su. Development of generalized photovoltaic model using MATLAB/SIMULINK, Proceedings of the World Congress on Engineering and Computer Science 2008, WCECS 2008, October 22 - 24, San Francisco, USA, 2008.
- [2] R. Hernanz, C. Martín, J. J. Belver, L. Lesaka, Z. Guerrero, E. Puelles Pérez. Modelling of photovoltaic module, International Conference on Renewable Energies and Power Quality, (ICREPQ'10) Granada (Spain), 23th to 25th March, 2010.
- [3] D. Sera, R. Teodorescu, P. Rodriguez. PV panel model based on datasheet values, IEEE International Symposium on Industrial Electronics, ISIE 2007, June 4-7 2007, Vigo, Spain, ISBN: 978-1-4244-0754-5, pp. 2392-2396, 2007.
- [4] R. K. Nema, Savita Nema, Gayatri Agnihotri. Computer Simulation Based Study of Photovoltaic Cells/Modules and their Experimental Verification, International Journal of Recent Trends in Engineering, Vol 1, No. 3, May 2009
- [5] M. G. Villalva, J. R. Gazoli, E. R. Filho. Comprehensive Approach to Modeling and Simulation of Photovoltaic Arrays, IEEE Transactions on Power Electronics, v. 24, n. 5, 1198 – 1208, May 2009.

IMPLEMENTATION OF “POWER QUALITY TEACHING TOY” (PSL) IN THE EDUCATIONAL PROCESS IN BULGARIA

Nikolay Gourov¹⁾, George Milushev²⁾

¹⁾Department of Electrical Measurements, Technical University - Sofia, 8 Kl. Ohridski Blvd., 1000 - Sofia, Bulgaria, phone: +359 2 965 23 66, e-mail: nrg@tu-sofia.bg

²⁾Department of Electrical Measurements, Technical University - Sofia, 8 Kl. Ohridski Blvd., 1000 - Sofia, Bulgaria, phone: +359 2 965 23 80, e-mail: gm@tu-sofia.bg

Abstract. *The attractive simulation “Power Quality Teaching Toy” aimed to help visually understanding the single and three phase power quality problems. It has been translated on Bulgarian by a team from Electrical Measurements Department of TU-Sofia and was implemented in the educational process for the first time during the last educational year. The results were better understanding by the students the physical effects of different events and controls, as well as the harmonics influence. The team plan to propose to PSL and to Mr. Alex McEachern personally, to add the Bulgarian translation to the web-published versions of PQTT.*

Keywords: *Interactive education, Self study, Power quality, Electrical power supply, Software simulation*

1. INTRODUCTION

Nowadays, more and more traditional teaching methods are replaced by interactive. Trainees from object of the educational process where they passively listen and watch what the teacher, read and then learned it respectively increasingly become the subject of training where they self-solve problems creatively and work individually on specific projects. Accordingly, the teacher does not provide ready knowledge and serves as a kind of filter for the useful knowledge but incite students and helps them to find their own solutions by participating actively in the learning process.

This tendency is particularly facilitated by the introduction of information technologies in education. They allow relatively easy to create training programs with interactive activities that simulate real-life situations and help students to be innovative and learn about real situations that rarely occur in practice, is difficult to find and can not be ordered optionally.

In the case of electrical energy efficiency during design and commissioning activities and for the evaluation of the power quality electrical quality analyzers are used. They are complex and relatively expensive instruments whose use must be preceded by training of personnel for safety, proper use of equipment, its setting and grid connection.

The physical nature of the processes and problems in three-phase systems, their understanding and their repeated replay to analyze, require visual simulation in real or laboratory medium.

Any malfunction of the electrical power supply raises discrepancy of the parameters of electricity, which ensure the normal operation of equipment and are defined as parameters of power quality. Simulation and reproduction of such discrepancies is sometimes difficult, expensive and resource-intensive task.

The most inexpensive and yet very useful option is software simulations. In this case the software is fully responsible to simulate and demonstrate on the computer display various changes of parameters of electricity. This helps students to understand the most common causes of malfunctions and to get used to diagnose them quickly and without mistakes. Thus they learn better how to react in different situations they may encounter in practice.

2. “POWER QUALITY TEACHING TOY” IN THE BULGARIAN LANGUAGE EDUCATION ON POWER QUALITY

An example of such a product is a software simulator Power Quality Teaching Toy developed by Power Standards Lab (PSL). It is accessible and comprehensive tool for simulation of almost any possible discrepancies in power systems. Due to these qualities the software was fully translated into Bulgarian and steps had took to the PSL for the official recognition of translation and respectively its inclusion in future versions of the program.

Fig. 1 shows the main screen of the program. From this screen relevant sub-screens can be chosen through which students become acquainted to various aspects of power quality. They can vary different parameters and watch clearly how this affects the shape of the voltage, current, etc.



Fig. 1

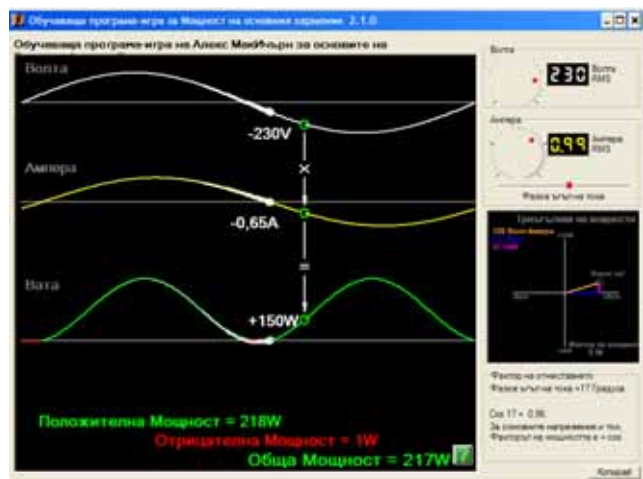


Fig. 2

On Fig. 2 is depicted "Fundamental power flow" screen. Here students can watch how the amplitudes of current and voltage and the phase angle of the current influence the power. They may vary the three parameters and monitor the change of the curves and power triangle diagram (active, reactive and full). The power factor is calculated on this screen too.

Fig. 3 shows the screen “Fundamental sequence vectors“. Here students can explore virtually balanced, unbalanced and phase-to-phase system. They can show or hide the main neutral, to see the influence of the magnitudes of different sequences (positive, negative and zero), the influence of the relative angle of the negative and zero sequence. They may also hide or show the vector sum.

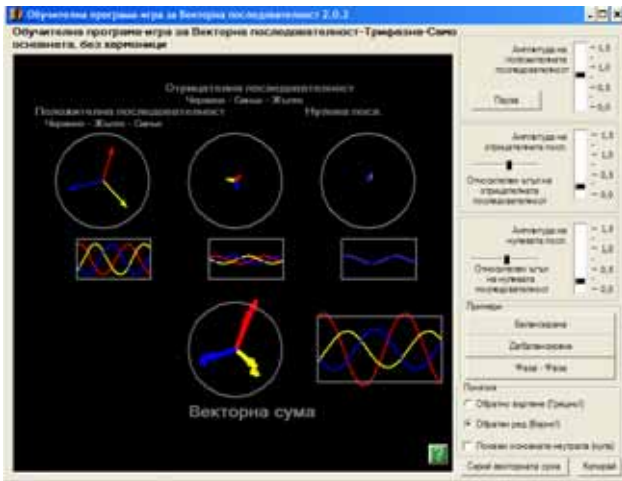


Fig. 3

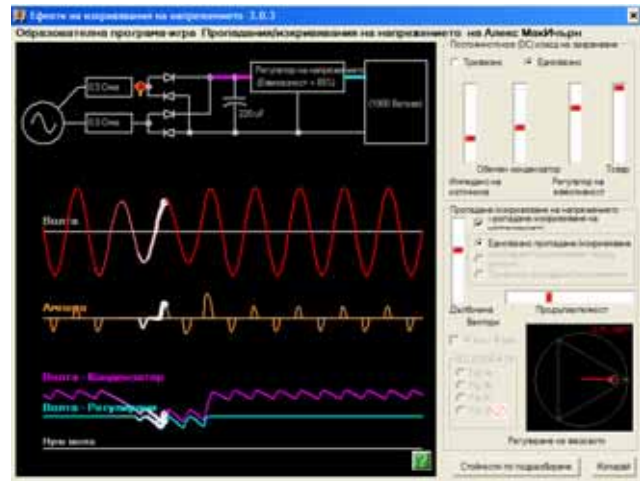


Fig. 4

On Fig. 4 is depicted screen “Voltage Dip/Sag Effects“. It can simulate single phase/three phase power supply, hide (show) voltage dip/sag respectively for single and three phase power. There are options for adjusting the amplitude and/or duration of dip/sag, show (hide) the vector phase to phase. Here students can see various figures from the standard IEC 61000-4-34.



Fig. 5

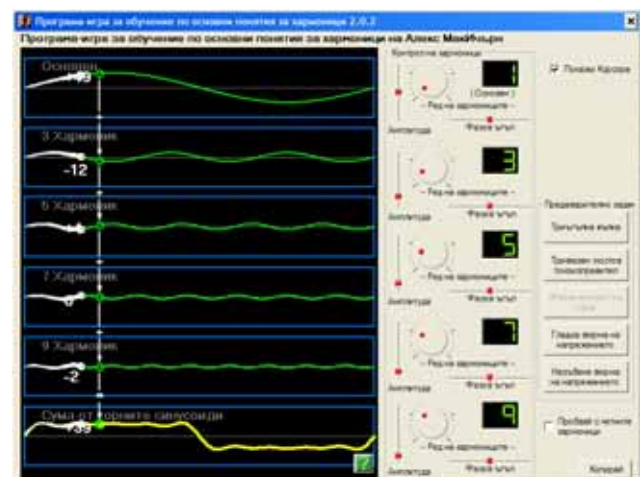


Fig. 6

On Fig. 5 is shown the screen "Flicker". Here students can regulate the amplitude and frequency of the flicker and see how it affects the perception of it. It should be noted that the screen can be annoying migraine headaches and is not advisable to be viewed by people with epileptic seizures.

Fig. 6 depicts the screen “Harmonics concept”. Here odd and even harmonics can be traced; amplitude and phase angle of harmonics can be varied. Students can watch pre-set waveforms. It is possible to show (hide) the cursor.

Fig. 7 presents the screen “Harmonic power flow” The screen is similar to the “Fundamental power flow” but here except changing the amplitude of voltage and current, and changing the phase angle of the current is possible to choose the order of harmonic currents and show (hide) cursor.

On Fig. 8 is shown screen “Harmonic sequencing”. Here students can choose harmonic order to visualize the sequence of harmonics. Showing (hiding) of cursor is possible.

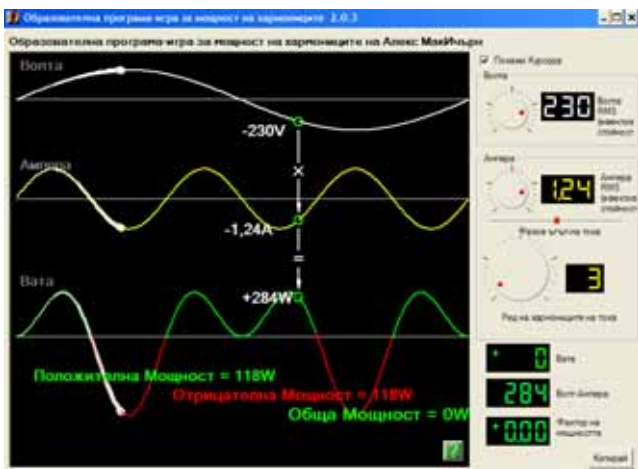


Fig. 7

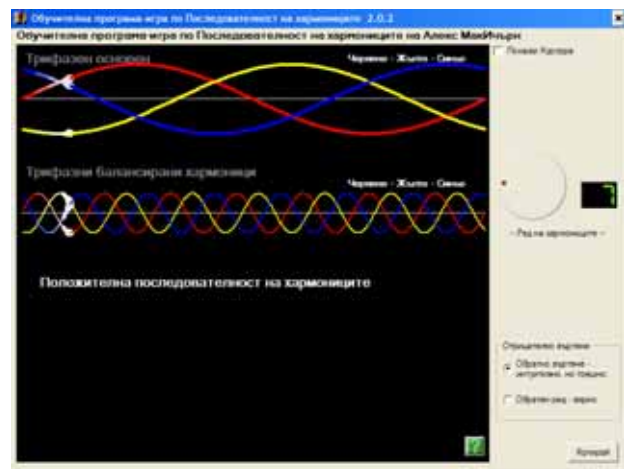


Fig. 8

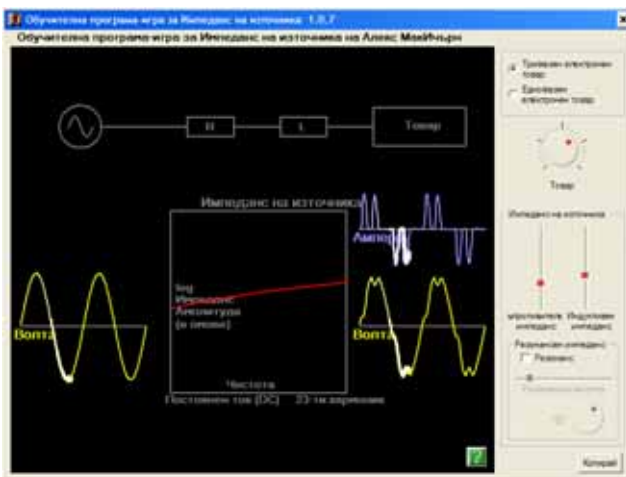


Fig. 9

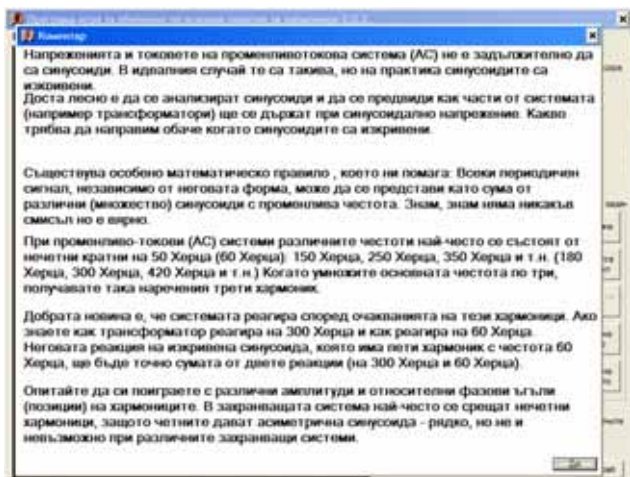


Fig. 10

Fig. 9 depicts screen “Source impedance and distortion”. The type (three-phase electronic and single phase electronic) of the load can be chosen. Varying the source impedance (resistive and inductive) is possible. Simulation of the resonance impedance as well as varying the resonant frequency and Q-factor are possible too.

Each screen has a corresponding help screen through which the user can familiarize himself with the basics and dependencies related to a preview of a screen. Access

to help screens is possible by clicking on icon with depicted question mark (?) on every screen. Sample help screen (to screen “Harmonic concepts”) are shown on Fig. 10.

3. CONCLUSION

The paper is devoted to the application in the educational process in Bulgaria of the software simulator named “Power Quality Teaching Toy” developed by Power Standards Lab. The program is completely translated into Bulgarian language and all necessary steps had taken for the translation to be included in future official releases of the software.

Using the program, students can actually learn about various aspects of power quality without physical simulation of related processes (or wait for their actual occurrence in practice). Users can see the real impact of different parameters on power quality and realize in practice how main electrical quantities are changing when these parameters are varying.

References

- [1] <http://www.wisegeek.com/what-is-interactive-learning.htm>, as visited on 15.09.2012
- [2] <http://www.powerstandards.com/PQTeachingToyIndex.php>, as visited on 15.09.2012

THE E-LEARNING OF THEORETICAL ELECTRICAL ENGINEERING

Tsvetomir Dobrev, Rosen Pasarelski, Teodora Pasarelska

Department Telecommunications, New Bulgarian University, Street: Montevideo No10,
1610 Sofia, Bulgaria, phone: +3592 81619 e-mail: telecom@nbu.bg
e-mail: ts.dobrev@gmail.com; rpasarelski@mail.bg; tedy_54@abv.bg

Abstract: *One of more important tasks of technology in education is to influence creativity upon the studying practice, to work out methods based on science and to reach some definite didactic aims. Learning role in the technology of education in telecommunications is the lab studies and e-learning which comes of the specificity of that definite science – the theoretical electrical engineering. In these lab studies the theoretical knowledge is put under a check and is also hardened. In New Bulgarian University (NBU), teaching theoretical electronics is combined with practice that motivates the students and urges them to see connection between the theory and the practice. The organization and the way of practicing as a part of these practical courses in the program of the Telecommunications Department at NBU are considered in this article.*

Key words: *Laboratorial studies, technology in e-learning, organization the education of the theoretical electric engineering.*

1. INTRODUCTION

One of more important tasks of technology in education is to influence creativity upon the studying practice, to work out methods based on science and to reach some definite didactic aims. Learning role in the technology of education in telecommunications is the lab studies and e-learning which comes of the specificity of that definite science – the theoretical electrical engineering. In these lab studies the theoretical knowledge is put under a check and is also hardened. At the same time, during these lab studies lots of questions appear and the students are trying to give appropriate answers all by themselves. In this way they form a sense of scientific work and develop some interests which, most of the time, are wider than these in the schedules. Through e-learning the students develop their thinking abilities and they also acquire a habit of organizing practical training. For example, in our university – The NBU, there is an e-learning system named “Moodile”. Using this system, the students are able to read their lectures and try to give appropriate answers to the questions. The e-learning help students to acquire a good habit for organizing their education process and more specifically in the field of theoretical electrical engineering. In NBU, teaching theoretical electronics is combined with practice that motivates the students and urges them to see connection between the theory and the practice [1]. The organization and the way of practicing as a part of these practical courses in the program of the Telecommunications Department at NBU are considered in this article.

2. ADVANTAGES OF E-LEARNING AND HIS INTRODUCTION FOR THE PURPOSES OF TRAINING IN THEORETICAL ELECTRONICS

The development of e-learning products and the provision of e-learning opportunities is the one of the most rapidly expanding areas of education and training, not only as a testing method, but also as a leading in the training of students and students in different disciplines. A significant problem at this moment occurs in the implementation of the electronic training in this discipline, because ignorance assesses the methods and approaches in future developments.

In substance, the electronic training assisted development of the training and allowed students to seek resources necessary in educational process. Today e-learning, as a known - "is-learning" - is on the path to displace and improve the traditional training. It is very popular in disciplines such as computer technologies and telecommunications.

Unfortunately evaluation and measurement methods are not so popular in Bulgaria, but in the course of time they are being monitored in several universities. The advantages of this way of evaluation can not be considered either little or minor. In the era of high technology and the rapid pace of development of computer technology, we are prone to develop ways of assessment, such as e-learning. The rich tools we have now give us the opportunity not only to integrate the e-assessment but to develop to such an extent that to become a referable way for both students and teachers.

The ways for the electronic evaluation are different and depend on both software program and the teacher. During the electronic course, it must be taken into account the number of the trainees and the way that they evaluate the students. In addition to all the above the teacher has to considerate the type and the specification of the discipline. It is also important to analyze the mindset of the students, whether they will considerate these kind of evaluation. In most cases, such an approach would have been profitable, not only in the training in theoretical electronics, but in other disciplines. This leads to both win the audience and the students. There are other ways of electronic assessment which can be representing in universities if they want. At this time there are both paper works and projects which are the main type of evaluation. Considering the new age, the electronic training would lead to minimize the discontent of the students and also would make them to decide whether they would like to take a test and to receive their grades in home. We are striving to achieve these results applying e-learning not only in theoretical electronics but also in other disciplines.

Another advantage of the introduction of e-learning is that we can make real connection with the professor or the teacher we want in real time. This will lead to a reduction of pointless standing in lecturer rooms in universities [3], [4].

3. RESULTS OF THE INTRODUCTION OF E- LEARNING IN STUDYING THE THEORETICAL ELECTRONICS

Theoretical training in electronics should establish regular evaluation of the students that will help them during their training. It is also good to introduce laboratory

(practical) forms of learning theory to course as a NBU and the opportunity to work with real equipment. In this way, students will be encouraged to do something good for yourself, which would bring them dividends in the form of assessments and would help them with their development in the field of computer science and telecommunications. "Periodic evaluation" shall mean continuous assessment during the learning process conducted by the teacher in what form he chooses – practical, written or electronic form. Whatever form teacher to choose it would be appropriate to include the electronic form, because she will give the student the opportunity to prepare himself considering that he already has the lectures of the course uploaded on Internet. Materials uploaded to Internet assist for the development of thinking. Students must synthesize and process the information in such that it can help them in evaluating or in the future. Thanks to the e-learning the development of the students is better because it leads not only to autodidaction but also to retrieve and learn useful information.

Bottom you can see the results of the latest survey of students at NBU where e-learning was introduced 10 years ago and it developed every year more and more. In the study involved students from the Department of Telecommunications 120 people, mainly first and second year, who have passed training in theoretical electronics [2].

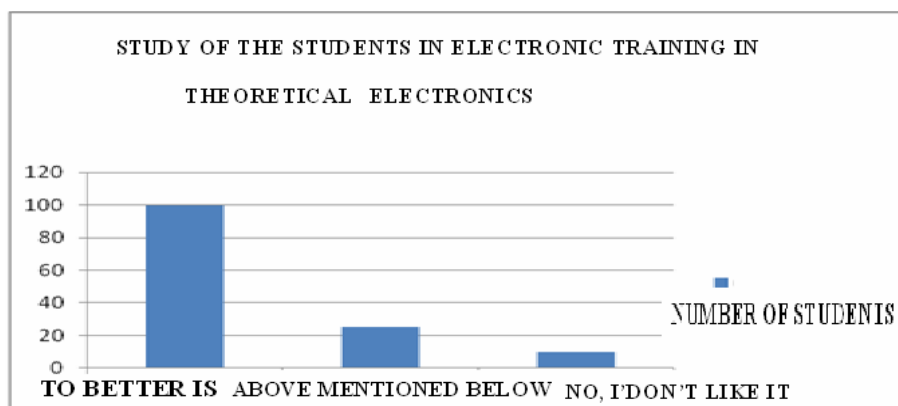


Fig. 1. Graphics, showing the satisfaction of the students of electronic training from the Department of "Telecommunications" - Theoretical electronics

From the graph we understand that the majority of the respondents fully agreed with the introduction of e-learning. They believe that it helps them learn the material better and enables them to acquire specific technical and professional skills. However, it should not be left in the background the current measurement, as it leads students to discipline. Forcing them to attend lectures and practical activities that in our University are required and desirable, teachers gain vision for each student and see what its development is and what to emphasize, in case they have not understood what is important.

For students, it is important to see the meaning of their visit to the lectures and exercises, with this in mind the assessment may be multi. That said, consider the following: for example, if you enter such assessment must have several components that students need to be evaluated.

For example: **T1** (*current assessment 1*) - control work;
T2 (*current assessment 2*) - exchange work;
T3 (*current estimate 3*) - discussion.

Another option for evaluation is as follows: T1 (coursework), T2 (discussion), T3 (practical training). The most profitable and the best is suitable third option, which you can see below. Option three assessment in TE – T1 (electronic test), T2 (discussion), T3 (practical task). Under this option, the student is allowed to decide between an electronic test that may be of material that has been taken to date, or is fixed in advance by the teacher in the discipline, in the case of - TE. It also allows, in attendance of the lectures to get a score, depending on whether he is active or not. The third but not least - the practical task which develops thinking technical skills and to apply in practice, what learned in theory.

Moreover, thus allowing the student to self-analysis, self-assessment and to give an opinion, either during the lecture or in electronic form. Based on this we can see that e-learning should become the number one goal, at the start of a given year and to discuss how to assess for training - Theoretical electronics [2].

As we know, according to traditional didactic, organizational learning is a form of education, which involves collaboration between educators and learners to build knowledge and skills to apply them in the learning process of the students. This is appropriate in order to be processed information from learners and this so complicated dynamic process to be most effective. Thanks to the introduction of e-learning in the process of studying the subject - Theoretical electronics, there is a better success rate of students. As this is achieved, thanks to the unlimited access of internet and integrated learning environment. E-learning in general has both advantages and disadvantages [2], [3].

ADVANTAGES OF E-LEARNING

- ✓ Individualization of training
- ✓ Quick and easy access to the requested information
- ✓ Ability to group assessment and training
- ✓ Evaluation of results achieved in the year of the process of training
- ✓ Opportunity for access to the educational content, at any time Communication between trainees and exchanging opinions and comments, during the training process
- ✓ Minimize the cost of training.

Precisely the construction of e-learning induce us to speak about On-line learning, Web-based learning, virtual classrooms and universities, "digital" cooperation and technology support to DE (Distance Education). Thanks to e-learning, as some call it and transposition into the learning process and in the technical disciplines, but more closely in learning - Theoretical electronics - not only helps the process of studying the subject, but it enriches it. This is due to the many opportunities facing students

(learners), that changing the status quo and implementing rational and imaginative thinking in students, giving them the opportunity to apply what they have learned in theory, in a laboratory environment (during practice) and electronically.

E-learning is not only new to the technical disciplines but to all of the educational systems in our country. It is with this distinguished, NBU, who has introduced e-learning in all subjects 10 years ago, we can make a comparison – Before / After its introduction. That is why e-learning and its approaches are very important to the development of the training programs and structuring the curriculum in which students will be trained not only in theoretical electronics, but in general [3].

4. CONCLUSION

In conclusion we can say that the implementation of e-learning in the training of Theoretical Electronics has to previously analyze the attitudes of the students, to develop approaches to facilitate teachers and students. This requires the development of the training programs to provide those options - to introduce lectures and other aids century integrated electronic environment that also serve to help students. Furthermore, e-learning serves as the introduction of multimedia files and other like, through which facilitates the learning and reducing the cost. Also, introduction of integrated electronic learning environment leads to innovative teaching methods and the introduction of new method of assessment in higher education [2], [3].

References

- [1] T. Stefanova – part of presentation “The learning of the telecommunications”, Department of “Telecommunications”, New Bulgarian University, 2009.
- [2] R. Pasarelski – part of lectures "Training of the telecommunications", Department of “Telecommunications”, New Bulgarian University, 2011.
- [3] T. Dobrev – part of scientific development "E-learning of the telecommunications", Department of “Telecommunications”, New Bulgarian University, 2012.
- [4] T. Pasarelska – part of lectures "Training of the telecommunications", Department of “Telecommunications”, New Bulgarian University, 2011.

ОПТИМИЗИРАНЕ НА ОРГАНИЗАЦИЯТА ПРИ ПРОВЕЖДАНЕТО И НА РЕЗУЛТАТИТЕ ОТ ОЛИМПИАДИТЕ ПО ТЕОРЕТИЧНА ЕЛЕКТРОТЕХНИКА СЪС СТУДЕНТИТЕ ОТ ЕЛЕКТРОТЕХНИЧЕСКИТЕ СПЕЦИАЛНОСТИ НА ТЕХНИЧЕСКИТЕ ВУЗ

Таня Методиева Стоянова¹, Георги Рашков Георгиев²,

^{1,2}Катедра “Теоретична и измервателна електротехника”,

РУ “Ангел Кънчев”, ул. „Студентска” №8

тел.: ¹(00359 82) 888 502, ²(00359 82) 888 412

e-mail: ¹tstoyanova@uni-ruse.bg, ²grashkov@uni-ruse.bg

Резюме: В публикацията се разглеждат въпроси, свързани с оптимизиране на организацията и на резултатите от провеждането на Олимпиади по Теоретична електротехника (ТЕ) със студентите от електротехническите специалности на техническите ВУЗ (Вътрешни и Републикански кръгове). Ползността от провеждането на такива олимпиади със студентите е безспорно и необходимостта от тяхното провеждане си остава. Олимпиадите допринасят за значителното повишаване на нивото на знанията по дисциплината Теоретична електротехника, която е базова за студентите от електротехническите специалности, при тяхното обучението в Образователно-квалификационната степен “Бакалавър”.

Олимпиадите създават и засилват състезателния дух у студентите в съответния ВУЗ и между отделните ВУЗ-ове. Събуждат интереса на състезателите към по-нататъшно активно участие, както в няколко поредни олимпиади по ТЕ, така и към студентските научни сесии, към международните проекти. Дават още и допълнителна възможност за получаване на информация за нивото на обучение на студентите в отделните ВУЗ и стремежът на всеки от тях да го подобрява във всяко отношение.

Ключови думи: Олимпиада по Теоретична електротехника, Вътрешни кръгове, Републикански кръг

1. ВЪВЕДЕНИЕ

Тази публикацията е продължение на предходна такава [1], която разглежда влиянието, необходимостта и полезните резултати от провеждането на Олимпиади по Теоретична електротехника със студентите от електро-техническите специалности на техническите ВУЗ (Вътрешни и Републикански кръгове). Провеждането на такава олимпиада е безспорно полезно, както за допълнителната подготовка на студентите, така и за по-голям интерес към дисциплината Теоретична електротехника, която е базова за студентите от електротехническите специалности при тяхното обучението в Образователно-квалификационната степен “Бакалавър”. Изучаването ѝ в първи и втори курс от една страна затруднява състезателите, защото още не са придобили достатъчно базови знания.

Допълнителните сбирки за подготовка на участниците в олимпиадите дават възможност за натрупване у тях на повече знания, както по Теоретична електротехника, така и по прилаганата в нея математика. Трябва да се отчете и участието в тези сбирки на значително по-големия брой студенти, отколкото е броят на състезателите в Републиканските кръгове.

2. СЪСТОЯНИЕ НА ПРОБЛЕМА – ВЪТРЕШНИ КРЪГОВЕ, РЕПУБЛИКАНСКИ КРЪГОВЕ – ОРГАНИЗАЦИЯ, ТЕМАТИКА, ПОДГОТОВКА, ПОДБОР НА УЧАСТНИЦИТЕ

Организатори на Републиканския кръг на Олимпиадата по ТЕ в съответната учебна година са преподавателите от катедрата по ТЕ на ВУЗ-а домакин, определен на ротационен принцип предходната година от участниците в нея. Подготовката започва с изпращане на официални покани от ВУЗ-а домакин, до катедрите по ТЕ на всички технически ВУЗ-ове в България. В тези покани се публикуват вече утвърдени от всички досегашни участници:

- правила за провеждане на Републиканското състезание;
- тематика на Републиканската студентска олимпиада (PCO) по ТЕ;
- правила за проверка и оценяване на работата на състезателите, както и за тяхното класиране;
- график за даване на предложенията на съответните ВУЗ-ове за техни членове на проверяващото жури;
- правила за подготовка на вариант за задачи за PCO по ТЕ от всеки ВУЗ-участник.

Тематиката на Олимпиадата е по избрани раздели от материала, изучаван по дисциплината Теоретична електротехника от студентите от електротехническите специалности на техническите ВУЗ-ове. Те са посочени в поканата, изпратена от ВУЗ-а домакин. На PCO по ТЕ студентите решават три задачи от тези раздели. Условието на задачите са предложени от ВУЗ-овете, участници в PCO. Сутринта, преди започването на Републиканския кръг, журито ги групира във варианти по подходящ начин, така че да се избегне всякаква субективност. Случайно подбран състезател изтегля един от тези варианти, в присъствието на останалите участници в състезанието, което е анонимно като конкурсен изпит. След приключване на състезанието журито, което се състои от три комисии (за всяка от задачите има отделна комисия), включващи преподаватели от различни ВУЗ-ове, проверява работите на състезателите и класира участниците индивидуално и по отбори. Във всеки отбор участват пет студента, но в неговия състезателен бал се включват точките само на първите четирима състезатели, с максимален брой точки. Победителите до трето място в двете класации получават материални награди и грамоти, осигурени от ВУЗ-а домакин.

Републиканският кръг на Студентската олимпиада по дисциплината ТЕ се провежда обикновено през месец май на текущата учебна година. ВУЗ-ът дома-

кин предлага датата за провеждане на РСО по ТЕ и посочва дата, до която останалите ВУЗ-ове трябва да дадат своето съгласие. Когато всички тези въпроси се изяснят, домакинът съставя програмата за провеждане на състезанието и я изпраща на останалите ВУЗ-ове.

Подготовката на своите състезатели всеки ВУЗ прави сам, като това се осъществява от преподаватели по ТЕ от едноименните катедри чрез провеждане на допълнителни занятия. Подборът на участниците и селекцията им в отборите става след провеждане на Вътрешни кръгове, които са обикновено два. Те предхождат Републиканския кръг.

За подобряване на организацията по провеждането на РСО по ТЕ би било по-добре:

- изпращането на официалните покани от ВУЗ-а домакин, до катедрите по ТЕ на всички технически ВУЗ-ове в България да стане най-късно до средата на месец декември от текущата учебна година;
- правилата за провеждане на Републиканското състезание, свързани с броя на състезателите в отборите, проверката и оценяването на състезателите, както и за тяхното класиране, да се спазват стриктно и да не им се правят, макар и частични промени по време на текущото състезание;
- необходима е по-голяма съгласуваност между ВУЗ-овете по отношение на вариантите на задачите за Републиканския кръг. Съдържанието на тези задачи трябва да съответства на тематиката, обявена в официалната покана, но не е необходимо да се фиксират методите, по които могат да бъдат решавани тези задачи;
- би трябвало да отпадне ограничението участниците в РСО по ТЕ да са студенти само до трети курс на обучение на бакалавърската степен, а да могат да участват и четвъртокурсници, ако те желаят.

Оказва се, че провеждането на Олимпиадата по ТЕ през месец май води до прекомерно натоварване, както на студентите, така и на преподавателите по ТЕ. От една страна е свързано с провеждането на много мероприятия едновременно – Студентски научни сесии, олимпиади по Математика и Програмиране и още форуми, отнасящи се към Майските празници на науката и техниката. От друга страна тогава е и краят на летния семестър на студентите-бакалаври. Освен това различните ВУЗ-ове имат различни графици на учебния си процес. Необходимо и възможно е да се съгласуват ВУЗ-овете и да се определи по-подходящ период, например месец април. Затова се налага ВУЗ-ът домакин да направи проучване по този въпрос още със започването на текущата учебна година и да предложи варианти за дата за РСО по ТЕ. Своето мнение по този въпрос ВУЗ-овете-участници трябва да изложат до края на месец ноември на текущата учебна година, така че официалната покана да бъде направена навреме.

3. РЕЗУЛТАТИ

Провеждането на РСО по ТЕ има безспорни и полезни резултати:

– Организираните допълнителни занятия по ТЕ със студенти, подготвяни за участие в Олимпиадата по ТЕ, повишава тяхната подготовка по дисциплината Теоретична електротехника и засилва интереса им към нея, особено като се има предвид, че по учебен план часовете по ТЕ стават все по-малко и се преместват все по-напред в обучението на бакалаврите [1, 2, 3]. Студентите, които участват в допълнителната подготовка, са по-голям брой от състезателите в отборите и са едно сериозно ядро в студентската общност;

– Създава се състезателен дух у участниците в Олимпиадите по ТЕ, както по време на Вътрешните кръгове, така и на Републиканския кръг;

– Увеличаването на знанията на студентите по ТЕ е предпоставка и за разширяването на базата на техните знания, необходима както за следващите електротехнически предмети (като Електрически измервания, Полупроводникови елементи и т.н.), така и за формирането им като специалисти.

– Стимулира вече участвали студенти в една Олимпиада, да участват и в следващи такива.

– Предизвиква поява на интерес у студентите към изследователската работа и следващо тяхно участие в Научни конференции и други форуми. След като завършат магистърската си степен на обучение, много бивши състезатели в РСО по ТЕ, се насочат към участие в конкурси за докторанти и асистенти, както по ТЕ, така и по други изучавани вече от тях дисциплини по време на тяхното обучение;

– Събужда се интересът на тези студенти и към участие в международни проекти;

– При Републиканския кръг се осъществяват контакти както между студентите от различните технически ВУЗ-ове, така и между техните преподаватели по ТЕ. Така става възможно да бъде получена допълнителна информация за обучението както по ТЕ, така и по други изучавани дисциплини, за обучението и базата на ВУЗ-а домакин. Дава се възможност да се „сверяват часовниците“ по много страни на обучението в техническите ВУЗ-ове в България. Получава се един много полезен обмен на опит.

– В разговорите и дискусиите по време на самите Олимпиади, които не се ограничават само в рамките на няколко състезателни часа, се получава много полезно взаимно опознаване, както и уеднаквяване на позициите по важни проблеми, едно сплотяване на колегията. То е много полезно при възникване на дебати в образователната система и защитата на общите позиции.

4. ИЗВОДИ

1. Републикански и Вътрешни кръгове на Олимпиади по Теоретична електротехника трябва да се провеждат, защото води до получаването на редица по-

ложителни резултати в образователно, методично, научно и социално направление.

2. Подобряването на организацията и технологията на провеждане на Олимпиадите по ТЕ трябва да е постоянен приоритет както на домакините, така и на всички участници.

3. Създадената вече доста дълголетна традиция трябва да бъде съхранена, за да бъде здрава основа на обучението по Теоретична електротехника.

Литература

- [1] Стоянова, Т. М., Г. Р. Георгиев, В. М. Младенов. Влияние, необходимост и полезни резултати от провеждането на Олимпиади по Теоретична електротехника със студентите от електротехническите специалности на техническите ВУЗ, Sozopol 19...22 Sept 2010., *Advanced Aspects of Theoretical Electrical Engineering*, Part 1, Sozopol, Bulgaria, pp. 148...151, ISSN: 1313-9479, 2010.
- [2] http://www.uni-ruse.bg/ECTS_package/New/Erasmus_ECTS_InfoPack_FEEA_Bg.pdf
- [3] <http://fa.tu-sofia.bg>

CREATION OF REGIONAL ELECTRIC TRANSMISSION NETWORK MODELS BY USING DATABASE RELATED SOFTWARE SOLUTION

Petar Krstevski, Rubin Taleski, Jordancho Angelov, Aleksandra Krkoleva, Kliment Naumoski, Aleksandar Paunoski

¹Power Systems Department, Faculty of Electrical Engineering and Information Technologies
Ss Cyril and Methodius University, Rugjer Boskovic bb, 1000 Skopje

Republic of Macedonia

²AD MEPSO, Orce Nikolov bb, 1000 Skopje

Republic of Macedonia

Abstract. *The newest trends of regional electricity markets development and integration, creation of large continental electricity grids which will incorporate renewable power sources, highlight the need for using of regional electric transmission models for load flow calculations in many different analyses.*

This paper shows a database related software solution which enables creation of regional network models from national network models. This solution is developed in the framework of the European FP7 project SEETSOC [1] as Model Creator for Day Ahead Congestion Forecast as part of the Transmission System Planning & Operation Tool application [2]. It also includes creation of forecasted network models on a base of existing models, and network model data preparation for load flow calculations. This proposed solution is developed in coordination with the Transmission System Operators from South Eastern Europe and is adapted to its requirements.

Keywords: *transmission network, load flow*

1. INTRODUCTION

According to the European Strategic Energy Technology Plan [3] and the European Electricity Grid Initiative [4] the main aims for further development of the electricity grids in Europe are: enabling transmission and distribution of up to 35% of electricity from renewable power sources, creation of integrated pan-European Electricity Market, optimization of the electric power system operational costs and increasing the security supply. In order to achieve these goals efficient performing of different types of power system analyses and procedures is required. The integration of renewable energy sources into transmission networks requires advanced power system planning studies. The integration of the electricity markets is impeded by the congestion at the interconnection lines between countries and it is dependent of the Congestion Management procedures [5,6] and the increasement of the cross border transmission capacity by interconnection lines construction. The security of supply is also dependent of the transmission networks reliability.

All of the above mentioned analyses and procedures comprise load flow calculations and they cannot be performed only on a national level using the transmission

network model of one country and network model equivalents for the neighboring networks, because of the increased exchange of power between countries, the increased number of interconnecting power lines etc.

Today transmission network models covering multiple countries in a region are used for Congestion Management in the cross border capacity calculation and allocation and Day-Ahead Congestion Forecast (DACF) coordinated procedures [7,8], performed by the transmission system operators in the European Network of Transmission System Operators for Electricity (ENTSO-E).

The software solution presented in this paper is developed for creation of regional forecasted network models for DACF but it can be used for other purposes described above. The solution enables import or export of network models from UCTE Data Exchange Format (UCTE-DEF) [9], which is standard format used for network model description and exchange in ENTSO-E.

2. MODEL CREATOR FOR DACF

The Model Creator is developed as a database related software solution, which is a new approach, and enables management with the network models on an easy manner [10,11]. The solution provides storage of different national and regional network models and enables creation of regional network models by merging national network model, creation of forecasted network models, import and export to UCTE-DEF, model compare etc. It includes input data validation and advanced network topology check in order to eliminate possible errors in the models and to prepare them for load flow calculations.

The Model Creator module consists of the following sub modules:

- Format Converter & Storage Sub Module,
- Export Data Sub Module,
- Model Merger Sub Module,
- Model Builder Sub Module,
- Load Adjustment & Automated Model Generator Sub Module,
- Model Compare Sub Module.

The principle structure of the Model Creator is shown on Fig. 1.

As it is presented on Fig. 1 the database takes central place in this software solution, while the sub modules are performing different types of actions to the network data thus creating new network models.

The database is consisted of two data tables DB Input Tables and DB Output Tables. The DB Input Tables are used for storage of different network models, which can be: national or regional models - merged by using this software; forecasted or snapshot models – with data collected from SCADA. The structure of DB Input Tables is similar to the UCTE- DEF. The DB Output tables are used for storage of the data from the network models which are prepared for load flow calculation and its structure is adapted for the load flow calculation procedure.

The functionalities of the sub modules are described in the following sub sections.

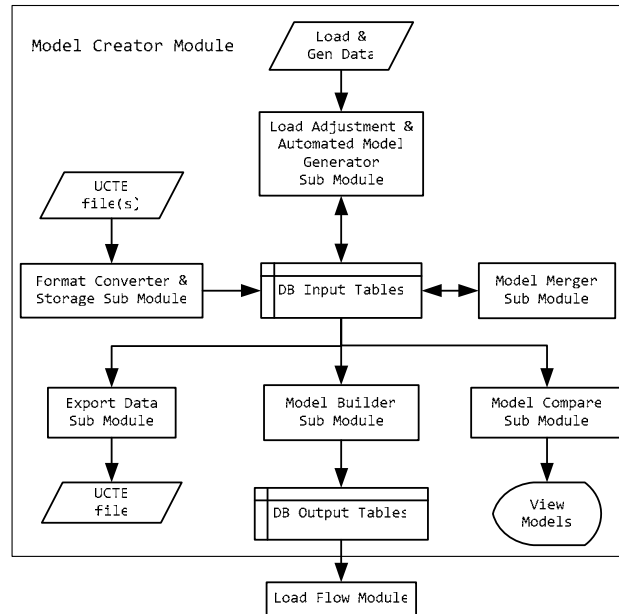


Fig. 1. Principle diagram of the Model Creator

2.1. Format Converter & Storage Sub Module

The Format Converter and Storage Sub Module provides connection between raw network model data contained in a UCTE-DEF formatted ASCII file and the DB Input Tables in the database. It reads one or more UCTE formatted files describing national or regional networks, incorporates error checking and warning mechanisms that check the validity of the input data and stores the data into the database for further use. In this procedure the code, date and the time of a network model are extracted from its file name and put into the database. This data is used for identification of different network models.

2.2. Export Data Sub Module

This sub module allows export of a selected network model from the database to UCTE-DEF file format. The selection of the model is done by the user by entering its code, date and time.

2.3. Model Merger Sub Module

The Model Merger Sub Module enables creation of regional network models by merging national network models. It is one of the most important features of the Model Creator alongside with the creation of forecasted models.

The model merging procedure starts with selection of multiple national network models from the DB Input Tables. The data from these models is put into a single dataset. Afterwards the connection of the networks is done at the bordering, so called X-nodes. In the connection process certain active power imbalance could appear in the merged network model. This imbalance is distributed at the boundaries of the re-

gion and the regional network model is finally created and written to the Input DB Tables [7].

In order to enable description of transmission networks which are part of greater synchronously interconnected power system and network model merging the UCTE-DEF includes definition of X -nodes as fictitious nodes located at the electric middle or at the geographical boundary on the interconnecting power lines [7]. When we want to represent a network which is a part of an interconnected power system the power flows at the interconnection lines are simulated by adding load or generation at the X -nodes. This way the active power balance of the model is maintained.

Because the exact power flows at the interconnection lines are not known before the creation of the merged network model and load flow calculation, often estimated values are set by the TSOs in its national network models as load and generation at X -nodes. The active power balance P_{BALQQ} of a national network QQ is equal to the sum of load minus generation at its X -nodes. It is positive if the country exports active power or negative if the country imports power and it can be calculated by using the following equation:

$$P_{BALQQ} = \sum_{i \in XQQ} (P_i - G_i) \quad (1)$$

where XQQ is a set of X -nodes at the national network model QQ .

Because estimated power flows at the interconnection lines are used sometimes different TSOs can use different flows in their models for the same interconnection line i.e. different injections for the same X -node. Therefore if the networks are simply connected at X -nodes an active power imbalance appears i.e. the power balance of the region calculated as sum of national balances of the countries from the region, differs from the sum of injected power at the X -nodes located on the boundary of the region. The X -nodes at the boundary of the region are known as non-paired X -nodes and marked as set XNP . This imbalance P_{ImBAL} can be calculated by the equation (2):

$$P_{ImBAL} = \sum_{j \in C} P_{BALj} - \sum_{i \in XNP} (P_i - G_i) \quad (2)$$

where C is the set of countries in the region.

In order to achieve active power balance in the merged regional network model this imbalance has to be somehow distributed to the non-paired X -nodes. The proposed software solution distributes the power imbalance over a subset of selected non-paired X -nodes XS and the distribution method is pro rata regarding to the previous (old) active power injection by using equation (3) [10,11].

$$\Delta P_i = P_{ImBAL} \cdot \frac{|(P_i^{old} - G_i^{old})|}{\sum_{j \in XS} |(P_j^{old} - G_j^{old})|}, i \in XS \quad (3)$$

If only loads with zero active power injections have been selected, the additional load would be distributed over selected nodes equally.

At the end of the merging procedure the status of both sections of each interconnection is checked. If the topology status is not equal for both sections, the whole interconnection line is switched off, as well as the corresponding X-node.

2.4. Model Builder Sub Module

The Model Builder Sub Module is used for preparation of the data from a model selected from DB Input Tables for load flow calculation. This sub module changes the data structure of a network model into a more suitable form for load flow calculations and performs different tests of the network model in order to ensure efficient and correct calculation of load flow.

For example, the data structure of the Input DB Tables is similar to UCTE- DEF and it contains different data tables for lines and transformers, also there are additional tables which describe the voltage regulation properties and tap position of a transformer etc. Therefore this data format is not appropriate for the load flow calculation which require list of branches with its equivalent parameters, no matter whether they are lines transformers etc. and list of nodes and its power injections.

This sub module includes the following functionalities in order to ensure efficient and correct calculation of load flow:

- small impedance branches and bus coupler elimination;
- topology check;
- node numbering (indexing), assigning index 0 to the global slack node;
- active power balance check;
- per unit conversion and calculation of line and transformers parameters;
- model data writing into the DB Output Tables.

2.5. Load Adjustment and Automated Model Generation Sub Module

The Load Adjustment and Automated Model Generator allows creation of forecasted national network models by using existing base network models from the database and input data from the user. This functionality is very important for DACF but it is also useful for cross border capacity calculation and power system planning studies.

Because the network elements parameters and the way they are connected are not changing in time the most of the network data for the forecasted network model can be taken from the, so called, base model. The other data that is changeable with time have to be provided by the user. In this software solution a special LAAMG CSV file format, for this purpose, was developed. The program enables creation of future network models for multiple hours during the day. The user should enter the following additional data for each hour:

- total system active power load,

- total active power import/export,
- active power generation at generation nodes,
- active power load at certain nodes,
- changes of network topology.

The LAAMG Sub Module is used in a three step procedure. In the first step, an empty LAAMG CSV file is created. It contains list of all generation and load nodes from the base model, but no data for the future load or generation.

In the second step, the data for total system active power load and total import or export, for each hour for the forecasted models, should be added to the LAAMG CSV file. Also the active power generation at each generation node should be entered from the generation schedule. The data for some load nodes can be added if it is available. For each load node without provided load for the forecasted model, the user sets whether the load data will be taken from the base model or to be adjusted *pro rata* in order to meet total system load. The changes of the network topology i.e. the switching of certain network elements should also be entered in the LAAMG CSV file.

In the third step the forecasted network models are created by using the data from the base scenario and from the LAAMG CSV file and written to DB Input Tables. More detailed information for the LAAMG CSV file format and the pro rata calculation of forecasted load is provided in [10,11].

2.5. Model Compare Sub Module

The Model Compare Sub Module enables visualization of the network model data and visual comparison of different network models. This is very useful when handling with many different network models in the database so the user can compare them and find similarities or differences between them.

3. CONCLUSION

From this paper we can conclude that the presented database related software solution for storage and creation of regional network models and forecasted network models could be very useful in the every day work of operational planning of the TSOs. The software facilitates the creation of network models for DACF, cross border capacity calculation and also it can be used for power system planning purposes. This solution can also be used for these purposes by researchers.

References

- [1] SEETSOC, FP7EN/239453, [Online]. Available: <http://seetsoc.ntua.gr/>
- [2] Open Transmission System Planning & Operation Tool, SEETSOC. [Online]. Available: <http://www.opentspot.com/>
- [3] European Strategic Energy Technology, [Online]. Available: http://ec.europa.eu/energy/technology/set_plan/set_plan_en.htm

- [4] European Electricity Grid Initiative [Online]. Available: <http://www.egi.eu/>
- [5] European Transmission System Operators (ETSO), "Evaluation of congestion management methods for cross-border transmission", Florence Regulators Meeting, November, 1999.
- [6] IAEW Aachen University of Technology, CONSENTEC, "Analysis of the Electricity Network Capacities and Identification of Congestion", Final Report, December 2001.
- [7] ENTSO-E, UCTE Operation Handbook, Appendix A4 - Policy P4: Coordinated Operational Planning, approved by the UCTE Steering Committee on 3 May, 2006.
- [8] UCTE: DACF Procedure, UCTE Annual Report, 2003.
- [9] UCTE Subgroup Network models and forecast tools: UCTE data exchange format for load flow and three phase short circuit studies (UCTE – DEF) Version 2.
- [10] V. Maldenov, M. Kostic, R. Taleski, N. Sijakovic: SEETSOC – Deliverable 5.2.2, December 2011.
- [11] P. Krstevski, J. Angelov, R. Taleski, A. Krkoleva, K. Naumoski, A. Paunoski, "Facilitating DACF by Implementation of Integrated Software Solutions", European Energy Market (EEM), 2012 9th International Conference on the, 10-12 May, 2012

SEETSOC RBM PROGRAMM –STRUCTURE AND IMPLEMENTATION

*Costin Cepisca, Alexandru Lazar, George Seritan,
Sorin Dan Grigorescu, Mircea Covrig*

Department of Electrical Measurements and Apparatus, University POLITEHNICA of Bucharest,
313 Splaiul Independentei, zip code 060042, Bucharest, Romania, phone: +4021-402 91 49,
e-mail: george.seritan@upb.ro

***Abstract.** The paper presents an overview of the Regional Balancing Systems designed for the South-East European regional energy market. We present the implementation of the server-side components that aggregate the participants' bids and schedule transactions according to the rules of the balancing mechanisms. A set of results on trial data is presented as a benchmark of the system, along with a short discussion of the main choices for implementation.*

***Keywords:** energy market, energy regulation, regional balancing*

1. INTRODUCTION

Set up of national day – ahead balancing mechanisms looks essential for the security of electricity supply in each country. National Balancing Mechanism (BM) is unavoidable market instrument for the Transmission System Operators (TSO) dispatching service for solving the power imbalances and network constraints in his control area. During the operating (delivery) day, the TSO balances the market and dispatches generation according to dispatch schedule. Intra – day deliveries on the BM is primarily meant to resolve the balancing needs of those Balance Responsible Parties (BRP) that are unable to meet their obligations.

The same phases can also be imagined for a regional context, where the schedules address cross – border power exchanges, with the important advantage [4]. The SEETSOC project addresses the needs of South-East European TSOs in harmonization and integration of the region with the rest of the European power network. One of objectives of project is design, development and testing of the regional balancing mechanism module (RBM) and his integration with all modules in the SEETSOC platform [1].

RBM procures up-ward regulation in power deficient area and down-ward regulation in power surplus area at Regional Market for Balancing Energy (RMBE) prices. RMBE is of interest, particularly, for releasing cross – border constraints (power flows kept at or below limits) and for the control areas with permanent/temporary weak balancing resources. Resolving deviations from Cross Border (CB) exchange schedule by seeking bids and offers via the RBM to reduce or increase generated output as appropriate would raise the question of additional capacity payment; this could be achieved by acquisition of ancillary System Services (SS) on the centralized national (regional) market prior to offering on the RMBE.

2. SEETSOC RBM PROGRAM

The SEETSOC RBM program is a set of software modules which implements the regional balance mechanisms used by market operators as the backbone of the energy market transactions. The RBM software solution for both the Day-Ahead and Intraday RMBE functions of the business process is described in the SEETSOC deliverable D5.1.2 – Software Implementation [2].

The RBM for both the day-ahead and intraday transactions determines the transaction volumes and payments resulting from the selected offers in a three – step procedure, namely:

- Placing of offers for each balancing interval and each balance energy type followed by their formal acceptance / rejection.
- Offer selection. A fixed and firm schedule bidding for the balance energy is carried out that ensures transaction selection and pricing, i.e. the establishment of regional market for balance energy clearing prices.
- Notification and transaction settlement. The schedule is executed during the dispatching day (D). For each balancing interval, the imbalance quantity – price pair is established based on the final dispatch order for the BE purchase.
- In order to support this three-step procedure, the RBM has to perform an additional set of tasks, such as:
 - Managing the users who are placing bids and performing transactions
 - Allowing the operators to monitor the transactions and record any difference between scheduled and delivered quantities
 - Generating reports of the performed transactions for the use of the operators

3. HOW DOES RBM SOFTWARE WORK?

For TSOs

The representatives of each TSO can submit bids to be considered for transactions, usually from the web interface accessible to them. The bids are encoded in a standard XML format, so they can be generated by any in-house tools compliant with the standard with only trivial modifications – but a reference implementation of such a graphical tool, which can also submit the offers by connecting directly to the server, is also provided [3], [4].

Once the bids are accepted, they enter the selection process and the representatives are notified if they were accepted for scheduling, as well as of any necessary change of delivery parameters. Representatives can also track the status of their bids in real-time, and have access to all the bids they have submitted through a simple web interface – figure 1.

ID	Ack Time	View	Accepted
1	2012-04-15 18:16:44	Click here to view	Yes
2	2012-04-15 18:17:04	Click here to view	Yes
None	2012-04-15 18:22:04	Click here to view	No
3	2012-04-15 18:22:08	Click here to view	Yes
4	2012-04-15 18:22:57	Click here to view	Yes
5	2012-04-15 18:23:13	Click here to view	Yes
6	2012-04-15 18:23:29	Click here to view	Yes
7	2012-04-15 18:51:09	Click here to view	Yes
8	2012-04-15 18:52:37	Click here to view	Yes
9	2012-04-15 19:14:10	Click here to view	Yes
10	2012-04-15 23:12:43	Click here to view	Yes

Copyright (c) UPB, 2010-2011

Fig. 1. User interface: viewing the bid history

For operators

Market operators can perform offer selection and scheduling from a dedicated interface, and can keep the delivery statuses up-to-date using a simple web interface. As scheduled transactions are performed, they can generate the required payment information.

Operators can also perform user management functions as well as various maintenance operations which are required for the smooth functioning of the RBM system.

Viewing Merit Order

Tertiary Upward Regulation Merit Order

Merit order and clearing:

Submit order for verification and committing:

Interval 1

Transactions:

Buying:

Offering Party	Offer ID	Bid ID	Price	Quantity	Complete	Original Quantity
Example TSO 1 1	2	25	165	Yes	N/A	
Example TSO 2 1	2	25	165	Yes	N/A	
Example TSO 1 2	2	25	165	Yes	N/A	
Example TSO 2 2	2	25	165	Yes	N/A	
Example TSO 1 3	2	25	165	Yes	N/A	
Example TSO 2 3	2	25	165	Yes	N/A	
Example TSO 1 4	2	25	165	Yes	N/A	
Example TSO 2 4	2	25	165	Yes	N/A	
Example TSO 1 1	3	25	190	Yes	N/A	
Example TSO 2 1	3	25	10	No	190	

Fig. 2. Operator interface for generating merit order information

Id:	1
Party Id:	1
Bid Id:	24
Bid Type:	1
Eng Type:	2
Offer Id:	8
Delivery Date:	2012-05-05
Interval:	1
Qty:	1700
Mcp:	4775
Orig Price:	3300
Transactioned:	<input checked="" type="checkbox"/>
Final Price:	3300
Final Qty:	1700
<input type="button" value="Submit"/>	

Fig. 3. Administrator interface: editing the parameters of a scheduled transaction

3. THE SEETSOC RBM IMPLEMENTATION

The server-side software modules are implemented in the Python programming language, using web2py – a well-established, enterprise-class, Open Source framework, distributed under a highly permissive license – to integrate the back-end business logic with the user interface. The choice of Python and web2py makes the RBM program effectively platform-agnostic: it can run on any operating system that can run Python and a web server (including Windows, Linux and Mac OS X), and can use any widely-available database management system – including the popular MySQL and PostgreSQL, but also highly scalable systems such as MongoDB.

Some of its functions, which are required for integration with desktop clients, are also available through web services implemented using the standard SOAP protocol.

These two traits result in a great deal of deployment flexibility. Platforms can even be switched seamlessly – it is possible to move from one hosting system to another, changing everything, from the web server to the database management system used, and the system will continue to run without any data loss. Secure access can be granted using the HTTPS protocol, which is supported by any modern web browser and operating systems, and results in a well-encrypted, secure communication that ensures the security of transaction-related data.

The reference desktop client is implemented in C++, using the cross-platform application framework Qt – an Open Source application framework for desktop applications that runs on all major operating systems and even on mobile platforms. However, the platform is not tied to its use – as the encoding of the bids is an open standard, any client that complies with it can be used.

4. TEST RESULTS FOR THE SYSTEM

Offers have been uploaded and system tests were performed to ensure the proper functionality of the whole modules assembly.

Downward Tertiary regulation

Data were loaded in XML format files and the program filters data in conformity with the specifications; the results are presented in Table 1. Sell and buy issues were treated separately and the accepted offers are specified. The accepted offers are marked A in the last three columns of the Table.

Table 1. Downward Tertiary regulation

TERTIARY REGULATION OFFERS										
	Sender	No	Transaction_Day	Trans_Interval	Time Stamp (Server)	Type	Direction			
Offer										
Pair	TSO1	1	21.01.2012	2	20.01.2012 12:23	Sell	Downward	1	2	3
Price	TSO1	1	21.01.2012	2	20.01.2012 12:23	Sell	Downward	40	45	50
Quantity	TSO1	1	21.01.2012	2	20.01.2012 12:23	Sell	Downward	15	12	22
Accepted	TSO1	1	21.01.2012	2	20.01.2012 12:23	Sell	Downward	A	A	A
Offer										
Pair	TSO2	2	21.01.2012	2	20.01.2012 10:10	Sell	Downward	1	2	3
Price	TSO2	2	21.01.2012	2	20.01.2012 10:10	Sell	Downward	25	30	33
Quantity	TSO2	2	21.01.2012	2	20.01.2012 10:10	Sell	Downward	20	22	37
Accepted	TSO2	2	21.01.2012	2	20.01.2012 10:10	Sell	Downward	A	A	A
Offer										
Pair	TSO3	3	21.01.2012	2	20.01.2012 15:12	Buy	Downward	1	2	3
Price	TSO3	3	21.01.2012	2	20.01.2012 15:12	Buy	Downward	30	32	35
Quantity	TSO3	3	21.01.2012	2	20.01.2012 15:12	Buy	Downward	10	12	14
Accepted	TSO3	3	21.01.2012	2	20.01.2012 15:12	Buy	Downward	A	A	A
Offer										
Pair	TSO4	4	21.01.2012	2	20.01.2012 15:01	Buy	Downward	1	2	3
Price	TSO4	4	21.01.2012	2	20.01.2012 15:01	Buy	Downward	33	40	51
Quantity	TSO4	4	21.01.2012	2	20.01.2012 15:01	Buy	Downward	17	19	11
Quantity	TSO4	4	21.01.2012	2	20.01.2012 15:01	Buy	Downward	A	A	A

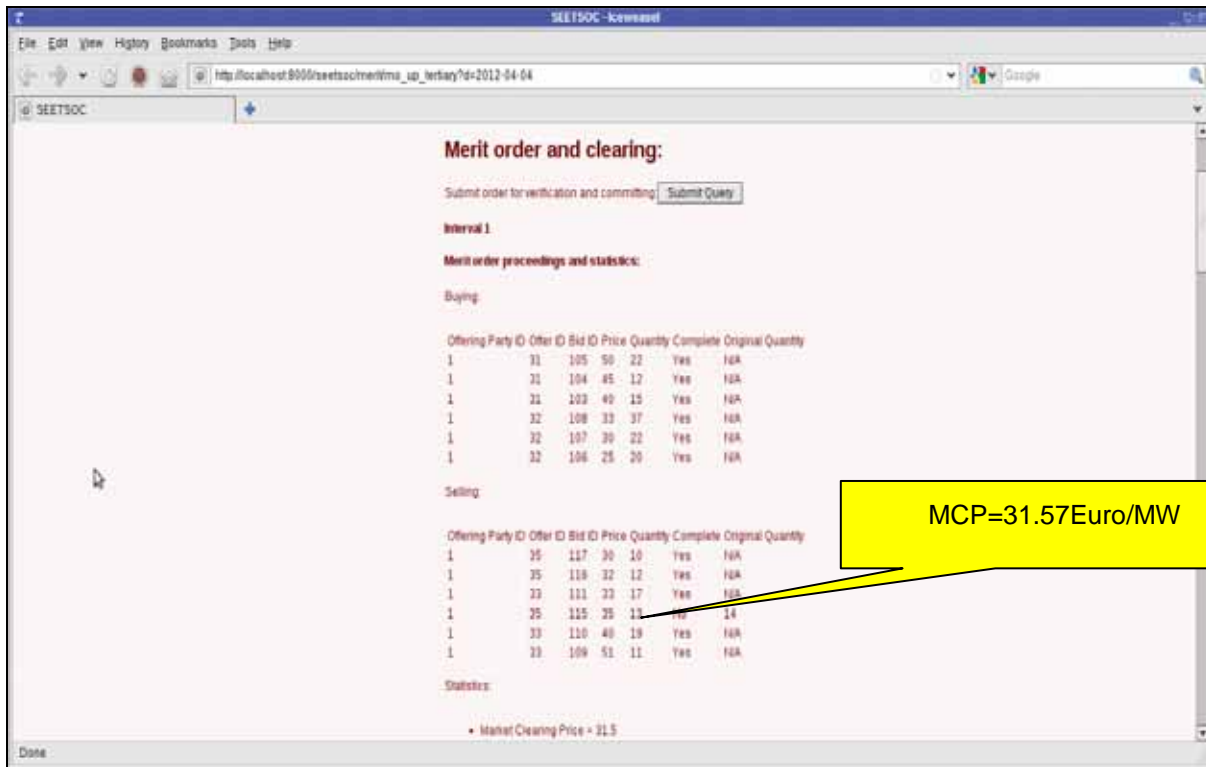


Fig. 4. Software results for Clearing Price - Downward Tertiary Regulation

5. CONCLUSIONS

The RBM system has a modular design using standard interfaces and XML-formatted messaging, web-based interfaces and web services for the system users. It could also be a stand-alone program which can be installed anywhere in a TSO's operational network and integrated into the existing Market Management Systems (MMS) which are used in the TSO run centralized electric markets.

Acknowledgment

The authors would like to acknowledge the contribution of all partners of the SEETSOC consortium for their contributions to the realization of the project no.TREN/FP7EN/239453.

References

- [1] *** RBM Software Analysis and Design, SEETSOC Deliverable D5.1.1., SEETSOC Project
- [2] *** RBM Software Implementation, SEETSOC Deliverable D5.1.2, SEETSOC Project
- [3] Costin Cepisca, Alexandru Lazar, Sorin Dan Grigorescu, George Seritan, Database structure support for bid interface, Proceedings of WSEAS Intl. Conference Recent Researches in System Science, Corfu, 2011, pp.394-397
- [4] Costin Cepisca, Alexandru Lazar, Sorin Dan Grigorescu, George Seritan, Desktop Client Bid Interface, Workshop SEETSOC, Bucharest, may 13, 2011, pp.26-36G
- [5] Xiao-Ping Zhang, Analysis of Electricity Markets with Equilibrium Models, IEEE Press, 2010

CALCULATION OF NETWORK TRANSFER CAPACITIES USING UCTE FILE FORMAT

Nikolay Baldzhiev, Ivan Evgeniev, Velizar Bodurski, Valeri Mladenov

Faculty of Automation, Technical University of Sofia,
blvd. Kliment Ohridski 8, Sofia, Bulgaria

Abstract. *In the paper algorithms for calculation of NTC – Network Transfer Capacity and ATC – Available Transmission Capacity are reviewed. By using the contents of the UCTE file format (Universal format for exchanging data about power grids) a power network model can be created using a software module thus allowing simulation of the transfer/transmission capacities of the network by changing power of generator nodes.*

Keywords: *NTC, ATC, Power Grids, Simulation, UCTE*

1. INTRODUCTION

One of the important tasks of the Power engineer working with power lines is to know for a given period what the transfer capacity is during different power conditions. This can prevent outages, and the lines can be used with greater efficiency. In order to apply algorithms for calculation of NTC and ATC, a model of the power lines/gird should be created. This can be achieved using UCTE file format, which is European standard for describing data exchange between power grids. A software module was developed to create a power network model from the UCTE file. Once the model is created power generator nodes can be changed in order to simulate lower or higher power consumption. This is done by defining Import and Export lists of generators. In order to simulate increased consumption, the load for the Import generators is increased using specific algorithms. From the other side – the export list – the load is decreased. This leads to increased amount of power load for lines connecting the import and export generator nodes. The increasing and decreasing of power load is done by steps. On each step depending on the algorithm, the Import List are increased, the export list generator nodes are decreased. This module is sent to Load Flow calculation procedure that detects the outages in the lines. If there aren't outages, the next step is performed. Additionally a list of outages can be created, so every time when calculation is made, one of the line is set to be an outage. These simulations are important, because there is an EU rule, which requires N+1 rule to be applied. The meaning of the rule is to provide security/stability if there is a failure/outage/power down in one of the power line, the rest can work without it. The software module provides the configuration of the NTC calculations, and the results from the associated calculations are saved in the database.

2. THE CALCULATION METHODOLOGY AND ALGORITHM

The software module uses flow chart depicted in Figure 1. The first step of the algorithm is to select a power grid model. The second step is to define what will be the Export Area and Import Area. Multiple countries (only countries in the previously opened model) can be selected. Power distribution algorithms should be selected for both Export and Import areas. The increase step in MW, and Max Simulation Range in MW should be defined before proceed to next step. With defining the Outage and Monitoring list, all of the necessary steps for configuring NTC calculations are done.

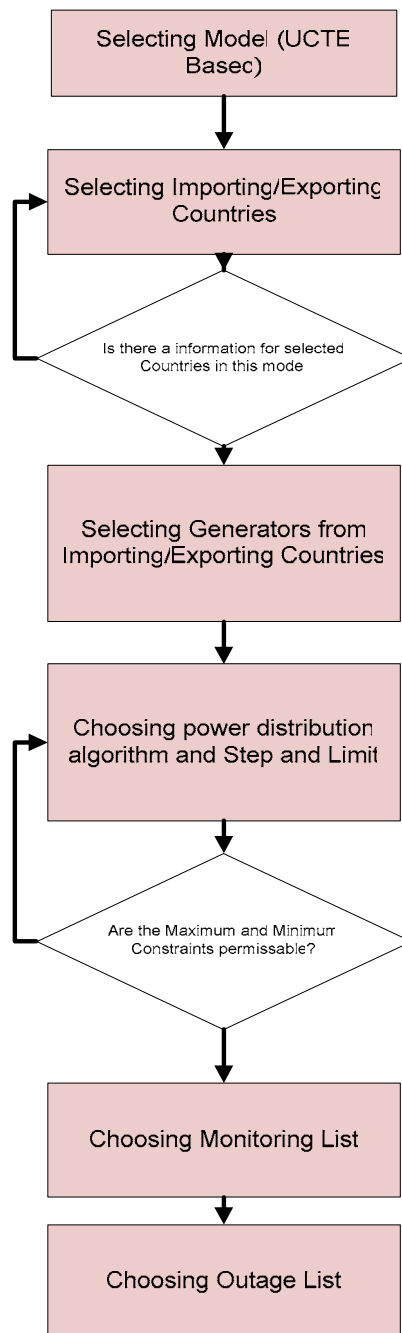


Fig. 1. Flow chart of the module

Definition of:

- Outage list,
- Monitoring list,
- Exporting system/systems,
- Importing system/systems,
- Step to increase/decrease production/consumption,
- Max limit of increase/decrease of production/consumption,
- Type of production and/or consumption change:
 - I. Proportional to reserve (dPg),
 - II. Proportional to engagement (Pg),
 - III. According to generation Shift list.
- Voltage and load flow thresholds to be reported for the concerned border-direction-period.

NTC/ATC calculation and reporting for the concerned border-direction-period (for year ahead, month ahead and week ahead time periods):

- Usage of defined settings under step (2) for NTC calculation.
- Base case calculation: n-1 calculation for base case (without increase/ decrease in production/consumption).
- Reporting on contingencies in base case (voltage out of limits or load flows out of limits).
- Change case calculation: n-1 calculation for each defined step of increase/decrease of production/consumption until the defined limit is reached (for increase/decrease of production/consumption usage of algorithm for defined type of production and/or consumption change: Proportional to reserve (dPg), Proportional to engagement (Pg), According to generation Shift list).
- Reporting on contingencies in change case (voltage out of limits or load flows out of limits).
- In all steps during the calculation of NTC values, the Capacity Module stores the model in a binary file.
- Calculation of TTC (Total Transfer Capacities) for the concerned border-direction-period:

$$TTC = BCE + \Delta E_{max}$$

Where:

BCE – is the Base Case Exchange (these values are scheduled),
 ΔE_{max} – is the Maximum shift of generation that can be assigned to areas without any violation of the N-1 security principle.

- Calculation and reporting on overall NTC/ATC calculation results for the concerned border-direction-period:

$$\begin{aligned} TTC &= BCE + \Delta E \\ NTC &= TTC - TRM \\ ATC &= NTC - AAC \end{aligned}$$

Where:

The values of TRM can be selected in two different ways:

- TRM is the predefined Technical Reliability Margin (100 MW for 400 kV OHLs, 50MW for 220 kV OHLs),
- The value of TRM can be manually selected.

AAC – is the Already Allocated Capacity in the past for the concerned border-direction-period.

- Creation of the final NTC/ATC calculation report and storage in DB. NTC/ATC evaluation and reporting for the concerned border-direction-period (for the week ahead (optionally), day ahead and intra-day periods):
- Usage of stored NTC results from the past,
- Usage of stored allocation results from the past,
- Algorithm for available transmission capacity - ATC evaluation:

$$ATC_{\text{new}} = ATC_{\text{old}} - AAC \pm RM$$

Where:

ATC_{new} – is the new evaluated value of available transfer capacity,

ATC_{old} – is the old value of available transfer capacity,

AAC – is the Already Allocated Capacity in the past for the concerned border-direction-period,

RM – is the reliability margin for the concerned border-direction-period.

Creation of final NTC/ATC evaluation report is stored in database.

3. POWER DISTRIBUTION ALGORITHMS

In order to simulate export from one area to another, the generation of energy should be increased in the exporting area, while the generation of energy should be decreased in the importing country. The generation of energy of the importing country is decreased by the same amount as the increase in generation of the exporting country. For example, if the total increase of generation in the exporting country is 1000 MW, the total decrease of generation in the importing country should be 1000 MW. The means to distribute 1000 MW to the generators depends on the selected algorithm:

- Proportional To Reserve – This algorithm is based on the assumption that generation will be increased/decreased based on the reserve capacity of the generators (the difference between the current rate of generation and the maximum permissible). In particular, if a generator has a maximum permissible power of 200MW, but works on 100MW, there is a 100MW reserve. Thus, for each of the generators, the reserve is calculated and the increased power is distributed proportionally to the reserves.
- Proportional To Engagement – This algorithm distributes the increase of generation based on the current rate of generation, so generators that generate

more will have a larger coefficient and more power should be distributed from them.

- Generation Shift List – Here, generators generate power according to a merit order taking into account the maximum and minimum production.

The user enters values for the Step and Limit parameters. Limit is the total power increased at the end of the simulation and Step is the amount of power that should be increased in each step. For example, if the limit is 1000 MW and the Step is 100 MW, there will be 10 steps and each increasing power by 100 MW. The first step will be 100 MW, the second step 200 MW, the third 300 MW and so on until the 1000 MW limit is reached. If the first algorithm i.e. proportional to reserve, is selected, the program checks for constraints (maximum and minimum levels), so that if a particular generator generates more than the maximum permissible power, this particular row in the table list (Fig. 2) will be coloured in red - otherwise it is white. The same check is carried out for generators that are in the importing area, but these are compared to the minimum permissible power, since most generators have a minimum working limit and cannot work under this limit.

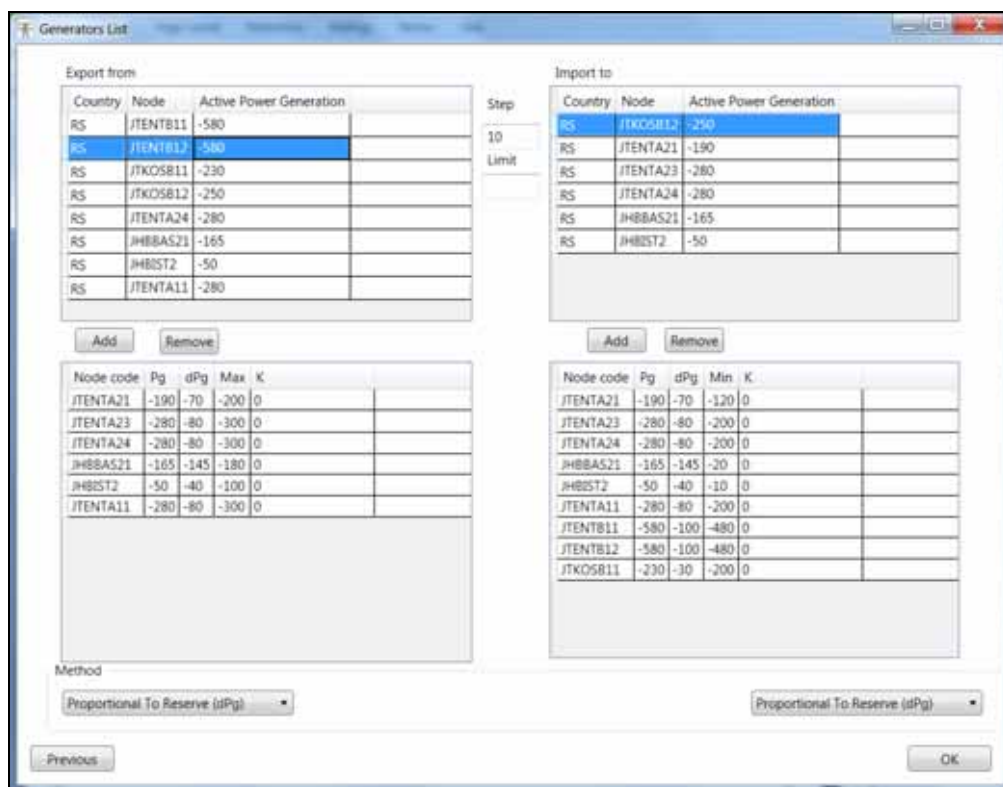


Fig. 2. Generators list table

4. CONCLUSION

A methodology for simulation and calculation of NTC and ATC based on using UCTE file is studied in this paper. By using the software module developed for Transmission Capacity, the power engineer can simulate and calculates where the

weak points of the network – where outages will appear, and whether the lines will be effectively used.

Aknowldgements

The software module used for calculation and simulation is developed under the Work Package 3 of project no. TREN/FP7EN/239453 SEETSOC. Valuable information was provided by Mr. Nenad Sijakovich from Serbian TSO about algorithms used for calculation of NTC and ATC.

References

- [1] N. Baldzhiev, V. Mladenov “Seetsoc Deliverable Report Work Package 3.5”
- [2] UCTE Subgroup “Network models and forecast tools ”UCTE data exchange format for load flow and three phase short circuit studies”
- [3] S. Jacobs and C. P. Bean, “Fine particles, thin films and exchange anisotropy,” in Magnetism, vol. III, G. T. Rado and H. Suhl, Eds. New York: Academic, 1963, pp. 271–350.

USING GEOGRAPHICAL INFORMATION SYSTEM IN POWER NETWORKS

*Nikolay Baldzhiev, Velizar Bodurski, Georgi Tzenov,
Ivan Evgeniev, Valeri Mladenov,*

Faculty of Automation, Technical University of Sofia,
blvd. Kliment Ohridski 8, Sofia, Bulgaria

Abstract. *In the paper are presented features and advantages of using geographical information system in the field power networks. Visualization of power grids, transformer substations and generators can be automatically generated using data from UCTE file and assigning to them GPS Coordinates. Helpful information can be gathered from web services like weather information, population of given visualizing all kinds of data on one screen. This would provide another point of view and source of information for the Power engineers and analytics.*

Keywords: *GIS, Power Grids, GPS, UCTE*

1. INTRODUCTION

Geographical Information System (GIS) is a software module that can visualize POI – Points of Interests. In this case they are Power Lines, Transformers and Generators. GIS module is customizable and can be used for interactive visualizing of results of other modules.

The GIS module is customizable and can be used for interactive visualizing of the results of the other modules. GIS uses OpenStreetMap web services for downloading the contents of the map. Features such as searching through an interactive map, navigation with GPS coordinates are also useful when interacting with it.

2. STRUCTURE OF THE GIS

The GIS Project contains four subprojects. The GIS visualization layer, TabGis-Control – provide interactive menus and features such as extensibility that functionalities from other modules can be implemented in it. The UCTE Map provider converts the UCTE files and assign them with a GPS coordinates. This way, nodes from the UCTE file, can be visualized on the screen.

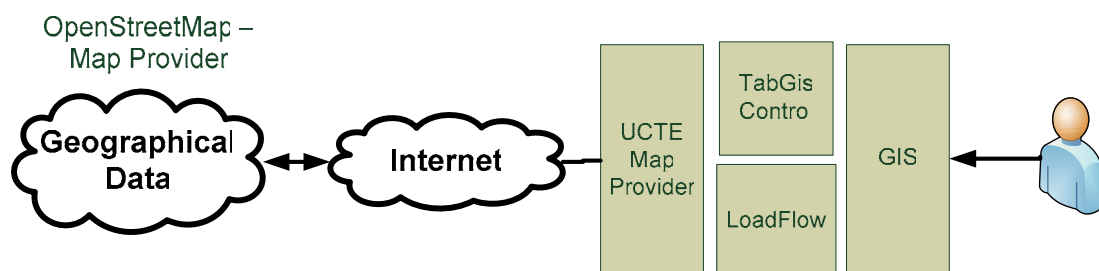


Fig. 1. The GIS structure

There are two choices regarding the implementation of the GIS system. Web based GIS system and Desktop Application (Windows application)

- Web Application – works on every platform, but is hard to manage, secure and support. There is considerably higher security risk.
- Desktop Application – This technology can provide rich user experience, smooth animations, and validation of data. The technology is also very flexible and various features can be implemented with it.

2.1. Desktop Application

The GIS is implemented as a desktop application. Following features are available by using this approach:

- Advanced visualization techniques. If there is a need, we can easily display real time data, trends and complex animations.
- Enhanced security – we can implement any security protocol, and also – without application there is no access to database. This will eliminate need of internet browsers, and internet servers to host the application
- Deployment only to authorized personals – access to data will be only through application, and internet is only for data exchange.
- Deployment with “One Click” technology. Last version of application is stored on server, and with one click, user can execute application locally.
- Easily connection with pc hardware or services on local PC if there is a need (OPC server, PLC trough serial communication or other)
- Real-time validation of data, or other complex logic
- Application can use Web Services
- Advanced file compression, encryption, interpretation

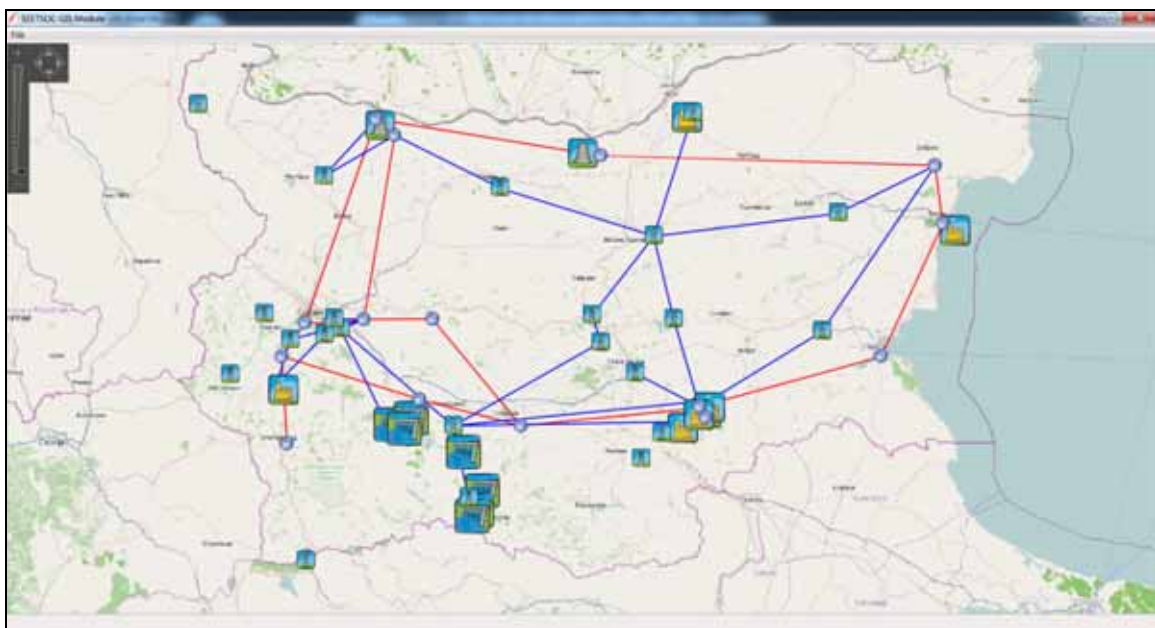


Fig. 2. A Model of Bulgarian Major Power Network visualized in the GIS.

2.2. Web Application

Internet applications run on a specialized Web Server which is a host. This server is also the host of the web applications. Additionally, a database server is required on a separate server, so two servers should be connected in order to exchange information.

Features of the Web based technology

- Runs on every platform, and almost every Internet browser
- There is no need of deployment, only updating server
- Can use web services

There are some drawbacks for internet application:

- Need of 24/7 support for internet server and backup
- Need of constantly updating internet server and internet browsers to prevent hack from exploits

3. CONSIDERATION FOR MAP PROVIDERS

The decision according to the aforementioned choices was to implement the GIS system as a desktop application. There is one major drawback in Web GIS. Almost every map provider (Google, Yahoo, Microsoft etc.) has limitations in the use of the free version of the maps that are incompatible with the purpose of the system under design. To use, for example, Google maps in a web site, all uploaded information must be visible to every user in the internet. The site must be non-password protected and publicly visible. Microsoft and Yahoo have similar conditions for using their maps. In order to have secure and non-visible maps for everyone, Web GIS must be obtained with corporate license which is beyond the scope of a research project.

On the other hand, if choosing a desktop application, only the geographical data such as terrain, towns and other can be downloaded. All the geographical data can be visualized in a background layer. On the front layer, POI (Points of interests) from the project's database can be added without compromising the security model of the visualized data. In that way, a map provider database is not used but only the geographical data.

The description of the major map providers follows. By using a desktop application, most of the drawbacks stemming from the license the map providers offer are not valid.

- Google Maps
- Microsoft Bing Maps
- MapQuest
- Yahoo Maps
- OpenStreetMap

3.1. Google Maps

Google maps are the most used GIS system in the world today. The system is free, for demonstration purposes, and for embedding in Web sites. The down-side of free version is the code must be made publicly visible, and open source. This isn't

appropriate for the GIS project since the Power Network Models represents the infrastructure that may be critical for a country's security and thus it cannot be made available online to any user in the Internet. There is a paid version but the prices and conditions fell beyond the scope of the developed GIS requirements. Google maps also have very useful features such as:

- Full detailed map of all countries, with city, regional and municipality borders
- POI – Point of interests.
- Added points on map.
- 3D visualization of terrain.
- Measurement of roads, elevation and other
- Satellite pictures or Road Map view.
- Many useful services.
- Work on all smartphones (iPhone, Symbian, Android, Blackberry and etc)

3.2. Microsoft Bing Maps

There are many useful features in these maps, especially from the Developer's side. Microsoft has very good tools for development and easy integration with other applications. For the GIS project purposes, the tools and technology cover all the requirements and have been selected as the implementation platform for the GIS module. Some of the salient features they offer are:

- Terrain details are also available in 3D mode.
- Finding, viewing, and printing driving directions
- Traffic viewing (in several major cities)
- User points of interest that can be stored and shared
- Drawing on maps
- A location finder that can locate the user's location
- Integrated route calculation

3.3. MapQuest

Map Quest is one of the first digitalized maps. They are free for using, but there are no good tools for development.

MapQuest offers:

- Maps of all countries
- Road names, length, elevation and other information
- Very simple for using
- Used from Yellow Page services
- Working on some mobile phones

3.4. OpenStreetMap

OpenStreetMap allows you to view, edit and use geographical data in a collaborative way from anywhere on Earth.

- Maps can be download entirely, or partially for specific regions
- Roads, Cities, Towns, Villages, Country Borders, Rivers, Lakes, Airports
- Free to use

The biggest advantage of the OpenStreetMap is that it is free to use. Other map providers require payment or public visibilities of contents in order to use them. Final decision was to use OpenStreetMap, which is open and free. Many new features and POI was introduced when we started to work with it such as:

- Addresses
- Aerialway
- Aeroways
- Airports
- Barriers
- Boundaries
- Buildings
- Railway stations
- Waste Processing
- Waste Processing
- Waterways
- Power

4. CONCLUSION

Using modern technologies such as Geographical Information System provide a new way of representing information in the Power Networks. It is very easy to create a power model for any given country by using UCTE file which describes all of the objects/nodes in the power networks. Many advantages can be achieved with visual representation of the power networks such as: connectivity and relative distance to major cities and factories which are major consumers, visual representation of most often outages, regional and social information and statistics.

Aknowldgements

The software module used for calculation and simulation is developed under the Work Package 3 of project no. TREN/FP7EN/239453 SEETSOC. Valuable information was provided from all of the partners involved in the project and especially by Prof. Nicholas Harkiolakis and Prof. Panos Liastis.

References

- [1] Lambros Ekonomou, Panagiotis Karampelas WP3.1 Client Module Functional Specification
- [2] N. Baldzhiev, V. Mladenov "Seetsoc Deliverable Report Work Package 3.2"
- [3] UCTE Subgroup "Network models and forecast tools" UCTE data exchange format for load flow and three phase short circuit studies"